

BOSTON UNIVERSITY  
COLLEGE OF ENGINEERING

Dissertation

**MECHANICAL REALIZATION THEORY AND ITS APPLICATION  
TO MACHINERY EMULATION**

by

**WENYUAN CHEN**

B.E., Zhejiang University, China, 1996  
M.E., Zhejiang University, China, 1999

Submitted in partial fulfillment of the  
requirements for the degree of  
Doctor of Philosophy

2004

## Approved by

Advisor:

---

Pierre E. Dupont, Ph.D.  
Associate Professor, Aerospace and Mechanical Engineering

Second Reader:

---

James Gregory McDaniel, Ph.D.  
Associate Professor, Aerospace and Mechanical Engineering

Third Reader:

---

Allan D. Pierce, Ph.D.  
Professor, Aerospace and Mechanical Engineering

Fourth Reader:

---

John B. Baillieul, Ph.D.  
Professor, Chairman, Aerospace and Mechanical Engineering

Defense Chair:

---

Todd W. Murray, Ph.D.  
Assistant Professor, Aerospace and Mechanical Engineering

Dedicated to  
my parents  
elder sister and brother  
and  
wife  
for their unconditional love and support.

Science can amuse and fascinate us all, but it is engineering that changes the world.

Isaac Asimov (1920-1992)

## Acknowledgments

As an old saying says, “Where there is a will, there is a way.” The will to pursuing a Ph.D. degree sent me on a journey full of joy and pain. It cannot be reached without much diligence and persistence. More importantly, without a direction it can never be fulfilled. I am very pleased to acknowledge my advisor Professor Pierre E. Dupont for his patient and enthusiastic supervision. His outstanding technical insights, long-time encouragements and financial aid have proved invaluable through my Ph.D. study at BU.

I am greatly indebted to Professor James Gregory McDaniel for his enthusiasm and many discussions. I would like to thank Professor Allan D. Pierce and Professor John B. Baillieul for being my committee members. I have benefited from their outstanding knowledge and keen technical insights. Thanks to Professor Todd W. Murray for being my defense chair in my Ph.D. prospectus and dissertation defenses.

Thanks to David Campbell and Joseph Estano for their help in fabrication of mechanical emulators. Thanks to Sudeep Deshpande for his discussions and help in this research. Thanks to my colleagues in the BU Robotics, Dynamics and Control Laboratory and Intelligent Mechatronics Laboratory.

The research presented in this dissertation was sponsored by the US Office of Naval Research under the grant N00014-01-1-0155, titled “Design Methods for Machinery Emulators”. I also received a Boston University Presidential University Graduate Fellowship. I am very grateful for the generous funding support.

Finally, I wish to thank my wife Xuzheng Wang, my parents and family for their unconditional love and support for many years. Thanks to their belief in the importance of advanced education and knowledge. I would like to dedicate this dissertation to them.

**MECHANICAL REALIZATION THEORY AND ITS APPLICATION TO  
MACHINERY EMULATION**

(Order No.                    )

**WENYUAN CHEN**

Boston University, College of Engineering, 2004  
Major Professor: Pierre E. Dupont, Ph.D., Associate Professor  
Department of Aerospace and Mechanical Engineering

**ABSTRACT**

The realization of electromechanical dynamic systems possessing specified input-output dynamic properties is studied. Applications of this problem include the scaled shock and vibration testing of complicated structures, the design of electromechanical filters and the design of vibration absorbers. A two-step realization process is developed by which both passive and active systems can be realized. In the first step, a passive mechanical system is obtained, which is then modified in the second step to achieve active realization. For example, in machinery emulation, the goal is to design an electromechanical system which matches the vibrational energy flow at the locations where the machinery attaches to its foundation. In this case, the passive realization would correspond to the machinery when it is not in operation while the active realization would also account for the vibrational energy produced during machinery operation.

Two techniques have been developed to obtain realizable models for the design of passive mechanical systems. The first technique involves searching the parameterized space of congruent coordinate transformations relating input-output equivalent second order models for those that are realizable, i.e., those that can be directly interpreted as a network of mechanical elements. The second technique involves estimating realizable models which include both distributed and lumped mechanical elements directly from experimental machinery data. This approach utilizes a cost function dependent on accelerance and dynamic

mass errors. Active emulation is achieved by adding vibration sources, e.g., shakers, to the passive structure. These sources are driven under closed-loop control so as to produce the desired level of vibration at the output locations.

Experimental evaluation of these techniques has been carried out through the design of a modular, SISO machinery emulator, which can be adapted to match the mass and dynamic properties of a desired machine within a frequency range of interest. Experimental results demonstrating the effectiveness of the techniques for both passive and active emulation are presented.

# Contents

<b>List of Tables</b>	<b>xii</b>
<b>List of Figures</b>	<b>xiv</b>
<b>1 Introduction</b>	<b>1</b>
1.1 Dynamics of Machinery . . . . .	3
1.2 Mechanical Emulator Design Goals . . . . .	5
1.3 Passive and Active Emulator Design Approaches . . . . .	6
1.4 Organization of the Dissertation . . . . .	9
<b>2 Background and Related Work</b>	<b>12</b>
2.1 Frequency Ranges of Interest in Various Coordinate Directions . . . . .	13
2.2 Modeling Vibratory Mechanical Systems . . . . .	14
2.2.1 Model Identification and Reduction . . . . .	18
2.3 Prior Work on Mechanical Realization . . . . .	21
2.3.1 Frequency Domain Realization . . . . .	21
2.3.2 Time Domain Realization . . . . .	29
2.3.3 Navy Contractor Emulators . . . . .	32
2.4 Summary . . . . .	34
<b>3 Theory of Transformations Relating Realizations</b>	<b>37</b>
3.1 Structure of Realizable Second Order Models . . . . .	38



3.1.1	Mechanically Realizable Mass, Damping and Stiffness Matrices . . .	38
3.1.2	Desired Input and Output Influence Vectors or Matrices . . . . .	41
3.1.3	Mechanically Realizable Second Order Model . . . . .	44
3.2	Decomposition of the Congruent Coordinate Transformations . . . . .	46
3.3	Parameterization of the Orthogonal Component $R$ . . . . .	49
3.3.1	Aligning the Input and Output Influence Vectors (or Matrices) . . .	50
3.3.2	Converting to Realizable Damping and Stiffness Matrices . . . . .	57
3.4	Properties of Transformations Relating Realizable Models . . . . .	62
3.4.1	SISO Mechanical Realizations . . . . .	63
3.4.2	MIMO Mechanical Realizations . . . . .	67
3.5	Obtaining the Final Mass Matrix . . . . .	75
<b>4</b>	<b>Two Techniques for Obtaining Realizable Models</b>	<b>77</b>
4.1	Searching the Parameterized Space of Realization Transformations . . . . .	77
4.1.1	Approximate Solutions . . . . .	79
4.1.2	Approximation Error by Removing Connecting Elements with Small Values . . . . .	82
4.1.3	Numerical Examples . . . . .	85
4.2	Direct Estimation of Realizable Models from Experimental Data . . . . .	99
4.2.1	Direct Estimation Procedure . . . . .	99
4.2.2	Direct Estimation Examples . . . . .	102
<b>5</b>	<b>Mechanical Emulator Design Methodology</b>	<b>107</b>
5.1	Passive Emulator Design . . . . .	108
5.1.1	Modular Design . . . . .	108
5.1.2	Mass Matching Requirements . . . . .	110
5.1.3	Modeling the Passive Mechanical Emulator Model . . . . .	116
5.1.4	Estimation of Unknown Parameters in the Passive Emulator . . . .	119
5.1.5	Emulator Damping . . . . .	120

5.1.6	Design and Implementation Steps for Passive Emulators . . . . .	126
5.2	Active Emulator Design . . . . .	129
5.2.1	Selection of the Emulating Shaker and its Mounting Location . . . .	131
5.2.2	Feedforward/feedback Controller for the Emulating Shaker . . . . .	132
<b>6</b>	<b>Experimental Passive and Active Emulation</b>	<b>134</b>
6.1	Machinery Test Bed . . . . .	134
6.2	Accelerance Acquisition System . . . . .	136
6.3	Passive Mechanical Emulator . . . . .	139
6.3.1	Realizable Model Identification . . . . .	139
6.3.2	Design and Implementation of Passive Emulators . . . . .	143
6.3.3	Performance Evaluation of the Passive Mechanical Emulators . . . .	146
6.4	Design of an Active Mechanical Emulator . . . . .	147
6.4.1	Selection of the Emulating Shaker and its Mounting Location . . . .	147
6.4.2	Transfer Accelerance from the Emulating Shaker to the Attachment Point . . . . .	149
6.4.3	Identification of the Transfer Function $V(s)/F(s)$ . . . . .	150
6.4.4	Implementation of the Feedforward/feedback Controller . . . . .	153
6.4.5	Performance Evaluation of the Active Emulator . . . . .	154
<b>7</b>	<b>Conclusions</b>	<b>163</b>
<b>A</b>	<b>State Space Realizations</b>	<b>167</b>
<b>B</b>	<b>Approximation of Nonproportionally Damped Mechanical Systems: An Example</b>	<b>169</b>
<b>C</b>	<b>QR Factorization</b>	<b>174</b>
<b>D</b>	<b>Properties of the Orthogonal Transformation <math>R_e</math></b>	<b>176</b>

<b>E</b>	<b>Modeling the Base Structure of the Passive Mechanical Emulator</b>	<b>179</b>
E.1	Euler-Bernoulli Beam Model . . . . .	179
E.2	FEA Beam Model . . . . .	183
<b>F</b>	<b>Building Single-mode Oscillators from Distributed Mechanical Elements</b>	<b>186</b>
F.1	Modeling an Oscillator from Distributed Elements . . . . .	186
F.2	Distributed-parameter versus Lumped-parameter Oscillator . . . . .	190
<b>G</b>	<b>Analytical Model for Free-layer Damping Treatments</b>	<b>192</b>
<b>H</b>	<b><i>MATLAB/SIMULINK</i><sup>®</sup> Models for Active Emulation</b>	<b>194</b>
	<b>Bibliography</b>	<b>199</b>
	<b>Vita</b>	<b>206</b>

# List of Tables

2.1	Design Capabilities of Existing Methods versus this Research . . . . .	36
3.1	Number of Masses versus Dimension of the Solution Space . . . . .	59
3.2	Scaling the Final Mass Vector . . . . .	76
4.1	Parameters in the Parallel Model Estimated by Direct Estimation . . . . .	105
5.1	Notation for the parameters in the Passive Mechanical Emulator . . . . .	111
5.2	The Modal Loss Factors of the Free-layer Damping Treatments Calculated from the Measured Data (modal loss factor of the steel beam before treatments is $\eta_0 = 2.24 \times 10^{-3}$ , $n_d$ is the number of free damping layers, $\eta$ is modal loss factor of the spring steel beam after treatments.) . . . . .	123
5.3	Modal Loss Factor of the Constrained-layer Damping Treatments Calculated from Measured Data (loss factor of the steel beam before treatments $\eta_0 = 2.97 \times 10^{-3}$ , $n_d$ is number of constrained damping layers, $\eta$ is modal loss factor of the spring steel beam after treatments.) . . . . .	125
6.1	Parameters of the Identified Realizable Second Order Model for the Passive Mechanical Emulator . . . . .	141
6.2	Calculation of Desired Force for the Emulating Shaker, Experiment 1 . . . . .	155
6.3	Calculation of the Desired Force for the Emulating Shaker, Experiment 2 . . . . .	157
6.4	Magnitudes and Frequencies of Five Sinusoids, Experiment 3 . . . . .	159
6.5	Calculation of Desired Force for the Emulating Shaker, Experiment 3 . . . . .	161

6.6	Acceleration Magnitude for the Active Machinery and its Active Emulator at the Five Excitation Frequencies, Experiment 3 . . . . .	162
E.1	Parameters of the Base Structure in the Passive Mechanical Emulator . . .	180
F.1	Notation for Parameters in the Oscillator Model . . . . .	187

# List of Figures

1.1	A Schematic Example of a Passive Mechanical Emulator . . . . .	3
1.2	Dynamics of Machinery . . . . .	5
1.3	Two-step Mechanical Emulator Design Procedure . . . . .	7
1.4	The Passive Emulator Design Approach . . . . .	8
1.5	The Active Emulator Design Approach . . . . .	9
2.1	Attachment Points, Coordinate Directions of Equipment and Machinery . .	12
2.2	Serial Model . . . . .	22
2.3	Parallel Model Realization . . . . .	26
2.4	Parallel Model Realization II . . . . .	26
2.5	Serial Model . . . . .	27
2.6	Mechanical Emulator for COTS Cabinets . . . . .	33
3.1	A Simple Mechanical Model . . . . .	39
3.2	Mechanical System of a MIMO Driving-point Accelerance . . . . .	43
3.3	Mechanical System of a MIMO Transfer Accelerance . . . . .	43
3.4	Mechanical System of a MIMO Driving-point and Transfer Accelerance . .	44
3.5	Mechanical System of a SISO Transfer Accelerance . . . . .	65
4.1	Driving-point Accelerance of a Second Order Model . . . . .	87
4.2	Realizable Regions for the Driving-point Accelerance: Red - 7 connectors; Green - 8 connectors; Blue - 9 connectors; Magenta - 10 connectors; Cyan - 11 connectors; Black - 12 connectors. . . . .	88

4.3	Minimum Realizable Region for the Driving-point Accelerance . . . . .	89
4.4	Driving-point Accelerance of a Mechanical System with Ten Masses . . . . .	93
4.5	Realizable Region for a Four-mass System of a SISO Transfer Accelerance . . . . .	95
4.6	Realizable Regions for the Five-Mass Example . . . . .	98
4.7	Example 1: Driving-point Accelerance Comparison of Experimental Data and Identified Realizable Model . . . . .	104
4.8	Example 1: Identified Mechanical Model . . . . .	105
4.9	Example 2: Driving-point Accelerance of Experimental Data and the Ident- ified Realizable Model . . . . .	106
4.10	Example 2: Identified Mechanical Model . . . . .	106
5.1	Side View of the Passive Mechanical Emulator . . . . .	109
5.2	Emulator Undergoing Motions in the Horizontal, Vertical and Rotational Coordinates . . . . .	112
5.3	Oscillator Model with Free-Layer Damping Treatment . . . . .	121
5.4	Effect of Free Layer Damping Treatments . . . . .	122
5.5	Comparison Between the Measured Data, Prediction of the Oberst Equa- tion and the Polynomial of (5.30) . . . . .	124
5.6	Oscillator Model with Constrained-Layer Damping Treatments . . . . .	126
5.7	Effect of Constrained Layer Damping on Frequency and Amplitude . . . . .	127
5.8	Relation of Modal Loss Factor and the Amount of Constrained Layer Damp- ing Material . . . . .	128
5.9	Oscillator Model with Free-Layer Damping Treatments and a Spacer . . . . .	129
5.10	Feedforward/feedback Controller for the Emulating Shaker in Active Emu- lation . . . . .	132
6.1	Side View of the Machinery Test Bed . . . . .	136
6.2	Oscillators and Unbalanced Motor (back view) . . . . .	137
6.3	Accelerance Data Acquisition Schematic . . . . .	138

6.4	Driving-point Accelerance of Passive Machinery at its Attachment Point in the Horizontal Coordinate Direction . . . . .	140
6.5	Comparison between the Passive Machinery and its Realizable Second Order Model . . . . .	143
6.6	Comparison between the Passive Machinery and its Continuous and Lumped-parameter Hybrid Realizable Model: Realizable Model I . . . . .	144
6.7	Comparison between the Passive Machinery and its Continuous and Lumped-parameter Hybrid Realizable Model: Realizable Model II . . . . .	145
6.8	Example Passive Mechanical Emulator . . . . .	146
6.9	Driving-point Accelerance Comparison between Passive Machinery and its Passive Mechanical Emulator: Passive Mechanical Emulator I . . . . .	148
6.10	Driving-point Accelerance Comparison between Passive Machinery and its Passive Emulator: Passive Mechanical Emulator II . . . . .	149
6.11	The Transfer Accelerance from the Acceleration Pickup Location to the Mounting Location of the Emulating Shaker . . . . .	150
6.12	Comparison between the Identified Model and Experimental Data of the Transfer Function $V(s)/F(s)$ , Voltage Applied to the Emulating Shaker to the Emulating Shaker Generated Force . . . . .	151
6.13	Implementation of the Feedforward/feedback Controller for Active Emulation	154
6.14	Comparison between the Active Machinery and Active Emulator . . . . .	156
6.15	Comparison between Active Machinery and Active Emulator, Linear Scale .	157
6.16	Time Domain Comparison between the Active Machinery and Active Emulator, Experiment 2 . . . . .	158
6.17	Time Domain Close-up Comparison between the Active Machinery and Active Emulator, Experiment 2 . . . . .	159
6.18	Frequency Domain Comparison between the Active Machinery and Active Emulator, Experiment 2 . . . . .	160



6.19	Time Domain Comparison of Active Machinery and Active Emulator, Experiment 3 . . . . .	161
6.20	Frequency Domain Comparison of the Active Machinery and Active Emulator, Experiment 3 . . . . .	162
B.1	Nonproportionally Damped Mechanical System . . . . .	170
B.2	Approximation of a Nonproportionally Damped Mechanical System by a Proportionally Damped One . . . . .	171
B.3	Approximation of a Nonparallel Model by a Parallel Model: Strong Damping Coupling between Modes. . . . .	172
B.4	Approximation of a Nonparallel Model by a Parallel Model: Weak Damping Coupling between Modes. . . . .	173
E.1	Modeling the Base Structure of the Machinery Emulator . . . . .	181
E.2	FEA Beam Model . . . . .	184
F.1	Oscillator Model . . . . .	187
F.2	The Comparison between the Lumped-parameter Oscillator and Distributed-parameter Oscillator . . . . .	191
H.1	<i>SIMULINK</i> <sup>®</sup> Model of Attachment Point Acceleration Measurement and Feedforward/feedback Controller, Experiment 1 . . . . .	196
H.2	<i>SIMULINK</i> <sup>®</sup> Model of Attachment Point Acceleration Measurement and Feedforward/feedback Controller, Experiment 2 . . . . .	197
H.3	<i>SIMULINK</i> <sup>®</sup> Model of Attachment Point Acceleration Measurement and Feedforward/feedback Controller, Experiment 3 . . . . .	198

# Chapter 1

## Introduction

Our nature consists in motion; complete rest is death.

Blaise Pascal (1623-1662)

A ship's structure is comprised of four major components: its outer structure, the hull; its floors, the decks; a collection of internal structures, which reinforce the hull and support the ship decks; and finally the ship's equipment and machinery, mounted on the decks. The hull and internal structures must meet static loading requirements given by the maximum sea state to be encountered. In naval applications, dynamic considerations are also important. Shock energy transmitted from the surrounding water can damage deck-mounted equipment and machinery. In addition, machinery-generated vibration can be transmitted to the water leading to detection or the detonation of acoustically-activated mines. Thus, vibrational energy flow between the ship structure and shipboard machinery or equipment is an important problem in naval design.

Numerical methods such as finite element analysis (FEA) are often used to test the design of novel ship structures, however, these numerical methods have to make assumptions, such as the simplification of complex geometric shapes, the use of approximate boundary conditions, approximate damping representations and estimated material properties. Thus, experimental validation of a new design is often required, especially for large

and complex structures. When a structure is small and simple or the testing expenses are affordable, a full size physical model may be adopted for testing as is done in car crash tests.

For such expensive, large and complicated structures as ship structures, however, scaled vibration testing often has to be adopted to evaluate and improve their design. Thus, it is required to design and fabricate scaled ship structures as well as scaled equipment and machinery models. Scaled machinery models are referred to as machinery emulators here. This research work will focus on design and implementation of machinery emulators. They are inexpensive electromechanical systems which are able to reproduce the major dynamic properties of the actual equipment and machinery at the foundation attachment points where they are connected to the ship structures.

Depending on whether there are active moving components inside machinery such as rotors or not, mechanical emulators can be classified as two types: passive mechanical emulators and active mechanical emulators. The former emulates equipment or machinery when it is not in operation and the latter emulates machinery when it is operating. The mathematical definition of passivity refers to a system consisting only of elements such as masses, spring and dashpots which can only store or dissipate energy, but not internally generate energy [1].

There are two approaches to mechanical emulator design. The first is exact miniaturization, which is expensive and time-consuming. This research follows another approach, which is based on dynamic equivalence. It starts from the experimental measurement of the dynamic properties of the actual equipment and machinery at their foundation attachment points. Subsequently, a mathematical model directly realizable by mechanical elements is obtained by mechanical realization theory, which is developed here. A mechanical emulator is designed which approximates the dynamic properties of the actual equipment and machinery. In the later discussion, the word “machinery” is used to designate as both equipment and machinery. Passive machinery is referred to as machinery when it is not in operation while active machinery is designated as machinery when it is

operating.

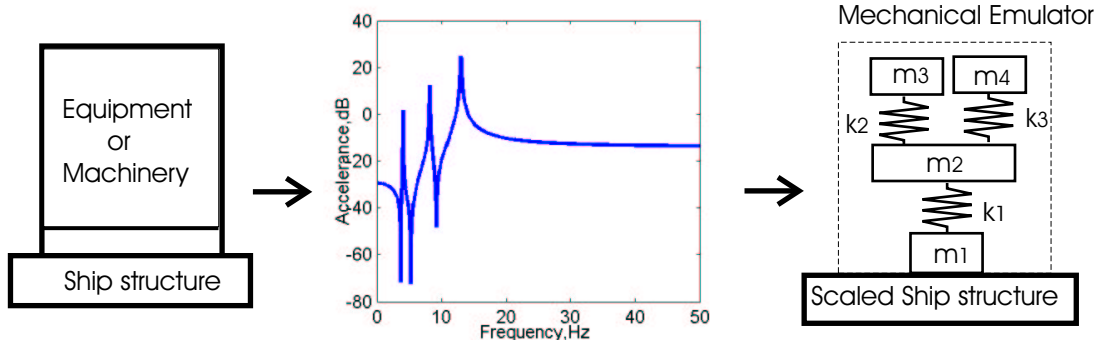


Figure 1.1: A Schematic Example of a Passive Mechanical Emulator

The schematic relation between the actual passive machinery and its mechanical emulator is illustrated in Figure 1.1. Suppose three modes dominate in the frequency response of an actual machinery. A properly designed four-mass mechanical emulator then may be used to replace this machinery in the scaled testing of the ship structure.

## 1.1 Dynamics of Machinery

Machinery is usually mounted on the decks by vibration isolators, which are resilient members such as metal springs, rubbers, elastomers, polymers, pneumatic mounts and even active isolators [2] [3] [4]. These isolators can reduce the vibrational energy transmission between decks and machinery. Modeling and scaling of the vibration isolators is complicated due to geometrical and material nonlinearities; their scaling is considered elsewhere, e.g. [5]. In this research, forces and accelerations are assumed to be measured above the isolators so that the emulator design problem can be treated independently. In addition, this decoupling allows the machinery dynamics to be modeled linearly.

Passive machinery acts as vibration absorbers to the ship structure. In this role, the vibration magnitude of the ship structure can be reduced at the resonant frequencies of passive machinery. Under this scenario, however, some components inside the machinery may undergo large magnitude motions, resulting in temporary malfunction and even

permanent damage.

As shown in Figure 1.2, the acceleration at the foundation is determined by the force exerted by the ship structure and the acceleration of machinery, that is,

$$a_f|_{\text{passive}} = A_{ff}F_f \quad (1.1)$$

where  $a_f|_{\text{passive}}$  is the vector of acceleration at the attachment points,  $A_{ff}$  is the accelerance matrix of the passive machinery at its attachment points and  $F_f$  is the vector of forces exerted by the ship structure to the passive machinery through the attachment points. Here, accelerance is defined as the ratio of acceleration to force. The driving-point accelerance means that the acceleration and force are measured at the same point and in the same direction. During testing, it can usually be measured by an impedance head which includes an accelerometer and force gauge.

When reciprocating or unbalanced machinery, such as diesel engines, electric motors of air conditioning units, are operational, the inevitable unbalance of rotating elements or the flow of fluids and steam causes the machinery to act as a vibration source to the ship structure. Usually, machinery operates at particular rotational speeds. If the operating frequency matches a resonant frequency of the ship structure, large vibration magnitudes of the ship structure will be generated. Vibrations can be transmitted to other vibration-sensitive equipment, to people and to the surrounding water, perhaps resulting in detonation of mines.

Suppose that machinery is freely suspended and turned on. The acceleration at the attachment points due to operation of machinery is decided by the following equation

$$a_f|_{\text{active}} = A_{fi}F_i \quad (1.2)$$

where  $A_{fi}$  is the transfer accelerance matrix from the internal forces to the attachment points and  $F_i$  is the vector of forces due to the moving components within the machinery.

Usually, only  $a_f|_{\text{active}}$  is available, which can be directly measured when the machinery is operating.

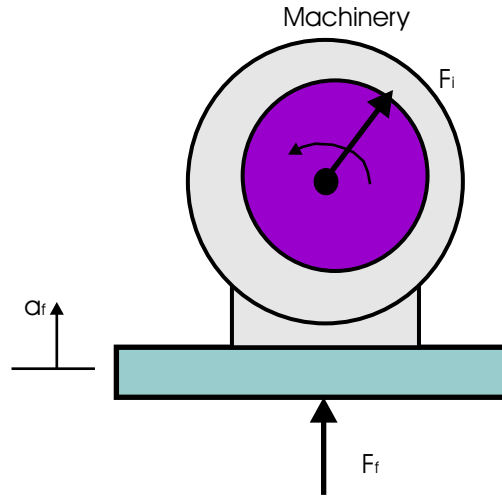


Figure 1.2: Dynamics of Machinery

The total response acceleration due to forces from the ship structure through mounts and forces from the internal moving components is given by the following equation

$$a_f = a_f|_{\text{passive}} + a_f|_{\text{active}} = A_{ff}F_f + A_{fi}F_i \quad (1.3)$$

## 1.2 Mechanical Emulator Design Goals

Mechanical emulators also must act as not only a vibration absorber but also a vibration source in the scaled vibration testing of a ship structure, just as machinery does while it is mounted on the actual ship structure. Generally speaking, machinery can undergo motions in six coordinate directions including three translations and three rotations. The complexity of mechanical emulator design strongly depends on the number of coordinate directions considered.

The coordinate directions can be separated into two groups, that is, those for which dynamic matching over a frequency range is needed and those in which the machinery

acts effectively as a rigid body for the desired frequency range. For the former case, there are modes in the frequency range of interest. In the latter case, it requires that passive machinery and its emulator have the same apparent inertia properties viewed from the foundation attachment points. In summary, the design goals of the passive mechanical emulator can be stated as follows:

1. Match mass and moment of inertia in the desired coordinate directions.
2. Match scalar accelerance or accelerance matrix within a range of frequency of interest in the desired coordinate directions at the foundation attachment points.

Since it is desired that the mechanical emulator must be able to reproduce the effect of machinery operation at its foundation attachment points, the active emulator design adds a third requirement that it should reproduce the operating effect of machinery, that is, accelerations at the attachment points in the desired directions.

### **1.3 Passive and Active Emulator Design Approaches**

To satisfy these design goals, a two-step design procedure is used, as depicted in Figure 1.3. In the first step, a passive mechanical emulator is designed to match the dynamic properties of passive machinery. In the next step, this passive emulator is modified into an active one by adding an active element like a shaker, referred to in the following as an emulating shaker driven by a controller to reproduce the foundation acceleration due to machinery operation.

As illustrated in Figure 1.4, the passive mechanical emulator design approach involves three major aspects: obtaining the accelerance data from the passive machinery; identifying the passive machinery model; and realizing the model with mechanical elements.

During experimental testing, the driving-point accelerances are collected from the experimental measurement of the actual passive machinery by collecting the driving forces and accelerations at the foundation attachment points. The passive machinery is excited

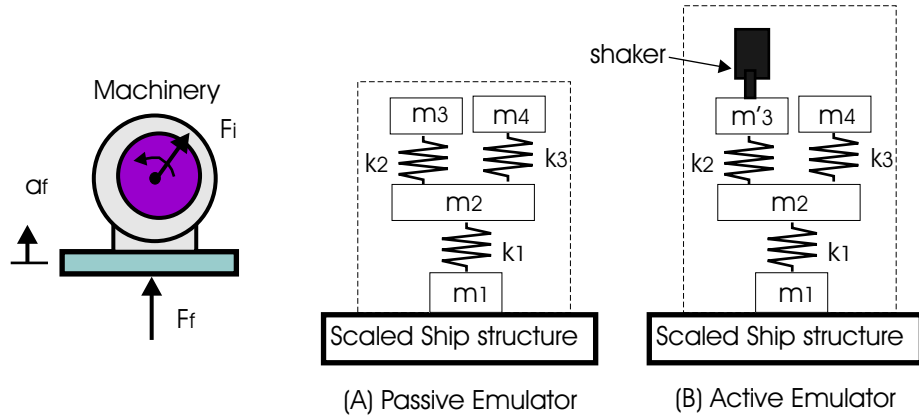


Figure 1.3: Two-step Mechanical Emulator Design Procedure

by shakers while the input forces and acceleration responses are measured by force gauges and accelerometers, respectively. The experimental data of the acceleration are acquired and processed by a dynamic spectrum analyzer.

As shown in Figure 1.4, two approaches are used to obtain the design of the mechanical emulator from the acceleration data. The first approach starts from the identification of mathematical models such as a state space model or a transfer function by model identification methods in the time domain and frequency domain, respectively, [6] [7]. If the order of the identified model is low, it can be directly used for the design of a mechanical emulator. Otherwise, model reduction methods are used to obtain reduced order models. The mechanical emulator model is achieved through the mechanical realization that converts an initial model to a form realizable by mechanical elements. Development of the mechanical realization methods is the major contribution in this research.

Alternatively, a nonlinear model estimation approach, developed in this research, can directly result in a realizable model with a desired model structure from the acceleration data. In this approach, a second order model form or other desired model form is selected in either the time domain or the frequency domain, and a cost function is defined in the frequency domain. Nonlinear optimization algorithms are employed to find the unknown parameters in the model. The advantage of this method is that all unknown parameters



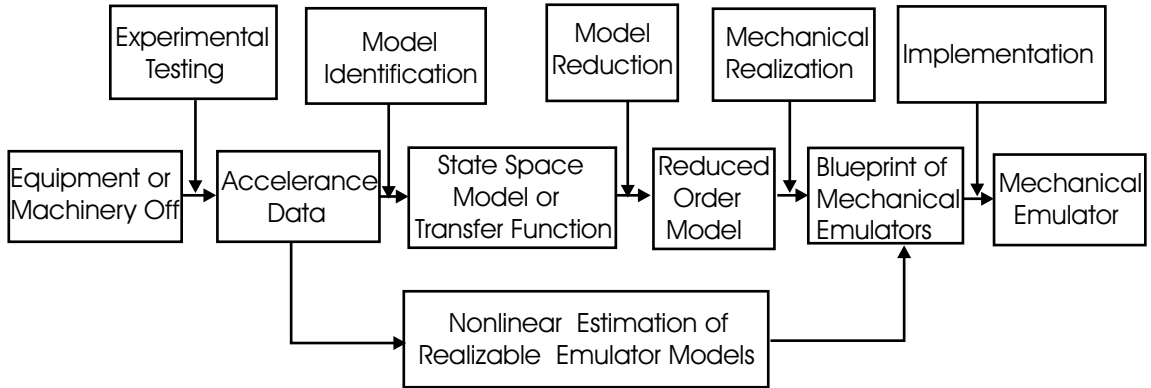


Figure 1.4: The Passive Emulator Design Approach

in the realizable model have direct relations to the mechanical elements in the mechanical emulator.

Once a realizable mechanical emulator model has been obtained, an emulator can be implemented using masses, dampers and springs. Experimental testing is used to verify that the realized mechanical emulator can reproduce the input/output dynamics of the actual passive machinery and to tune the emulator as needed.

After a passive emulator has been designed and implemented, an emulating shaker is used to reproduce the acceleration at the attachment points produced by machinery operation. The active emulator design approach mainly involves three aspects, as shown in Figure 1.5. For the first aspect, the foundation acceleration data of active machinery should be collected. For the second, the transfer acceleration between the location where the acceleration is measured and the location at which the emulating shaker mounts must be obtained. Finally, a feedforward/feedback controller should be designed and implemented for the emulating shaker.

When the active machinery has reached stable running condition, the acceleration data at its foundation are recorded by a dynamic signal analyzer. Meanwhile, after the mounting location of the emulating shaker is selected, the transfer acceleration between the foundation attachment points and the shaker mounting location can be experimentally determined or theoretically obtained from the passive emulator model. After that, the

desired force profile can be calculated from the machinery foundation acceleration data and the transfer acceleration of the passive emulator. To ensure that the emulating shaker follows the desired force profile, a feedforward/feedback controller is developed to obtain the voltage to be applied to the emulating shaker. Finally, experimental testing is carried out to evaluate the active emulator's performance under the same operating conditions as the active machinery.

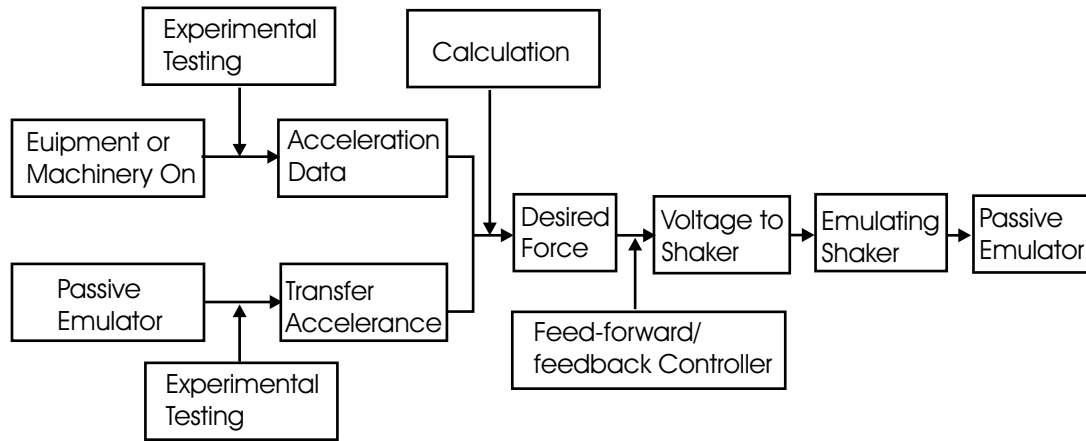


Figure 1.5: The Active Emulator Design Approach

## 1.4 Organization of the Dissertation

Chapter 2 provides background and a survey of the research work related to mechanical emulator design. It formalizes several concepts important to mechanical realization and includes a discussion of modeling vibratory mechanical systems. Second order models, state space models, transfer functions and their relationship are discussed. Many techniques in model identification and reduction for mechanical vibrational systems are reviewed. Prior work on mechanical realization including techniques in the frequency domain and in the time domain are discussed in detail. Finally, mechanical emulators designed and implemented by Navy contractors are discussed and analyzed. At the end of this chapter, a detailed comparison is carried out between the capabilities of the current realization

methods and Navy contractors emulators, and the results of this dissertation work.

A theory of transformations relating realizations is developed in Chapter 3. The structure of realizable second order models is analyzed, resulting in necessary realization conditions for mass, damping and stiffness matrices. Since a vibratory mechanical system can be described by an infinite number of second order models related via congruent coordinate transformations, those transformations are used to convert the initial second order model to realizable forms. Parameterization of the orthogonal component is discussed, including aligning the input and output influence vectors (or matrices) and converting the damping and stiffness matrices to desired forms. Finally, it is shown how to obtain the final mass matrix.

Two mechanical realization techniques are developed in Chapter 4. The first technique, which is applicable for a given second order model satisfying necessary realization conditions discussed in Chapter 3, involves searching for the realizable second order models in the parameterized space of realization transformations. Several numerical examples are provided to show the effectiveness of this technique. The second technique, direct estimation of realizable model, is developed to obtain a realizable model directly from experimental data. The estimation procedure including selection of a candidate model, choice of cost function and nonlinear search, is presented. Estimation examples with machinery experimental data are used to demonstrate the estimation process and effectiveness of this technique.

A mechanical emulator design methodology is developed in Chapter 5, including both passive emulation and active emulation. In the passive mechanical emulator design, SISO mechanical systems can be directly obtained from the realizable second order models by interpreting them as networks of mechanical elements. A model configuration in which oscillators do not have direct stiffness couplings, but damping couplings, is designed in Section 5.1 for passive mechanical emulators undergoing motions in multiple coordinate directions. Matching requirements of mass and moment of inertia between the passive machinery and its passive mechanical emulator are presented. Unknown parameters as-

sociated with mechanical elements can be obtained using the techniques from Chapter 4. The specified amount of damping is achieved by free-layer and constrained-layer damping treatments.

To reproduce the motions at the foundation attachment points due to machinery operation, the passive emulators are modified into active ones by incorporating active elements. In this research, a shaker under closed loop control is used. In Section 5.2, three important issues involving design of active emulators are addressed, including selection of the the emulating shaker, selection of its mounting location and design of a feedforward/feedback controller.

In Chapter 6, experimental passive and active emulators are presented. A machinery test bed and accelerance data acquisition are discussed. A realizable mechanical emulator model is identified with the measured driving-point accelerance of the machinery test bed and a passive mechanical emulator is fabricated. A feedforward/feedback controller is designed to control the emulating shaker to reproduce the foundation acceleration due to the effect of machinery operation. Experimental results for both passive and active emulation show good agreement of the input-output dynamic properties at the foundation attachment points between machinery and its passive/active mechanical emulator.

The contributions of this dissertation are summarized in Chapter 7. Directions for future research motivated by this work are also discussed.

## Chapter 2

# Background and Related Work

If I have seen further, it is because I have stood on the shoulders of giants.

Issac Newton (1642-1727)

Equipment and machinery is mounted to the ship structures at attachment points, as depicted in Figure 2.1. The number of these attachment points typically ranges from one to four. If the distances between these attachment points are small compared to the dimension of the ship structures, they may be treated as a single effective attachment point in a dynamic analysis.

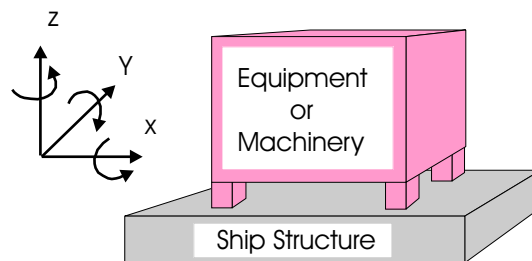


Figure 2.1: Attachment Points, Coordinate Directions of Equipment and Machinery

Machinery can undergo motions in six coordinate directions, which include three translational coordinates,  $x$ ,  $y$  and  $z$ , and three rotational coordinates,  $\theta_x$ ,  $\theta_y$  and  $\theta_z$ . At each attachment point, its dynamics can be described by the following equation in the Laplace

domain

$$a(s) = A(s)F(s) \tag{2.1}$$

where

$a(s)$  is the vector of acceleration  $s^2 \begin{bmatrix} x(s) & y(s) & z(s) & \theta_x(s) & \theta_y(s) & \theta_z(s) \end{bmatrix}^T$

$A(s)$  is the  $6 \times 6$  accelerance matrix

$F(s)$  is the vector of force  $\begin{bmatrix} F_x(s) & F_y(s) & F_z(s) & M_x(s) & M_y(s) & M_z(s) \end{bmatrix}^T$

Depending on the number of inputs and outputs, mechanical realization can be categorized as single-input, single-output (SISO) and multi-input, multi-output (MIMO). For example, when one is only interested in testing vibration in the vertical direction  $z$  and machinery has a single attachment point, this is a SISO mechanical realization problem. When one needs to test vibrations in multiple directions or with several attachment points, it requires design of a MIMO mechanical emulator.

## 2.1 Frequency Ranges of Interest in Various Coordinate Directions

If all fixed-base frequencies of machinery modes in a particular coordinate direction are higher than the upper limit of the frequency range of interest, the machinery can be emulated as a rigid body in this coordinate direction. Under this circumstance, only the mass and moment of inertia of the machinery in this coordinate direction need be matched by the mechanical emulator.

There are two different types of rigid-body mode matchings - translational and rotational. For the first type, according to Newton's second law, machinery and its mechanical emulator must possess the same apparent total mass in the coordinate direction. When there is no coupling between the translational and rotational coordinates, the apparent total mass is equal to the total mass. Otherwise, the apparent mass in the  $x$  or  $y$  coordinate direction is the combined effect of the total mass and moment of inertia. In the

second type, machinery and its mechanical emulator should possess the same moment of inertia with respect to the attachment points in the corresponding rotational coordinate directions, respectively.

Dynamic matching which concerns matching of corresponding modes between machinery and its mechanical emulator can be carried out in several different model representations. These model types are described below.

## 2.2 Modeling Vibratory Mechanical Systems

Vibratory mechanical systems can be modeled either by analytical approaches, for instance, Newton's second law, Lagrange's equation, or by numerical approaches such as finite element analysis, or by experimental tests such as sinusoidal sweeps and impulse responses. Whatever approach is used, modeling a vibratory mechanical system results in three types of model representations: second order model, state space model and transfer function. The first two are in the time domain and the last one is in the frequency domain. Each is described below.

### 1. Second Order Model

By choosing an  $n \times 1$  vector  $q$  as the set of coordinates, an  $m \times 1$  vector  $u$  as the input vector which is often an external force vector, and a  $p \times 1$  vector  $y$  as the output vector which can be displacement, velocity, acceleration or even their combination, a vibration system can be expressed as

$$\begin{aligned} M\ddot{q} + C\dot{q} + Kq &= Fu \\ y &= H_dq + H_v\dot{q} + H_a\ddot{q} \end{aligned} \tag{2.2}$$

Here, the matrix  $M$  is the  $n \times n$  mass matrix, which usually is a positive definite and symmetric matrix. In the case of lumped masses,  $M$  is a diagonal matrix. The matrix  $C$  is the  $n \times n$  damping matrix, which is a positive (semi-) definite and symmetric

matrix. In the case of proportional damping,  $C = \alpha M + \beta K$ , where  $\alpha$  and  $\beta$  are constants [8]. It should be noted that all damping from the  $\alpha M$  term corresponds to skyhook dashpots which are attached to a fixed ground - a situation which is impossible to achieve in machinery emulation. In practice, it is difficult to model damping mechanisms. For structures with light damping, a proportional damping assumption may be used [9]. The matrix  $K$  is the  $n \times n$  stiffness matrix, which is a positive (semi-) definite and symmetric matrix.  $F$  is the  $n \times m$  input influence vector (or matrix), which is determined by the location of excitations.  $H_d$ ,  $H_v$  and  $H_a$  are the output influence vectors (or matrices) of displacement, velocity and acceleration, respectively. These matrices depend on what outputs are measured. In most circumstances, acceleration signals at different locations are picked up by accelerometers. In this case,  $H_d = H_v = 0$ , while  $H_a \neq 0$ . Throughout this research, only acceleration outputs are considered.

## 2. State Space Model

By choosing the state variable vector as  $x = \begin{bmatrix} q & \dot{q} \end{bmatrix}^T$ , the second order model (2.2) can be transformed to a state space model, which is widely used in the control field

$$\begin{aligned} \dot{x} &= Ax + Bu \\ y &= Gx + Du \end{aligned} \tag{2.3}$$

where the matrix  $A$  is the  $2n \times 2n$  state matrix,  $A = \begin{bmatrix} 0 & I \\ -M^{-1}K & -M^{-1}C \end{bmatrix}$ . The matrix  $B$  is the  $2n \times m$  input matrix,  $B = \begin{bmatrix} 0 & M^{-1}F \end{bmatrix}^T$ . The matrix  $G$  is the  $p \times 2n$  output matrix,  $G = \begin{bmatrix} H_d & 0 \end{bmatrix} + \begin{bmatrix} 0 & H_v \end{bmatrix} + H_a \begin{bmatrix} M^{-1}K & M^{-1}C \end{bmatrix}$ . The matrix  $D$  is the  $p \times m$  direct transmission matrix,  $D = H_a M^{-1}F$ .

The state space representation which is not unique, depends on the choice of state



variables. The different representations are related to each other by coordinate transformations. By properly choosing coordinate transformations, realizations with special properties can be obtained. In the structural dynamics area, modal realization, McMillan normal form realization [10] and balanced realization [11] are widely used, which can be found in the appendix A.

### 3. Transfer Function

A transfer function is the ratio of the Laplace transformation of the outputs to the Laplace transformation of the inputs with zero initial conditions [12]. For single-input single-output systems, the transfer function can be expressed as

$$H(s) = \frac{Y(s)}{U(s)} = \frac{\sum_{i=0}^{i=m} b_i s^i}{\sum_{j=0}^{j=n} a_j s^j} = c_0 \frac{\prod_{i=1}^{i=m} (s - z_i)}{\prod_{j=1}^{j=n} (s - p_j)} \quad (2.4)$$

where  $Y(s)$  and  $U(s)$  are the Laplace transformations of the scalar output and scalar input, respectively. The quantity  $s$  is a complex variable. The coefficients  $a_i$ 's are determined by the intrinsic properties of the mechanical systems. The coefficients  $b_i$ 's are determined by both the intrinsic properties of the systems and choices of inputs and outputs.  $c_0$  is a coefficient.  $z_i$ 's and  $p_j$ 's are zeros and poles, respectively. For multi-input and multi-output systems, the transfer function matrix should be used as

$$Y(s) = H(s)U(s) \quad (2.5)$$

where  $Y(s)$  is an  $p \times 1$  vector of inputs,  $U(s)$  is a  $m \times 1$  vector of outputs and  $H(s)$  is a  $p \times m$  transfer function matrix.

Usually, the transfer function data can be obtained by experimental testing with a sinusoidal sweep in a frequency range.

Several conventional notations are reviewed here, which are used later in the text.

### 1. Dynamic Stiffness

The dynamic stiffness is the ratio of the Laplace transformation of the input force to the Laplace transformation of the output displacement.

### 2. Mechanical Impedance

The mechanical impedance is the ratio of the Laplace transformation of the input force to the Laplace transformation of the output velocity.

### 3. Dynamic Mass

The dynamic mass is the ratio of the Laplace transformation of the input force to the Laplace transformation of the output acceleration.

### 4. Driving point and Transfer Relationships

If the input and output are measured at the same attachment point and in the same coordinate direction, the relationship is called a driving-point relationship. Otherwise, it is called a transfer relationship.

The above model representations are related to each other. The conversion from a second order model to a state space model has been discussed earlier. The inverse transformation is necessary in mechanical realization if a state space model is identified from model identification. For this purpose, several methods are available [13] [14] [10] [15] [16] [17] and [18].

By Laplace transformation of (2.2) and (2.3), and after simple manipulations, the relationship between the second order model, state space model and transfer function can be found as

$$Y(s) = (H_d + H_v s + H_a s^2)(Ms^2 + Gs + K)^{-1}FU(s) = [C(sI - A)^{-1}B + D]U(s) \quad (2.6)$$

The second order model representation and state space model representation of a system are not unique since the internal coordinates can be chosen arbitrarily. Different

representations are related to each other through coordinate transformations. The transfer function of a system is unique, however, and is invariant with respect to the choice of coordinates.

Since the mechanical emulator design starts with the identification of a model of one of these three types from acceleration experimental data, model identification and reduction are briefly discussed below.

### 2.2.1 Model Identification and Reduction

Many mature time-domain and frequency-domain techniques are available for the purpose of model identification. In most cases, the identified parameters in the specified model do not have explicit physical meaning. In mechanical emulator design, however, the identified parameters must have an explicit relationship to the mechanical elements in the emulator model. Therefore, new identification techniques are needed so that the unknown parameters can be directly related to mechanical elements. For this purpose, several widely used methods of model identification in the time domain and frequency domain are reviewed here. Since the order of the identified model may be high, model reduction may be necessary. Model reduction techniques are briefly reviewed at the end of this subsection.

In the time domain, a state space model is widely employed for model identification. Many identification techniques are available, such as the Eigensystem Realization Algorithms (ERA) and ERA with Data Correlations (ERA/DC) [19] [20] [21] [22], the Q-Markov cover algorithm [23] [24] [25], Numerical Algorithms for Subspace State Space System Identification (N4SID) [26] [27]. All these methods attempt to find the matrices  $A$ ,  $B$ ,  $C$  and  $D$  in the state space model (2.3). For example, the well known ERA obtains the matrices in the state space model through minimizing the error between the Hankel matrix and the experimental data. The Hankel matrix is formed through the shifted Markov parameters, which is also known as the discrete-time impulse response functions. Furthermore, the order of state space model is determined by the number of the largest

singular values of the Hankel matrix. In [28], performances of several system identification methods for flexible structures were compared by using an FEM two-input, two-output model of a structure.

The major drawback of most time domain model identification techniques is that a large error in the vicinity of anti-resonances may exist although a high accuracy curve matching in the time domain can be achieved [29]. Another drawback of those methods for mechanical emulator realization is that the unknown parameters in the state space do not directly relate to physical elements.

The identification of frequency response functions (FRFs) in the modal analysis community falls in the category of the frequency domain identification. Because an enormous number of methods are available, only a few are reviewed here. The circle-fitting method expresses the FRF as a weighted summation of terms of modes and identifies the modal parameters through a least squares algorithm at each mode. The frequency response curve in the Nyquist plot is a circle at the vicinity of its resonance [30]. The Ewins-Gleeson method, which is valid for lightly damped structures, also expresses the FRF as a weighted summation of terms of modes. Its resonance frequencies, however, are determined by the peaks in the FRF data and its  $N$  weighting coefficients are solved with data at  $N$  frequency points [31]. The rational fraction polynomial method is one of the most widely used frequency domain methods. This method formulates the error between the analytical frequency response function and experimental data as a set of linear equations with unknown coefficients of the numerator and denominator in the rational fraction FRF. Subsequently, a least squares procedure is adopted to obtain the unknown coefficients [32].

All frequency domain model identification methods discussed above did not consider noise. Since noise ubiquitously exists in the input and output measurement, however, the method of estimator for linear systems (EliS) can be applied to identify a transfer function [33]. This method formulates the transfer function identification as a nonlinear weighted least squares problem. The weighting factors are chosen as reciprocals of variances of the errors at frequency points. It is solved by using numerical methods for solving nonlinear

least squares problems, such as Newton-Gauss method and Levenberg-Marquardt method.

If the order of the identified model is high, model reduction has to be used to obtain a reduced order model. Many model reduction techniques are available in both the finite element analysis and control communities. Several popularly used methods are reviewed here. Guyan's model reduction [34] is based on the viewpoint of static structural analysis. Its basic idea is to eliminate the subset of coordinates, at which no forces are applied. The set of coordinates in the reduced model is a subset of the initial coordinates. The generalized dynamic reduction uses a subset of eigenvectors of the full order model to form a transformation between the full order and reduced order models [35]. Modal reduction is a conceptually simple reduction method, which omits the coordinates in the modal realization (A.1) corresponding to: (1) high decay rates, or (2) high resonance frequencies, or (3) large magnitudes of poles [11].

When the modal density of equipment and machinery is high, however, balanced reduction through balanced realization (A.3) by Moore has good performance for it minimizes the error between frequency response functions of the full order model and reduced order model, by removing the most uncontrollable and unobservable coordinates [36]. It has a drawback, however, that the reduced order model may not preserve passivity. A passive system can only absorb or dissipate energy, but not generate energy. To overcome this drawback, the passivity preserving balanced reduction by Chen and Wen [37] can be used. This method is more effective than modal reduction to obtain reduced-order models of equipment and machinery from the viewpoints of the frequency, time and shock spectra domains [38]. Simplified representations of complicated vibratory subsystems with a high modal density such as equipment were obtained through the Dirichlet to Neumann or DtN map by Barbone, et al. [39] [40] [41] [42].

The time-domain and frequency-domain models from identification and reduction may not be in a form corresponding to a mechanical system. Therefore, it is necessary to apply mechanical realization techniques to convert these models to a form directly realizable by mechanical elements. The problem of mechanical realization can be defined in terms of

models, which must be interpreted as networks of mechanical elements or be converted to a form in which such an interpretation can be made. In the time domain, mechanical elements including masses, dashpots and springs may be directly obtained from the mass, damping and stiffness matrices in a given second order model, which has already been transformed to realizable form. Otherwise, this model has to be converted to such a form. In the frequency domain, a given transfer function has to be decomposed into a form from which mechanical elements can be obtained.

## **2.3 Prior Work on Mechanical Realization**

A variety of techniques have been developed which specifically address the identification of, or conversion to, a model in realizable form. In the frequency domain, the inverse eigenvalue/vibration approach and methods from electric network synthesis are available. In the time domain, serial realizations and parallel realizations may be obtained through special coordinate transformations. In addition, Navy contractors have designed and fabricated several mechanical emulators for commercial-off-the-shelf (COTS) cabinets, pumps and heat exchangers. These techniques are described below.

### **2.3.1 Frequency Domain Realization**

In the frequency domain, mechanical realization can be formulated as a problem of how to determine the distribution of mass, damping and stiffness from a given transfer function or from a set of poles and zeros which correspond to resonance frequencies and anti-resonance frequencies, respectively. There have been two bodies of work developed to solve this problem. The first is the inverse eigenvalue/vibration approach developed by researchers in mathematics and mechanics. The second approach is based on electrical network synthesis theory.

## Inverse Eigenvalue/Vibration Approach

The inverse eigenvalue/vibration problem concerns how to determine the mass, damping and stiffness matrices in the second order model (2.2) so that the realized system possesses the required resonance frequencies. It contrasts with the direct problem which studies the relationship between the input and output given a known distribution of mass, damping and stiffness. Prior work on the inverse vibration problem is limited to isospectral mechanical systems, which possess the same set of resonance frequencies, but have different mass, damping and stiffness matrices. There are several survey articles available, for example, [43] [44] [45] [46] [47].

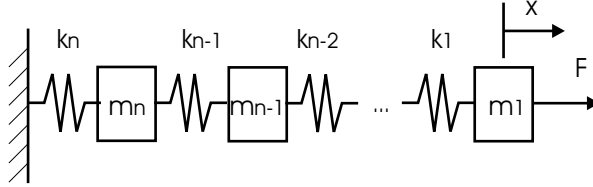


Figure 2.2: Serial Model

A widely studied inverse vibration problem is to determine the masses and springs in the serial model illustrated in Figure 2.2 with two given sets of real scalars  $\{\lambda_1, \lambda_2, \dots, \lambda_n\}$  and  $\{\mu_1, \mu_2, \dots, \mu_{n-1}\}$ [45]. The set  $\{\lambda_1, \lambda_2, \dots, \lambda_n\}$  are eigenvalues of the matrix  $A = M^{-1/2}KM^{-1/2}$ , where  $M$  and  $K$  are mass and stiffness matrices to be determined. The set  $\{\mu_1, \mu_2, \dots, \mu_{n-1}\}$  consists of eigenvalues of the matrix  $\hat{A}$ , which is obtained by deleting the last row and last column of  $A$ . The solution to this inverse vibration problem exists only if the given two sets satisfy the following interlacing conditions

$$0 \leq \lambda_1 < \mu_1 < \lambda_2 < \mu_2 < \dots < \mu_{n-1} < \lambda_n \quad (2.7)$$

When damping is incorporated in the serial model, however, the elements in the two given sets are usually complex numbers and do not satisfy the interlacing conditions. A method was presented to solve the inverse vibration problem of a serial model with damping, through the approach of the quadratic matrix pencil  $Q(s) = s^2I + sC + K$ ,

where  $C$  and  $K$  are, respectively, damping and stiffness matrices in [48]. Starting from a known serial model, the method can find serial models with equivalent properties, but there still remains a question of what requirements should be imposed on the sets of  $\lambda_i$  and  $\mu_j$ .

There have been other inverse vibration techniques which can generate more complicated models, for example, [49] [50] [51] [52]. The resulting models from these methods, however, do not have corresponding physical structures. Therefore, the application of the inverse vibration approach is very limited for the purpose of realization of mechanical emulators. In the next subsection, a more powerful realization approach by applying electrical network synthesis is discussed.

### **Electrical Network Synthesis Applied to Mechanical Realization**

As early as the 1930's, Norton designed mechanical systems like loudspeakers in terms of the circuit theory [53] [54]. The monograph *Mechanical Filters in Electronics* by Johnson covered how to apply the equivalence of passive electrical and mechanical elements to the design of high-Q mechanical filters [53]. The electromechanical analogy is widely used today in design and simulation of micro-electro-mechanical systems (MEMS), [55] [56] [57] [58] [59].

There are two types of electromechanical analogy. One type is the mobility analogy by which velocity is analogous to voltage and force to current. In terms of elements, a mass, dashpot and spring correspond to a capacitor, resistor and inductor, respectively. Under this type of analogy, a mechanical system has the same network topology as its equivalent electrical system [53]. Another type of the electromechanical analogy is the impedance analogy in which force is analogous to voltage and velocity to current. In this approach, a mass, dashpot and spring are analogous to an inductor, resistor and capacitor, respectively. Since the impedance analogy is more understandable, this analogy is adopted in the following discussion.

Using the electromechanical analogy, most of results in electrical network synthesis,



which is a well-developed field, can be employed for mechanical realization. Electrical network synthesis is a theory on how to design electrical circuits, such as filters, with desired input-output behaviors. Its history can be found in the review article written by Darlington [54]. Books by Guillemin [60], Valkenburg [61] and Baher [1], are thorough references in this field.

For any passive electrical or mechanical system, which is a stable system without internal energy-generating sources, the driving-point relationship in the frequency domain should satisfy the positive realness requirement first given by Otto Brune in complete form in his doctoral thesis in 1931. A positive-real transfer function  $P(s)$ , where  $s$  is a complex number, is defined as follows:

**Definition 2.1.** [60] *A function  $P(s)$  is termed a positive real function if it satisfies the following two conditions: (1) all coefficients are real; (2) the real part of  $P(s)$  is positive for any complex number  $s$  with a positive real part, i.e.,  $\operatorname{Re}\{P(s)\} \geq 0$  for  $\operatorname{Re}\{s\} \geq 0$ .*

Positive realness is the necessary and sufficient condition for a given driving-point transfer function to be realized by a passive mechanical system. The requirement of the positive realness is equivalent to the passivity requirement. Furthermore, a positive real transfer function has the property that its reciprocal is also a positive real function [1].

Mechanical realization can be carried out by expanding a given positive real transfer function into special forms in which parameters are directly related to physical components. These expansion forms determine the topology of the realized mechanical systems. In the following discussion, realization of mechanical systems without damping, which is analogous to the synthesis of an LC (inductor-capacitor) electrical network, is used to demonstrate realization procedures. Other realizations such as realization of mechanical systems with mass and damping or with damping and stiffness, follow similar procedures. At the end of the following discussion, realization of mechanical systems with mass, damping and stiffness is briefly discussed.

Besides the positive realness requirement, the driving-point accelerance  $A(s)$  of a me-

chanical system without damping should also satisfy  $A(j\omega) + A(-j\omega) = 0$  for all real numbers  $\omega$ , where  $j = \sqrt{-1}$ . Such a driving-point accelerance is a reactance function or Foster function, which implies no energy dissipation in the mechanical system. In general, it can always be expressed in the following form

$$A(s) = c_0 \frac{\prod_{i=1}^n (s^2 + \mu_i^2)}{\prod_{j=0}^n (s^2 + \lambda_j^2)} \quad (2.8)$$

where  $c_0$  is a positive real constant, and  $\mu_i$  ( $i = 1, 2, \dots, n$ ) and  $\lambda_j$  ( $j = 1, 2, \dots, n$ ) are positive real numbers, which satisfy the interlacing conditions  $0 \leq \lambda_0 < \mu_1 < \lambda_1 < \mu_2 < \lambda_2 < \dots < \mu_n < \lambda_n$ . All poles ( $j\lambda_j$  and  $-j\lambda_j$ ) and zeros ( $j\mu_i$  and  $-j\mu_i$ ) alternate on the imaginary axis. This explains why the interlacing conditions (2.7) is required in the inverse vibration approach while building a serial model.

By expanding the accelerance (2.8) into different forms, we have the following canonical realizations, which are defined as those with the minimum number of spring elements between masses.

#### 1. Parallel Model Realization I

The reciprocal of the accelerance (2.8) can be expressed in a *partial fraction expansion* form as follows

$$\frac{1}{A(s)} = m_0 + \frac{k_0}{s^2} + \sum_{j=1}^n \frac{m_j k_j}{m_j s^2 + k_j} \quad (2.9)$$

which corresponds to the mechanical system as illustrated in Figure 2.3. According to the above expansion, the antiresonance frequencies of the driving-point accelerance happen at the fixed-base resonance frequencies of oscillators, given by

$$\omega_j = \sqrt{\frac{k_j}{m_j}} \quad (2.10)$$

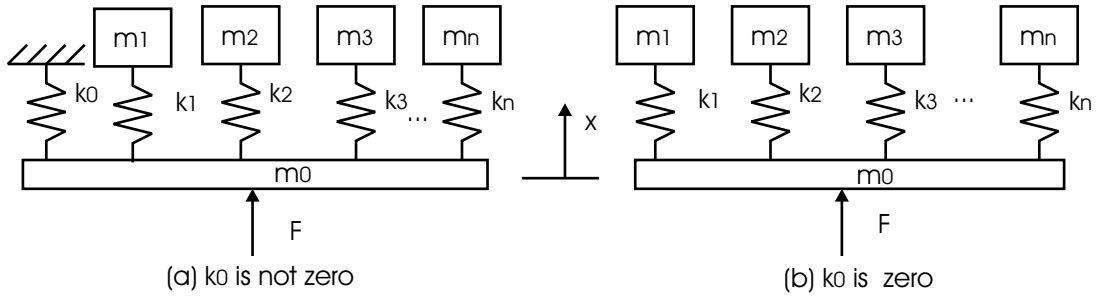


Figure 2.3: Parallel Model Realization I

## 2. Parallel Model Realization II

Another parallel model realization can be achieved by expressing the accelerance (2.8) in a *partial fraction expansion* form as

$$A(s) = \frac{1}{m_0} + \frac{s^2}{k_0} + \sum_{j=1}^{j=n} \frac{s^2}{m_j s^2 + k_j} \quad (2.11)$$

which is shown in Figure 2.4, where the accelerance is defined as

$$A(s) = \frac{\sum_{i=0}^{i=n} s^2 X_i(s)}{F(s)} \quad (2.12)$$

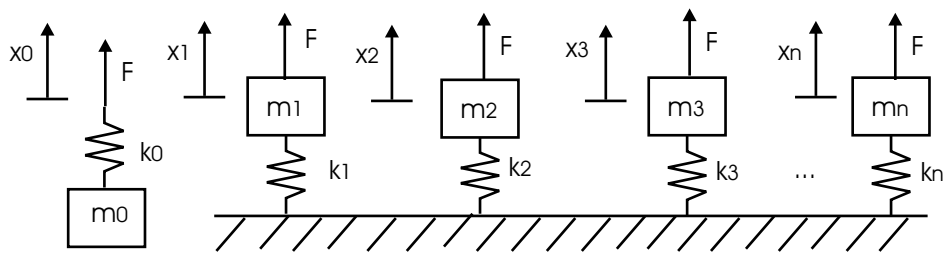


Figure 2.4: Parallel Model Realization II

## 3. Serial Model Realization

A serial model realization of the accelerance (2.8) can be obtained through a *con-*

*tinued fraction expansion* form as follows

$$\frac{1}{A(s)} = m_0 + \frac{1}{\frac{s^2}{k_1} + \frac{1}{m_1 + \frac{1}{\frac{s^2}{k_2} + \dots}}} \quad (2.13)$$

In the above expansion, the last element may be a mass or a spring, as illustrated in Figure 2.5 (a) and (b), respectively. This is decided by the properties of the given accelerance.

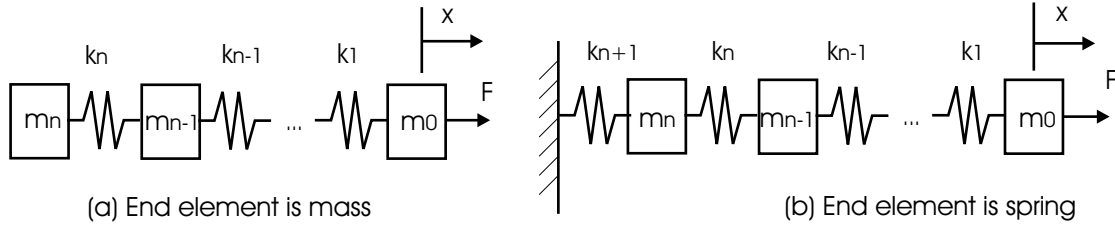


Figure 2.5: Serial Model

#### 4. Parallel/Serial and Serial/Parallel Combination Realization

The accelerance (2.8) can also be expressed in combination of a *partial fraction expansion* form and *continued fraction expansion* form, which result in a parallel/serial realization or serial/parallel realization.

From a practical viewpoint, the realizations of Figures 2.3 (b) and 2.5 (a) are good model forms for mechanical emulators since skyhook springs are prohibited in mechanical emulators and they have the minimum number of springs. These two realizations have the following properties:

##### 1. Total Mass

$$m_t = \sum_{i=0}^{i=n} m_i = \left\{ \frac{1}{A(s)} \right\}_{s=0} \quad (2.14)$$

##### 2. Base Mass

$$m_b = m_0 = \left\{ \frac{1}{A(s)} \right\}_{s=\infty} \quad (2.15)$$

From the above two properties, it can be concluded that the driving-point dynamic mass of a vibratory mechanical system without skyhook elements approaches its base mass at very low frequency and its total mass at very high frequency. In this scenario, according to (2.9), the number of modes is equal to the number of lumped masses in the system. Moreover, since two equivalent mechanical realizations have the same transfer function, they must have the same amount of total mass and base mass.

When damping is incorporated, mechanical realization is analogous to RLC (resistor-inductor-capacitor) network realization. Different from a reactance accelerance, the driving-point accelerance of a damped mechanical system cannot be realized as a parallel or serial model unless it satisfies certain constraints. A parallel model realization can be obtained only when the given accelerance can be expressed as follows

$$\frac{1}{A(s)} = m_0 + \sum_{i=1}^{i=n} \frac{m_i(c_i s + k_i)}{m_i s^2 + c_i s + k_i} \quad (2.16)$$

A serial model realization is achievable only if the given accelerance can be expanded in the following continued fraction expansion

$$\frac{1}{A(s)} = m_0 + \frac{1}{\frac{c_1}{s} + \frac{k_1}{s^2} + \frac{1}{m_1 + \frac{1}{\frac{c_2}{s} + \frac{k_2}{s^2} + \dots}}} \quad (2.17)$$

For mechanical realization of SISO driving-point mechanical systems without damping or with proportional damping, the inverse eigenvalue/vibration approach can give a serial realization and electric network synthesis can conveniently generate both serial realization and parallel realization. However, for a vibratory mechanical system with nonproportional damping, one cannot obtain mechanical realizations with these two approaches except for some special cases. Another limitation of these two approaches is their difficulty in dealing with SISO transfer mechanical systems and MIMO mechanical realization problems. Time

domain realization discussed below, however, can overcome these limitations.

### 2.3.2 Time Domain Realization

In the time domain, a second order model is often used to describe a vibratory mechanical system. If the second order model is in realizable form, the elements of its mass, damping and stiffness matrices are directly related to the mechanical elements of the mechanical system. Otherwise, this model may be converted to realizable form by congruent coordinate transformations. Available methods consider how to convert a given second order model to a serial model realization or to a parallel model realization. These methods are limited to the cases of either no damping or proportional damping.

Before discussing these realization methods, second order models for the realizable parallel and serial realizations of Figure 2.3 (b) and 2.5 (a) are derived below. Denoting the displacement of the  $i'$ th mass from its equilibrium point as  $x_i$ , then the second order models are obtained as follows.

#### Parallel Model Realization

The parallel model can be described by

$$\begin{aligned} M_p \ddot{x} + C_p \dot{x} + K_p x &= e_1 u \\ y &= e_1^T \dot{x} \end{aligned} \tag{2.18}$$

where the subscript  $p$  stands for “parallel” and the matrices are defined as

$$\begin{aligned}
 M_p &= \begin{bmatrix} m_0 & & & & \\ & m_1 & & & \\ & & m_2 & & \\ & & & \ddots & \\ & & & & m_n \end{bmatrix} \\
 C_p &= \beta K_p \\
 K_p &= \begin{bmatrix} \sum_{i=1}^{i=n} k_i & -k_1 & -k_2 & & -k_n \\ -k_1 & k_1 & & & \\ -k_2 & & k_2 & & \\ & & & \ddots & \\ -k_n & & & & k_n \end{bmatrix}
 \end{aligned} \tag{2.19}$$

In the parallel realization, the mass matrix is a diagonal matrix with  $m_0 \geq 0$ ,  $m_i > 0$ ,  $i = 1, 2, \dots, n$  and the stiffness matrix is a border diagonal matrix with  $k_i > 0$ ,  $i = 1, 2, \dots, n$ . If there is no damping, then  $\beta = 0$ .

### Serial Model Realization

The serial model is given by

$$\begin{aligned}
 M_s \ddot{x} + C_s \dot{x} + K_s x &= e_1 u \\
 y &= e_1^T \ddot{x}
 \end{aligned} \tag{2.20}$$

where the subscript  $s$  stands for “serial” and the matrices and vectors are defined as

$$\begin{aligned}
 M_s &= \begin{bmatrix} m_0 & & & & \\ & m_1 & & & \\ & & m_2 & & \\ & & & \ddots & \\ & & & & m_n \end{bmatrix} \\
 C_s &= \beta K_s \\
 K_s &= \begin{bmatrix} k_1 & -k_1 & & & \\ -k_1 & k_1 + k_2 & -k_2 & & \\ & -k_2 & k_2 + k_3 & & \\ & & & \ddots & \ddots \\ & & & & -k_n & k_n \end{bmatrix} \\
 e_1 &= \begin{bmatrix} 1 & 0 & \cdots & 0 \end{bmatrix}^T
 \end{aligned} \tag{2.21}$$

In this realization, the mass matrix is diagonal with  $m_0 \geq 0$ ,  $m_i > 0$ ,  $i = 1, 2, \dots, n$  and the stiffness matrix is tridiagonal with  $k_i > 0$ ,  $i = 1, 2, \dots, n$ . If there is no damping, then  $\beta = 0$ .

It is well known that any undamped or proportionally damped mechanical system can be converted to serial and parallel realizations in the sense of the same driving-point relationship. For the SISO mechanical system, the conversion from a general mechanical system without damping or with proportional damping to a serial model was studied through a coordinate transformation by Falk [62]. The algorithm for finding the coordinate transformation was also presented there. It was used to obtain equivalent serial models from mechanical systems with complicated spring couplings in [63]. The conversion from a general mechanical model to a parallel model was obtained through the normal mode theory by O’Hara and Cunniff [64]. O’Hara and Cunniff’s result was generalized to a



mechanical system undergoing three-dimensional vibration by Pierce [65].

To obtain a serial model realization, it is necessary to find a transformation which can convert any symmetric stiffness matrix to a tridiagonal stiffness matrix. To this end, there are several methods available in matrix computation, including Givens' method by Givens' rotations, Householder's method by Householder's reflections and Lanczos' method by a recursive process [66] [67]. These tridiagonalization methods have been widely used to calculate eigenvalues of symmetric matrices. No result with these methods, however, is available for the purpose of mechanical realization except [68], where the Householder's method was used to obtain a tridiagonal stiffness matrix satisfying the required resonance frequencies.

In order to obtain a parallel model realization, however, a transformation which can change any symmetric stiffness matrix to a border diagonal stiffness matrix, is required. A method in [67] can perform this task.

The advantage of time domain realization techniques is that mechanical elements can be directly obtained from the realizable second order model converted from the given second order model via special congruent coordinate transformations. Algorithms of these transformations are available in matrix computation. Another advantage of time domain realization techniques is that they may be used to deal with SISO transfer mechanical realization and MIMO mechanical realization problems. The major limitation of these techniques, however, is that they cannot handle realization of nonproportionally damped vibratory mechanical systems because the available coordinate transformations cannot convert the damping and stiffness matrices to the desired realizable forms simultaneously.

### **2.3.3 Navy Contractor Emulators**

The design and fabrication of a variety of mechanical emulators was carried out by the Navy laboratories and contractors. Exact miniaturization and modal reduction were two approaches adopted by them [38]. Exact miniaturization was used to obtain scaled mechanical models for commercial-off-the-shelf (COTS) cabinets, as shown in Figure 2.6 [69].

Lumped masses or bags of beads were attached on the shelves to emulate the mass effect of equipment and damping.

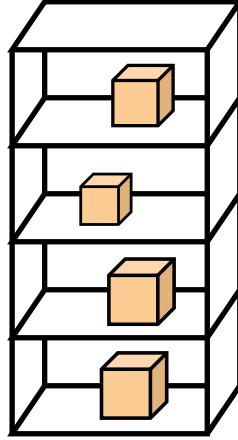


Figure 2.6: Mechanical Emulator for COTS Cabinets

Modal reduction was also used to design emulators of equipment cabinets [69]. These emulators were designed to match the scaled mass and the lowest four fundamental fixed-base frequencies corresponding to bending, torsional and axial deflection. The damping within the emulators was obtained by enclosing the head of the emulator in beads made of damping materials.

Additional emulators were built to model components such as heat exchangers [70]. In this design case, the mechanical emulator was designed to match the scaled mass, the center of mass and rotary inertia of the heat exchanger. Damping was matched by filling the hollow components and the surrounding container with granular damping materials.

Some theoretical and experimental results on passive and active mechanical emulation were reported in Deshpande's master thesis [71]. A passive mechanical emulator was designed for a scaled machinery test bed comprised of modular components. Although damping was considered in the design, the polymeric damping treatments used had to be iteratively modified through experiment to achieve the desired level. For active emulation, the feasibility of using a shaker to reproduce the effect of active machinery was tested on the scaled machinery test bed. A PD feedback controller was used to control the shaker

to generate the desired motion at the attachment point.

## 2.4 Summary

Prior work on mechanical realization with second order models mainly focused on undamped or proportionally damped vibratory mechanical systems due to the difficulty in dealing with nonproportional damping. Both frequency domain and time domain realization techniques can be used to obtain two special realization forms, that is, parallel and serial model realizations for a SISO driving-point accelerance. No techniques are available, however, for solving more complicated realization problems such as SISO transfer accelerances or MIMO accelerances. Although modal decoupling can result in a realization in which all oscillators are attached to a fixed base, this kind of realization does not work for mechanical emulator design since skyhook elements are prohibited.

Furthermore, all currently available realization techniques cannot deal with nonproportional damping without approximation. As demonstrated with an example in Appendix B, however, the approximation of nonproportional damping by proportional damping can introduce significant errors if there is strong damping coupling between modes associated with oscillators. Therefore, to obtain high fidelity realizable second order models, it is important to incorporate nonproportional damping.

To overcome disadvantages of current realization methods, this dissertation research develops a general and systematic realization theory for both passive and active mechanical emulator design with consideration of arbitrary viscous damping in design and implementation. A comparison between the design capabilities of existing methods and the goals of this research is carried out in Table 2.1. This research considers the realization of mechanical systems with multiple attachment points and multiple coordinate directions which can be uncoupled or coupled. In theory, an infinite number of modes can be dealt with, but in practice, the number of important modes is on the order of ten. Transformations for realizing SISO and MIMO mechanical systems are discussed in Chapter 3. Two

numerical methods for obtaining realizable models are developed in Chapter 4. A design methodology for passive and active emulator design is developed in Chapter 5 and experimental emulation is carried out in Chapter 6. Arbitrary viscous and structural damping are considered in the design and implementation of mechanical emulators.

Table 2.1: Design Capabilities of Existing Methods versus this Research

Capability	FDR in Section 2.3.1	TDR in Section 2.3.2	Work in [69] [70]	Work in [71]	This Research
Number of Attachment Points	1	1	1	1	Multiple
Number of coordinate Directions	1	1 or multiple	4 (uncoupled)	1	Multiple (coupled or uncoupled)
Number of Modes	theory = $\infty$	Theory = $\infty$	4	Theory= $\infty$ ; Practice=up to 10	Theory= $\infty$ ; Practice=up to 10
Systematic Passive Emulation Theory	N/A	N/A	No	SISO	SISO and MIMO
Design with Damping	No or proportional damping	No or proportional damping	No	Viscous damping	Viscous and structural damping
Semi-analytical Damping Treatment	N/A	N/A	No	Empirical	Based on relations between loss factor and number of damping layers.
Active Emulation	N/A	N/A	No	Tested feasibility on machinery test bed.	Developed systematic design method using a feed-forward/feedback controller.

FDR: Frequency Domain Realization

TDR: Time Domain Realization

## Chapter 3

# Theory of Transformations Relating Realizations

A journey of a thousand miles begins with a single step.

Lao Zi, Ancient Chinese Philosopher

A vibratory mechanical system in general can be described by an infinite number of second order models. These models are related to each other by congruent coordinate transformations. The theory to be developed here is used to find the transformations, each of which corresponds to a specific second order model which can be directly interpreted as a network of mechanical elements. The structure and properties of realizable second order models will be analyzed, in particular, for vibratory mechanical systems without skyhook elements since no skyhook elements are permitted in mechanical emulators.

To overcome the difficulty in directly finding a transformation corresponding to a realization, a technique of decomposing the transformation into a product of three components is adopted. The first component is the inverse of the square root of the initial mass matrix, which is used to mass normalize the given second order model. The second component, which is an orthogonal matrix, is used to align the input and output influence vectors

(or matrices) and to convert the damping and stiffness matrices to desired forms. For undamped or proportionally damped mechanical systems, parallel model and serial model realizations can always be obtained by proper selection of this orthogonal component. For nonproportionally damped mechanical systems, however, this component has to be parameterized by a finite set of free parameters. Finally, the last component is the square root of the final mass matrix which is obtained from the null space vector of the damping or stiffness matrix.

### **3.1 Structure of Realizable Second Order Models**

Mechanically realizable mass, damping and stiffness matrices possess special properties. Moreover, input and output influence vectors (or matrices) also should have special forms for realizable second order models. These two issues are discussed in detail below.

#### **3.1.1 Mechanically Realizable Mass, Damping and Stiffness Matrices**

Several assumptions have been made in this research. Since skyhook springs and dampers cannot be implemented in machinery emulation, all models discussed below preclude them. Another assumption in this research is that each mass in the system is connected to at least one mass by at least one spring or one spring and dashpot, that is, there are no isolated masses in the mechanical emulator design. Viscous damping is assumed in the second order models since it can be explicitly represented. Structural damping will also be used when it is necessary to model continuous elements with Euler-Bernoulli's beam model, which is covered in Chapter 5.

A stiffness or damping matrix realizable by mechanical elements must satisfy several properties. Since these requirements are the same for both types of matrices, a realizable stiffness matrix is used to demonstrate them. The simple mechanical system of Figure 3.1 is used here to illustrate these properties. The mass and stiffness matrices are expressed

as follows

$$M = \begin{bmatrix} m_0 & & & \\ & m_1 & & \\ & & m_2 & \\ & & & m_3 \end{bmatrix}$$

$$K = \begin{bmatrix} k_1 + k_2 + k_4 & -k_1 & -k_2 & -k_4 \\ -k_1 & k_1 + k_3 & 0 & -k_3 \\ -k_2 & 0 & k_2 & 0 \\ -k_4 & -k_3 & 0 & k_3 + k_4 \end{bmatrix} \quad (3.1)$$

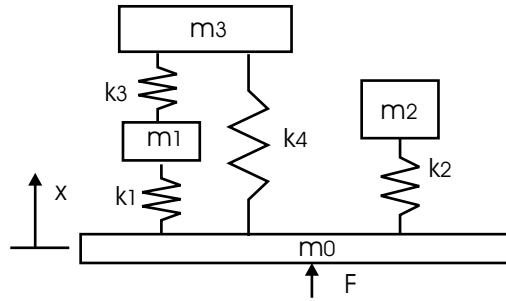


Figure 3.1: A Simple Mechanical Model

The stiffness matrix can be decomposed in the following form [72]

$$K = C_K K_D C_K^T \quad (3.2)$$

where the connectivity matrix is  $C_K = \begin{bmatrix} 1 & 1 & 1 & 0 & 1 \\ 1 & -1 & 0 & 1 & 0 \\ 1 & 0 & -1 & 0 & 0 \\ 1 & 0 & 0 & -1 & -1 \end{bmatrix}$  and the nonnegative



diagonal matrix is  $K_D =$  
$$\begin{bmatrix} 0 & & & & \\ & k_1 & & & \\ & & k_2 & & \\ & & & k_3 & \\ & & & & k_4 \end{bmatrix}.$$

The connectivity matrix  $C_K$  shows how all masses are connected by springs. The first column of  $C_K$  represents the rigid body mode of the system in Figure 3.1, corresponding to the zero element of  $K_D$ . The other columns of  $C_K$  indicate connections between pairs of masses. For example, the third column represents the connection between  $m_0$  and  $m_2$  by stiffness  $k_2$  in  $K_D$ . For a mechanical system with  $n$  masses and  $n_k$  springs,  $C_K$  is an  $n \times (n_k + 1)$  matrix and  $K_D$  is an  $(n_k + 1) \times (n_k + 1)$  diagonal matrix.

Similarly, a mechanically realizable damping matrix  $C$  can also be decomposed as  $C = C_C C_D C_C^T$ , where  $C_C$  is a connectivity matrix and  $C_D$  is a diagonal matrix with nonnegative diagonal elements. It should be noted that  $C_C$  is not necessarily equal to  $C_K$ . If the damping matrix is proportional to the stiffness matrix, however, they have the same connectivity matrix, i.e.,  $C_K = C_C$ . It should be noted that in general, a proportional damping matrix  $C$  can be expressed as  $C = \alpha M + \beta K$ , where  $\alpha$  and  $\beta$  are two constants.

For the mechanical emulator design, however,  $\alpha$  has to be zero since the term  $\alpha M$  leads to skyhook dampers which are prohibited. Therefore, the damping and stiffness matrices must share the same null space vector  $\begin{bmatrix} 1 & 1 & \dots & 1 \end{bmatrix}^T$  corresponding to a resonance frequency of zero, that is,  $null(C_0) = null(K_0)$ . At this frequency, all masses undergo the same motion and the whole structure moves like a rigid body.

It can be summarized that the mechanically realizable mass, damping and stiffness matrices must satisfy the following realization conditions:

$$M = \text{diag}\left(\begin{bmatrix} m_0 & m_1 & \dots & m_n \end{bmatrix}\right), m_i > 0$$

$$C = C^T, C_{ii} > 0, C_{ij} \leq 0, C \begin{bmatrix} 1 & 1 & \dots & 1 \end{bmatrix}^T = 0$$

$$K = K^T, K_{ii} > 0, K_{ij} \leq 0, K \begin{bmatrix} 1 & 1 & \dots & 1 \end{bmatrix}^T = 0 \quad (3.3)$$

where  $i, j = 0, 1, 2, \dots, n$  and  $i \neq j$ .

The most important task in mechanical realization is to find techniques to convert mass, damping and stiffness matrices obtained from experimental input-output data to a form satisfying the realization conditions (3.3).

### 3.1.2 Desired Input and Output Influence Vectors or Matrices

As discussed in Chapter 2, mechanical realization can be categorized as single-input, single-output (SISO) and multi-input, multi-output (MIMO). Depending on where the excitation force is applied and the output acceleration is measured, SISO systems can be further classified as driving-point realizations and transfer realizations. For MIMO systems, a third category is added for those realizations involving both driving-point and transfer accelerances. The desired input and output influence vectors or matrices are discussed below.

#### 1. SISO Mechanical Realizations

In a driving-point realization, the acceleration and force are measured at the same attachment point and in the same coordinate direction. A SISO transfer realization involves an acceleration and force measured at different attachment points or in different coordinate directions.

Without loss of generality, it is assumed that for the driving-point case, the input force is excited and the output acceleration is measured at the first coordinate. Thus, the input and output influence vectors have the following relationship

$$F_f = H_f^T = e_1 \quad (3.4)$$

where  $e_1$  is an element of the standard basis for  $R^n$ , which has a 1 at its first

component and 0's elsewhere.

In a similar fashion, for the transfer case, the input force is assumed excited at the first coordinate and the output acceleration is assumed measured at the second coordinate

$$\begin{aligned} F_f &= e_1 \\ H_f &= e_2^T \end{aligned} \tag{3.5}$$

where  $e_2$  is an element of the standard basis for  $R^n$ , which has a 1 at its second component and 0's elsewhere.

## 2. MIMO Mechanical Realizations

Denote the set of indices of coordinates at which excitation forces are applied as  $I_f$  and the set of indices of coordinates at which accelerations are measured as  $I_a$ . An initial MIMO second order model (3.9) can be categorized as one of the following three types:

### (a) Driving-point Accelerance

In this case,  $I_f = I_a$ , which means the forces are applied and accelerations are measured at the same set of coordinates, as shown in Figure 3.2. In the final realizable model (3.13), without loss of generality, it is assumed that  $I_f = I_a$  correspond to the first  $m$  coordinates, as depicted in Figure 3.2. The input and output influence matrices in (3.13) are given by

$$F_f = H_f^T = \begin{bmatrix} e_1 & e_2 & \cdots & e_m \end{bmatrix} \tag{3.6}$$

### (b) Transfer Accelerance

In this case, it has  $I_f \cap I_a = \emptyset$ . This means there is no common coordinate at which an excitation force is applied and an acceleration is measured. In the

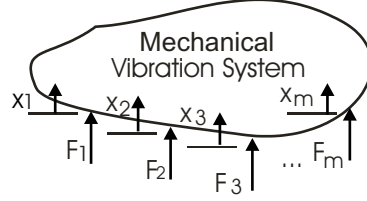


Figure 3.2: Mechanical System of a MIMO Driving-point Accelerance

final realizable model (3.13), without loss of generality, it is assumed that the excitation forces are applied at the first  $m$  coordinates and the accelerations are measured at the next  $p$  coordinates, as depicted in Figure 3.3. Obviously,  $m$  and  $p$  must satisfy  $m + p \leq n$ . Thus, the input and output influence matrices in the realizable model (3.13) are given by

$$F_f = \begin{bmatrix} e_1 & e_2 & \cdots & e_m \end{bmatrix}$$

$$H_f^T = \begin{bmatrix} e_{m+1} & e_{m+2} & \cdots & e_{m+p} \end{bmatrix} \quad (3.7)$$

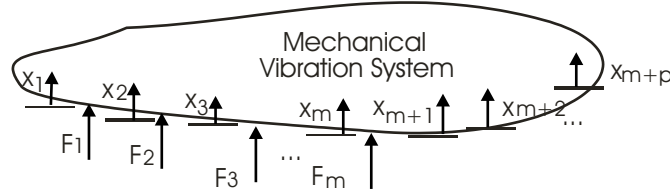


Figure 3.3: Mechanical System of a MIMO Transfer Accelerance

(c) Driving-point and Transfer Accelerance

This is the most comprehensive case which satisfies  $I_f \cap I_a \neq \emptyset$ , as shown in Figure 3.4. Without loss of generality, it is assumed in the final realizable model (3.13) that the excitation forces are applied at the first  $m$  coordinates and the accelerations are measured at the first  $r$  coordinates and the  $m + 1$ 'th,  $m + 2$ 'th,  $\dots$ ,  $m + (p - r)$ 'th coordinates, where  $r \leq \min(m, p)$ , as depicted in Figure 3.4.

The input and output influence matrices are given by

$$F_f = \begin{bmatrix} e_1 & e_2 & \cdots & e_m \end{bmatrix}$$

$$H_f^T = \begin{bmatrix} e_1 & e_2 & \cdots & e_r & e_{m+1} & e_{m+2} & \cdots & e_{m+(p-r)} \end{bmatrix} \quad (3.8)$$

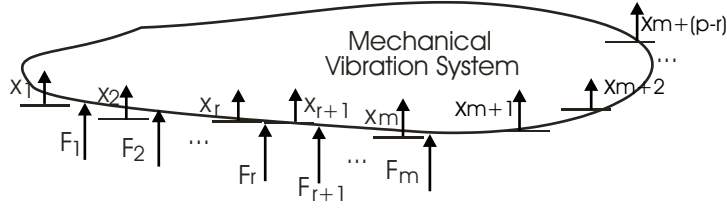


Figure 3.4: Mechanical System of a MIMO Driving-point and Transfer Accelerance

### 3.1.3 Mechanically Realizable Second Order Model

In the time domain, congruent coordinate transformations can be applied in mechanical realization since the input-output relationship and symmetry of mass, damping and stiffness matrices need to be preserved. An initial second order model which describes the driving-point relationship of a mechanical system without skyhook elements is given by

$$M_0 \ddot{x} + C_0 \dot{x} + K_0 x = F_0 u$$

$$y = H_0 \ddot{x} \quad (3.9)$$

where the mass matrix  $M_0 = M_0^T > 0$ , the damping matrix  $C_0 = C_0^T \geq 0$  and the stiffness matrix  $K_0 = K_0^T \geq 0$ . Assume that there are  $n$  masses in a vibratory mechanical system. Thus, the mass, damping and stiffness matrices are  $n \times n$  square matrices. The relationship between the input influence vector (or matrix)  $F_0$  and output influence vector (or matrix)  $H_0$  depends on the coordinates in which the inputs and outputs are chosen. In the simplest case, if the initial model (3.9) describes a driving-point accelerance, then it satisfies  $F_0 = H_0^T$ .

Choose a coordinate transformation

$$x = Tq \quad (3.10)$$

where  $T$  is an unknown nonsingular matrix.

Substituting (3.10) into (3.9) yields

$$\begin{aligned} M_0 T \ddot{q} + C_0 T \dot{q} + K_0 T q &= F_0 u \\ y &= H_0 T \ddot{q} \end{aligned} \quad (3.11)$$

Premultiplying the above equation by the transpose of the coordinate transformation  $T$ , one obtains

$$\begin{aligned} T^T M_0 T \ddot{q} + T^T C_0 T \dot{q} + T^T K_0 T q &= T^T F_0 u \\ y &= H_0 T \ddot{q} \end{aligned} \quad (3.12)$$

which can be rewritten as

$$\begin{aligned} M_f \ddot{q} + C_f \dot{q} + K_f q &= F_f u \\ y &= H_f \ddot{q} \end{aligned} \quad (3.13)$$

where  $M_f$ ,  $C_f$ ,  $K_f$ ,  $F_f$  and  $H_f$  are, respectively, the final mass, damping and stiffness matrices, and the input influence vector (or matrix) and output influence vector (or matrix).

They are defined as

$$\begin{aligned} M_f &= T^T M_0 T \\ C_f &= T^T C_0 T \\ K_f &= T^T K_0 T \end{aligned}$$

$$\begin{aligned}
F_f &= T^T F_0 \\
H_f &= H_0 T
\end{aligned}
\tag{3.14}$$

If the final second order model (3.13) is realizable, the mass, damping and stiffness matrices  $M_f$ ,  $C_f$  and  $K_f$  must satisfy the realization conditions (3.3). Furthermore, the input and output influence vectors (or matrices) must be in the desired forms provided in Subsection 3.1.2. Therefore, the necessary conditions for a second-order system to be mechanically realizable are that (3.3) is satisfied and that the input and output influence matrices can be transformed to one of (3.4) to (3.7).

Generally speaking, it is difficult to directly find the congruent coordinate transformation corresponding to a realizable model. Therefore, in this research, the transformation is decomposed as a product of several components so that each component can be found separately. This will be covered in the following section.

## 3.2 Decomposition of the Congruent Coordinate Transformations

The realizing congruent coordinate transformations can be decomposed into a product of three components as follows

$$T = M_0^{-1/2} R M_f^{1/2} \tag{3.15}$$

The first component, the inverse of the square root of the initial mass matrix, is used to mass normalize the initial second order model (3.9). The second component  $R$  is an orthogonal matrix which should perform two tasks: (1) align the input and output influence vectors (or matrices) to the desired forms; (2) convert the damping and stiffness matrices to the desired realizable forms in which all of off-diagonal elements are negative. The orthogonal matrix has the following properties: (1) it can preserve the identity mass matrix in the mass normalized second order model; (2) it belongs to an orthogonal group

which can be easily parameterized. The last component is the square root of the final mass matrix  $M_f$ .

After subsequently applying each component of the transformation  $R$ , the initial second order model (3.9) or the second order model obtained in the previous step is changed to a new form. The model obtained after each transformation step is given below.

Denote the first coordinate transformation as

$$x = M_0^{-1/2} z \quad (3.16)$$

Substituting this transformation into (3.9) and pre-multiplying by  $M_0^{-1/2}$ , yields the mass normalized second order model

$$\begin{aligned} \ddot{z} + C_z \dot{z} + K_z z &= F_z u \\ y &= H_z \ddot{z} \end{aligned} \quad (3.17)$$

with its matrices defined by

$$\begin{aligned} C_z &= M_0^{-1/2} C_0 M_0^{-1/2} \\ K_z &= M_0^{-1/2} K_0 M_0^{-1/2} \\ F_z &= M_0^{-1/2} F_0 \\ H_z &= H_0 M_0^{-1/2} \end{aligned} \quad (3.18)$$

Denote the second coordinate transformation as

$$z = R w \quad (3.19)$$

where  $R$  is an orthogonal matrix, that is,  $R^{-1} = R^T$ .

Substituting the above transformation into (3.17) and pre-multiplying by  $R^T$ , yields a



new second order model

$$\begin{aligned} \ddot{w} + C_w \dot{w} + K_w w &= F_w u \\ y &= H_w \ddot{w} \end{aligned} \tag{3.20}$$

with matrices defined by

$$\begin{aligned} C_w &= R^T C_z R \\ K_w &= R^T K_z R^T \\ F_w &= R^T F_z \end{aligned} \tag{3.21}$$

$$H_w = H_z R \tag{3.22}$$

Finally, denote the third coordinate transformation as

$$w = M_f^{1/2} q \tag{3.23}$$

Substituting the above transformation into (3.20) and pre-multiplying by  $M_f^{1/2}$ , yields the following second order model

$$\begin{aligned} M_f \ddot{q} + C_f \dot{q} + K_f q &= F_f u \\ y &= H_f \ddot{q} \end{aligned} \tag{3.24}$$

with its matrices defined by

$$\begin{aligned} C_f &= M_f^{1/2} C_w M_f^{1/2} \\ K_f &= M_f^{1/2} K_w M_f^{1/2} \\ F_f &= M_f^{1/2} F_w \\ H_f &= H_w M_f^{1/2} \end{aligned} \tag{3.25}$$

It should be noted that the input and output influence vectors (or matrices) in the model (3.20) are already in the desired forms except for a scaling factor. The last transformation scales the input and output influence vectors (or matrices) in the model (3.20). These two influence vectors (or matrices) satisfy

$$\begin{aligned}\frac{F_w}{\|F_w\|} &= \frac{F_f}{\|F_f\|} \\ \frac{H_w}{\|F_w\|} &= \frac{H_f}{\|H_f\|}\end{aligned}\tag{3.26}$$

### 3.3 Parameterization of the Orthogonal Component $R$

As discussed in Section 3.2, the orthogonal component  $R$  in the congruent coordinate transformation  $T$  must carry out two tasks when it is applied to the mass normalized model (3.17). First, this component needs to align the input and output influence vectors (or matrices)  $F_z$  and  $H_z$  in (3.17) to the desired forms  $F_w$  and  $H_w$  in (3.20). Second, the component  $R$  subsequently should convert the damping matrix  $C_z$  and the stiffness matrix  $K_z$  to the desired forms  $C_w$  and  $K_w$  in (3.20), in which all diagonal elements are positive and all off-diagonal elements are nonpositive.

Consequently, the orthogonal component  $R$  can be decomposed as a product of two orthogonal matrices

$$R = R_{IO}R_e\tag{3.27}$$

In the above equation, the component  $R_{IO}$  performs the first task; and  $R_e$  carries out the second task while preserving the input and output influence matrices obtained in the previous step.

Two matrix computation algorithms can be used as the orthogonal component  $R_e$ , as discussed in Subsection 2.3.2, resulting in parallel or serial realizations with no damping or proportional damping. There is no general algorithm to find this orthogonal component  $R_e$  when nonproportional damping exists, however. This research adopts parameterization

of this orthogonal component to find the total congruent coordinate transformation  $T$  in (3.15).

In the following two subsections, how to obtain the above two orthogonal components  $R_{IO}$  and  $R_e$  are discussed. The first component  $R_{IO}$  is obtained below and another component  $R_e$  will be determined in the later subsection.

### 3.3.1 Aligning the Input and Output Influence Vectors (or Matrices)

After applying the transformation  $R_{IO}$  to the mass normalized model (3.17), a new model can be obtained. Denote the coordinate transformation as

$$z = R_{IO}\tilde{z} \quad (3.28)$$

Substituting (3.28) into the mass normalized model (3.17) and pre-multiplying by  $R_{IO}^T$  yields the following model

$$\begin{aligned} \ddot{\tilde{z}} + C_{\tilde{z}}\dot{\tilde{z}} + K_{\tilde{z}}\tilde{z} &= F_{\tilde{z}}u \\ y &= H_{\tilde{z}}\tilde{z} \end{aligned} \quad (3.29)$$

in which the matrices are defined by

$$\begin{aligned} C_{\tilde{z}} &= R_{IO}^T C_z R_{IO} \\ K_{\tilde{z}} &= R_{IO}^T K_z R_{IO} \\ F_{\tilde{z}} &= R_{IO}^T F_z \\ H_{\tilde{z}} &= H_z R_{IO} \end{aligned} \quad (3.30)$$

The first orthogonal component  $R_{IO}$  of the transformation  $R$  can be obtained by  $QR$  factorization of the input and output influence vectors (or matrices). In this  $QR$  factorization, a matrix is decomposed into a product of an orthogonal matrix and an

upper triangular matrix. A property of this method, which is proved in Appendix C, is that a matrix whose column vectors are perpendicular to each other can be factored as a product of an orthogonal matrix and a diagonal matrix. This property is used extensively in the following discussion.

### 1. SISO Driving-point Accelerance

Recall (3.4) in Section 3.1.2. After aligning the input and output influence vectors  $F_z$  and  $H_z$  in (3.17) via the orthogonal transformation  $R_{IO}$ , the input and output influence vectors  $F_{\tilde{z}}$  and  $H_{\tilde{z}}$  in (3.29) should satisfy the following relationship

$$\frac{F_{\tilde{z}}}{\|F_{\tilde{z}}\|} = \frac{H_{\tilde{z}}^T}{\|H_{\tilde{z}}^T\|} = e_1 \quad (3.31)$$

Suppose the  $QR$  factorization of the input and output influence vectors  $F_z$  and  $H_z$  has the following form

$$F_z = H_z^T = Q \begin{bmatrix} \|F_z\|e_1 & 0 & \cdots & 0 \end{bmatrix} \quad (3.32)$$

where  $Q$  is an orthogonal matrix.

Consequently, the orthogonal component  $R_{IO}$  is found as follows

$$R_{IO} = Q \quad (3.33)$$

### 2. SISO Transfer Accelerance

The input and output influence vectors in the final realizable second order model (3.13) must have the form in (3.5). Thus, after aligning the input and output influence vectors with the orthogonal transformation  $R_{IO}$ , the input and output influence vectors  $F_{\tilde{z}}$  and  $H_{\tilde{z}}$  in (3.29) should satisfy the following relationship

$$\frac{F_{\tilde{z}}}{\|F_{\tilde{z}}\|} = e_1$$

$$\frac{H_{\bar{z}}}{\|H_{\bar{z}}\|} = e_2^T \quad (3.34)$$

Therefore, the orthogonal component  $R_{IO}$  should satisfy

$$\begin{aligned} F_{\bar{z}} &= R_{IO}^T F_z = \|F_z\| e_1 \\ H_{\bar{z}} &= H_z R_{IO} = \|H_z\| e_2^T \end{aligned} \quad (3.35)$$

or equivalently

$$R_{IO}^T \begin{bmatrix} F_z & H_z^T \end{bmatrix} = \begin{bmatrix} \|F_z\| e_1 & \|H_z\| e_2 \end{bmatrix} \quad (3.36)$$

According to the property of  $QR$  factorization, suppose the matrix  $\begin{bmatrix} F_z & H_z^T \end{bmatrix}$  can be factorized as follows

$$\begin{bmatrix} F_z & H_z^T \end{bmatrix} = Q \begin{bmatrix} \|F_z\| e_1 & \|H_z\| e_2 \end{bmatrix} \quad (3.37)$$

Therefore, the orthogonal component  $R_{IO}$  is obtained as follows

$$R_{IO} = Q \quad (3.38)$$

### 3. MIMO Accelerances

The input and output influence matrices in the final realizable model (3.13) must be in one of the forms given by (3.6), (3.7) and (3.8). It depends on the realization type to which the given model (3.9) belongs. QR factorization of the input and output influence matrices can also be used to align these matrices to the desired forms.

#### (a) Driving-point Accelerance

In this case, the input influence matrix is the transpose of the output influence matrix, i.e.,  $F_z = H_z^T$  in the model (3.17). After aligning them to the correct

form by the orthogonal transformation  $R_{IO}$ ,  $F_{\bar{z}}$  and  $H_{\bar{z}}$  in (3.29) should satisfy

$$\begin{aligned}
 F_{\bar{z}} = R_{IO}^T F_z &= \begin{bmatrix} \|f_{z_1}\|e_1 & \|f_{z_2}\|e_2 & \cdots & \|f_{z_m}\|e_m \end{bmatrix} \\
 H_{\bar{z}} = H_z R_{IO} &= \begin{bmatrix} \|f_{z_1}\|e_1^T \\ \|f_{z_2}\|e_2^T \\ \cdots \\ \|f_{z_m}\|e_m^T \end{bmatrix}
 \end{aligned} \tag{3.39}$$

Suppose the  $QR$  factorization of  $F_z$  is given by

$$Q \begin{bmatrix} \|f_{z_1}\|e_1 & \|f_{z_2}\|e_2 & \cdots & \|f_{z_m}\|e_m \end{bmatrix} = F_z \tag{3.40}$$

where  $Q$  is an orthogonal matrix. The orthogonal component  $R_{IO}$  is then obtained as follows

$$R_{IO} = Q \tag{3.41}$$

(b) Transfer Accelerance

In this case, the input and output influence matrices in the final realizable model (3.13) must possess the form given by (3.7). Thus, after aligning  $F_z$  and  $H_z$  in the model (3.17) by the orthogonal transformation  $R_{IO}$ , the input and output influence matrices  $F_{\bar{z}}$  and  $H_{\bar{z}}$  in the model (3.29) should satisfy the following relationships

$$\begin{aligned}
 F_{\bar{z}} = R_{IO}^T F_z &= \begin{bmatrix} \|f_{z_1}\|e_1 & \|f_{z_2}\|e_2 & \cdots & \|f_{z_m}\|e_m \end{bmatrix} \\
 H_{\bar{z}} = H_z R_{IO} &= \begin{bmatrix} \|h_{z_1}\|e_{m+1}^T \\ \|h_{z_2}\|e_{m+2}^T \\ \cdots \\ \|h_{z_p}\|e_{m+p}^T \end{bmatrix}
 \end{aligned} \tag{3.42}$$

or equivalently

$$R_{IO}^T \begin{bmatrix} F_z & H_z^T \end{bmatrix} = \begin{bmatrix} \|f_{z_1}\|e_1 & \cdots & \|f_{z_m}\|e_m & \|h_{z_1}\|e_{m+1} & \|h_{z_2}\|e_{m+2} & \cdots & \|h_{z_p}\|e_{m+p} \end{bmatrix} \quad (3.43)$$

where  $f_{z_i}$  ( $i = 1, 2, \dots, m$ ) is the  $i$ 'th column vector of  $F_z$  and  $h_{z_i}$  ( $i = j, 2, \dots, p$ ) is the  $j$ 'th row vector of  $H_z$ .

Suppose  $QR$  factorization of the matrix  $\begin{bmatrix} F_z & H_z^T \end{bmatrix}$  is given by

$$Q \begin{bmatrix} \|f_{z_1}\|e_1 & \cdots & \|f_{z_m}\|e_m & \|h_{z_1}\|e_{m+1} & \|h_{z_2}\|e_{m+2} & \cdots & \|h_{z_p}\|e_{m+p} \end{bmatrix} = \begin{bmatrix} F_z & H_z^T \end{bmatrix} \quad (3.44)$$

The orthogonal component  $R_{IO}$  is then given by the following equation

$$R_{IO} = Q \quad (3.45)$$

(c) Driving-point and Transfer Accelerance

The input and output influence matrices in the final realizable model (3.13) must have the form given by (3.8). Thus, after the orthogonal transformation  $R_{IO}$ , the input and output influence matrices  $F_{\bar{z}}$  and  $H_{\bar{z}}$  in (3.29) should satisfy the following relationships

$$F_{\bar{z}} = R_{IO}^T F_z = \begin{bmatrix} \|f_{z_1}\|e_1 & \|f_{z_2}\|e_2 & \cdots & \|f_{z_m}\|e_m \end{bmatrix}$$

$$H_z = H_z R_{IO} = \begin{bmatrix} \|f_{z_1}\| e_1^T \\ \|f_{z_2}\| e_2^T \\ \vdots \\ \|f_{z_r}\| e_r^T \\ \|h_{z_{(r+1)}}\| e_{m+1}^T \\ \|h_{z_{(r+2)}}\| e_{m+2}^T \\ \cdots \\ \|h_{z_p}\| e_{m+(p-r)}^T \end{bmatrix} \quad (3.46)$$

To fulfill the above requirements, the component  $R_{IO}$  can be decomposed as a product of two orthogonal transformations

$$R_{IO} = R_{F_z} R_{H_z} \quad (3.47)$$

In (3.47), the first component  $R_{F_z}$  satisfies

$$R_{F_z}^T F_z = \begin{bmatrix} \|f_{z_1}\| e_1 & \|f_{z_2}\| e_2 & \cdots & \|f_{z_m}\| e_m \end{bmatrix} \quad (3.48)$$

Suppose the  $QR$  factorization of  $F_z$  is given by

$$Q_{F_z} \begin{bmatrix} \|f_{z_1}\| e_1 & \|f_{z_2}\| e_2 & \cdots & \|f_{z_m}\| e_m \end{bmatrix} = F_z \quad (3.49)$$

where  $Q_{F_z}$  is an orthogonal matrix. The first component  $R_{F_z}$  then can be chosen as

$$R_{F_z} = Q_{F_z} \quad (3.50)$$

From (3.48), the first  $m$  column vectors of  $R_{F_z}$  (or  $Q_{F_z}$ ) should be equal to  $f_{z_i}/\|f_{z_i}\|$  ( $i = 1, 2, \dots, m$ ), respectively. According to (3.8),  $H_z R_{F_z}$  should



have the following form

$$H_z R_{F_z} = \begin{bmatrix} \|f_{z_1}\| e_1^T \\ \|f_{z_2}\| e_2^T \\ \vdots \\ \|f_{z_r}\| e_r^T \\ \bar{H}_z \end{bmatrix} \quad (3.51)$$

where  $\bar{H}_z = \begin{bmatrix} 0_{(p-r) \times m} & \tilde{H}_z \end{bmatrix}$  and  $\tilde{H}_z$  is a  $(p-r) \times (n-m)$  matrix.

The second component  $R_{H_z}$  of the transformation  $R_{IO}$  needs to preserve  $e_j$ 's ( $j = 1, 2, \dots, m$ ) and should convert (3.51) to the the following form

$$(H_z R_{F_z}) R_{H_z} = \begin{bmatrix} \|f_{z_1}\| e_1^T \\ \|f_{z_2}\| e_2^T \\ \vdots \\ \|f_{z_r}\| e_r^T \\ \|h_{z_{(r+1)}}\| e_{m+1}^T \\ \|h_{z_{(r+2)}}\| e_{m+2}^T \\ \dots \\ \|h_{z_p}\| e_{m+(p-r)}^T \end{bmatrix} \quad (3.52)$$

Suppose the  $QR$  factorization of  $\tilde{H}_z^T$  is given by

$$Q_{H_z} \begin{bmatrix} \|h_{z_{(r+1)}}\| \tilde{e}_1 & \|h_{z_{(r+2)}}\| \tilde{e}_2 & \dots & \|h_{z_p}\| \tilde{e}_{m+p} \end{bmatrix} = \tilde{H}_z^T \quad (3.53)$$

where  $Q_{H_z}$  is an orthogonal matrix and  $\tilde{e}_i$  is an element of the standard basis for  $R^{n-m}$ , which has a 1 at its  $i$ 'th component and 0's elsewhere.

The equation (3.53) can be rewritten into

$$\begin{bmatrix} \|h_{z(r+1)}\| \tilde{e}_{m+1}^T \\ \|h_{z(r+2)}\| \tilde{e}_{m+2}^T \\ \vdots \\ \|h_{z_p}\| \tilde{e}_{m+p}^T \end{bmatrix} Q_{H_z}^T = \tilde{H}_z \quad (3.54)$$

or equivalently

$$\begin{bmatrix} \|h_{z(r+1)}\| \tilde{e}_{m+1}^T \\ \|h_{z(r+2)}\| \tilde{e}_{m+2}^T \\ \vdots \\ \|h_{z_p}\| \tilde{e}_{m+p}^T \end{bmatrix} = \tilde{H}_z Q_{H_z} \quad (3.55)$$

Thus, the second component  $R_{H_z}$  in (3.47) is given by

$$R_{H_z} = \begin{bmatrix} I_{m \times m} & 0 \\ 0 & Q_{H_z} \end{bmatrix} \quad (3.56)$$

It should be noted that  $R_{H_z}$  preserves  $e_i$ 's ( $i = 1, 2, \dots, m$ ).

Consequently, from (3.47), (3.50) and (3.56), the component  $R_{IO}$  of the transformation  $R$  in (3.27) is given by

$$R_{IO} = R_{F_z} R_{H_z} = Q_{F_z} \begin{bmatrix} I_{m \times m} & 0 \\ 0 & Q_{H_z} \end{bmatrix} \quad (3.57)$$

### 3.3.2 Converting to Realizable Damping and Stiffness Matrices

After aligning the input and output influence vectors (or matrices) as described in the preceding subsection, a second orthogonal component  $R_e$  needs to be applied to convert the damping and stiffness matrices in the model (3.29) to the desired forms in which all diagonal elements are positive and all off-diagonal elements are nonnegative. This

orthogonal component  $R_e$  must simultaneously preserve the input and output influence vectors (or matrices) in the model (3.29). After applying the second transformation  $R_e$ , the model (3.29) results in the model (3.20). Denote the coordinate transformation

$$\tilde{z} = R_e w \quad (3.58)$$

Substituting the above transformation into (3.29) and pre-multiplying  $R_e^T$ , yields the following second order model which is the same as (3.20)

$$\begin{aligned} \ddot{w} + C_w \dot{w} + K_w w &= F_w u \\ y &= H_w \ddot{w} \end{aligned} \quad (3.59)$$

in which

$$\begin{aligned} C_w &= R_e^T C_{\tilde{z}} R_e \\ K_w &= R_e^T K_{\tilde{z}} R_e \\ F_w &= R_e^T F_{\tilde{z}} \\ H_w &= H_{\tilde{z}} R_e \end{aligned} \quad (3.60)$$

It should be noted that the input and output influence vectors (or matrices) in the model (3.29) have been already in the desired forms only with a lack of scaling. In addition, the transformation  $R_e$  does not change their forms. These two influence vectors (or matrices) satisfy

$$\begin{aligned} \frac{F_{\tilde{z}}}{\|F_{\tilde{z}}\|} &= \frac{F_w}{\|F_w\|} = \frac{F_f}{\|F_f\|} \\ \frac{H_{\tilde{z}}}{\|H_{\tilde{z}}\|} &= \frac{H_w}{\|H_w\|} = \frac{H_f}{\|H_f\|} \end{aligned} \quad (3.61)$$

The component  $R_e$  is obtained below for each type of mechanical realization.

### 1. SISO Accelerances

For mechanical realization of SISO accelerances, the orthogonal component  $R_e$  should preserve the input and output influence vectors  $F_{\tilde{z}}$  and  $H_{\tilde{z}}$  given by (3.31) or (3.35). This component thus should have the following form

$$R_e = \begin{bmatrix} I_{n_{io} \times n_{io}} & 0 \\ 0 & \tilde{R}_e \end{bmatrix} \quad (3.62)$$

where  $I_{n_{io} \times n_{io}}$  is an  $n_{io} \times n_{io}$  identity matrix and  $\tilde{R}_e$  is an  $(n - n_{io}) \times (n - n_{io})$  orthogonal matrix. Here, the number  $n_{io}$  is determined by the type of SISO accelerances

$$n_{io} = \begin{cases} 1 & \text{for SISO driving-point accelerances} \\ 2 & \text{for SISO transfer accelerances} \end{cases} \quad (3.63)$$

Therefore,  $R_e$  belongs to the orthogonal group  $O(n - n_{io})$  and can be parameterized by  $(n - n_{io})(n - n_{io} - 1)/2$  free parameters for a mechanical system with  $n$  masses. The relationship between the number of masses and the dimension of the solution space of transformations is listed in Table 3.1.

Table 3.1: Number of Masses versus Dimension of the Solution Space

Number of Masses	Dim (Solution Space) for Driving-point Accelerances	Dim (Solution Space) for Transfer Accelerances
1	0	0
2	0	0
3	1	0
4	3	1
5	6	3
6	10	6
7	15	10
8	21	15
9	28	21
10	36	28

For realizing the driving-point accelerance with no damping or proportional damping, serial and parallel model realizations can be obtained by choosing  $R_e$  as special orthogonal transformations. To obtain a serial model,  $R_e$  can be chosen as a product of two orthogonal matrices, i.e.,  $R_e = HS$ , where  $H$  is the Householder's transformation [67] of the stiffness matrix  $K_{\bar{z}}$  in (3.29) and  $S$  is a diagonal matrix in which diagonal elements are  $-1$ 's at rows of positive off-diagonal elements of  $H^T K_{\bar{z}} H$  and  $1$ 's at other rows. To find a parallel model,  $R_e$  can be chosen as a product of two orthogonal matrices, i.e.,  $R_e = PS$ , where  $P$  is in form of  $\begin{bmatrix} 1 & \\ & \tilde{P} \end{bmatrix}$  and  $S$  is a diagonal matrix in which diagonal elements are  $-1$ 's at rows of positive off-diagonal elements of  $P^T K_{\bar{z}} P$  and  $1$ 's at other rows. Here  $\tilde{P}$  can be chosen as the eigenvector matrix of the matrix from deleting the first row and column of  $K_{\bar{z}}$  in the model (3.29) [67]. The same transformation can be used to convert the proportional damping matrix to realizable form.

## 2. MIMO Accelerances

For realizing MIMO accelerances, the orthogonal component  $R_e$  should preserve the input and output influence matrices given by (3.39), or (3.42) or (3.46).  $R_e$  can be expressed as

$$R_e = \begin{bmatrix} I_{n_{io} \times n_{io}} & 0 \\ 0 & \tilde{R}_e \end{bmatrix} \quad (3.64)$$

where  $I_{n_{io} \times n_{io}}$  is an  $n_{io} \times n_{io}$  identity matrix and the matrix  $\tilde{R}_e \in O(n - n_{io})$ . Here, the number  $n_{io}$  is determined by the type of MIMO accelerances

$$n_{io} = \begin{cases} m & \text{for MIMO driving-point accelerances} \\ m + p & \text{for MIMO transfer accelerances} \\ m + p - r & \text{for MIMO driving-point and transfer accelerances} \end{cases} \quad (3.65)$$

Therefore,  $R_e$  belongs to the orthogonal group  $O(n - n_{io})$  which can be parameterized

by  $(n - n_{io})(n - n_{io} - 1)/2$  free parameters.

In summary, the number of free parameters for the component  $R_e$  increases quadratically with the increment of the number of masses in a mechanical system. These free parameters can be chosen as either 2-dimensional rotation angles or reflection angles. In this research, the product of a series of 2-dimensional rotation transformations is adopted as the orthogonal component  $R_e$ . Two-dimensional rotations, also known as Givens rotations, have been widely used to convert symmetric matrices to tridiagonal matrices in solving symmetric matrix eigenvalue problems [67].

In general,  $R_e$  can be expressed as

$$R_e = \prod_{i=1}^{i=n_p} R_i \quad (3.66)$$

where  $R_i$  is the  $i$ 'th 2-D rotation matrix. Since matrix multiplications do not commute, there are many possible orders of multiplication. To find realizable second order models from a given model, one only needs to use  $R_e$  with a specific order of multiplication. Because of periodicity of the cosine and sine functions, the range for each angle can be chosen from 0 to  $2\pi$ . These are not the minimum ranges to cover all of  $O(n - n_{io})$ .

For instance, the orthogonal component  $R_e$  in (3.27), associated with a four-mass mechanical system of SISO driving-point accelerance, can be parameterized by three 2-dimensional rotational angles. These three 2-D rotation transformations which preserve the driving-point input and output influence vectors are given by

$$R_{\theta_1} = \begin{bmatrix} 1 & & & & \\ & \cos\theta_1 & -\sin\theta_1 & & \\ & \sin\theta_1 & \cos\theta_1 & & \\ & & & & 1 \end{bmatrix}$$

$$\begin{aligned}
R_{\theta_2} &= \begin{bmatrix} 1 & & & \\ & 1 & & \\ & & \cos\theta_2 & -\sin\theta_2 \\ & & \sin\theta_2 & \cos\theta_2 \end{bmatrix} \\
R_{\theta_3} &= \begin{bmatrix} 1 & & & \\ & \cos\theta_3 & -\sin\theta_3 & \\ & & 1 & \\ & \sin\theta_3 & \cos\theta_3 & \end{bmatrix}
\end{aligned} \tag{3.67}$$

The second orthogonal component  $R_e$  in the orthogonal transformation  $R$  then can be expressed as

$$R_e(\theta_1, \theta_2, \theta_3) = R_{\theta_1} R_{\theta_2} R_{\theta_3} \tag{3.68}$$

After parameterization of  $R_e$ , the realizations can be found by search in the solution space of the congruent coordinate transformations. This will be discussed in the next chapter. Moreover, realizations with special requirements such as a minimum number of connecting elements may be obtained through considering additional constraints during the search.

### 3.4 Properties of Transformations Relating Realizable Models

The initial second order model (3.9) and its final realizable model (3.13) have many properties. Only those properties associated with mass are discussed below, including those for SISO mechanical realizations and MIMO mechanical realizations. Properties related to damping and stiffness can be obtained by following similar approaches to those presented here.

### 3.4.1 SISO Mechanical Realizations

If the initial second order model (3.9) describing SISO accelerances can be converted to the final second order model (3.13), these two second order models must satisfy the following theorem.

**Theorem 3.1.** *The given second order model (3.9) describing SISO accelerances and its final second order model (3.13) satisfy the following identity*

$$H_0 M_0^{-1} F_0 = H_f M_f^{-1} F_f = \begin{cases} \frac{1}{m_{f_1}} & \text{for a driving-point accelerance} \\ 0 & \text{for a transfer accelerance} \end{cases} \quad (3.69)$$

where  $m_{f_1}$  is the first mass in the final mass matrix  $M_f = \text{diag} \left( \begin{bmatrix} m_{f_1} & m_{f_2} & \cdots & m_{f_n} \end{bmatrix} \right)$ .

*Proof.* From (3.14),

$$\begin{aligned} F_0 &= (T^T)^{-1} F_f \\ H_0 &= H_f T^{-1} \\ M_0 &= (T^T)^{-1} M_f T^{-1} \end{aligned} \quad (3.70)$$

Thus,

$$H_0 M_0^{-1} F_0 = H_f T^{-1} [(T^T)^{-1} M_f T^{-1}]^{-1} (T^T)^{-1} F_f = H_f M_f^{-1} F_f \quad (3.71)$$

#### 1. Driving-point Accelerance Case

Because  $F_f = e_1$ ,  $H_f^T = e_1$ , and  $M_f = \text{diag} \left( \begin{bmatrix} m_{f_1} & m_{f_2} & \cdots & m_{f_n} \end{bmatrix} \right)$

$$\begin{aligned} H_0 M_0^{-1} F_0 = H_f M_f^{-1} F_f &= e_1 \text{diag} \left( \begin{bmatrix} m_{f_1} & m_{f_2} & \cdots & m_{f_n} \end{bmatrix} \right)^{-1} e_1^T \\ &= m_{f_1}^{-1} e_1 e_1^T = m_{f_1}^{-1} \end{aligned}$$



2. Transfer Accelerance Case

Because  $F_f = e_1$ ,  $H_f^T = e_2$ , and  $M_f = \text{diag} \left( \begin{bmatrix} m_{f_1} & m_{f_2} & \cdots & m_{f_n} \end{bmatrix} \right)$ ,

$$H_0 M_0^{-1} F_0 = H_f M_f^{-1} F_f = e_1 \text{diag} \left( \begin{bmatrix} m_{f_1} & m_{f_2} & \cdots & m_{f_n} \end{bmatrix} \right)^{-1} e_2^T = m_{f_1}^{-1} e_1 e_2^T = 0 \quad (3.72)$$

□

Theorem 3.1 means that all equivalent realizable second order models describing the same SISO driving-point accelerance must have the same mass at the driving location although their remaining parts may be totally different. For the transfer accelerance case, there is a corollary stated below.

**Corollary 3.1.** *Mass normalization of the initial second order model (3.9) describing the SISO transfer accelerance can recover perpendicularity between the input influence vector and the output influence vector, i.e.,  $H_z F_z = 0$ .*

This corollary is important since the input and output influence vectors in the final realizable model should be perpendicular to each other. This corollary can be proven below.

*Proof.* The inner product between the input influence vector and the output influence vector in the mass normalized second order model (3.17) is given by

$$H_z F_z = (H_0 M_0^{-1/2})(M_0^{-1/2} F_0) = H_0 M_0^{-1} F_0 \quad (3.73)$$

According to Theorem 3.1, thus it holds

$$H_z F_z = 0 \quad (3.74)$$

□

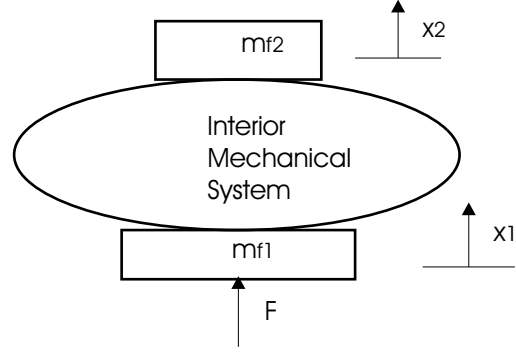


Figure 3.5: Mechanical System of a SISO Transfer Accelerance

The final mass vector  $m_f = \begin{bmatrix} m_{f_1} & m_{f_2} & \cdots & m_{f_n} \end{bmatrix}$  needs to be scaled by Theorem 3.1 for the driving-point accelerance case. Just as driving-point systems fix the driving mass, transfer systems shown in Figure 3.5, must possess the same mass at the driving location and the mass at the location where the acceleration is measured although the interior mechanical systems vary from one system to another. In this case, the final mass vector  $m_f$  should be scaled according to the following Theorem.

**Theorem 3.2.** *The input influence vector and the output influence vector in the mass normalized second order model (3.17) describing a SISO transfer accelerance should satisfy the following relationships*

$$\begin{aligned} \|F_z\| &= \|M_0^{-1/2}F_0\| = \frac{1}{\sqrt{m_{f_1}}} \\ \|H_z\| &= \|H_0M_0^{-1/2}\| = \frac{1}{\sqrt{m_{f_2}}} \end{aligned} \quad (3.75)$$

or equivalently

$$\begin{aligned} m_{f_1} &= \frac{1}{\|F_z\|^2} = \frac{1}{\|M_0^{-1/2}F_0\|^2} \\ m_{f_2} &= \frac{1}{\|H_z\|^2} = \frac{1}{\|H_0M_0^{-1/2}\|^2} \end{aligned} \quad (3.76)$$

which can be proven below.

*Proof.* Suppose the eigenvalue decomposition of the initial mass matrix is given by

$$M_0 = VDVT^T \quad (3.77)$$

where  $V$  is the eigenvector matrix which is an orthogonal matrix, that is,  $V^T = V^{-1}$  and  $D$  is a diagonal matrix with positive diagonal elements. The square root of  $M_0$  thus can be calculated by

$$M_0^{1/2} = VD^{1/2}V^T \quad (3.78)$$

Furthermore, it holds

$$M_0 = VDVT^T = (VD^{1/2})(D^{1/2}V^T) = (VD^{1/2}M_f^{-1/2})M_f(M_f^{-1/2}D^{1/2}V^T) \quad (3.79)$$

Since  $M_0 = (T^T)^{-1}M_fT^{-1}$ ,  $T$  can be chosen as

$$T^{-1} = M_f^{-1/2}D^{1/2}V^T \quad \text{or} \quad T = VD^{-1/2}M_f^{1/2} \quad (3.80)$$

Then

$$F_z = M_0^{-1/2}F_0 = (VD^{1/2}V^T)^{-1}(T^T)^{-1}F_f = (T^TVD^{1/2}V^T)^{-1}F_f \quad (3.81)$$

Substituting (3.80) into (3.81) yields

$$\begin{aligned} F_z = M_0^{-1/2}F_0 &= (T^TVD^{1/2}V^T)^{-1}F_f \\ &= \left[ \left( VD^{-1/2}M_f^{1/2} \right)^T VD^{1/2}V^T \right]^{-1} F_f \\ &= VM_f^{-1/2}F_f \\ &= V \frac{1}{\sqrt{m_{f_1}}} e_1 \\ &= \frac{1}{\sqrt{m_{f_1}}} v_1 \end{aligned} \quad (3.82)$$

where  $v_1$  is the first column vector in the orthogonal eigenvector matrix  $V$ . Therefore, the

following relationship holds

$$\|F_z\| = \|M_0^{-1/2}F_0\| = \frac{1}{\sqrt{m_{f_1}}} \quad (3.83)$$

In the similar way, the following relationship can be proven

$$\|H_z\| = \|H_0M_0^{-1/2}\| = \frac{1}{\sqrt{m_{f_2}}} \quad (3.84)$$

□

### 3.4.2 MIMO Mechanical Realizations

Similar results as discussed above for SISO accelerances can be obtained for MIMO accelerances. If the initial second order model (3.9) describing MIMO accelerances can be converted to the final second order model (3.13), these two second order models must satisfy the following theorem.

**Theorem 3.3.** *The given second order model (3.9) describing SISO accelerances and its final second order model (3.13) satisfy the following identities*

1. *MIMO Driving-point Accelerance*

$$H_0M_0^{-1}F_0 = H_fM_f^{-1}F_f = \text{diag}\left(\left[\begin{array}{cccc} \frac{1}{m_{f_1}} & \frac{1}{m_{f_2}} & \cdots & \frac{1}{m_{f_m}} \end{array}\right]\right) \quad (3.85)$$

2. *MIMO Transfer Accelerance*

$$H_0M_0^{-1}F_0 = H_fM_f^{-1}F_f = 0_{p \times m} \quad (3.86)$$

3. *MIMO Driving-point and Transfer Accelerance*

$$H_0M_0^{-1}F_0 = H_fM_f^{-1}F_f = \text{diag}\left(\left[\begin{array}{cccccc} \frac{1}{m_{f_1}} & \frac{1}{m_{f_2}} & \cdots & \frac{1}{m_{f_r}} & 0 & \cdots & 0 \end{array}\right]\right) \quad (3.87)$$

where  $m_{f_i}$  ( $i = 1, 2, \dots, m$ ) is the mass at which the  $i$ 'th force is applied .

*Proof.* From (3.71), it is known

$$H_0 M_0^{-1} F_0 = H_f M_f^{-1} F_f \quad (3.88)$$

For each type of accelerances, its corresponding necessary realization condition is proven below.

### 1. Driving-point Accelerance

Since  $F_f = H_f^T = \begin{bmatrix} e_1 & e_2 & \dots & e_m \end{bmatrix}$  and  $M_f = \text{diag} \left( \begin{bmatrix} m_{f_1} & m_{f_2} & \dots & m_{f_n} \end{bmatrix} \right)$ ,

$$H_0 M_0^{-1} F_0 = H_f M_f^{-1} F_f = \text{diag} \left( \begin{bmatrix} \frac{1}{m_{f_1}} & \frac{1}{m_{f_2}} & \dots & \frac{1}{m_{f_m}} \end{bmatrix} \right) \quad (3.89)$$

### 2. Transfer Accelerance

With consideration of (3.7) and  $M_f = \text{diag} \left( \begin{bmatrix} m_{f_1} & m_{f_2} & \dots & m_{f_n} \end{bmatrix} \right)$ , it yields

$$\begin{aligned} H_0 M_0^{-1} F_0 &= H_f M_f^{-1} F_f \\ &= \begin{bmatrix} e_{m+1}^T \\ e_{m+2}^T \\ \vdots \\ e_{m+p}^T \end{bmatrix} \begin{bmatrix} m_{f_1} & & & \\ & m_{f_2} & & \\ & & \ddots & \\ & & & m_{f_n} \end{bmatrix}^{-1} \begin{bmatrix} e_1 & e_2 & \dots & e_m \end{bmatrix} \\ &= \begin{bmatrix} e_{m+1} & e_{m+2} & \dots & e_{m+p} \end{bmatrix}^T \begin{bmatrix} m_{f_1}^{-1} e_1 & m_{f_2}^{-1} e_2 & \dots & m_{f_m}^{-1} e_m \end{bmatrix} \\ &= 0_{p \times m} \end{aligned} \quad (3.90)$$

### 3. Driving-point and Transfer Accelerance

With consideration of  $M_f = \text{diag} \left( \begin{bmatrix} m_{f_1} & m_{f_2} & \dots & m_{f_n} \end{bmatrix} \right)$  and (3.8),

$$H_0 M_0^{-1} F_0 = H_f M_f^{-1} F_f$$

$$\begin{aligned}
&= \begin{bmatrix} e_1 & e_2 & \cdots & e_r & e_{m+1} & e_{m+2} & \cdots & e_{m+(p-r)} \end{bmatrix}^T \\
&\quad \begin{bmatrix} m_{f_1} & & & & & & & \\ & m_{f_2} & & & & & & \\ & & \ddots & & & & & \\ & & & m_{f_n} & & & & \end{bmatrix}^{-1} \begin{bmatrix} e_1 & e_2 & \cdots & e_m \end{bmatrix} \\
&= \begin{bmatrix} e_1 & e_2 & \cdots & e_r & e_{m+1} & e_{m+2} & \cdots & e_{m+(p-r)} \end{bmatrix}^T \\
&\quad \begin{bmatrix} m_{f_1}^{-1}e_1 & m_{f_2}^{-1}e_2 & \cdots & m_{f_m}^{-1}e_m \end{bmatrix} \\
&= \begin{bmatrix} M_r^{-1} & 0 \\ 0 & 0 \end{bmatrix}_{p \times m} \tag{3.91}
\end{aligned}$$

where  $M_r = \text{diag} \left( \begin{bmatrix} m_{f_1} & m_{f_2} & \cdots & m_{f_r} \end{bmatrix} \right)$ .

□

For the driving-point accelerance, the final mass vector should be scaled according to the following corollary associated with Theorem 3.3.

**Corollary 3.2.** *The masses at the driving points are related to the input influence and output influence matrices in the mass normalized model (3.17) as follows*

$$m_{f_i} = \frac{1}{\|f_{z_i}\|^2} = \frac{1}{\|h_{z_i}\|^2} \quad (i = 1, 2, \dots, m) \tag{3.92}$$

where  $f_{z_i}$  ( $i = 1, 2, \dots, m$ ) is the  $i$ 'th column vectors of  $F_z$  and  $h_{z_i}$  ( $i = 1, 2, \dots, m$ ) is the  $i$ 'th row vectors of  $H_z$ . In addition, the column vectors of  $F_z$  are perpendicular to each other, i.e.,  $f_{z_i}^T f_{z_j} = 0$  for  $i \neq j$ ; the row vectors of  $H_z$  are perpendicular to each other too, i.e.,  $h_{z_i} h_{z_j}^T = 0$  for  $i \neq j$ .

*Proof.* Denote the mass normalized input and output influence matrices in (3.17) as

$$F_z = M_0^{-1/2} F_0 = \begin{bmatrix} f_{z_1} & f_{z_2} & \cdots & f_{z_m} \end{bmatrix}$$

$$H_z = H_0 M_0^{-1/2} = \begin{bmatrix} h_{z_1} \\ h_{z_2} \\ \vdots \\ h_{z_m} \end{bmatrix} \quad (3.93)$$

According to Theorem 3.3,

$$H_z F_z = H_0 M_0^{-1} F_0 = \text{diag} \left( \left[ \frac{1}{m_{f_1}} \quad \frac{1}{m_{f_2}} \quad \cdots \quad \frac{1}{m_{f_m}} \right] \right) \quad (3.94)$$

Therefore,

$$h_{z_i} f_{z_i} = \frac{1}{m_{f_i}}$$

$$h_{z_i} f_{z_j} = 0 \quad \text{for } i \neq j \quad (3.95)$$

Since  $h_{z_i} = f_{z_i}^T$ , the equation (3.95) can be rewritten as follows

$$h_{z_i} h_{z_i}^T = \frac{1}{m_{f_i}}$$

$$h_{z_i} h_{z_j}^T = 0 \quad \text{for } i \neq j$$

$$f_{z_i}^T f_{z_j} = 0 \quad \text{for } i \neq j \quad (3.96)$$

Thus, the following relationship holds

$$m_{f_i} = \frac{1}{\|f_{z_i}\|^2} \quad (i = 1, 2, \dots, m) \quad (3.97)$$

Since  $f_{z_i} = h_{z_i}^T$  ( $i = 1, 2, \dots, m$ ), it yields

$$m_{f_i} = \frac{1}{\|f_{z_i}\|^2} = \frac{1}{\|h_{z_i}\|^2} \quad (i = 1, 2, \dots, m) \quad (3.98)$$

□

For the transfer accelerance, the following corollary associated with Theorem 3.3 provides the reason why the second component in the transformation (3.15) should be an orthogonal matrix.

**Corollary 3.3.** *The product of the input influence matrix and the output influence matrix in the mass normalized second order model (3.17) from the given second order model (3.9) which describes a MIMO transfer accelerance is a zero matrix, that is,  $H_z F_z = 0_{p \times m}$ .*

*Proof.* According to (3.17), the inner product between the input influence vector and the output influence vector in the mass normalized second order model is

$$H_z F_z = H_0 M_0^{-1/2} M_0^{-1/2} F_0 = H_0 M_0^{-1} F_0 = 0_{p \times m} \quad (3.99)$$

In the above derivation, the equation (3.86) in Theorem 3.3 has been used. □

For the transfer accelerance, in the final realizable model (3.13), the final mass vector needs to be scaled according to the following theorem.

**Corollary 3.4.** *The masses at the excitation points and the acceleration measurement points are related to the input influence and output influence matrices in the mass normalized second order model (3.17) as follows*

$$m_{f_i} = \frac{1}{\|f_{z_i}\|^2} \quad (i = 1, 2, \dots, m)$$

$$m_{f_j} = \frac{1}{\|h_{z_j}\|^2} \quad (j = i - m; i = m + 1, m + 2, \dots, m + p) \quad (3.100)$$



where  $f_{z_i}$  ( $i = 1, 2, \dots, m$ ) is the  $i$ 'th column vector of  $F_z$  and  $h_{z_j}$  ( $j = 1, 2, \dots, p$ ) is the  $j$ 'th row vector of  $H_z$ .

*Proof.* Denote the mass normalized input and output influence matrices in (3.17) as

$$\begin{aligned} F_z &= M_0^{-1/2} F_0 = \begin{bmatrix} f_{z_1} & f_{z_2} & \cdots & f_{z_m} \end{bmatrix} \\ H_z &= H_0 M_0^{-1/2} = \begin{bmatrix} h_{z_1} \\ h_{z_2} \\ \vdots \\ h_{z_p} \end{bmatrix} \end{aligned} \quad (3.101)$$

According to (3.13), (3.15) and (3.7), it yields

$$F_f = T^T F_0 = M_f^{1/2} R^T M_0^{-1/2} F_0 = M_f^{1/2} R^T F_z \quad (3.102)$$

that is,

$$M_f^{-1/2} \begin{bmatrix} e_1 & e_2 & \cdots & e_m \end{bmatrix} = \begin{bmatrix} R^T f_{z_1} & R^T f_{z_2} & \cdots & R^T f_{z_m} \end{bmatrix} \quad (3.103)$$

or equivalently

$$\begin{bmatrix} \frac{1}{\sqrt{m_{f_1}}} & \frac{1}{\sqrt{m_{f_2}}} & \cdots & \frac{1}{\sqrt{m_{f_m}}} \end{bmatrix} = \begin{bmatrix} R^T f_{z_1} & R^T f_{z_2} & \cdots & R^T f_{z_m} \end{bmatrix} \quad (3.104)$$

Therefore, the following relations hold

$$\frac{1}{\sqrt{m_{f_i}}} e_i = R^T f_{z_i} \quad (i = 1, 2, \dots, m) \quad (3.105)$$

Thus, with consideration of the fact that  $R$  is an orthogonal matrix, the following relations hold

$$m_{f_i} = \frac{1}{\|f_{z_i}\|^2} \quad (i = 1, 2, \dots, m) \quad (3.106)$$

In the similar way, the following relations can be proved

$$m_{f_i} = \frac{1}{\|h_{z_j}\|^2} \quad (i = m + 1, m + 2, \dots, m + p; j = i - m) \quad (3.107)$$

□

For the driving-point and transfer accelerance, the final mass vector  $m_f$  in (3.13) should be scaled according to the following Corollary 3.5.

**Corollary 3.5.** *The masses at the coordinates where excitation forces are applied and where accelerations are measured are related to the input influence and output influence matrices in the mass normalized second order model (3.17) as follows*

$$\begin{aligned} m_{f_i} &= \frac{1}{\|f_{z_i}\|^2} \quad (i = 1, 2, \dots, m) \\ m_{f_{(m+j)}} &= \frac{1}{\|h_{z_{(r+j)}}\|^2} \quad (j = 1, 2, \dots, p - r) \end{aligned} \quad (3.108)$$

where  $f_{z_i}$  ( $i = 1, 2, \dots, m$ ) is the  $i$ 'th column vector of  $F_z$  and  $h_{z_j}$  ( $j = 1, 2, \dots, p$ ) is the  $j$ 'th row vector of  $H_z$ .

*Proof.* Denote the mass normalized input and output influence matrices in (3.17) as

$$\begin{aligned} F_z &= M_0^{-1/2} F_0 = \begin{bmatrix} f_{z_1} & f_{z_2} & \cdots & f_{z_m} \end{bmatrix} \\ H_z &= H_0 M_0^{-1/2} = \begin{bmatrix} h_{z_1} \\ h_{z_2} \\ \vdots \\ h_{z_p} \end{bmatrix} \end{aligned} \quad (3.109)$$

where  $f_{z_i}$ 's and  $h_{z_j}$ 's are column vectors of the input influence matrix and row vectors of the output influence matrix in the mass normalized second order model (3.17), respectively.

According to (3.13), (3.15) and (3.8), it yields

$$F_f = T^T F_0 = M_f^{1/2} R^T M_0^{-1/2} F_0 = M_f^{1/2} R^T F_z \quad (3.110)$$

that it,

$$M_f^{-1/2} \begin{bmatrix} e_1 & e_2 & \cdots & e_m \end{bmatrix} = R^T \begin{bmatrix} f_{z_1} & f_{z_2} & \cdots & f_{z_m} \end{bmatrix} \quad (3.111)$$

or equivalently

$$\begin{bmatrix} \frac{1}{\sqrt{m_{f_1}}} e_1 & \frac{1}{\sqrt{m_{f_2}}} e_2 & \cdots & \frac{1}{\sqrt{m_{f_m}}} e_m \end{bmatrix} = \begin{bmatrix} R^T f_{z_1} & R^T f_{z_2} & \cdots & R^T f_{z_m} \end{bmatrix} \quad (3.112)$$

Therefore, the following relations hold

$$\frac{1}{\sqrt{m_{f_i}}} e_i = R^T f_{z_i} \quad (i = 1, 2, \dots, m) \quad (3.113)$$

With consideration of the fact that the transformation  $R$  is an orthogonal matrix, the following relations hold

$$m_{f_i} = \frac{1}{\|f_{z_i}\|^2} \quad (i = 1, 2, \dots, m) \quad (3.114)$$

In a similar way, by considering  $H_z$ , the following relations can also be proved

$$m_{f_{(m+j)}} = \frac{1}{\|h_{z_{(r+j)}}\|^2} \quad (j = 1, 2, \dots, p-r) \quad (3.115)$$

□

It should be noted that the first  $r$  masses can also be calculated by  $m_{f_i} = \frac{1}{\|h_{z_i}\|^2}$ , ( $i = 1, 2, \dots, r$ ) since it holds  $f_{z_i} = h_{z_i}^T$  ( $i = 1, 2, \dots, r$ ).

### 3.5 Obtaining the Final Mass Matrix

After the damping and stiffness matrices  $C_w$  and  $K_w$  in the model (3.59) have been put in the correct form, the final mass matrix  $M_f$  in the realizable model (3.13) can be obtained by solving for the null space vectors of the damping and stiffness matrices in (3.20) and scaling according to results proved in Section 3.4. Since it is assumed that no skyhook elements are permitted, the damping and stiffness matrices share the same null space vector. Therefore, only one of these two matrices is enough for determining the mass matrix in the realizable model (3.13). According to the realization conditions given in (3.3), the damping and stiffness matrices in (3.13) satisfy

$$\begin{aligned} K_f \begin{bmatrix} 1 & 1 & \cdots & 1 \end{bmatrix}^T &= 0 \\ C_f \begin{bmatrix} 1 & 1 & \cdots & 1 \end{bmatrix}^T &= 0 \end{aligned} \quad (3.116)$$

According to (3.25), (3.116) is equivalent

$$\begin{aligned} C_w \sqrt{m_f} &= 0 \\ K_w \sqrt{m_f} &= 0 \end{aligned} \quad (3.117)$$

where  $m_f$  is the final mass vector, i.e.,  $m_f = \begin{bmatrix} m_{f_1} & m_{f_2} & \cdots & m_{f_n} \end{bmatrix}$ .

The unit null space vector can be obtained from either  $C_w$  or  $K_w$ . The final mass vector then is obtained by scaling this null space vector accordingly so that the base mass and total mass of the system is preserved, as shown in Table 3.2.

Obviously, the final mass matrix  $M_f$  is dependent on the choice of the orthogonal transformation  $R_e$ . Only for undamped and proportionally damped mechanical systems can this transformation be explicitly obtained by available algorithms in matrix computation. Therefore, for realizing nonproportionally damped vibratory mechanical systems, the key task to finding a realizable second order model using the congruent coordinate

Table 3.2: Scaling the Final Mass Vector

Type of Mechanical Realization	Theorems
SISO Driving-point Accelerance	Theorem 3.1
SISO Transfer Accelerance	Theorem 3.2
MIMO Driving-point Accelerance	Theorem 3.3 or Corollary 3.2
MIMO Transfer Accelerance	Corollary 3.4
MIMO Driving-point and Transfer Accelerance	Theorem 3.3 or Corollary 3.5

transformations is to obtain the orthogonal transformation  $R_e$  described in this chapter. Two methods for obtaining a realizable model are presented in the next chapter, including a technique for searching the space of the realizable transformations.

## Chapter 4

# Two Techniques for Obtaining Realizable Models

Everything should be made as simple as possible, but not simpler.

Albert Einstein (1879-1955)

Two methods are presented for obtaining realizable models. The first involves searching the space of realization transformations, parameterized by a finite set of free parameters as described in Chapter 3. This method starts with a given second order model satisfying the realization conditions discussed in Chapter 3. The second technique involves a direct estimation of realizable models from experimental input-output data. Both techniques are described below.

### 4.1 Searching the Parameterized Space of Realization Transformations

For a given second order model (3.9), congruent coordinate transformations  $T$  can be applied to obtain realizable second order models. Recall from (3.15) and (3.27) that these

congruent coordinate transformations  $T$  have been decomposed as

$$T = M_0^{-1/2} R M_f^{1/2} = M_0^{-1/2} (R_{IO} R_e) M_f^{1/2} \quad (4.1)$$

The first component  $M_0^{-1/2}$  is readily available from the given second order model (3.9) and the second component  $R_{IO}$  can be obtained via  $QR$  factorization of the input and output influence vectors (or matrices) in (3.29). Also, the last component  $M_f^{1/2}$  can be obtained by solving the null space vectors of the damping and stiffness matrices in (3.20) and scaling them according to theorems or corollaries listed in Table 3.2.

Therefore, the key task to obtain mechanical realizations is to find  $R_e$  in (4.1). An explicit solution is available only for a SISO driving-point accelerance with either no damping or proportional damping. In general,  $R_e$  belongs to an orthogonal group which can be parameterized by a finite number of free parameters. The dimension of the space of realizable transformations increases quadratically with the number of masses in mechanical systems.

When the number of masses is small, e.g., 3 or 4, an exhaustive search can be carried out and the search results can be easily visualized. For mechanical systems with more masses, however, it is impractical to use this search technique. Moreover, it is difficult to incorporate additional search criteria, such as minimizing the number of springs and dashpots with this approach. In these cases, other efficient search techniques [73] [74] [75] must be used. For those cases amenable to search of the transformation space, a cost function is needed.

As has been shown in Chapter 3, a realizable second order model satisfies (3.3) in which all off-diagonal elements of the stiffness and damping matrices must be nonpositive. A natural way to choose the cost function as

$$J(\theta) = w_1 S_K + w_2 S_C \quad (4.2)$$

where  $\theta$  is the vector of rotation angles,  $S_K$  is the summation of all positive off-diagonal elements in the stiffness matrix and  $S_C$  is the summation of all positive off-diagonal elements in the damping matrix. In order to balance the contributions from the stiffness and damping matrices, two weighting factors are given as

$$\begin{aligned} w_1 &= 1 \\ w_2 &= \frac{\text{trace}(K)}{\text{trace}(C)} \end{aligned} \quad (4.3)$$

where  $\text{trace}(\cdot)$  is defined as the summation of diagonal elements of a matrix. Since the congruent orthogonal transformation does not change the trace of a matrix, the weighting factor  $w_2$  actually is a constant.

With cost function (4.2), a wide choice of optimization techniques can be used to find the angle vector  $\theta$ . Once the cost function reaches zero, the search stops, resulting in a realization. During a nonlinear search, a small jump in a random direction with a random magnitude may have to be applied if the search converges to a local minimum.

In practice, however, a mechanical realization may not be found for a high-dimensional system due to the problems associated with optimization techniques applied to nonlinear systems. In those cases when the cost function does not reach zero, but does reach a small positive number, then an approximate realizable second order model may be obtained by removing all small positive off-diagonal elements as discussed below.

#### 4.1.1 Approximate Solutions

An approximate realizable model may be obtained by removing small positive elements from the damping and stiffness matrices. When this process is applied, however, the resulting damping and stiffness matrices are not singular any more. Since the damping and stiffness matrices should have the same null space vector relating to the final mass vector, further operations are needed to restore the singularities and null space vector. To this end, singular value decomposition (SVD) [76] can be applied.



Denote the damping and stiffness matrices after removing small positive off-diagonal elements as  $C$  and  $K$ , respectively. Their SVD's can be written as

$$\begin{aligned} C &= U_C S_C V_C^T \\ K &= U_K S_K V_K^T \end{aligned} \quad (4.4)$$

where  $U_C$ ,  $V_C$ ,  $U_K$  and  $V_K$  are  $n \times n$  orthogonal matrices and  $n$  is the number of masses. The diagonal matrix  $S_C$  is expressible as  $diag(\left[ \begin{array}{cccc} \sigma_{C_1} & \sigma_{C_2} & \cdots & \sigma_{C_n} \end{array} \right])$  and its nonnegative singular values  $\sigma_{C_i}$  ( $i=1, 2, \dots, n$ ) are ordered from the largest to the smallest. Another diagonal matrix  $S_K$  is expressible as  $diag(\left[ \begin{array}{cccc} \sigma_{K_1} & \sigma_{K_2} & \cdots & \sigma_{K_n} \end{array} \right])$  and its nonnegative singular values  $\sigma_{K_i}$  ( $i=1, 2, \dots, n$ ) are also ordered from the largest to the smallest.

Since the zeroed positive off-diagonal elements were very small, the lowest singular values  $\sigma_{C_n}$  and  $\sigma_{K_n}$  should be very close to zero. Therefore, their corresponding column vectors  $v_{C_n}$  and  $v_{K_n}$  in the matrices  $V_C$  and  $V_K$  can be approximately considered as the null space vectors of the matrices  $C$  and  $K$ , respectively, since

$$\begin{aligned} C v_{C_n} &= U_C S_C V_C^T v_{C_n} = U_C S_C V_C^T v_{C_n} = U_C S_C \left[ \begin{array}{cccc} 0 & 0 & \cdots & 1 \end{array} \right]^T = \sigma_{C_n} u_{C_n} \\ K v_{K_n} &= U_K S_K V_K^T v_{K_n} = U_K S_K V_K^T v_{K_n} = U_K S_K \left[ \begin{array}{cccc} 0 & 0 & \cdots & 1 \end{array} \right]^T = \sigma_{K_n} u_{K_n} \end{aligned} \quad (4.5)$$

where  $v_{C_n}$  and  $v_{K_n}$  are the  $n$ 'th column vectors in the matrices  $V_C$  and  $V_K$ , respectively. Here  $u_{C_n}$  and  $u_{K_n}$  are the  $n$ 'th column vectors of the matrices  $U_C$  and  $U_K$ , respectively.

In general, the approximate null space vectors  $v_{C_n}$  and  $v_{K_n}$  are not equal. To balance the approximation error induced from the damping and stiffness matrices, an approximate null space vector for both damping and stiffness matrices is constructed by averaging  $v_{C_n}$  and  $v_{K_n}$  as

$$v = \frac{v_{C_n} + v_{K_n}}{2} \quad (4.6)$$

Consequently, the final mass matrix  $m_f$  can be obtained according to Table 3.2. By applying the congruent coordinate transformation  $M_f^{1/2}$  to the matrices  $C$  and  $K$ , two new matrices are obtained as

$$\begin{aligned}\tilde{C}_f &= M_f^{1/2} C M_f^{1/2} \\ \tilde{K}_f &= M_f^{1/2} K M_f^{1/2}\end{aligned}\quad (4.7)$$

where all off-diagonal elements in the matrices  $\tilde{C}_f$  and  $\tilde{K}_f$  are nonpositive.

Since the final mass matrix is obtained from the vector  $v$ , the matrices  $\tilde{C}_f$  and  $\tilde{K}_f$  do not strictly satisfy

$$\begin{aligned}\tilde{C}_f \begin{bmatrix} 1 & 1 & \dots & 1 \end{bmatrix}^T &= 0 \\ \tilde{K}_f \begin{bmatrix} 1 & 1 & \dots & 1 \end{bmatrix}^T &= 0\end{aligned}\quad (4.8)$$

In order to make the final realizable model (3.13) possess a rigid body mode, the approximate final damping and stiffness matrices can be constructed by modifying their diagonal elements. The following two steps can be carried out:

1. Subtract the diagonal elements from the damping and stiffness matrices  $\tilde{C}_f$  and  $\tilde{K}_f$

$$\begin{aligned}\tilde{\tilde{C}}_f &= \tilde{C}_f - D_{\tilde{C}_f} \\ \tilde{\tilde{K}}_f &= \tilde{K}_f - D_{\tilde{K}_f}\end{aligned}\quad (4.9)$$

where  $D_{\tilde{C}_f}$  is the diagonal matrix constructed from the main diagonal of the matrix  $\tilde{C}_f$  and  $D_{\tilde{K}_f}$  is the diagonal matrix constructed from the main diagonal of the matrix  $\tilde{K}_f$ .

2. Set the absolute value of the sum of each row as the diagonal elements

$$C_f = \tilde{\tilde{C}}_f + \text{diag}(|\text{sum}(\tilde{\tilde{C}}_f)|)$$

$$K_f = \tilde{K}_f + \text{diag}(|\text{sum}(\tilde{K}_f)|) \quad (4.10)$$

where  $\text{sum}(\cdot)$  is a column vector with each element as a sum of all elements in a row of a matrix.  $C_f$  and  $K_f$  are the final realizable damping and stiffness matrices, which share the same null space vector  $\begin{bmatrix} 1 & 1 & \dots & 1 \end{bmatrix}^T$ .

Similarly, an approximate realizable second order model may be obtained by removing small connecting elements from a realizable second order model. This process is straightforward as discussed below.

#### 4.1.2 Approximation Error by Removing Connecting Elements with Small Values

Realizable second order models obtained through either exhaustive search or other search methods may possess mechanical elements with very small values. To make it easy to implement mechanical emulators under this circumstance approximate realizable second order models can be obtained by removing these mechanical elements. Since total mass in the realization must be preserved, only damping and stiffness elements may be removed.

Suppose that according to the decomposition in (3.2), the stiffness matrix in the realizable second order model (3.13) can be expressible as

$$K_f = C_{K_f} K_{D_{K_f}} C_{K_f}^T \quad (4.11)$$

where the connectivity matrix  $C_{K_f}$  depends on the couplings between masses. Here, the nonnegative diagonal matrix  $K_{D_{K_f}}$  can be expressed as  $\text{diag}(\begin{bmatrix} 0 & k_1 & k_2 & \dots & k_{n_k} \end{bmatrix})$ , where  $k_i$  ( $i=1, 2, \dots, n$ ) are positive spring constants and  $n_k$  is the number of springs in the realization.

By removing the small diagonal elements in the matrix  $K_{D_{K_f}}$  and the corresponding column vectors in the matrix  $C_{K_f}$ , an approximate stiffness matrix  $\tilde{K}_f$  can be obtained

as

$$\tilde{K}_f = C_{\tilde{K}_f} K_{D_{\tilde{K}_f}} C_{\tilde{K}_f}^T \quad (4.12)$$

where  $C_{\tilde{K}_f}$  is the connectivity matrix after removing the column vectors associated with small spring constants,  $K_{D_{\tilde{K}_f}}$  is the diagonal matrix after removing the small spring constants. Note that the approximate stiffness matrix  $\tilde{K}_f$  is still in realizable form. The omitted stiffness elements are included in the following matrix  $K_r$

$$K_r = K_f - \tilde{K}_f \quad (4.13)$$

In a similar way as discussed above, an approximate damping matrix can also be obtained as

$$\tilde{C}_f = C_{\tilde{C}_f} C_{D_{\tilde{C}_f}} C_{\tilde{C}_f}^T \quad (4.14)$$

where  $C_{\tilde{C}_f}$  is the connectivity matrix after removing the column vectors associated with small dashpots,  $C_{D_{\tilde{C}_f}}$  is the diagonal matrix after removing the small dashpots. The removed damping elements are included in the following matrix

$$C_r = C_f - \tilde{C}_f \quad (4.15)$$

Therefore, an approximate realizable second order model is obtained as

$$\begin{aligned} M_f \ddot{x} + \tilde{C}_f \dot{x} + \tilde{K}_f x &= F_f u \\ y &= H_f \ddot{x} \end{aligned} \quad (4.16)$$

Suppose that the acceleration of the original second order model (3.13) is  $A(s)$  and the acceleration of the approximate second order model (4.16) is  $\tilde{A}(s)$ . The original acceleration  $A(s)$  is given by

$$A(s) = H_f s^2 (M_f s^2 + C_f s + K_f)^{-1} F_f \quad (4.17)$$

The approximate accelerance  $\tilde{A}(s)$  is expressible as

$$\tilde{A}(s) = H_f s^2 (M_f s^2 + \tilde{C}_f s + \tilde{K}_f)^{-1} F_f \quad (4.18)$$

The approximation error  $E(s)$  induced by removing the small connecting elements is expressed as

$$E(s) = A(s) - \tilde{A}(s) \quad (4.19)$$

To simplify the approximate error, the following identity is used.

$$(A + B)^{-1} = A^{-1} - (A + B)^{-1} B A^{-1} \quad (4.20)$$

Using (4.20), the approximation error can be rewritten as

$$E(s) = A(s) - \tilde{A}(s) = -H_f s^2 \Delta (M_f s^2 + \tilde{C}_f s + \tilde{K}_f)^{-1} F_f \quad (4.21)$$

where  $\Delta = (M_f s^2 + C_f s + K_f)^{-1} (C_r s + K_r)$ .

Usually, the relative error  $E(s)A^{-1}(s)$  is more useful, but its expression is so complicated that it is not helpful in determining how the omitted connecting elements are related to the approximation error. In particular, for a SISO mechanical system, the relative error can be expressed as

$$\frac{E(s)}{A(s)} = F_f^T (C_r s + K_r) (M_f s^2 + \tilde{C}_f s + \tilde{K}_f)^{-1} F_f \quad (4.22)$$

which means the relative error is equal to the (1, 1) element in the square matrix  $(C_r s + K_r)(M_f s^2 + \tilde{C}_f s + \tilde{K}_f)^{-1}$  dependent on the complex number  $s$ .

Norms such as the  $H_2$  and  $H_\infty$  norms of the approximation error may be adopted as

$$\begin{aligned} \|E(s)\|_\infty &= \|A(s) - \tilde{A}(s)\|_\infty = \max_\omega |A(j\omega) - \tilde{A}(j\omega)| \quad \text{SISO case} \\ \|E(s)\|_\infty &= \|A(s) - \tilde{A}(s)\|_\infty = \max_\omega \sigma_{max}(A(j\omega) - \tilde{A}(j\omega)) \quad \text{MIMO case} \end{aligned}$$

$$\|E(s)\|_2 = \sqrt{\frac{1}{2\pi} \int_{-\infty}^{\infty} \text{trace} \left( (A(j\omega) - \tilde{A}(j\omega))^H (A(j\omega) - \tilde{A}(j\omega)) \right) d\omega} \quad (4.23)$$

where  $\sigma_{max}$  denotes the largest singular value of a matrix.

### 4.1.3 Numerical Examples

In this section, several numerical examples are used to demonstrate how searching the space of realizable congruent transformations is carried out. Each example involves five steps as listed below.

1. Check whether the given model (3.9) satisfies (3.3) and figure out which type of mechanical realization it belongs to;
2. Mass normalize the given second order model, resulting in a new second order model (3.17) with an identity mass matrix;
3. Put the input and output influence vectors (or matrices) into the desired forms with the orthogonal component  $R_{IO}$ ;
4. Convert the damping and stiffness matrices into desired forms while preserving the input and output vectors (or matrices) with another orthogonal component  $R_e$ ;
5. Solve for the final mass matrix  $M_f$ .

In each numerical example discussed below, only the fourth step is detailed since the other steps were discussed in detail in Chapter 3.

#### Mechanical Realization of SISO Driving-point Accelerances

Here, two examples of mechanical systems describing driving-point accelerances are used to demonstrate both an exhaustive search and a nonlinear search using (4.2) in the space of parameterized congruent coordinate transformations,  $R_e$ .

#### Example 1: Four-mass Mechanical System

An initial second order model in realizable form with its accelerance shown in Figure 4.1 is given by

$$\begin{aligned}
 & \begin{bmatrix} 7.6941 & 0 & 0 & 0 \\ 0 & 0.0220 & 0 & 0 \\ 0 & 0 & 0.2502 & 0 \\ 0 & 0 & 0 & 0.1616 \end{bmatrix} \ddot{x} + \begin{bmatrix} 0.3770 & -0.0177 & -0.1450 & -0.2143 \\ -0.0177 & 0.0178 & 0 & -0.0001 \\ -0.1450 & 0 & 0.1450 & 0 \\ -0.2143 & -0.0001 & 0 & 0.2144 \end{bmatrix} \dot{x} \\
 & + \begin{bmatrix} 14444 & 0 & -10633 & -3810 \\ 0 & 474 & -474 & 0 \\ -10633 & -474 & 11528 & -421 \\ -3810 & 0 & -421 & 4232 \end{bmatrix} x = \begin{bmatrix} 1 \\ 0 \\ 0 \\ 0 \end{bmatrix} u \\
 & y = \begin{bmatrix} 1 & 0 & 0 & 0 \end{bmatrix} \ddot{x}
 \end{aligned} \tag{4.24}$$

The magnitude level at low frequencies is close to the reciprocal of the total mass. In particular, at zero frequency, it is exactly the reciprocal of total mass. In contrast, the magnitude at the high frequency range closely approaches the reciprocal of the base mass.

According to Table 3.1, the number of 2-D rotation free parameters is 3. With the orthogonal transformation matrix (3.68), the result of the exhaustive search in the solution space is shown in Figure 4.2, where a three-degree angle grid is used. The shaded areas are realizable regions with colors specifying different numbers of connecting elements between masses. It would be expected that realizations with fewer connecting elements are located at the boundary between realizable and unrealizable regions because some elements in damping and stiffness matrices change their signs at the boundary.

According to the properties of the orthogonal component  $R_e$ , given in Appendix D, realizations in different regions are related to each other by permutation matrices. By removing all redundant realizable regions, the minimum set of the realizable regions can

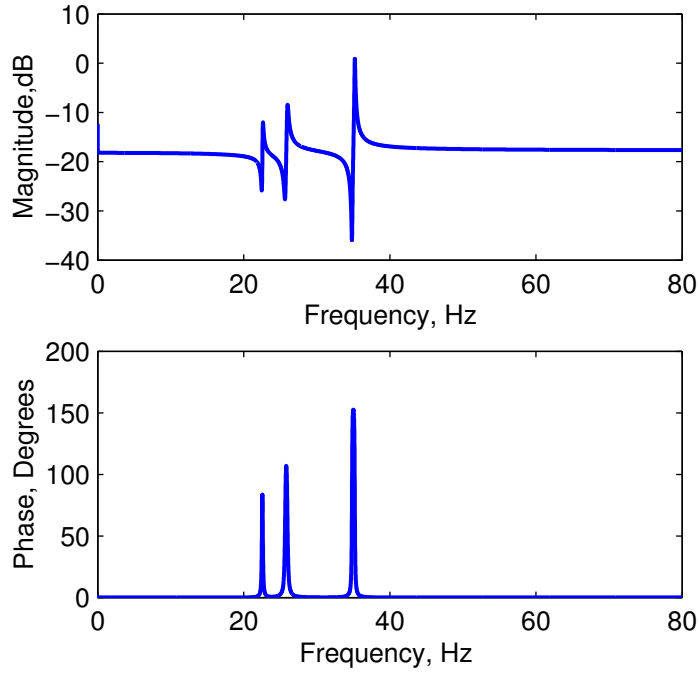


Figure 4.1: Driving-point Accelerance of a Second Order Model

be obtained and is depicted in Figure 4.3. Two realization examples from this region are presented here. They possess the same accelerance as the initial second order model (4.24). Since the initial model (4.24) is already a realization with the fewest connecting elements, the following examples have more connecting elements.

**Realization 1:** When angles are chosen as  $\theta_1 = 300^\circ$ ,  $\theta_2 = 90^\circ$  and  $\theta_3 = 200^\circ$ , the realizable second order model is obtained as follows

$$\begin{bmatrix} 7.6941 & & & \\ & 0.2179 & & \\ & & 0.1616 & \\ & & & 0.0542 \end{bmatrix} \ddot{q} + \begin{bmatrix} 0.3770 & -0.1236 & -0.2143 & -0.0391 \\ -0.1236 & 0.1279 & 0 & -0.0043 \\ -0.2143 & 0 & 0.2144 & -0.0001 \\ -0.0391 & -0.0043 & -0.0001 & 0.0435 \end{bmatrix} \dot{q}$$



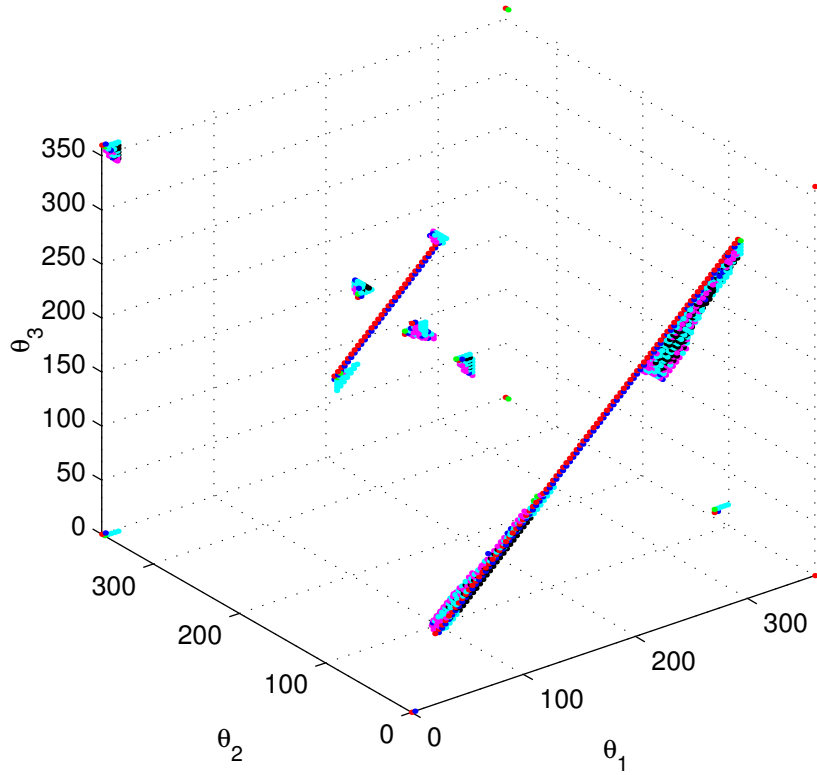


Figure 4.2: Realizable Regions for the Driving-point Accelerance: Red - 7 connectors; Green - 8 connectors; Blue - 9 connectors; Magenta - 10 connectors; Cyan - 11 connectors; Black - 12 connectors.

$$\begin{aligned}
 & + \begin{bmatrix} 14444 & -9774 & -3810 & -860 \\ -9774 & 10358 & -387 & -197 \\ -3810 & -387 & 4232 & -34 \\ -860 & -197 & -34 & 1091 \end{bmatrix} q = \begin{bmatrix} 1 \\ 0 \\ 0 \\ 0 \end{bmatrix} u \\
 & y = \begin{bmatrix} 1 & 0 & 0 & 0 \end{bmatrix} \ddot{q}
 \end{aligned} \tag{4.25}$$

In this realization, there is one more damping element and two more stiffness elements than the original realization (4.24).

**Realization 2:** When angles are given by  $\theta_1 = 300^\circ$ ,  $\theta_2 = 80^\circ$  and  $\theta_3 = 200^\circ$ , a realizable second order model with fully populated damping and stiffness matrices is

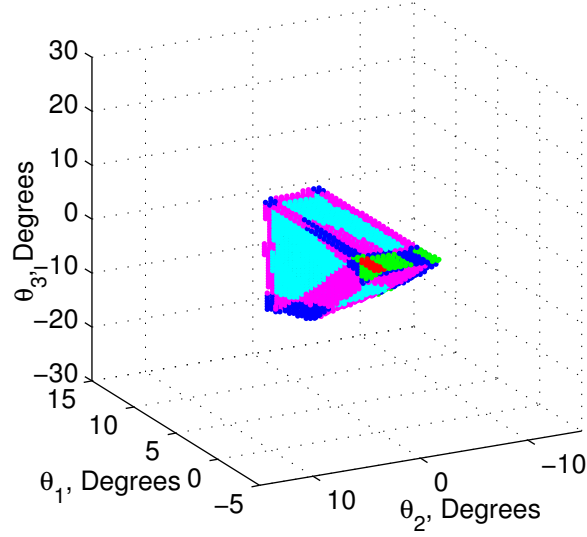


Figure 4.3: Minimum Realizable Region for the Driving-point Accelerance

achieved as follows

$$\begin{aligned}
 & \begin{bmatrix} 7.6941 \\ 0.1945 \\ 0.2131 \\ 0.0262 \end{bmatrix} \ddot{q} + \begin{bmatrix} 0.3770 & -0.1022 & -0.2623 & -0.0125 \\ -0.1022 & 0.1147 & -0.0101 & -0.0024 \\ -0.2623 & -0.0101 & 0.2789 & -0.0066 \\ -0.0125 & -0.0024 & -0.0066 & 0.0214 \end{bmatrix} \dot{q} \\
 & + \begin{bmatrix} 14444 & -8960 & -5161 & -323 \\ -8960 & 9280 & -212 & -107 \\ -5161 & -212 & 5478 & -105 \\ -323 & -107 & -105 & 535 \end{bmatrix} q = \begin{bmatrix} 1 \\ 0 \\ 0 \\ 0 \end{bmatrix} u \\
 & y = \begin{bmatrix} 1 & 0 & 0 & 0 \end{bmatrix} \ddot{q}
 \end{aligned} \tag{4.26}$$

Although the initial model (4.24) and two realizations (4.25) and (4.26) have different mass, damping and stiffness matrices, they have several common features: (1) the same driving-point accelerance; (2) the same total mass and base mass; (3) the same damping

and stiffness associated with the base mass.

### Example 2: Ten-mass Mechanical System

According to Table 3.1, the number of 2-dimensional rotation parameters for a ten-mass system is 36 so an exhaustive search of this space is impractical. Therefore, a nonlinear search with the cost function defined by (4.2) is carried out. The vectors and matrices in the second order model (3.29) after mass normalization and alignment of input and output influence vectors are given below. The given damping matrix is not a weighted sum of the mass and stiffness matrices.

$$\begin{aligned}
 C_{\ddot{z}} &= 10^{-2} \times \begin{bmatrix} 2.7128 & 0.5884 & 0.9063 & 0.3057 & 0.2789 & 0.0366 & -0.5277 & 0.3770 & -0.8588 & 0.1026 \\ 0.5884 & 2.2130 & -0.4462 & 0.1803 & -0.5566 & -0.0037 & 0.1355 & 0.3250 & 0.7427 & -0.2086 \\ 0.9063 & -0.4462 & 3.2407 & 0.1044 & -0.7221 & 0.1187 & 0.2252 & 0.5407 & 0.8267 & 0.1413 \\ 0.3057 & 0.1803 & 0.1044 & 2.4779 & -0.0200 & -0.5379 & -0.1216 & -0.8723 & 0.8624 & -0.1269 \\ 0.2789 & -0.5566 & -0.7221 & -0.0200 & 2.5065 & -0.5251 & -0.0023 & 0.3179 & -0.1601 & -0.0073 \\ 0.0366 & -0.0037 & 0.1187 & -0.5379 & -0.5251 & 3.2081 & -0.3332 & 0.0705 & 0.0055 & -0.0668 \\ -0.5277 & 0.1355 & 0.2252 & -0.1216 & -0.0023 & -0.3332 & 2.9139 & -0.3074 & -0.2305 & 0.1764 \\ 0.3770 & 0.3250 & 0.5407 & -0.8723 & 0.3179 & 0.0705 & -0.3074 & 2.7448 & 0.5058 & -0.6769 \\ -0.8588 & 0.7427 & 0.8267 & 0.8624 & -0.1601 & 0.0055 & -0.2305 & 0.5058 & 2.5958 & 0.5924 \\ 0.1026 & -0.2086 & 0.1413 & -0.1269 & -0.0073 & -0.0668 & 0.1764 & -0.6769 & 0.5924 & 3.5425 \end{bmatrix} \\
 K_{\ddot{z}} &= 10^4 \times \begin{bmatrix} 1.6685 & 0.5279 & 0.2255 & 0.0964 & 0.2052 & 0.1663 & -0.3627 & 0.0432 & -0.6797 & 0.0093 \\ 0.5279 & 1.1712 & -0.0615 & -0.0742 & 0.0952 & 0.0664 & -0.1747 & -0.2261 & 0.3368 & -0.2184 \\ 0.2255 & -0.0615 & 1.3728 & -0.1508 & -0.3500 & 0.0709 & 0.2709 & -0.0669 & 0.3985 & 0.1844 \\ 0.0964 & -0.0742 & -0.1508 & 1.5194 & -0.0821 & -0.0457 & 0.0360 & -0.0362 & 0.4447 & 0.0249 \\ 0.2052 & 0.0952 & -0.3500 & -0.0821 & 1.7704 & -0.0591 & -0.0855 & -0.0525 & 0.2505 & -0.2485 \\ 0.1663 & 0.0664 & 0.0709 & -0.0457 & -0.0591 & 1.9298 & -0.0199 & 0.1753 & 0.1535 & 0.0034 \\ -0.3627 & -0.1747 & 0.2709 & 0.0360 & -0.0855 & -0.0199 & 1.3734 & -0.1139 & -0.0153 & 0.2045 \\ 0.0432 & -0.2261 & -0.0669 & -0.0362 & -0.0525 & 0.1753 & -0.1139 & 1.6008 & 0.0808 & -0.1654 \\ -0.6797 & 0.3368 & 0.3985 & 0.4447 & 0.2505 & 0.1535 & -0.0153 & 0.0808 & 1.5770 & 0.3236 \\ 0.0093 & -0.2184 & 0.1844 & 0.0249 & -0.2485 & 0.0034 & 0.2045 & -0.1654 & 0.3236 & 1.9318 \end{bmatrix} \\
 F_{\ddot{z}} &= H_{\ddot{z}}^T = \begin{bmatrix} 1 & 0 & 0 & 0 & 0 & 0 & 0 & 0 & 0 & 0 \end{bmatrix}^T
 \end{aligned}$$

The initial guess for the set of 2-dimensional rotation angles was generated by random numbers within the angle range from 0 to  $2\pi$ . The Nelder-Mead nonlinear minimization method was used for the search. At each iteration, a maximum of 2500 evaluations of the cost function was permitted. The search terminates when a realizable model is found.

Since the search is initiated by random numbers, results vary from trial to trial. The results of one trial, comprising six iterations, are as follows.

$$\begin{aligned}
 & M_f = \text{diag}([ 1.0000 \quad 0.5897 \quad 0.2208 \quad 0.3018 \quad 0.4610 \quad 0.3100 \quad 0.3778 \quad 0.1229 \quad 0.3782 \quad 0.5211 ]) \\
 C_f = 10^{-2} \times & \begin{bmatrix} 2.7128 & -0.4864 & -0.0520 & -0.1772 & -0.5985 & -0.2404 & -0.2864 & -0.0659 & -0.4470 & -0.3590 \\ -0.4864 & 1.8425 & -0.0005 & -0.0719 & -0.5606 & -0.0152 & -0.2845 & -0.0205 & -0.0673 & -0.3355 \\ -0.0520 & -0.0005 & 0.7682 & -0.1320 & -0.0733 & -0.1213 & -0.0533 & -0.0006 & -0.1780 & -0.1572 \\ -0.1772 & -0.0719 & -0.1320 & 0.8836 & -0.0622 & -0.1643 & -0.0609 & -0.0001 & -0.1234 & -0.0916 \\ -0.5985 & -0.5606 & -0.0733 & -0.0622 & 1.4538 & -0.0001 & -0.0023 & -0.0123 & -0.0421 & -0.1024 \\ -0.2404 & -0.0152 & -0.1213 & -0.1643 & -0.0001 & 0.8747 & -0.2050 & -0.0001 & -0.0992 & -0.0291 \\ -0.2864 & -0.2845 & -0.0533 & -0.0609 & -0.0023 & -0.2050 & 1.2671 & -0.0013 & -0.2212 & -0.1522 \\ -0.0659 & -0.0205 & -0.0006 & -0.0001 & -0.0123 & -0.0001 & -0.0013 & 0.1040 & -0.0004 & -0.0028 \\ -0.4470 & -0.0673 & -0.1780 & -0.1234 & -0.0421 & -0.0992 & -0.2212 & -0.0004 & 1.2354 & -0.0569 \\ -0.3590 & -0.3355 & -0.1572 & -0.0916 & -0.1024 & -0.0291 & -0.1522 & -0.0028 & -0.0569 & 1.2867 \end{bmatrix} \\
K_f = 10^4 \times & \begin{bmatrix} 1.6685 & -0.4698 & -0.0265 & -0.1705 & -0.1809 & -0.2239 & -0.1058 & -0.0074 & -0.1632 & -0.3205 \\ -0.4698 & 1.0694 & -0.0007 & -0.0809 & -0.1432 & -0.0702 & -0.2497 & -0.0315 & -0.0041 & -0.0193 \\ -0.0265 & -0.0007 & 0.3609 & -0.0754 & -0.0129 & -0.0278 & -0.0135 & -0.0422 & -0.0718 & -0.0900 \\ -0.1705 & -0.0809 & -0.0754 & 0.4805 & -0.0295 & -0.0759 & -0.0004 & -0.0068 & -0.0407 & -0.0004 \\ -0.1809 & -0.1432 & -0.0129 & -0.0295 & 0.6300 & -0.1016 & -0.0522 & -0.0001 & -0.1088 & -0.0008 \\ -0.2239 & -0.0702 & -0.0278 & -0.0759 & -0.1016 & 0.6269 & -0.0876 & -0.0359 & -0.0008 & -0.0033 \\ -0.1058 & -0.2497 & -0.0135 & -0.0004 & -0.0522 & -0.0876 & 0.6655 & -0.0096 & -0.1182 & -0.0285 \\ -0.0074 & -0.0315 & -0.0422 & -0.0068 & -0.0001 & -0.0359 & -0.0096 & 0.1967 & -0.0178 & -0.0453 \\ -0.1632 & -0.0041 & -0.0718 & -0.0407 & -0.1088 & -0.0008 & -0.1182 & -0.0178 & 0.5453 & -0.0199 \\ -0.3205 & -0.0193 & -0.0900 & -0.0004 & -0.0008 & -0.0033 & -0.0285 & -0.0453 & -0.0199 & 0.5280 \end{bmatrix} \\
& F_f = H_f^T = [ 1 \quad 0 \quad 0 \quad 0 \quad 0 \quad 0 \quad 0 \quad 0 \quad 0 \quad 0 ]^T
 \end{aligned}$$

As expected, this model has the same driving-point accelerance as the initial model, as depicted in Figure 4.4. The damping and stiffness matrices have many small connecting elements which may be removed by the technique discussed in Subsection 4.1.2. The number of damping and stiffness elements which need to be kept depends on the desired approximate error limit. After the damping elements smaller than 0.001 and stiffness elements less than 50 have been removed, for instance, the resulting approximate damping and stiffness matrices are given by

$$C_a = 10^{-2} \times \begin{bmatrix} 2.5949 & -0.4864 & 0 & -0.1772 & -0.5985 & -0.2404 & -0.2864 & 0 & -0.4470 & -0.3590 \\ -0.4864 & 1.6671 & 0 & 0 & -0.5606 & 0 & -0.2845 & 0 & 0 & -0.3355 \\ 0 & 0 & 0.5885 & -0.1320 & 0 & -0.1213 & 0 & 0 & -0.1780 & -0.1572 \\ -0.1772 & 0 & -0.1320 & 0.5969 & 0 & -0.1643 & 0 & 0 & -0.1234 & 0 \\ -0.5985 & -0.5606 & 0 & 0 & 1.2615 & 0 & 0 & 0 & 0 & -0.1024 \\ -0.2404 & 0 & -0.1213 & -0.1643 & 0 & 0.7310 & -0.2050 & 0 & 0 & 0 \\ -0.2864 & -0.2845 & 0 & 0 & 0 & -0.2050 & 1.1493 & 0 & -0.2212 & -0.1522 \\ 0 & 0 & 0 & 0 & 0 & 0 & 0 & -0.0000 & 0 & 0 \\ -0.4470 & 0 & -0.1780 & -0.1234 & 0 & 0 & -0.2212 & 0 & 0.9695 & 0 \\ -0.3590 & -0.3355 & -0.1572 & 0 & -0.1024 & 0 & -0.1522 & 0 & 0 & 1.1063 \end{bmatrix}$$

$$K_a = 10^4 \times \begin{bmatrix} 1.6685 & -0.4698 & -0.0265 & -0.1705 & -0.1809 & -0.2239 & -0.1058 & -0.0074 & -0.1632 & -0.3205 \\ -0.4698 & 1.0646 & 0 & -0.0809 & -0.1432 & -0.0702 & -0.2497 & -0.0315 & 0 & -0.0193 \\ -0.0265 & 0 & 0.3602 & -0.0754 & -0.0129 & -0.0278 & -0.0135 & -0.0422 & -0.0718 & -0.0900 \\ -0.1705 & -0.0809 & -0.0754 & 0.4797 & -0.0295 & -0.0759 & 0 & -0.0068 & -0.0407 & 0 \\ -0.1809 & -0.1432 & -0.0129 & -0.0295 & 0.6291 & -0.1016 & -0.0522 & 0 & -0.1088 & 0 \\ -0.2239 & -0.0702 & -0.0278 & -0.0759 & -0.1016 & 0.6228 & -0.0876 & -0.0359 & 0 & 0 \\ -0.1058 & -0.2497 & -0.0135 & 0 & -0.0522 & -0.0876 & 0.6651 & -0.0096 & -0.1182 & -0.0285 \\ -0.0074 & -0.0315 & -0.0422 & -0.0068 & 0 & -0.0359 & -0.0096 & 0.1966 & -0.0178 & -0.0453 \\ -0.1632 & 0 & -0.0718 & -0.0407 & -0.1088 & 0 & -0.1182 & -0.0178 & 0.5404 & -0.0199 \\ -0.3205 & -0.0193 & -0.0900 & 0 & 0 & 0 & -0.0285 & -0.0453 & -0.0199 & 0.5234 \end{bmatrix}$$

In so doing, 26 dashpots out of 45 dashpots and 8 springs out of 45 springs have been removed. The accelerance of the approximate model is also depicted in Figure 4.4.

## Mechanical Realization of SISO Transfer Accelerances

Two examples of SISO transfer accelerances are presented here. The first example is a four-mass system and the second is a five-mass system. The angle regions where realizations exist are found by exhaustive search in the solution space of congruent coordinate transformations.

### 1. Four-mass Example

According to Table 3.1, the dimension of the solution space of the congruent coordinate transformation is one. Assume the force excitation is applied at the first coordinate and the acceleration is measured at the second coordinate. To preserve the input and output influence vectors  $e_1$  and  $e_2$ , the orthogonal transformation  $R_e$

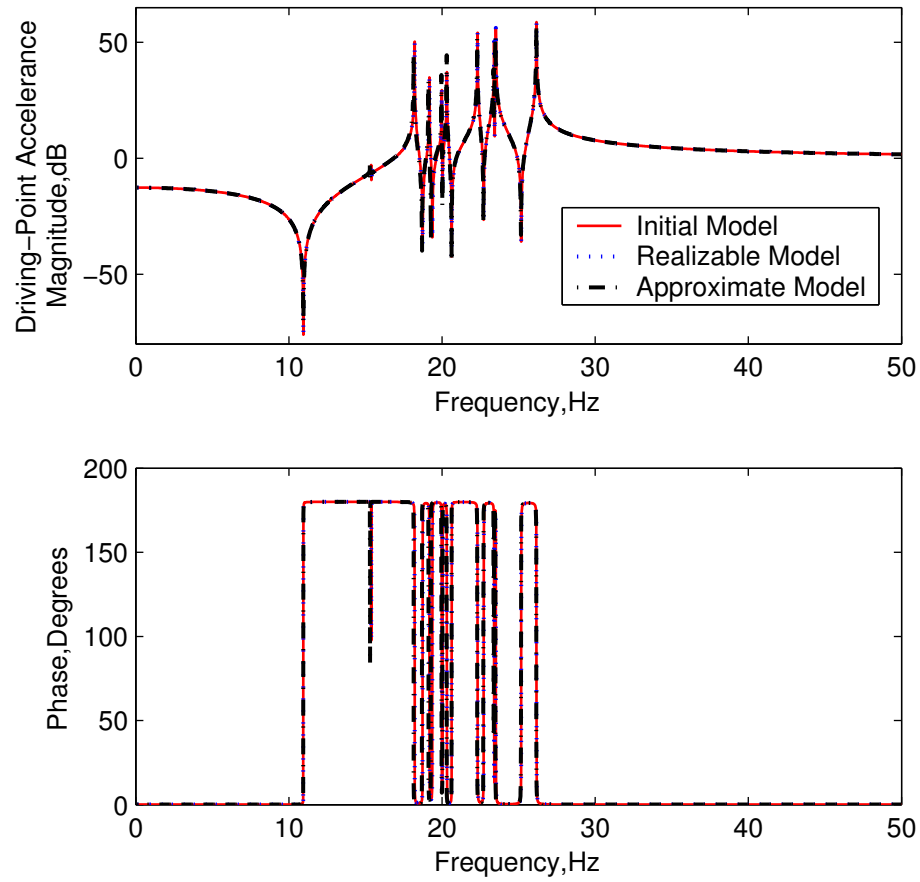


Figure 4.4: Driving-point Accelerance of a Mechanical System with Ten Masses

should have the following form

$$R_e = \begin{bmatrix} 1 & 0 & 0 & 0 \\ 0 & 1 & 0 & 0 \\ 0 & 0 & \cos\theta & -\sin\theta \\ 0 & 0 & \sin\theta & \cos\theta \end{bmatrix} \quad (4.27)$$

An initial second order model describing a transfer accelerance of a four-mass system

is given by

$$\begin{aligned}
& \begin{bmatrix} 2180 & -780 & -164 & -168 \\ -780 & 2211 & -513 & -110 \\ -164 & -513 & 1027 & 2 \\ -168 & -110 & 2 & 76 \end{bmatrix} \ddot{x} + \begin{bmatrix} 6100 & -5560 & 614 & 112 \\ -5560 & 10928 & -6735 & 120 \\ 614 & -6735 & 13163 & 154 \\ 112 & 120 & 154 & 32 \end{bmatrix} \dot{x} \\
& + \begin{bmatrix} 44840 & -31595 & -3245 & 1290 \\ -31595 & 55460 & -13255 & 1460 \\ -3245 & -13255 & 42380 & 790 \\ 1290 & 1460 & 790 & 320 \end{bmatrix} x = \begin{bmatrix} 2 \\ 4 \\ -1 \\ 4 \end{bmatrix} u \\
& y = \begin{bmatrix} -20 & 3 & 5 & 2 \end{bmatrix} \ddot{x} \quad (4.28)
\end{aligned}$$

By exhaustive search, the angle region where realizations exist, is presented in Figure 4.5. Here, a 0.1 degree angle grid is used and realizations exist in the region ranging from  $233.8^\circ$  to  $263.4^\circ$ . It should be noted that some realizations may exist between  $233.7^\circ$  and  $233.8^\circ$  and between  $263.4^\circ$  and  $263.5^\circ$ . With a finer angle grid, it is found that the number of damping elements can range from five to six. This is also true for the stiffness elements. Since the number of them cannot reach five at the same time, the total number of connecting elements in realizations range from eleven to twelve. At the angle  $263.4912^\circ$ , the realization with the fewest stiffness elements is obtained as follows

$$\begin{bmatrix} 2.0000 & 0 & 0 & 0 \\ 0 & 5.0000 & 0 & 0 \\ 0 & 0 & 5.2086 & 0 \\ 0 & 0 & 0 & 0.7914 \end{bmatrix} \ddot{q} + \begin{bmatrix} 8.0000 & -1.0000 & -4.1626 & -2.8374 \\ -1.0000 & 13.0000 & -7.5460 & -4.4540 \\ -4.1626 & -7.5460 & 14.4830 & -2.7744 \\ -2.8374 & -4.4540 & -2.7744 & 10.0658 \end{bmatrix} \dot{q}$$

$$\begin{aligned}
& + \begin{bmatrix} 80.0000 & -20.0000 & -41.3192 & -18.6808 \\ -20.0000 & 90.0000 & -55.9819 & -14.0181 \\ -41.3192 & -55.9819 & 97.3011 & -0.0000 \\ -18.6808 & -14.0181 & -0.0000 & 32.6990 \end{bmatrix} q = \begin{bmatrix} 1 \\ 0 \\ 0 \\ 0 \end{bmatrix} u \\
& y = \begin{bmatrix} 0 & 1 & 0 & 0 \end{bmatrix} \ddot{q} \quad (4.29)
\end{aligned}$$

which indicates no direct stiffness connection between the third and fourth masses.

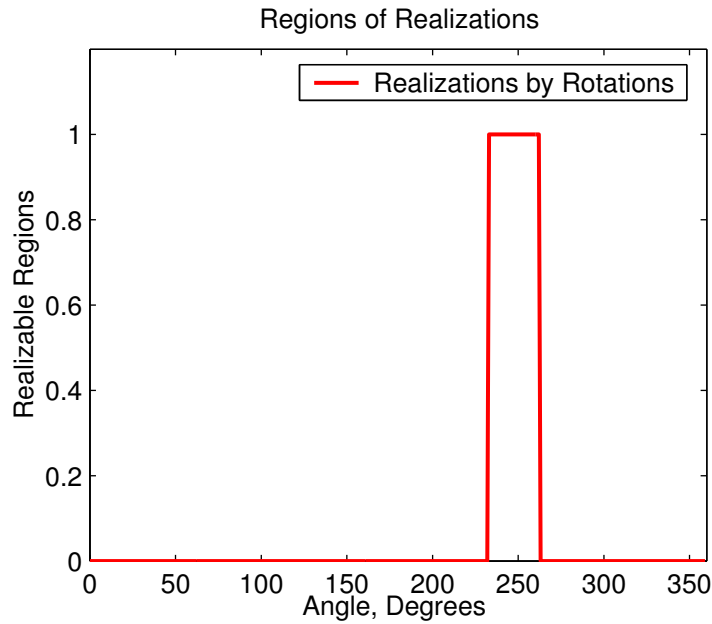


Figure 4.5: Realizable Region for a Four-mass System of a SISO Transfer Accelerance

## 2. Five-mass Example

In this case, the dimension of the solution space is three, according to Table 3.1. Assume the force excitation is applied at the first coordinate and the acceleration is measured at the second one.

The orthogonal transformation  $R_e$  thus is given by

$$R_e = R_{\theta_1} R_{\theta_2} R_{\theta_3} \quad (4.30)$$



where  $R_{\theta_1}$ ,  $R_{\theta_2}$  and  $R_{\theta_3}$  are expressible as

$$R_{\theta_1} = \begin{bmatrix} 1 & 0 & 0 & 0 & 0 \\ 0 & 1 & 0 & 0 & 0 \\ 0 & 0 & \cos\theta_1 & -\sin\theta_1 & 0 \\ 0 & 0 & \sin\theta_1 & \cos\theta_1 & 0 \\ 0 & 0 & 0 & 0 & 1 \end{bmatrix}$$

$$R_{\theta_2} = \begin{bmatrix} 1 & 0 & 0 & 0 & 0 \\ 0 & 1 & 0 & 0 & 0 \\ 0 & 0 & 1 & 0 & 0 \\ 0 & 0 & 0 & \cos\theta_2 & -\sin\theta_2 \\ 0 & 0 & 0 & \sin\theta_2 & \cos\theta_2 \end{bmatrix}$$

$$R_{\theta_3} = \begin{bmatrix} 1 & 0 & 0 & 0 & 0 \\ 0 & 1 & 0 & 0 & 0 \\ 0 & 0 & \cos\theta_3 & 0 & -\sin\theta_3 \\ 0 & 0 & 0 & 1 & 0 \\ 0 & 0 & \sin\theta_3 & 0 & \cos\theta_3 \end{bmatrix}$$

The initial second order model of the transfer accelerance is given by

$$\begin{bmatrix} 36.0632 & 0.2743 & 7.0077 & 37.1531 & -14.0227 \\ 0.2743 & 16.5796 & -6.7431 & 5.5551 & 2.1107 \\ 7.0077 & -6.7431 & 17.1533 & 16.6964 & -13.3775 \\ 37.1531 & 5.5551 & 16.6964 & 61.9214 & -25.8255 \\ -14.0227 & 2.1107 & -13.3775 & -25.8255 & 17.8591 \end{bmatrix} \ddot{x} +$$

$$\begin{aligned}
& \begin{bmatrix} 97.2937 & -57.5426 & 91.8234 & 72.4757 & -38.5575 \\ -57.5426 & 62.9875 & -56.3684 & -51.0698 & 29.9845 \\ 91.8234 & -56.3684 & 92.8620 & 64.1156 & -37.4205 \\ 72.4757 & -51.0698 & 64.1156 & 60.7210 & -27.3858 \\ -38.5575 & 29.9845 & -37.4205 & -27.3858 & 34.8577 \end{bmatrix} \dot{x} + \\
& \begin{bmatrix} 931.9559 & -207.5005 & 567.4285 & 768.4827 & -618.2834 \\ -207.5005 & 383.5154 & -262.6956 & -186.1123 & 172.2111 \\ 567.4285 & -262.6956 & 514.7016 & 383.3350 & -393.4070 \\ 768.4827 & -186.1123 & 383.3350 & 709.9495 & -487.2931 \\ -618.2834 & 172.2111 & -393.4070 & -487.2931 & 544.2288 \end{bmatrix} x = \begin{bmatrix} 1.9574 \\ -0.2111 \\ 0.5512 \\ 0.4620 \\ -1.2316 \end{bmatrix} u \\
& y = \begin{bmatrix} 0.5045 & 1.1902 & -1.0998 & -0.3210 & 1.0556 \end{bmatrix} \ddot{x}
\end{aligned} \tag{4.31}$$

which is not in realizable form.

An exhaustive search of transformation space results in Figure 4.6, where realizations exist in the shaded regions. Here, a uniform angle grid of one degree in each search direction is used. According to the properties of the orthogonal transformation  $R_e$  discussed in Appendix D, any one of the six realizable regions includes all possible realizations since realizations in other realizable regions can be mapped to those in this region by permutation matrices. For example, at  $\theta_1 = 36.60^\circ$ ,  $\theta_2 = 235.98^\circ$  and  $\theta_3 = 319.82^\circ$ , a realization with fully populated damping and stiffness matrices is found as follows

$$\begin{bmatrix} 2.0000 & 0 & 0 & 0 & 0 \\ 0 & 5.0000 & 0 & 0 & 0 \\ 0 & 0 & 1.9995 & 0 & 0 \\ 0 & 0 & 0 & 3.9998 & 0 \\ 0 & 0 & 0 & 0 & 10.0008 \end{bmatrix} \ddot{q} +$$

$$\begin{aligned}
 & \begin{bmatrix} 8.5000 & -1.0000 & -4.9993 & -2.0001 & -0.5006 \\ -1.0000 & 13.3000 & -7.9989 & -4.0002 & -3.0009 \\ -4.9993 & -7.9989 & 23.1945 & -9.9978 & -0.1984 \\ -2.0001 & -4.0002 & -9.9978 & 16.1483 & -0.1501 \\ -0.5006 & -0.3009 & -0.1984 & -0.1501 & 1.1500 \end{bmatrix} \dot{q} + \\
 & \begin{bmatrix} 130.0000 & -20.0000 & -34.9942 & -24.9996 & -50.0063 \\ -20.0000 & 92.0000 & -29.9954 & -39.9999 & -2.0047 \\ -34.9942 & -29.9954 & 89.9780 & -14.9956 & -9.9928 \\ -24.9996 & -39.9999 & -14.9956 & 84.9939 & -4.9989 \\ -50.0063 & -2.0047 & -9.9928 & -4.9989 & 67.0028 \end{bmatrix} q = \begin{bmatrix} 1 \\ 0 \\ 0 \\ 0 \\ 0 \end{bmatrix} u \\
 & y = \begin{bmatrix} 0 & 1 & 0 & 0 & 0 \end{bmatrix} \ddot{q}
 \end{aligned} \tag{4.32}$$

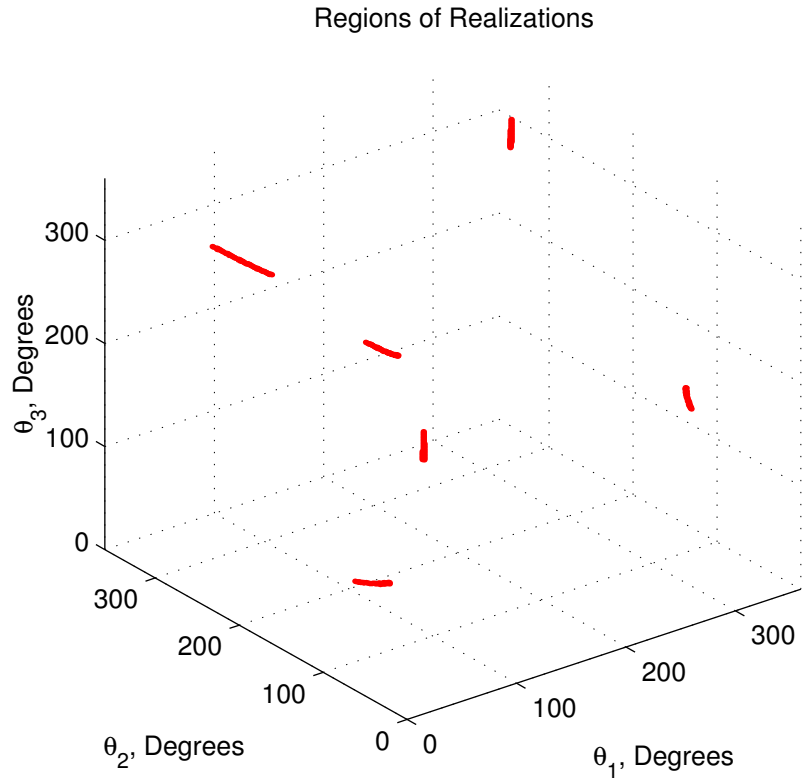


Figure 4.6: Realizable Regions for the Five-Mass Example

These numerical examples have demonstrated that searching the parameterized space of the realization transformations can be effective. This technique assumes that an initial second order model satisfies the necessary conditions appearing at the end of Section 3.1. In contrast, if experimental data are available from machinery, a direct estimation technique for realizable models can be used, which is described below.

## **4.2 Direct Estimation of Realizable Models from Experimental Data**

Experimental frequency response function (FRF) data can be easily acquired from passive machinery. Alternatively, in the application of filter design, a desired transfer function is specified. In either case, it is desired to obtain a mechanical model matching the input-output data. Under these scenarios, a direct model estimation technique can be used, resulting in mechanical realizations possessing a preselected model form.

This technique involves three important aspects: selection of candidate realizable models; choice of appropriate cost functions; and a nonlinear search for unknown parameters in the realizable models. Once a candidate model form is chosen, defined in either the time domain or the frequency domain, the key task is to find the unknown parameters, which have direct relations to the mechanical elements in the model. The cost function should be defined to minimize the error between the experimental FRF data and the FRF of the desired model. Starting from initial guesses for unknown parameters, nonlinear search methods are then applied to estimate these unknown parameters.

### **4.2.1 Direct Estimation Procedure**

As a candidate model form, one can adopt any second order model satisfying all necessary realization conditions discussed in Chapter 3, any transfer function expandable into a desired form, or any other model form corresponding to a physical realization.

To facilitate implementation of mechanical emulators, however, simple realizable mod-

els should be selected whenever possible. In particular, for proportionally damped mechanical systems, canonical model realizations such as parallel or serial realizations should be chosen. Moreover, while damping is nonproportional and light, as discussed in Appendix B, a parallel realization or a serial realization may be used to approximate the desired dynamic properties. In this case, it should be noted that damping is not necessarily assumed to be proportional damping, that is, the damping matrix is not a weighted sum of mass and stiffness matrices per se. For highly damped mechanical systems with strong damping couplings between modes, as also discussed in Appendix B, parallel model realizations and serial model realizations cannot be used in general. Otherwise, significant errors may arise from approximation.

Passive machinery acts as a vibration absorber at its antiresonance frequencies in its foundation driving-point accelerance, as discussed in Chapter 1. Therefore, a cost function should ensure matching of amplitudes and frequencies at both resonance and antiresonance frequencies. Assume all accelerances are put in a column vector form. The cost function for the  $j$ 'th accelerance  $A_{m_j}(f_i)$  should consist of two parts, which are the accelerance error and dynamical mass error. Since these two errors are not necessarily of the same order of magnitude, the cost function for each accelerance is defined as a weighted summation to normalize their contributions

$$J_j = w_{1_j} \sum_{i=0}^{i=n} |A_{m_j}(f_i) - A_{r_j}(f_i)|^2 + w_{2_j} \sum_{i=0}^{i=n} \left| \frac{1}{A_{m_j}(f_i)} - \frac{1}{A_{r_j}(f_i)} \right|^2 \quad (4.33)$$

where the subscript  $m$  stands for “machinery”, the subscript  $r$  stands for “realization”.

In (4.33),  $A_{m_j}(f_i)$  and  $A_{r_j}(f_i)$  are accelerances of the  $j$ 'th machinery accelerance data from measurements and the  $j$ 'th accelerance in the realization at the frequency point  $f_i$ , respectively. The two weighting factors are given by

$$w_{1_j} = 1$$

$$w_{2j} = \frac{\sum_{i=0}^{i=n} |A_{m_j}(f_i)|^2}{\sum_{i=0}^{i=n} \left| \frac{1}{A_{m_j}(f_i)} \right|^2} \quad (4.34)$$

If one only needs to match the  $j$ 'th accelerance of a realization with experimental data, then the above cost function  $J_j$  is enough. Otherwise, a total cost function can be obtained by the following equation to match all accelerances simultaneously,

$$J = \sum_{j=1}^{j=n_A} \tilde{w}_j J_j \quad (4.35)$$

where  $n_A$  is the number of accelerances and  $\tilde{w}_j$ 's are weighting factors. These weighting factors should be chosen so that the contributions from all accelerances are balanced.

The resulting nonlinear optimization problem is solvable by many techniques, such as those discussed in [77]. In this research, the Nelder-Mead simplex method is adopted since it is robust for strongly nonlinear problems [78] [73]. To initiate the search, initial values should be provided for the unknown parameters. Good initial values may be obtained by comparing the accelerance of the model with initial values to the experimental accelerance. For a parallel or serial model realization, all initial masses can be assigned based on an understanding of the passive machinery mass properties. The initial spring constants  $k_{o_i}$  ( $i=1, 2, \dots, n-1$ ) then can be calculated from the following relations

$$k_{o_i} = m_{o_i} (2\pi f_{o_i})^2 \quad (4.36)$$

where  $m_{o_i}$  is the  $i$ 'th oscillator mass and  $f_{o_i}$  is the  $i$ 'th oscillator antiresonance frequency obtained from the experimental data.

The dimensionality of this nonlinear estimation depends on the number of unknown parameters in the realizable model form. For a second order model in parallel or serial form, given by (2.18) and (2.20), respectively, for a mechanical system with  $n$  masses, the

dimensionality is  $3n - 2$ . In contrast, if fully populated damping and stiffness matrices are adopted, the dimensionality is  $n^2$ . As discussed in Appendix B, a parallel model realization or a serial model realization may be a good approximation to a mechanical system with light damping. Although a realization with fully populated damping and stiffness matrices can model a given mechanical system accurately, it can be both difficult and expensive to implement, especially with a large number of masses. A tradeoff between them is to use a model with a border diagonal stiffness matrix and a fully populated damping matrix. In this case, the dimensionality is  $\frac{3n - 2}{2} + \frac{n^2}{2}$ , which is the average between the parallel model and the fully populated model. In so doing, damping is approximated, but this approximation may be quite accurate.

It often happens that the identified second order model has elements with small values compared to other elements of the same type. In this case, these elements may be removed, resulting in a simpler mechanical system without causing much error.

This direct estimation technique will be extensively used in the design of passive mechanical emulators in Section 5.1 of Chapter 5 and Section 6.3 of Chapter 6. Two examples of the approach are presented here.

### 4.2.2 Direct Estimation Examples

In this subsection, the procedure and performance of the direct model estimation are demonstrated with two examples, comprised of four and six masses, respectively. In the first example, a fully populated second order model is used while for the latter, a parallel model is adopted.

#### Four-mass Example

For this example, the driving-point accelerance data, shown in Figure 4.7, was collected from a mechanical system of four lumped masses connected by viscoelastic elements. The accelerance level in the low frequency range is flat, which indicates a rigid body mode. In addition, each mode should be associated with a mass. Thus, four masses are needed

in the realizable model. A fully populated second order model satisfying all realizability conditions, is chosen as follows

$$\begin{aligned}
 & \begin{bmatrix} |m_1| \\ |m_2| \\ |m_3| \\ |m_4| \end{bmatrix} \ddot{x} + \begin{bmatrix} \sum_{i=2}^{i=4} |c_{1i}| & -|c_{12}| & -|c_{13}| & -|c_{14}| \\ -|c_{21}| & \sum_{i=1, i \neq 2}^{i=4} |c_{2i}| & -|c_{23}| & -|c_{24}| \\ -|c_{31}| & -|c_{32}| & \sum_{i=1, i \neq 3}^{i=4} |c_{3i}| & -|c_{34}| \\ -|c_{41}| & -|c_{42}| & -|c_{43}| & \sum_{i=1, i \neq 4}^{i=4} |c_{4i}| \end{bmatrix} \dot{x} \\
 & + \begin{bmatrix} \sum_{i=2}^{i=4} |k_{1i}| & -|k_{12}| & -|k_{13}| & -|k_{14}| \\ -|k_{21}| & \sum_{i=1, i \neq 2}^{i=4} |k_{2i}| & -|k_{23}| & -|k_{24}| \\ -|k_{31}| & -|k_{32}| & \sum_{i=1, i \neq 3}^{i=4} |k_{3i}| & -|k_{34}| \\ -|k_{41}| & -|k_{42}| & -|k_{43}| & \sum_{i=1, i \neq 4}^{i=4} |k_{4i}| \end{bmatrix} x = e_1 u \\
 & y = e_1^T \dot{x}
 \end{aligned} \tag{4.37}$$

where absolute values are used to force the resulting mass, damping and stiffness elements to be nonnegative.

By initiating the nonlinear search with an initial guess of a parallel model realization, a mechanical realization is obtained, as depicted in Figure 4.8. As expected, very good accelerance matching in the range of frequency has been achieved, as illustrated in Figure 4.7.

### Six-mass Example

The driving-point accelerance from a machinery test bed is depicted in Figure 4.9. The



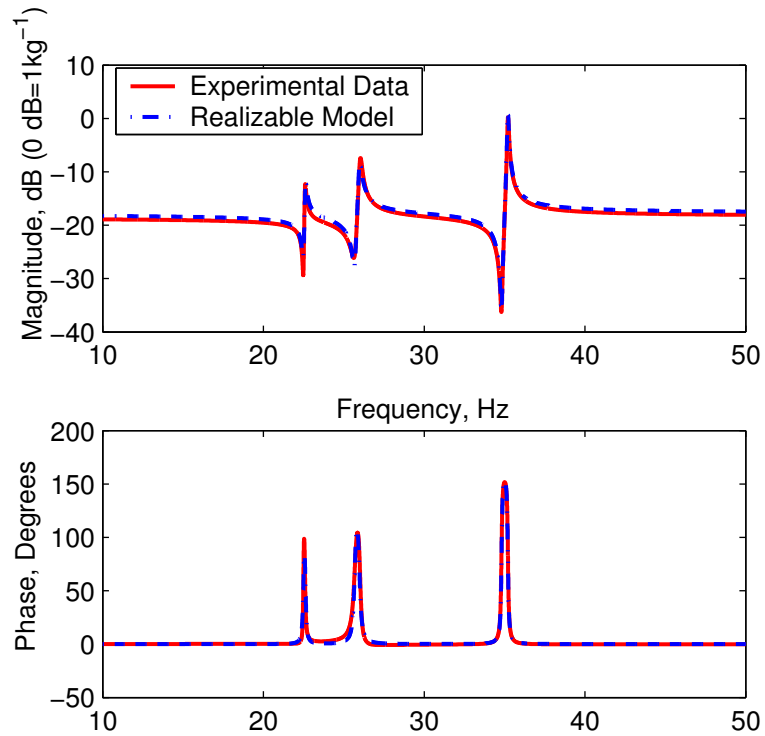


Figure 4.7: Example 1: Driving-point Accelerance Comparison of Experimental Data and Identified Realizable Model

plot reveals a rigid body mode along with five modes at higher frequencies. Since the modes exhibit sharp peaks around their resonance and antiresonance frequencies, a parallel model (2.18) can be used, as discussed in Appendix B. Note that in (2.18), the damping matrix is not assumed to be a weighted sum of the mass and stiffness matrices. Since the data below 10 Hz are noisy due to the usable frequency range of the impedance head, the cost function is defined between 10 Hz and 100 Hz. Using direct estimation, a parallel model, shown in Figure 4.10, is identified with its masses, dashpots and spring constants listed in Table 4.1. Magnitude comparison of the experimental and parallel model accelerances in Figure 4.9 indicates that good agreement has been achieved except for some amplitude discrepancy between 50 Hz and 70 Hz. Good agreement is also obtained in the phase plots, which are not included here.

In this subsection, two examples demonstrating direct estimation from experimental

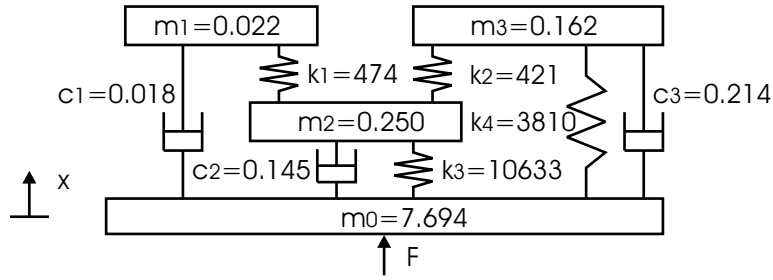


Figure 4.8: Example 1: Identified Mechanical Model

Table 4.1: Parameters in the Parallel Model Estimated by Direct Estimation

Number of Oscillator $i$	$m_i, kg$	$c_i, N \cdot s/m$	$k_i, N/m$	$f_i = \sqrt{k_i/m_i}, Hz$
0	1.876			
1	0.100	0.164	3161	28.30
2	0.0815	0.1621	4034	35.41
3	0.1586	0.173	8500	36.84
4	0.0351	0.0503	2815	45.08
5	0.0894	0.121	8787	49.89

data have been presented. This technique can also be used to estimate damping associated with a mode, as are discussed in Subsection 5.1.5. More complicated applications of this technique are addressed in Chapter 6, where a passive mechanical emulator is designed and implemented.

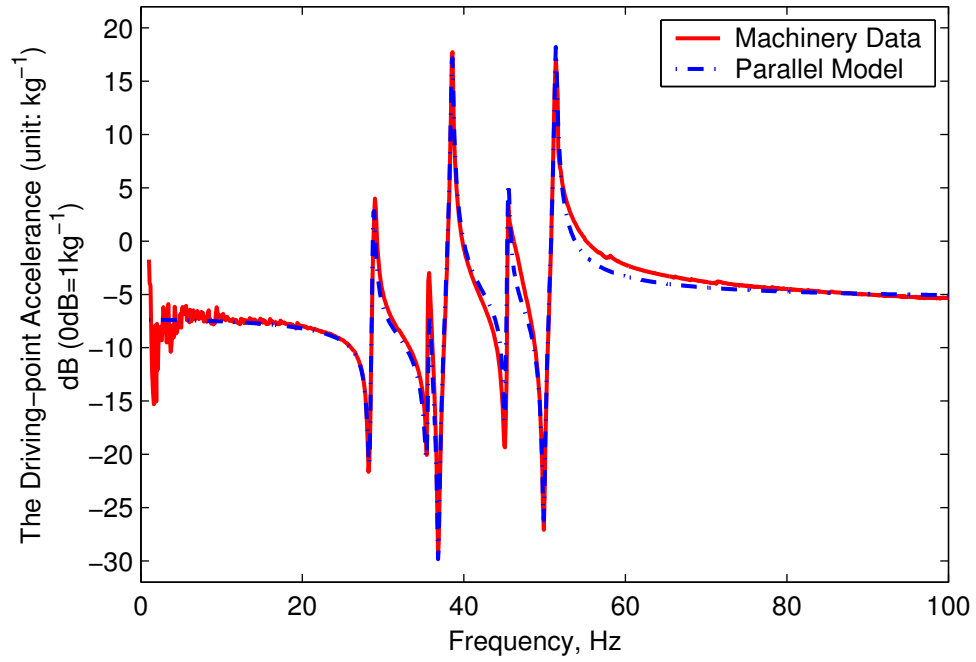


Figure 4.9: Example 2: Driving-point Accelerance of Experimental Data and the Identified Realizable Model

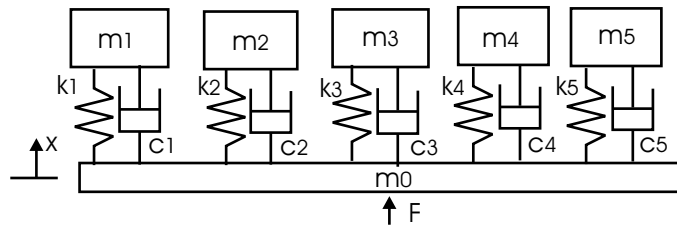


Figure 4.10: Example 2: The Identified Mechanical Model

## Chapter 5

# Mechanical Emulator Design

## Methodology

Technology feeds on itself. Technology makes more technology possible.

Alvin Toffler (1928- )

Given a model in realizable form, this chapter presents a systematic design methodology for implementing this model as a passive or active emulator. From the view of the attachment points where machinery is mounted to its supporting structure, machinery and its mechanical emulator must have the same dynamics, that is, they must have the same rigid body modes and frequency responses within the frequency range of interest. To this end, there are two design goals for a passive emulator: (1) matching mass and moment of inertia between machinery and its passive mechanical emulator; (2) matching their attachment point accelerances in the frequency range of interest. For active mechanical emulator design, a third design goal is to reproduce the attachment point acceleration of the operating machinery.

## 5.1 Passive Emulator Design

In this chapter, it is assumed that the passive mechanical emulator undergoes rigid-body motions in the horizontal, vertical and planar rotational coordinate directions, which should match those of the passive machinery as well as possible. In addition, the motion in the horizontal direction has many modes in the frequency range of interest. The design methodology presented here can be extended to the design of more complicated mechanical emulators, for example, those with many modes both in the horizontal and vertical directions.

### 5.1.1 Modular Design

While all undamped or proportionally damped mechanical systems can be converted to parallel model realizations in the form of (2.18), for nonproportionally damped mechanical systems, this is not the case. While realizations with border diagonal stiffness matrices (parallel springs) can always be obtained, the associated damping matrices may be fully populated. For ease of implementation, however, the realizable model should be made as simple as possible. Therefore, in the the passive mechanical emulator design discussed in this chapter, a border diagonal stiffness matrix is always used, and damping is approximated by minimizing the error between a model with the desired damping matrix and experimental data of the passive machinery. The guideline for choice of the desired damping matrix form is that it should be simple whenever possible. In the simplest case for implementation, a border diagonal matrix is also used, resulting in a parallel model realization. If the matching between the realizable model and experimental data is not as good as expected, more damping connections between oscillators may be required.

Following this approach, a passive emulator model is shown in Figure 5.1. It consists of a base frame, a round mounting rod, two identical vertical bars, an additional mass and a desired number of oscillators (eight in the figure). The base frame is fabricated from metal plates such that its modes lie above the frequency range of interest. The

round mounting rod stiffens the base frame and is used to mount oscillators to the frame by fixtures which are not shown in the figure. The additional mass is used to satisfy mass matching requirements and is connected to the base frame by two identical vertical bars with appropriately designed dimensions. Each oscillator is composed of block masses clamped on a spring steel plate with damping layers on its surface. Depending on the damping connections in the identified realizable model, damping elements may be applied between two oscillators, a situation not shown in Figure 5.1. The modular mechanical components for the oscillators and base frame were designed and fabricated as described in [71].

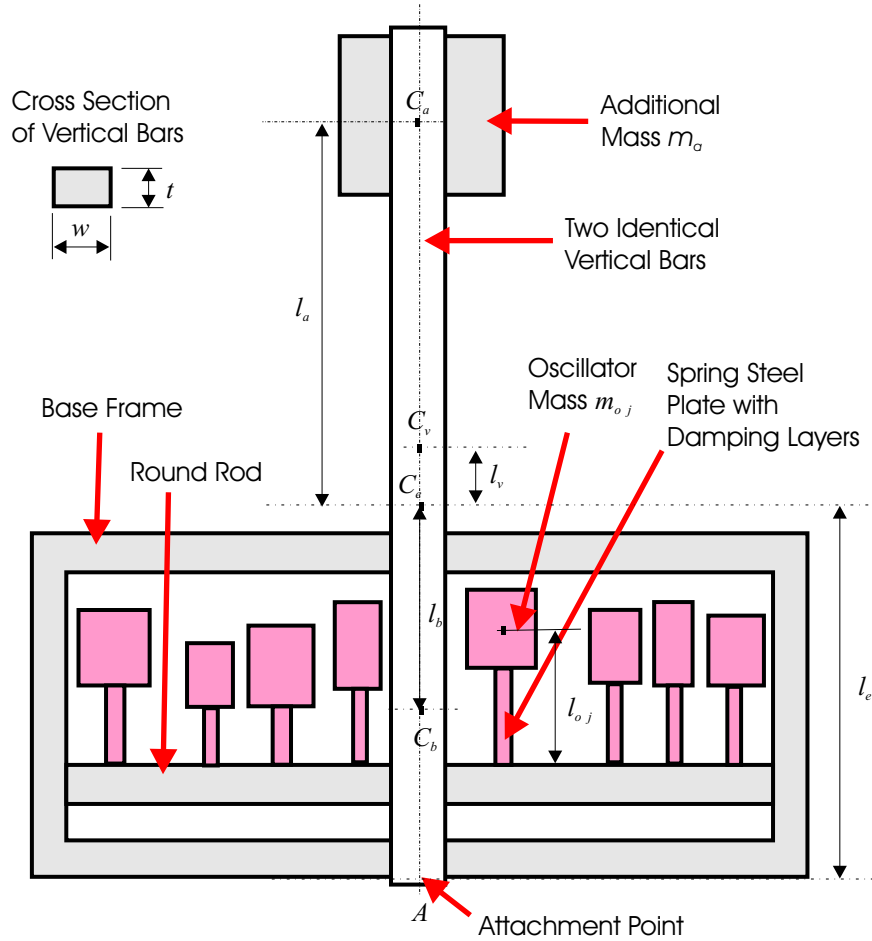


Figure 5.1: Side View of the Passive Mechanical Emulator

Since the mass of the base frame is far greater than that of an oscillator, the oscillator can be approximated as a block mass at the tip of a cantilever beam. An oscillator with the desired fixed-base resonance frequency can be obtained by adjusting the distance from the mounting fixture to the oscillator mass. Given the desired frequency of the oscillator, the length of the beam can be estimated either by a continuous model or by a lumped-parameter model, as described in Appendix F.

The substructure comprised of the two identical vertical bars connecting the additional mass and the base frame can be considered a rigid body if the fundamental mode of this substructure is outside the frequency range of interest. Due to the mass constraint, however, the two vertical bars are not very stiff and so the mode associated with bending of these bars may often fall within the frequency range of interest. In this situation, the two identical vertical bars should be designed so that this structural mode can match that passive machinery mode with apparent mass closest to the apparent mass of this structural mode.

The major parameters of the passive mechanical emulator are defined in Table 5.1.

### 5.1.2 Mass Matching Requirements

For matching of mass and moment of inertia, the passive machinery and its passive emulator can be idealized as the simple model depicted in Figure 5.2, where  $A$  is the attachment point of the passive machinery,  $m$  is the total mass,  $C$  is the center of mass and  $I_C$  is the moment of inertia with respect to the center of mass  $C$ .

To match rigid-body motions in the vertical coordinate direction, the passive machinery and its emulator should have the same total mass,  $m_m = m_e$ , where the subscripts  $m$  and  $e$  stand for “machinery” and “emulator”, respectively. Moreover, to match the rigid body rotational mode, the passive machinery and its emulator must possess the same moment of inertia with respect to the attachment point  $A$ ,  $I_{mA} = I_{eA}$ , where the second subscript stands for “attachment point”.

In the horizontal coordinate direction, however, the apparent mass viewed at the at-

Table 5.1: Notation for the parameters in the Passive Mechanical Emulator

Item	Definition	Determined by
$m_t$	Total mass of the passive mechanical emulator	Given passive machinery
$m_a$	Additional mass	Equation (5.13)
$m_b$	Total mass of the base frame, round rod and mounting fixtures	Less than the apparent base mass
$m_{o_j}$	$j'th$ oscillator mass	Estimation in Subsection 5.1.4
$m_v$	Mass of a vertical bar	Total and base masses
$I_{C_b}$	Moment of inertia of the base frame, round rod and mounting fixtures with respect to its own center of mass $C_b$	Equation (5.16)
$I_{C_v}$	Moment of inertia of the identical vertical bars with respect to its own center of mass $C_v$	$I_{C_v} = 1/12m_vL_v^2$ , where $L_v$ is the length of the vertical bars
$I_{C_{o_j}}$	Moment of inertia of the $j'th$ oscillator with respect to its center of mass $C_{o_j}$	Oscillator dimensions
$I_{C_a}$	Moment of inertia of the additional mass $m_a$ with respect to its center of mass $C_a$	Additional mass dimensions
$l_e$	Distance from the attachment point of machinery $A$ to that of the passive mechanical emulator $C_e$	Theorem 5.1
$l_a$	Distance from the additional mass center $C_a$ to the mass center of the passive mechanical emulator $C_e$	Equation (5.14)
$l_b$	Distance from the mass center of the base frame, round rod and mounting fixtures $C_b$ to the mass center of the passive mechanical emulator $C_e$	Mass center of $m_b$
$l_v$	Distance from the mass center of vertical bars $C_v$ to the mass center of the passive mechanical emulator $C_e$	Distance between $C_v$ and $C_e$
$l_{o_j}$	Length of the spring steel plate in the $j'th$ oscillator	Required spring constant in the model (5.17)
$E$	Complex Young's modulus of the two identical vertical bars with damping treatments, $E = E_0(1 + j\eta)$ , where $E_0$ is the elastic modulus which is a real number	Material (aluminum here)
$\eta$	Effective loss factor of the two identical vertical bars with damping treatments	Estimation in Subsection 5.1.4
$n_d$	Number of polymeric free damping layers or constrained damping layers	$\eta$ and (5.30) and (5.31)
$w$	Width of the two identical vertical bars	Estimation in Subsection 5.1.4
$t$	Thickness of the two identical vertical bars	Total and base masses



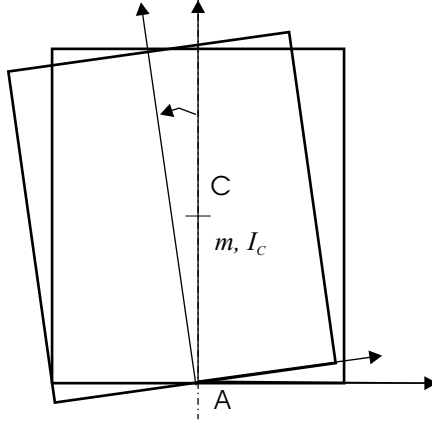


Figure 5.2: Emulator Undergoing Motions in the Horizontal, Vertical and Rotational Coordinates

attachment point is dependent on the total mass and on the moment of inertia  $I_A$  with respect to the attachment point  $A$ . Suppose that a horizontal force  $F$  is applied at the attachment point and the horizontal displacement  $x$  is measured at the same point. The equations of motion are given by the following

$$\begin{aligned}
 I_C \ddot{\theta} &= FL_C \\
 F &= m\ddot{x}_C \\
 x &= x_C + L_C\theta
 \end{aligned} \tag{5.1}$$

where  $x_C$  is the horizontal displacement of the mass center  $C$  and  $\theta$  is the angular displacement away from the vertical coordinate.

By manipulation of (5.1), the apparent mass in the horizontal coordinate direction, defined by the force and acceleration at the same point in the same coordinate direction, can be obtained as follows

$$m_{app}(s) = \frac{F(s)}{a(s)} = \frac{F(s)}{s^2 x(s)} = \frac{m}{1 + \frac{mL_C^2}{I_C}} \tag{5.2}$$

where *app* stands for “apparent mass”. According to this equation, it can be concluded

that the apparent mass  $m_{app}$  in the horizontal coordinate direction is less than the actual total mass  $m$ .

In order to ensure that the passive machinery and its emulator have the same motion in the horizontal coordinate under the same excitation, they must have the same apparent mass in the horizontal coordinate direction,

$$m_{m_{app}} = m_{e_{app}} \quad \text{or} \quad \frac{m_m}{1 + \frac{m_m L_{mC}^2}{I_{mC}}} = \frac{m_e}{1 + \frac{m_e L_{eC}^2}{I_{eC}}} \quad (5.3)$$

where  $L_{mC}$  is the distance from the attachment point of the passive machinery to its mass center and  $L_{eC}$  is the distance from the attachment point of the passive mechanical emulator to its mass center.

In summary, the mass matching requirements between the passive machinery and its passive emulator can be interpreted by the following three equations

$$\begin{aligned} m_m &= m_e \\ \frac{m_m}{1 + \frac{m_m L_{mC}^2}{I_{mC}}} &= \frac{m_e}{1 + \frac{m_e L_{eC}^2}{I_{eC}}} \\ I_{mA} &= I_{eA} \end{aligned} \quad (5.4)$$

These requirements can be reduced to the following theorem.

**Theorem 5.1.** *For the passive machinery and its emulator to have the same dynamic properties in the horizontal, vertical and planar rotational coordinates, they must possess the same total mass, the same location of the mass center with respect to the attachment point and the same moment of inertia with respect to the center of mass, that is,*

$$\begin{aligned} m_m &= m_e \\ L_{mC} &= L_{eC} \\ I_{mC} &= I_{eC} \end{aligned} \quad (5.5)$$

*Proof.* From the first and second equations in (5.4),

$$\frac{L_{mC}^2}{I_{mC}} = \frac{L_{eC}^2}{I_{eC}} \quad \text{or} \quad I_{mC} = \frac{L_{mC}^2}{L_{eC}^2} I_{eC} \quad (5.6)$$

By the parallel axis theorem, the third equation in (5.4) can be rewritten as

$$I_{mC} + m_m L_{mC}^2 = I_{eC} + m_e L_{eC}^2 \quad (5.7)$$

Substituting (5.6) into (5.7), yields

$$\frac{L_{mC}^2}{L_{eC}^2} I_{eC} + m_m L_{mC}^2 = I_{eC} + m_e L_{eC}^2 \quad (5.8)$$

which can be rewritten in the following form with consideration of  $m_m = m_e$ ,

$$m_m (L_{mC}^2 - L_{eC}^2) = \left(1 - \frac{L_{mC}^2}{L_{eC}^2}\right) I_{eC} \quad (5.9)$$

This can be further simplified as

$$(L_{mC}^2 - L_{eC}^2)(m_m L_{eC}^2 + I_{eC}) = 0 \quad (5.10)$$

Since the second term in the above equation does not vanish,

$$L_{mC} = L_{eC} \quad (5.11)$$

Substituting (5.11) into (5.6),

$$I_{mC} = I_{eC} \quad (5.12)$$

□

Theorem 5.1 can be easily extended to more complicated passive emulator design.

By Theorem 5.1, the additional mass  $m_a$  can be determined by

$$m_a = m_t - m_b - \sum_{j=1}^{j=n} m_{o_j} \quad (5.13)$$

where  $n$  is the number of oscillators in the passive mechanical emulator. For the current emulator model in Figure 5.1, the number of the oscillators is  $n = 8$ .

According to the mass center matching, the distance of the additional mass from the mass center of the passive mechanical emulator can be determined by

$$l_a = \frac{m_b l_b + m_v l_v + \sum_{j=1}^{j=n} m_{o_j} l_{o_j}}{m_a}, \quad (5.14)$$

where these parameters have been defined in Table 5.1.

Finally, Theorem 5.1 requires matching of moment of inertia with respect to the attachment point  $A$ . The mass distribution of the passive mechanical emulator should be designed to satisfy the the following constraint

$$I_{eC} = I_{mC} \quad (5.15)$$

Here, the moment of inertia of the passive mechanical emulator is given by

$$I_{eC} = (I_{C_b} + m_b l_b^2) + (I_{C_v} + m_v l_v^2) + \sum_{j=1}^{j=n} (I_{C_{o_j}} + m_{o_j} l_{o_j}^2) + (I_{C_a} + m_a l_a^2), \quad (5.16)$$

where all parameters have been defined in Table 5.1.

In practice, (5.15) can only be approximately satisfied since it is difficult to take into consideration all of the geometric details of the building components. Usually, only the dimensions of the components with large moments of inertia need to be designed carefully.

### 5.1.3 Modeling the Passive Mechanical Emulator Model

When using the model configuration in Figure 5.1 to implement a passive mechanical emulator, one must obtain a dynamic model describing its dynamics in the horizontal coordinate direction. Using a lumped-parameter model or a continuous model depends on whether the bending mode arising from the flexibility of the two vertical bars falls within the frequency range of interest.

Since the passive emulator model is composed of modular units, each unit can be modeled separately. Subsequently, the total model of the passive mechanical emulator can be obtained by the substructure synthesis method [79]. The advantage of this modeling method is that the models for the modular units are reusable.

Define the structure after removing all oscillators in Figure 5.1 as the base structure of the passive mechanical emulator. The attachment points of all oscillators approximately have the same acceleration in the horizontal coordinate direction as the base frame of the passive mechanical emulator. Therefore, the total driving-point accelerance can be obtained by

$$A_t(\omega) = \frac{1}{\frac{1}{A_b(\omega)} + \frac{1}{A_o(\omega)}} \quad (5.17)$$

where  $\omega$  is the frequency in radians per second,  $A_t(\omega)$  is the total driving-point accelerance of the passive mechanical emulator,  $A_b(\omega)$  is the driving-point accelerance of the base structure and  $A_o(\omega)$  is the driving-point accelerance of all oscillators.

The driving-point accelerance of the base structure  $A_b(\omega)$  can be chosen in two ways. In the first, it is selected as the apparent mass of the base structure if the first mode of the base structure has a frequency higher than the upper frequency limit. Under this scenario, the base structure acts like a rigid body without any bending in the two identical vertical bars. The driving-point accelerance of the base structure is given by

$$A_b(\omega) = m_{eapp} = \frac{m_e}{1 + \frac{m_e L_e^2}{I_e C}} \quad (5.18)$$

where the notations have been defined in Subsection 5.1.2. In this case, with the current configuration in Figure 5.1, the model (5.17) in the frequency domain is equivalent to the following second order model in the time domain with  $m_0 = m_b$

$$\begin{aligned} M_e \ddot{x} + C_e \dot{x} + K_e x &= F_e u \\ y &= H_e \ddot{x} \end{aligned} \quad (5.19)$$

which matrices are defined as follows

$$\begin{aligned} M_e &= \text{diag} \left( \begin{bmatrix} m_0 & m_{o_1} & m_{o_2} & \cdots & m_{o_8} \end{bmatrix} \right) \\ C_e &= \begin{bmatrix} \sum_{i=1}^{i=8} c_{o_i} & -c_{o_1} & -c_{o_2} & \cdots & -c_{o_8} \\ -c_{o_1} & c_{o_1} & & & \\ -c_{o_2} & & c_{o_2} & & \\ \vdots & & & \ddots & \\ -c_{o_8} & & & & c_{o_8} \end{bmatrix} \\ K_e &= \begin{bmatrix} \sum_{i=1}^{i=8} k_{o_i} & -k_{o_1} & -k_{o_2} & \cdots & -k_{o_8} \\ -k_{o_1} & k_{o_1} & & & \\ -k_{o_2} & & k_{o_2} & & \\ \vdots & & & \ddots & \\ -k_{o_8} & & & & k_{o_8} \end{bmatrix} \\ H &= F^T = \begin{bmatrix} 1 & 0 & 0 & \cdots & 0 \end{bmatrix} \end{aligned}$$

where  $m_0$  is the apparent base mass,  $e$  stands for “emulator”, the positive parameters  $m_{o_i}$ ,  $c_{o_i}$  and  $k_{o_i}$  ( $i = 1, 2, \dots, 8$ ) are masses, dashpots and springs of oscillators, respectively. Here, the damping matrix  $C_e$  is assumed as a border diagonal matrix, but in general it should be a fully dense realizable matrix.

The second approach to selecting the driving-point accelerance of the base structure

$A_b(\omega)$  is obtained by modeling the base structure using the continuous Euler-Bernoulli beam model, as discussed in Appendix E. This approach applies when the first structural mode of the base structure in Figure 5.1 falls within the frequency range of interest. Under this scenario, the structural mode of the base structure should be used to match the machinery mode that has the closest mass to the structural mode. This oscillator should be removed from the passive mechanical emulator.

All oscillators in Figure 5.1 share the same acceleration in the horizontal coordinate direction. For a border diagonal damping matrix, the driving-point acceleration of all oscillators  $A_o(\omega)$  in (5.17) can also be obtained in two ways. In the first, each oscillator is modeled according to the continuous Euler-Bernoulli beam model. Subsequently, the total model for all oscillators is obtained by the substructure synthesis method, given by

$$A_o(\omega) = \frac{1}{\sum_{i=1}^{i=n} \frac{1}{A_{o_i}(\omega)}}, \quad (5.20)$$

where  $A_{o_i}(\omega)$  is the driving-point acceleration of the  $i$ 'th oscillator, discussed in Appendix F.

Alternatively, the distributed elements of each oscillator can be approximately modeled by lumped-parameter elements, resulting in the acceleration  $A_o(\omega)$  given by

$$A_o(\omega) = \frac{1}{\sum_{i=1}^{i=n} \frac{1}{A_{o_i}(\omega)}}, \quad (5.21)$$

where the driving-point acceleration for the  $i$ 'th oscillator  $A_{o_i}$  is given by

$$A_{o_i}(\omega) = \frac{m_{o_i}s^2 + c_{o_i}s + k_{o_i}}{m_{o_i}(c_{o_i}s + k_{o_i})} \quad (5.22)$$

From (5.17) and (5.21), it can be shown that the anti-resonance frequencies in the driving-point acceleration of the emulator are located at the fixed-base resonance frequencies of the oscillators. Their amplitudes strongly depend on damping. This phenomenon

was called “Shock Spectrum Dip” by Cunniff and O’Hara [80], [81]. These fixed-base undamped resonance frequencies can be determined by

$$f_{o_i} = \frac{1}{2\pi} \sqrt{\frac{k_{o_i}}{m_{o_i}}} \quad (5.23)$$

The loss factors of the oscillators can be obtained by

$$\eta_{o_i} = 2\zeta_{o_i} = \frac{c_{o_i}}{\sqrt{k_{o_i}m_{o_i}}}, \quad (5.24)$$

where  $\eta_{o_i}$  is the damping ratio of the  $i$ 'th oscillator.

For a realizable damping matrix in general form, the total model of all oscillators  $A_o(\omega)$  can be obtained by

$$A_o(\omega) = -H\omega^2(-M\omega^2 + C\omega j + K)F \quad (5.25)$$

#### 5.1.4 Estimation of Unknown Parameters in the Passive Emulator

The unknown parameters in the emulator model (5.17) can be obtained by the direct estimation technique discussed in Section 4.2. The cost function for estimation is defined by

$$J = w_1 \sum_{i=0}^{i=n} |A_t(\omega_i) - A_m(\omega_i)|^2 + w_2 \sum_{i=0}^{i=n} \left| \frac{1}{A_t(\omega_i)} - \frac{1}{A_m(\omega_i)} \right|^2 \quad (5.26)$$

where  $A_m(\omega_i)$  is the driving-point accelerance of the passive machinery measured at the frequency  $\omega_i$  radians per second. Two weighting factors are picked as

$$\begin{aligned} w_1 &= 1 \\ w_2 &= \frac{S_1}{S_2} \end{aligned} \quad (5.27)$$

where  $S_1$  and  $S_2$  are defined by

$$S_1 = \sum_{i=0}^{i=n} |A_m(\omega_i)|^2 \quad (5.28)$$



$$S_2 = \sum_{i=0}^{i=n} \left| \frac{1}{A_m(\omega_i)} \right|^2 \quad (5.29)$$

After solving for all unknown parameters of the passive emulator, the model in Figure 5.1 can be assembled. Its performance should be evaluated experimentally. These two issues will be covered when the implementation of a representative mechanical emulator is described in Chapter 6.

### 5.1.5 Emulator Damping

The desired amount of damping can be achieved through surface damping treatments, which are designed to reduce noise or vibration by dissipating vibrational energy into other forms of energy, mainly heat [82]. Surface damping treatments, including both free-layer damping and constrained-layer damping, are adopted since they are easy to implement. There have been many books and articles on damping as well as the modeling and testing of damping treatments. Examples include the monologues [83], [84] and articles [85], [86], [87], [88], [89], [90].

Usually, it is difficult to precisely model damping since it depends on many factors such as the material properties, temperature, geometric configuration, and the underlying structure. Thus, semi-analytical equations in polynomial form are fit to experimental data according to the least squares method. Both free-layer damping treatments and constrained damping treatments are addressed below.

#### 1. Free-layer Damping Treatments

Free-layer damping treatments consist of layers of damping materials, often polymeric materials, applied to the surface of the structure, as depicted in Figure 5.3. When the structure undergoes deformation, the layers of damping material experience cyclic extensional deformation and so dissipate the mechanical energy. This kind of damping treatment can usually only achieve small loss factors since the extensional deformation is limited.

With free-layer damping treatments, the specified amount of damping can be obtained without significant change in structural stiffness because the damping layers are very soft in comparison. The analytical model between the effective loss factor and the number of free damping layers is called the Oberst equation and is discussed in Appendix G. Experimental measurements are carried out to verify whether the Oberst equation is applicable in the particular free-layer damping treatment material. The modal loss factors are calculated from the measured data associated with different numbers of damping layers and a polynomial is fit to the modal loss factors, resulting in the relation between the number of damping layers and the modal loss factor.

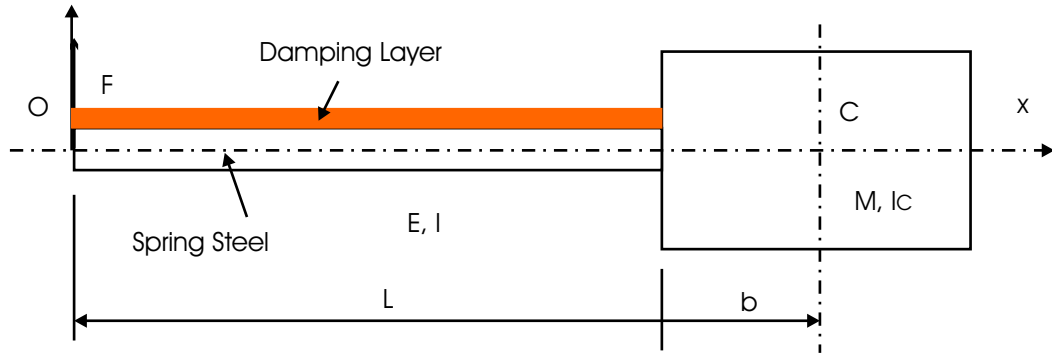


Figure 5.3: Oscillator Model with Free-layer Damping Treatment

In this research,  $3M^{TM}$  viscoelastic damping polymer 112P05 manufactured by  $3M^{TM}$  Industrial Business Electronics Markets Materials Division, is adopted for the free-layer damping treatment. It has a thickness of 0.005 inch for a single layer and a working temperature range from 0 to 65 Celsius degrees [91].

Since it is impossible to obtain the loss factor directly, indirect measurements are used here. In the experiments, an oscillator made from a known mass and a fixed-length spring steel beam with a particular number of 112P05 damping layers is mounted on the round rod of the base frame, which is hung by soft strings, and then the driving-point acceleration at the foundation attachment point is measured.

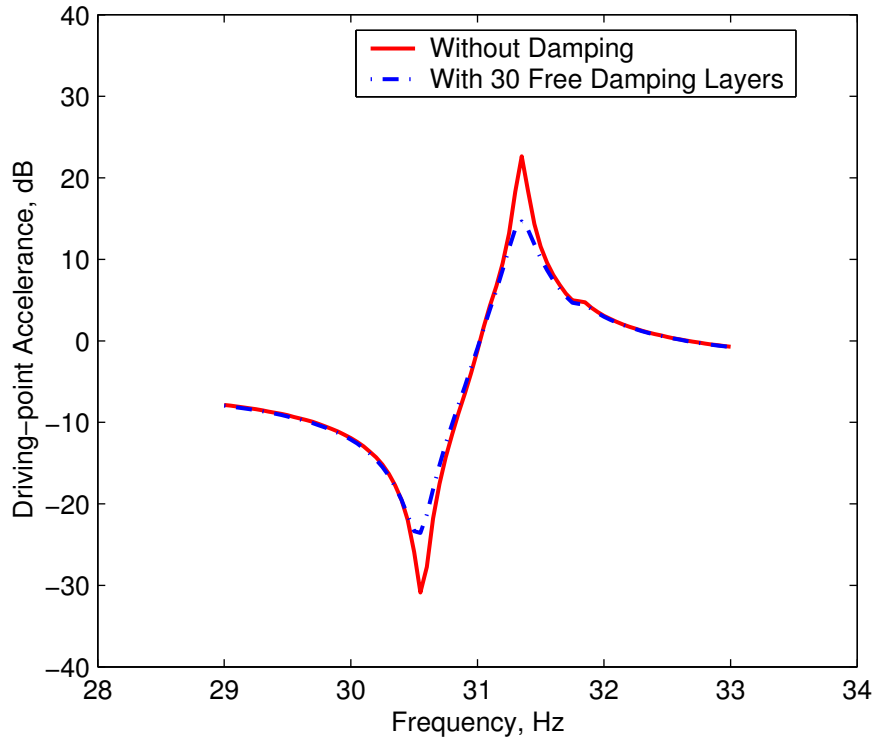


Figure 5.4: Effect of Free Layer Damping Treatments

For damping layer thicknesses between 0 to 30 layers, the driving-point accelerances are measured by slow sinusoidal sweeps, as shown in Figure 5.4. The damping layers do not significantly shift resonance and antiresonance frequencies even with many damping layers. The only significant difference before and after damping treatments of thirty 112P05 damping layers is that the magnitudes around resonance and antiresonance frequencies are changed.

With the direct estimation technique discussed in Section 4.2, a model of a lumped-parameter oscillator with a mass  $m_o$ , dashpot  $c_o$  and spring  $k_o$  connected to a base mass  $m_b$ , as depicted in Figure F.2, is used to fit each set of experimental data associated with a particular number of damping layers. The modal loss factors  $\eta$  then can be estimated by (5.24), as listed in Table 5.2. For the free layer damping treatment, as shown in Figure 5.5, the Oberst equation has very good matching with the measured data as long as the modal loss factor of the beam before treatments is

incorporated in the Oberst equation. The parameters of the damping layer used in the Oberst equation are obtained from the nomograph provided by 3M<sup>TM</sup> Corporation [91], which shows the relation of the viscoelastic damping polymers versus both the loss factor and storage modulus (the real part of the complex Young's modulus) for ranges of frequencies and temperatures.

Table 5.2: The Modal Loss Factors of the Free-layer Damping Treatments Calculated from the Measured Data (modal loss factor of the steel beam before treatments is  $\eta_0 = 2.24 \times 10^{-3}$ ,  $n_d$  is the number of free damping layers,  $\eta$  is modal loss factor of the spring steel beam after treatments.)

$n_d$	$\eta$	$n_d$	$\eta$	$n_d$	$\eta$
1	2.26	11	2.52	21	3.84
2	2.26	12	2.61	22	4.00
3	2.29	13	2.77	23	4.20
4	2.31	14	2.85	24	4.39
5	2.29	15	2.99	25	4.38
6	2.33	16	3.05	26	4.68
7	2.37	17	3.22	27	4.98
8	2.40	18	3.39	28	5.16
9	2.42	19	3.60	29	5.42
10	2.48	20	3.76	30	5.61

Since the loss factor is a rational function of the number of damping layers, as discussed in Appendix G, it is expected that a polynomial can be used to fit the experimental data. With the least squares method, the polynomial is obtained as follows

$$\eta = 10^{-3} \times (0.004305n^2 - 0.01672n + 2.2627) \quad (5.30)$$

With a desired loss factor, the number of free damping layers can be determined by (5.30).

## 2. Constrained-layer Damping Treatments

To obtain a large amount of damping, constrained-layer damping treatments should be used, as shown in Figure 5.6. A polymeric damping layer is constrained between

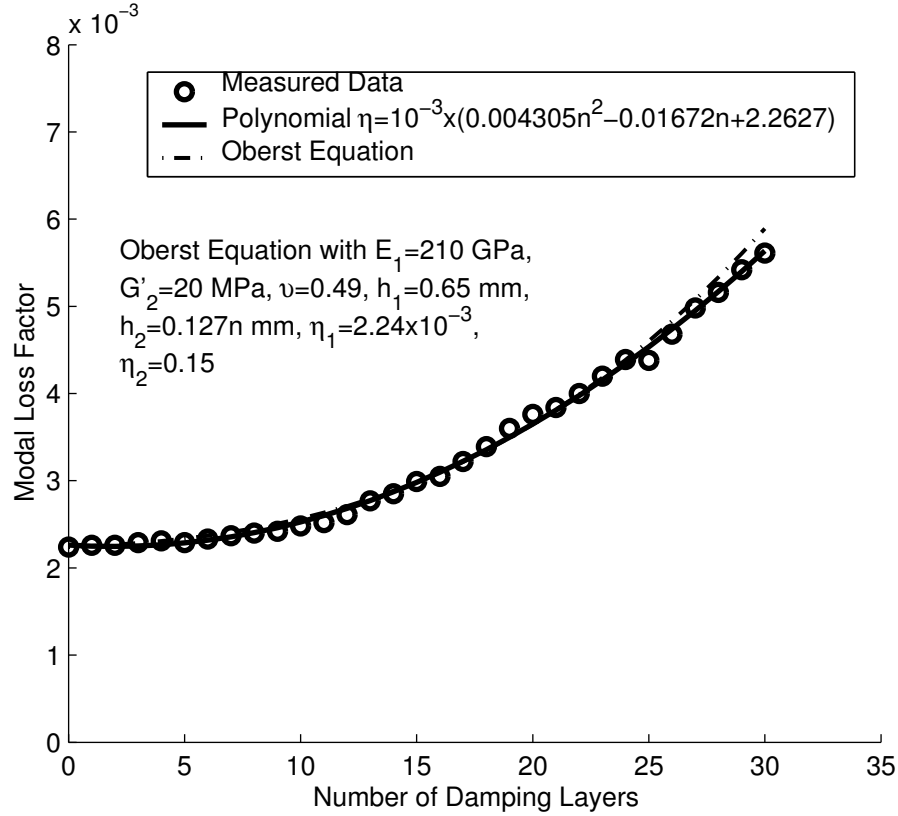


Figure 5.5: Comparison Between the Measured Data, Prediction of the Oberst Equation and the Polynomial of (5.30)

the spring steel beam and the constraining aluminum layer. If one constrained-layer damping layer is not enough to obtain the desired loss factor, then multiple layers can be applied. In contrast to the free-layer damping treatments, these treatments dissipate vibration energy mainly through shear deformations of the damping materials [82]. Modeling of the constrained-layer damping treatments, especially with multiple layers, is quite tedious. Therefore, a polynomial relating the loss factors to the number of layers is obtained based on experimental measurements.

In this research, *Dynaplate<sup>TM</sup>*, a light-weight aluminum constrained layer damper, is used, manufactured by Dynamic Control of North America, Inc. It consists of a thin polymeric damping layer and a constraining aluminum layer. Its specifications can be found in [92]. For this material, the indirect measurement method used in the

free-layer damping treatments is also used. Since the constrained damping layer is relatively stiff, the applied damping layers significantly stiffen the structure. The resonance and antiresonance frequencies increase as shown in Figure 5.7, as the number of layers  $n$  changes from 0 to 10. In addition, the magnitudes at the resonances and antiresonances change dramatically with increasing numbers of constrained damping layers.

Table 5.3: Modal Loss Factor of the Constrained-layer Damping Treatments Calculated from Measured Data (loss factor of the steel beam before treatments  $\eta_0 = 2.97 \times 10^{-3}$ ,  $n_d$  is number of constrained damping layers,  $\eta$  is modal loss factor of the spring steel beam after treatments.)

$n_d$	$\eta$	$n_d$	$\eta$
1	1.13	6	3.10
2	1.58	7	3.45
3	2.03	8	3.63
4	2.40	9	4.41
5	2.78	10	4.22

With the same technique used in the free-layer damping treatments, the modal loss factors are calculated from the measured data of driving-point accelerances with different numbers of constrained damping layers, as listed in Table 5.3. A third order polynomial is fit to the modal loss factors by the least-squares method, resulting in the relation between the number of constrained damping layers and the modal loss factor, given by

$$\eta = 10^{-3} \times (0.0203n^3 - 0.4723n^2 + 6.6957n + 3.8567) \quad (5.31)$$

In summary, several observations can be made on the use of damping treatments:

- (1) For free-layer damping, the farther away the damping layer is from the neutral axis, the more extensional deformation it undergoes. Thus the increment of the modal loss factor per damping layer increases as the number of damping layers increases. For

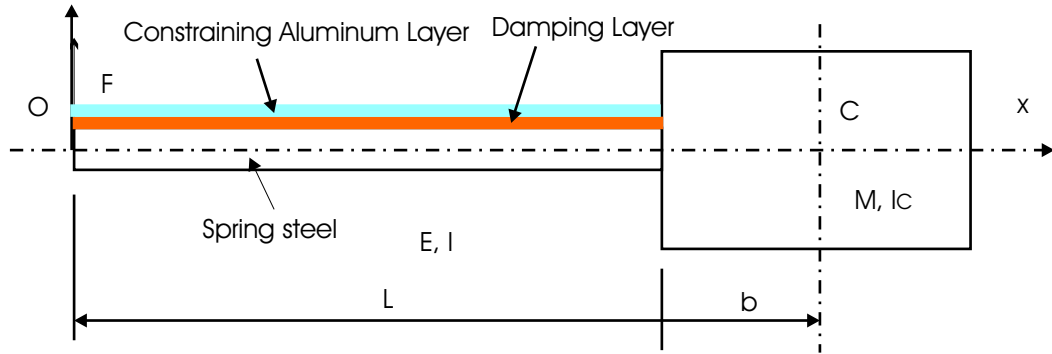


Figure 5.6: Oscillator Model with Constrained-layer Damping Treatments

the constrained-layer damping treatment, however, the increment of the modal loss factor per damping layer decreases as the number of damping layers increases when both ends of the damping layers are not clamped.

(2) By combining the free-layer and constrained-layer damping treatments, any desired amount of loss factor may be obtained quite accurately.

(3) Damping properties of polymeric layers depend on temperature, excitation frequency, dimensions and the configuration. Placing damping materials in the location where they will undergo the largest extensional deformation, maximizes their contribution to modal loss factor. For example, spacers can be used as shown in Figures 5.9 to increase damping.

### 5.1.6 Design and Implementation Steps for Passive Emulators

The design and implementation of passive mechanical emulators, as discussed in this section, are summarized below:

#### 1. Passive Mechanical Emulators with a Single Coordinate Direction

Step 1: Obtain the realizable second order model (3.13) by either one of the two techniques discussed in Chapter 4;

Step 2: Interpret the realizable mass, damping and stiffness matrices as a network of mechanical elements;

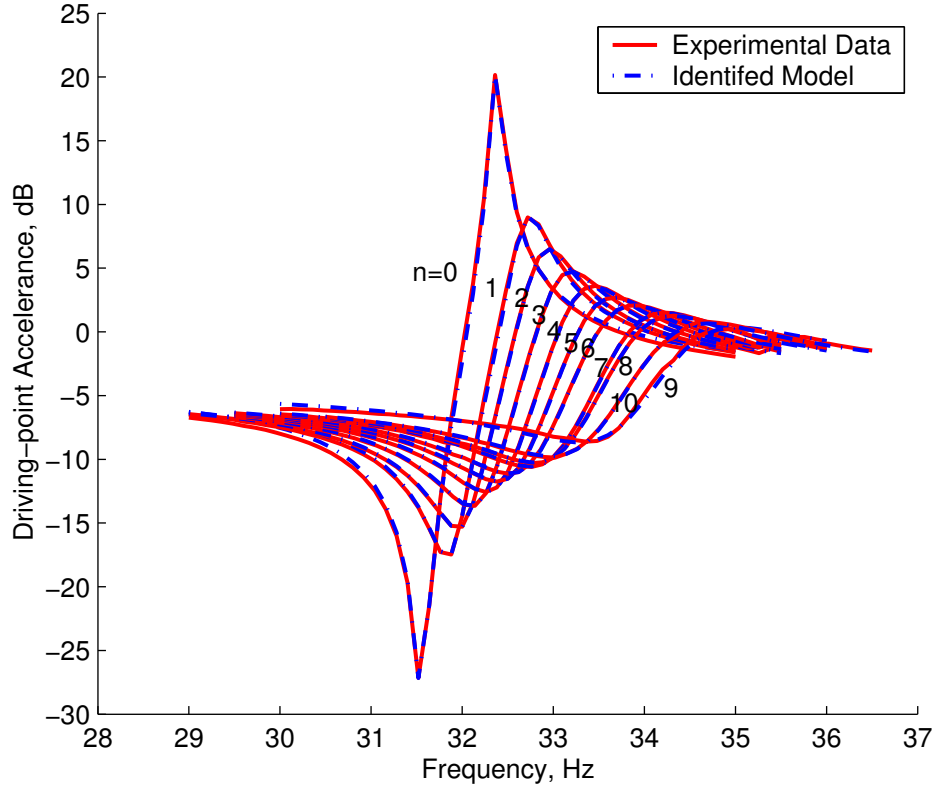


Figure 5.7: Effect of Constrained Layer Damping on Frequency and Amplitude

Step 3: Realize the desired mass, damping and stiffness by modular mechanical elements, including block masses, polymeric damping layers and elastic beams, respectively. The number of damping layers is determined by (5.30) and (5.31). After properly choosing the cross section, the length of each elastic beam can be determined by any nonlinear zero finding technique, as discussed in Appendix F.

## 2. Passive Mechanical Emulators with Multiple Coordinate Directions

Depending on whether motions in different coordinate directions are coupled or not, passive mechanical emulators can be categorized as two types. For the first type, there are no couplings of dynamic properties between different coordinate directions. Therefore, the apparent total and base masses in each coordinate direction are equal to the actual total and base masses, respectively. In this case, the steps for design and implementation of single coordinate direction emulators are simply repeated for



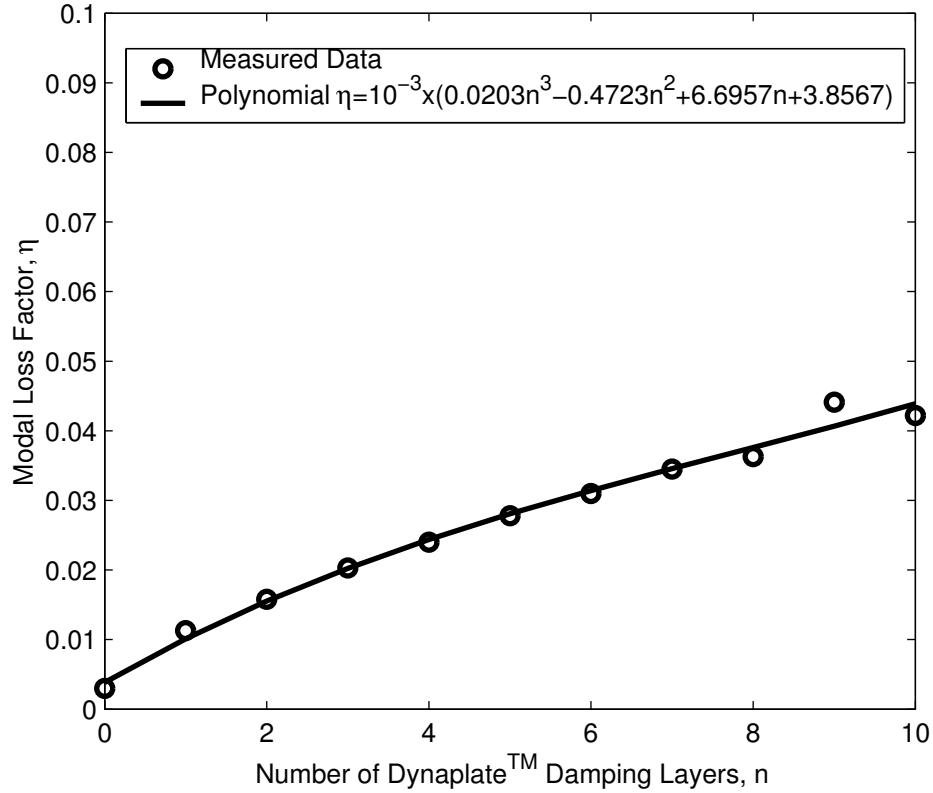


Figure 5.8: Relation of Loss Factor and Number of Constrained Damping Layers

each coordinate direction.

When the coordinate directions are coupled, however, the apparent total and base masses in each coordinate direction may be different from the actual total and base masses. In this case, the apparent total and base masses should be preserved as well as the actual total and base masses. The design and implementation steps are summarized as follows:

Step 1: Match the rigid body modes between passive machinery and its mechanical emulator according to Theorem 5.1 such that the apparent static total and base masses are preserved. After a base frame in Figure 5.1 is selected, the parameters  $m_b$  and  $l_b$  are determined and the additional mass  $m_a$  and the location of its mass center  $l_a$  are then determined by (5.13) and (5.14).

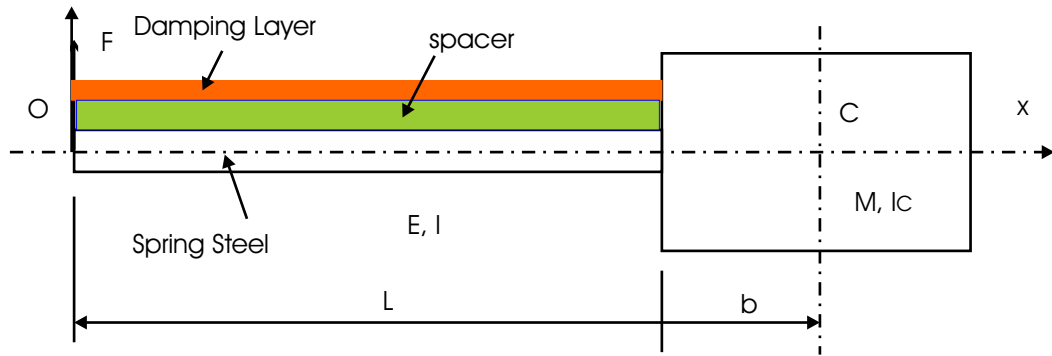


Figure 5.9: Oscillator Model with Free-layer Damping Treatments and a Spacer

Step 2: Obtain realizable models, by either of the two techniques in Chapter 4 for all the coordinate directions of interest. The total and base masses are not the actual ones, but apparent ones, respectively, which have been preserved in the first step.

Step 3: Check whether the structural mode due to the bending of vertical bars connecting the base frame and additional mass falls within the frequency range of interest or not. If it is higher than the upper frequency limit, no further work is necessary in this step. Otherwise, one has to use a continuous model or lumped and continuous hybrid model obtained from (5.17) in Step 2 and go back to Step 2. Under this scenario, to reduce computational time, the previously obtained oscillator parameters are fixed during model estimation in Step 2. Usually, there are two aspects to be determined, the dimensions of the cross section and the effective loss factor of the vertical bars.

Step 4: Implement the realizable models with mechanical elements. The geometric dimensions of mechanical elements should be designed so that (5.15) can be satisfied.

## 5.2 Active Emulator Design

During operation of machinery, many factors, such as unbalanced rotating elements, produce vibrations at the attachment points. These vibrations are mainly determined by the amplitudes and directions of the internal exciting forces, the transmission paths from those

forces to the attachment points and the dynamic interaction between active machinery and its mounting structures.

This attachment point vibration is reproduced by the addition of a shaker, referred to as an emulating shaker, to the passive emulator. The shaker's mounting location should be properly selected and its input voltage must be appropriately controlled. This research only focuses on reproducing translational motions of active machinery. Usually, at least one shaker should be used to reproduce motion in each coordinate direction. By using two separately mounted emulating shakers, rotational motions may be reproduced.

The advantage of using a shaker under closed-loop control is that a single shaker can reproduce an arbitrary acceleration profile. The active emulation problem is a type of command following control. A controller for the emulating shaker is needed so that the active emulator can reproduce the attachment point acceleration of the operating machinery. A feedback controller has to be used since it is difficult to accurately model the interaction between the emulating shaker and the passive mechanical emulator.

One way to implement feedback control is to compare the actual accelerations at the foundation attachment points of active machinery and that of its active emulator. If there is no additional external excitation on the active machinery, this is a good choice to design a feedback controller. Otherwise, the actual attachment point acceleration is affected not only by machinery operation but also by external excitation. In this scenario, it is misleading to compare the desired attachment point acceleration and the actual attachment point since the latter also includes the influence of external excitation.

In this research, a control approach is adopted in which the emulating shaker is commanded to reproduce the force at its mounting location in (1.2) that corresponds to the attachment point acceleration that occurs when there is no external loading. As given in (1.3), this approach provides for total attachment point acceleration to be a linear combination of the effects of internal and external forcing. This approach assumes that external excitation does not have much effect on the equivalent internal forcing of operating machinery. The goal of the controller for the emulating shaker is that the actual force this

shaker generates follows the desired force as closely as possible.

Design of an active mechanical emulator involves three aspects: selection of the emulating shaker, selection of its mounting location and design of a controller for the shaker. These are discussed below.

### 5.2.1 Selection of the Emulating Shaker and its Mounting Location

The basic guidelines for selecting an emulating shaker are that its output force within the range of frequency of interest must exceed the desired force and that its mass should not exceed the mass of the element on which it mounts since the same amount of mass as the emulating shaker should be removed from that element. For instance, in Figure 1.3, the mass  $m'_3$  satisfies

$$m'_3 = m_3 - m_{shaker} \quad (5.32)$$

where  $m_{shaker}$  is the emulating shaker mass.

Theoretically, the emulating shaker can be mounted anywhere. Because of the mass constraint  $0 < m_{shaker} < m_3$ , however, it is usually a good choice to mount the emulating shaker on the base frame of the passive mechanical emulator, as shown in Figure 6.8. Moreover, another advantage of this mounting location is that it usually requires shaker force of smaller magnitude.

After the mounting location is chosen, the transfer acceleration from the measured acceleration to the mounting location can be readily measured. The force which the shaker needs to generate is determined by the following equation

$$F(s) = \frac{a(s)}{A_{tf}(s)} \quad (5.33)$$

where  $a(s)$  is the attachment point acceleration of the active machinery and  $A_{tf}(s)$  is the transfer acceleration  $A_{tf}(s)$  from the location where the attachment point acceleration is measured to the mounting location of the emulating shaker. If the mounting location of

the emulating shaker is close to the attachment point, the transfer acceleration may be approximately chosen as the reciprocal of the apparent total mass of the passive mechanical emulator. An emulating shaker can be selected according to the estimated required force.

Based on the measured transfer acceleration  $A_{tf}(s)$  and the acceleration data  $a(s)$  at the attachment point of the active machinery, the force that the emulating shaker needs to generate can be computed from (5.33). If the actual force matches the capability of the selected emulating shaker, no further work is necessary. Otherwise, another emulating shaker must be selected.

### 5.2.2 Feedforward/feedback Controller for the Emulating Shaker

In this research, a PD controller is used in the feedback path together with a feedforward controller. Both make use of a dynamic model,  $V(s)/F(s)$ , between shaker voltage and force applied to the emulator. This controller is shown in Figure 5.10. The gain  $K_f$  is determined by the sensitivity of the force gauge and the gain set in the signal conditioner.

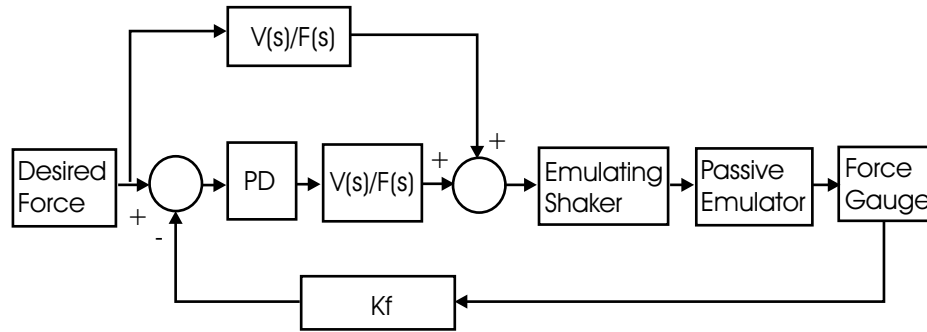


Figure 5.10: Feedforward/feedback Controller for the Emulating Shaker in Active Emulation

It is usually difficult to accurately obtain the transfer function  $V(s)/F(s)$  by an analytical method since the force which a shaker generates strongly depends on how the shaker and the mechanical emulator interact. This transfer function can, however, be readily obtained experimentally by model identification from measured data by a slow sinusoidal sweep.

In the feedforward/feedback controller, the desired force is determined by (5.33). If the acceleration is composed of several dominant harmonics, the force profile is likely to be dominated by these frequencies. In this case, the amplitude and phase angle of each frequency component in the force profile can be evaluated using (5.33). Otherwise, the time-domain force profile is obtained from the inverse Fourier transformation of  $F(s)$ .

## Chapter 6

# Experimental Passive and Active Emulation

Tell me, I forget. Show me, I remember. Involve me, I understand.

Xun Zi (About 310-237 B.C.), Ancient Chinese Philosopher

This chapter presents an experimental validation of the design procedures presented in the previous chapter. Rather than test a single machine, a machinery test bed was constructed which could represent systems with a variety of modes and variable internal forcing. The design of this test bed is first described followed by a description of the data acquisition system. A modular emulator test bed is then presented. Implementation of the passive and active emulator design rules is then illustrated along with an evaluation of the experimental results.

### 6.1 Machinery Test Bed

According to Navy machinery data, there are about 10 modes of interest in typical machinery. Modes from strong and direct couplings between machinery components and the machinery attachment points dominate in the frequency response data while those from

weak couplings do not have much contribution to the total response. The former are termed “major” modes and the latter “minor” modes.

An ideal machinery test bed should possess both major modes and minor modes and their couplings. A test bed thus designed is depicted in Figure 6.1, comprised of two aluminum frames connected by two steel plates. A total of eleven oscillators are mounted on the top and bottom frames. Each oscillator is comprised of block masses clamped on both sides of a piece of spring steel plate, as shown in Figure 6.2. Since steel has a very low loss factor, polymeric damping materials are attached to the steel plates to match the damping property of machinery modes. The attachment point assumed to mount machinery on its supporting structure is located at the bottom right corner of the machinery test bed. The design goal is that machinery and its emulator possess, with respect to the attachment point, the same dynamic properties in the horizontal and vertical translational coordinate directions as well as the planar rotational coordinate direction.

Two DC motors with eccentric masses fixed on their shafts are mounted on the machinery test bed, as shown in Figure 6.2, one on the top frame and another on the bottom frame. Their rotation speeds are tuned by control of supply voltages via potentiometers. In the experiments, it is noted that these speeds experience drift around the desired values due to such factors as shaft friction, resistance change in the potentiometers due to temperature change. It is possible to reduce this speed drift by using a feedback controller with an encoder.

The fixed-base resonance frequencies of eleven oscillators can be selected to lie between 10 Hz and 80 Hz. In addition, the two motors when they are turned off contribute two modes between 60 Hz and 70 Hz, which come from coupling between the mounting fixtures and motor masses. The machinery test bed also possesses a structural mode arising from the bending of the two steel plates connecting the top and bottom aluminum frames. Its first fundamental frequency is 25.3 Hz. Therefore, there are 14 modes in total between 10 Hz and 80 Hz.

Its major dimension parameters are: length  $l=22$  inches, width  $w=12$  inches and depth



$h=4$  inches. The total mass of the machinery test bed is  $m_t = 6.120$  kg.

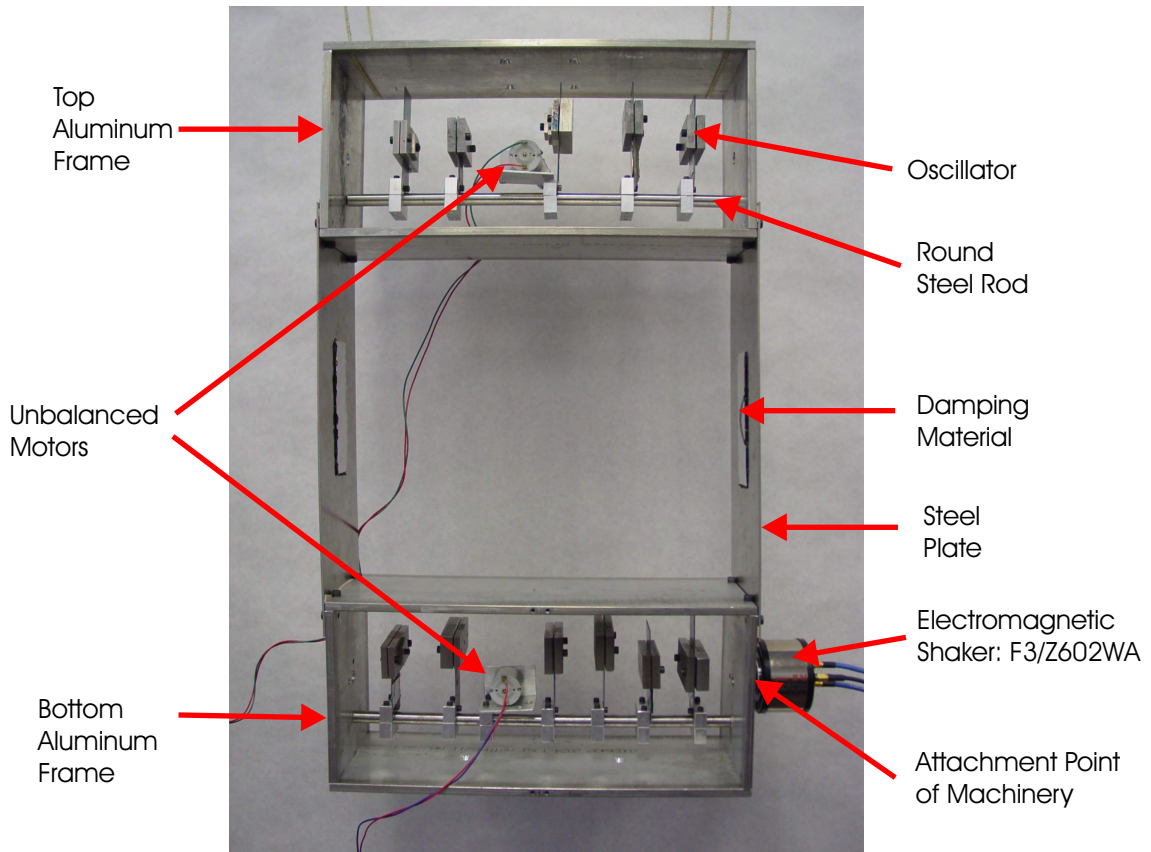


Figure 6.1: Side View of the Machinery Test Bed

## 6.2 Accelerance Acquisition System

The schematic accelerance measurement system, illustrated in Figure 6.3, consists of a power amplifier, a shaker, transducers (including a force gauge and an accelerometer), machinery under test, a signal conditioning amplifier and a dynamic signal analyzer. The signal conditioning amplifier can convert the high impedance charge signals from the impedance head to the voltage signals which are fed to the dynamic signal analyzer. The amplitudes of those signals can also be amplified by setting appropriate gains. The dynamic signal analyzer then can record and process the experimental data. Meanwhile,

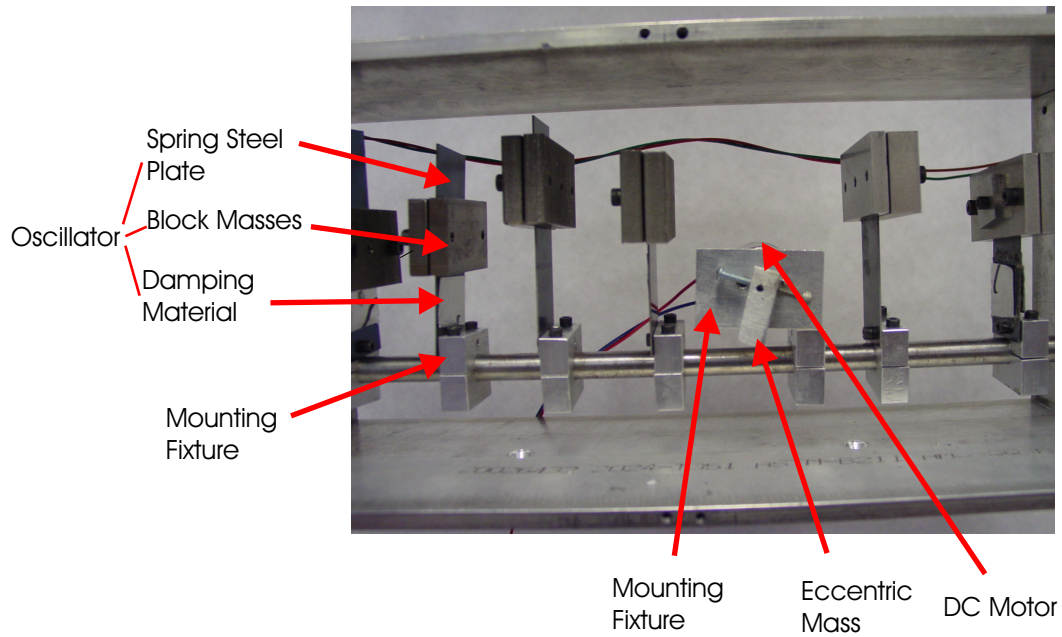


Figure 6.2: Oscillators and Unbalanced Motor (back view)

it also performs as a signal generator which provides the desired voltage to the shaker through the power amplifier.

To achieve the desired force levels, a Wilcoxon<sup>TM</sup> electromagnetic shaker *F3* with an impedance head *Z602WA* is used [93], together with power amplifier *PA7F*. There are several types of input force widely used in dynamic testing, such as hammer impact, stepped-sine, slow sinusoidal sweep and random force input. In order to improve the signal-to-noise ratio (SNR) and obtain high quality data in a frequency range of interest, a slow sinusoidal sweep is chosen in this study so that it is possible to obtain a good transfer function model by model identification. Any nonlinearity effects can be minimized by restricting the input voltage amplitude of the sweep.

The attachment point acceleration data should be measured either on a vibration table or when the passive machinery is unconstrained, that is, suspended. The latter method is used here and the machinery test bed is hung by soft strings to approximate free boundary conditions as best as possible. Under this situation, the rigid body modes have frequencies very close to 0 Hz. By maximizing the lengths of soft strings the frequency of

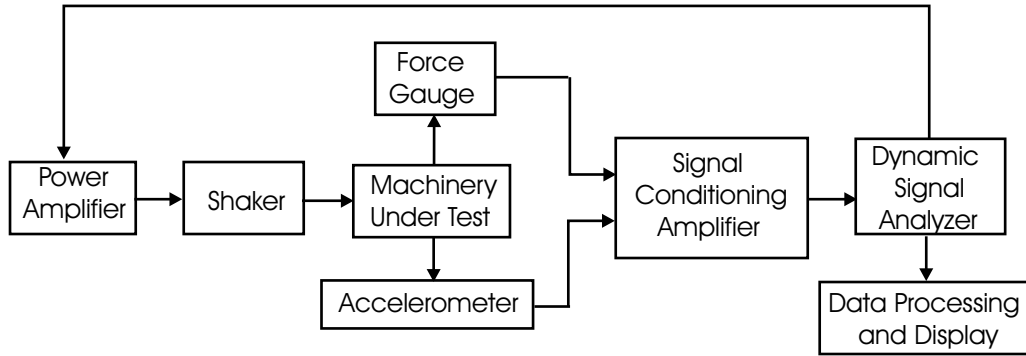


Figure 6.3: Accelerance Data Acquisition Schematic

any pendulum modes can be made as low as possible.

By swinging the machinery, the pendulum mode was found to have a frequency of 0.5 Hz. In addition, the shaker exerts a moment on machinery because of the off-center excitation, resulting in its planar rotation with respect to the hanging points on the machinery. The frequency of this rotational mode was found to be 3.5 Hz.

By applying a slow sinusoidal sweep in force, the driving-point accelerance of the passive machinery in the horizontal coordinate direction is obtained, as shown in Figure 6.4. Due to the restriction of the usable frequency range of the impedance head, the accelerance data under 10 Hz is quite noisy. The mode at 0.5 Hz labeled  $P$  is due to the pendulum effect and the mode at 3.5 Hz labeled  $R$  is due to the planar rotation of the machinery. In emulator design, one does not need to consider the pendulum mode at 0.5 Hz. To facilitate comparison, however, the machinery and emulator should have the same pendulum mode at 0.5 Hz. This requires the same hanging configuration for both.

The frequency range of interest in this design example is between 0 Hz and 80 Hz. Within this range, excluding the pendulum mode at 0.5 Hz, there are eight major modes and seven minor ones. Six of these seven major modes, labeled  $B_i$  ( $i = 1, 2, \dots, 6$ ) in Figure 6.4, are contributed by the six oscillators mounted on the bottom aluminum frame. One suspension mode at 3.5 Hz labeled  $R$  is due to the planar rotation. The last major mode labeled  $S$  arises from the bending of two steel plates connecting two aluminum

frames. Five of seven minor modes, labeled  $T_i$  ( $i = 1, 2, \dots, 5$ ), come from the oscillators mounted on the top aluminum frame. The remaining two modes, labeled  $M_1$  and  $M_2$ , are contributed from the two motor masses which act as oscillators when they interact with the fixtures through which they are mounted. By stiffening the mounting fixtures, these two motors can be moved out of the upper limit of frequency, 80 Hz.

As seen in Figure 6.4, the contributions from major modes in the frequency response are significant while those from minor modes are negligible. This is also true in the impulse response of passive machinery while experiencing an impulse excitation at the attachment point. Therefore, in the passive emulator design, only the major modes are included while the minor modes are discarded. Design of a passive mechanical emulator is described below.

### 6.3 Passive Mechanical Emulator

The design of a passive mechanical emulator involves three steps: identification of a realizable model from the accelerance data already obtained in Section 6.2; implementation of this model with mechanical elements; and experimental comparison between the passive machinery and its passive emulator.

#### 6.3.1 Realizable Model Identification

Recall that there are seven major modes in the frequency range of interest after all rigid body modes are excluded, which are matched according to mass matching requirements. Moreover, one minor mode with its label  $T_1$ , which is the most significant minor mode, is intentionally included to show that if necessary, minor modes can also be realized. Consequently, the passive mechanical emulator should possess nine modes in total. Since the driving-point accelerance, as shown in Figure 6.4, approaches a constant at low frequencies and also at high frequencies, a total of nine lumped masses are needed to design this emulator.

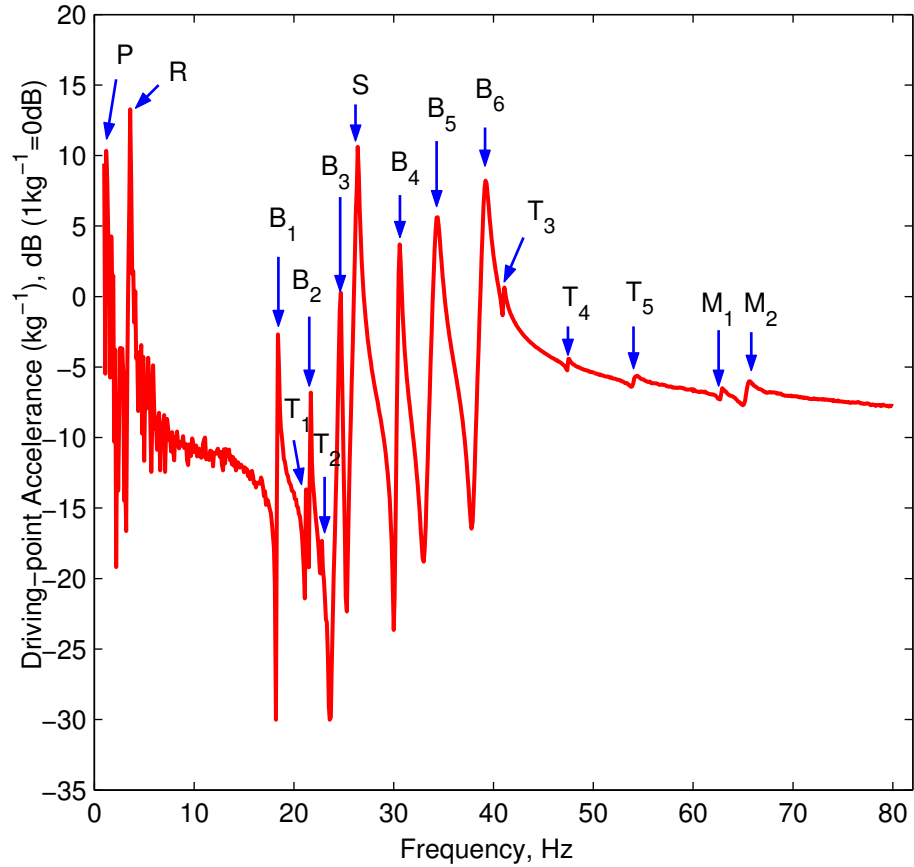


Figure 6.4: Driving-point Accelerance of Passive Machinery at its Attachment Point in the Horizontal Coordinate Direction

To obtain a realizable model from experimental driving-point accelerance, one should use the technique of direct estimation developed in Chapter 4. To ease passive mechanical emulator design and fabrication, a parallel model realization is chosen as given by (5.19).

To avoid the pendulum mode and rotational mode effects, the cost function (5.26) is defined in the frequency range 10 Hz to 80 Hz. The masses, dashpots and springs are identified by the nonlinear model estimation technique discussed in Section 4.2, as listed in Table 6.1. These oscillators are ordered from the lowest fixed-base resonance frequency to the highest. Here, the fixed-base undamped resonance frequencies are calculated by (5.23) and the loss factors are determined by (5.24). The lengths of spring steel plates of the oscillators are determined by the method discussed in Appendix F. The attachment

point driving-point accelerance of the identified realizable second order model matches very well with that of the machinery, as depicted in Figure 6.5.

Table 6.1: Parameters of the Identified Realizable Second Order Model for the Passive Mechanical Emulator

Apparent base mass  $m_0 = 2.3343\text{kg}$

Number of Oscillators	Mass (kg)	Dashpot ( $N \cdot s/m$ )	Spring ( $\times 10^3$ N/m)	Undamped Fixed-base Resonance Frequency (Hz)	Loss Factor $\eta$ ( $\times 0.01$ )	Length of Steel Plates (mm)
1	0.1016	0.0342	1.3321	18.2282	0.2939	47.5625
2	0.0559	0.0470	0.9832	21.1128	0.6338	53.8906
3	0.0470	0.0404	0.8602	21.5288	0.6355	56.8750
4	0.4420	0.8747	9.7547	23.6429	1.3322	18.2969
5	0.1115	0.1604	2.8132	25.2791	0.9057	34.1875
6	0.0962	0.1248	3.4265	30.0385	0.6874	31.1797
7	0.1512	0.5553	6.5083	33.0179	1.7703	22.6719
8	0.0959	0.3595	5.4320	37.8870	1.5747	24.8437

It can be found, however, that the resulting emulator structural mode from interaction between the base frame and the additional mass falls within the frequency range of interest. A continuous/lumped-parameter hybrid realizable model is therefore employed by substituting the driving-point accelerance of the base structure of the passive mechanical emulator  $A_{base}(\omega)$  into (5.17) with (E.10). In this case, the structural mode of the passive mechanical emulator can be matched with one of the modes of the passive machinery.

There are two ways to do this matching. First, the structural mode of the passive mechanical emulator is used to match any one of the passive machinery modes. Alternatively, this structural mode is matched with the passive machinery mode possessing the closest mass. It would be expected that the second approach can perform better.

Using the first approach, the structural mode of the passive mechanical emulator is required to match the highest frequency major mode  $B_6$  of the passive machinery in Figure 6.4. The eighth oscillator in Table 6.1 is thus removed and replaced by the base structure of the passive mechanical emulator. The total model of the passive mechanical

emulator is obtained according to (5.17) with the driving-point accelerance of the base structure given by (E.10). Since other modes have been matched very well, to reduce computational time, the width and effective loss factor of the two identical aluminum vertical bars in Figure 5.1 can be identified with the specified thickness of the vertical bars  $t = 0.25$  inches and the parameters of other oscillators fixed according to Table 6.1. The identified width is 0.590 inches and the effective loss factor of the two vertical bars is 0.0191. The comparison between the passive machinery and the identified continuous and lumped-parameter realizable model is carried out in Figure 6.6. Good agreement between the passive machinery and its hybrid realizable model is achieved again. In the frequency range between 45 Hz to 80 Hz, the amplitude of the identified realizable model is slightly higher than that of the passive machinery.

To obtain a better realizable model incorporating the structural mode of the passive mechanical emulator, the second matching approach was also implemented. By simple estimation, the structural mode of the passive mechanical emulator has a mass closest to the fifth oscillator in Table 6.1, which comes from the structural mode of the passive machinery  $S$  in Figure 6.4. The fifth oscillator in Table 6.1 is thus removed and replaced by the base structure of the passive mechanical emulator. Following the same procedure as used in the first approach, the width of the two identical aluminum vertical bars in Figure 5.1 is identified as 0.451 inches and the identified effective loss factor of the two vertical bars is 0.00923, with the previously specified thickness of the vertical bars  $t = 0.25$  inches and the parameters of other oscillators fixed according to Table 6.1. Comparison between the passive machinery and the newly identified continuous/lumped-parameter realizable model is carried out in Figure 6.6. Here, the structural mode of the passive mechanical emulator  $S_2$  has been matched with the structural mode of the passive machinery  $S$ . Very good agreement between the passive machinery and its hybrid realizable model is achieved and the magnitude difference between 45 Hz and 80 Hz is significantly improved.

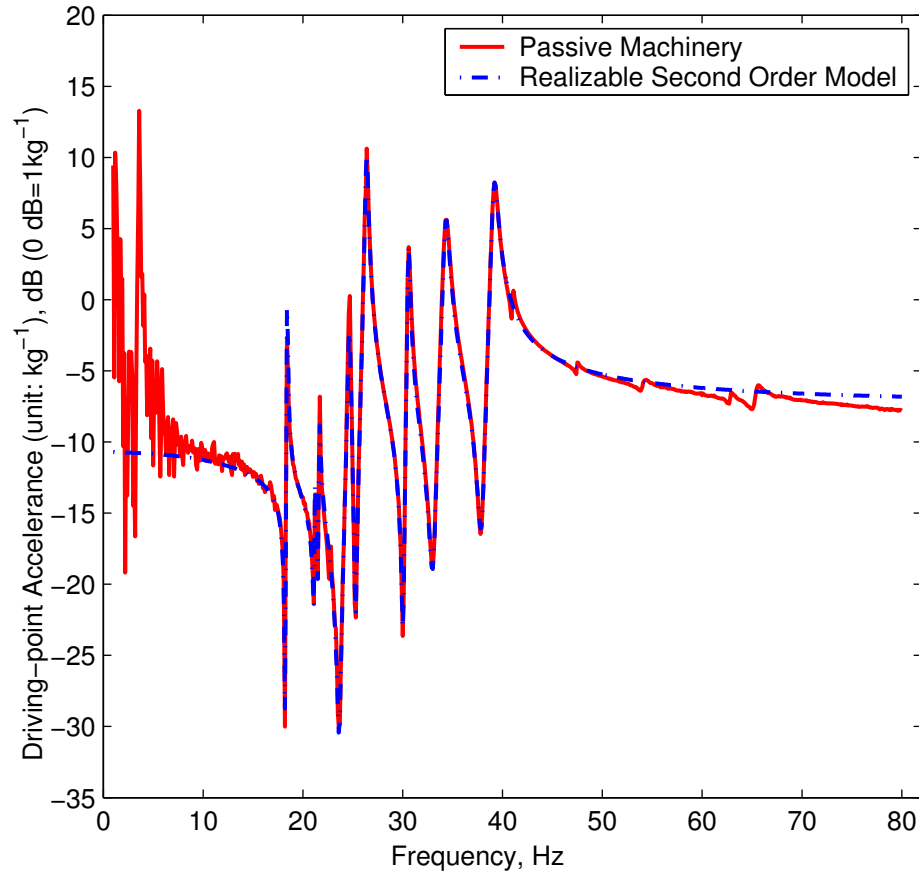


Figure 6.5: Comparison between the Passive Machinery and its Realizable Second Order Model

### 6.3.2 Design and Implementation of Passive Emulators

Two passive emulators for the machinery model of Figure 6.1, were designed and implemented according to the two identified hybrid realizable models in Figure 6.6 and Figure 6.7, respectively. The emulators, one of which is shown in Figure 6.6, are physical realizations of the passive emulator model in Figure 5.1. To make the effects of the pendulum mode and planar rotational mode comparable between the passive machinery and its emulator, the same hanging configuration during testing should be used. To this end, two horizontal aluminum bars used only for hanging testings, as shown in Figure 6.8. In the actual application of passive emulation, these two horizontal bars are not necessary. In



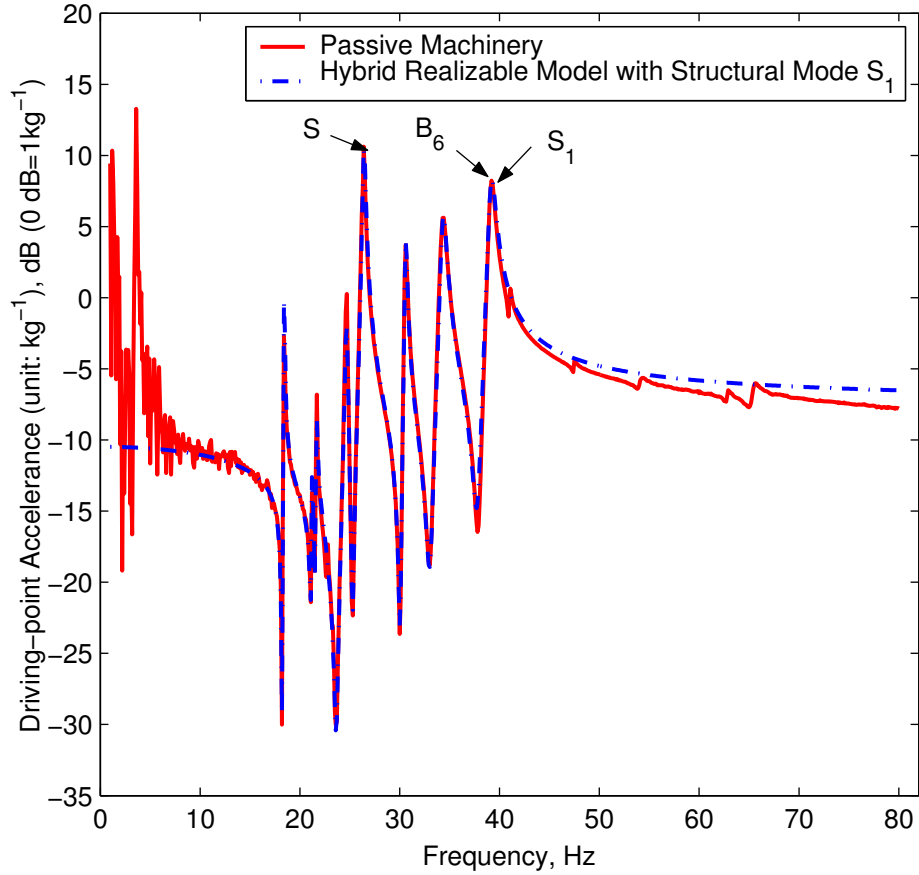


Figure 6.6: Comparison between the Passive Machinery and its Continuous and Lumped-parameter Hybrid Realizable Model: Realizable Model I

addition, the emulating shaker is turned off.

The identified hybrid realizable models, obtained in Subsection 6.3.1, can be used to solve for the parameters associated with the base structure. The base structure includes the base frame, the round rod, the two identical vertical bars, the additional mass and the mounting fixtures in Figure 5.1. The base frame plus the round rod made of steel, seven mounting fixtures made of aluminum and the emulating shaker have a total mass  $m_b = 1.931$  kg. Therefore, the additional mass  $m_a = 2.918$  kg, which is calculated according to (5.13). The location of the mass center of the additional mass then is determined as  $l_a = 8.81$  inches by using (5.14). The distribution of mass in the passive mechanical emulator is determined according to (5.15). Only the dimensions of the components with

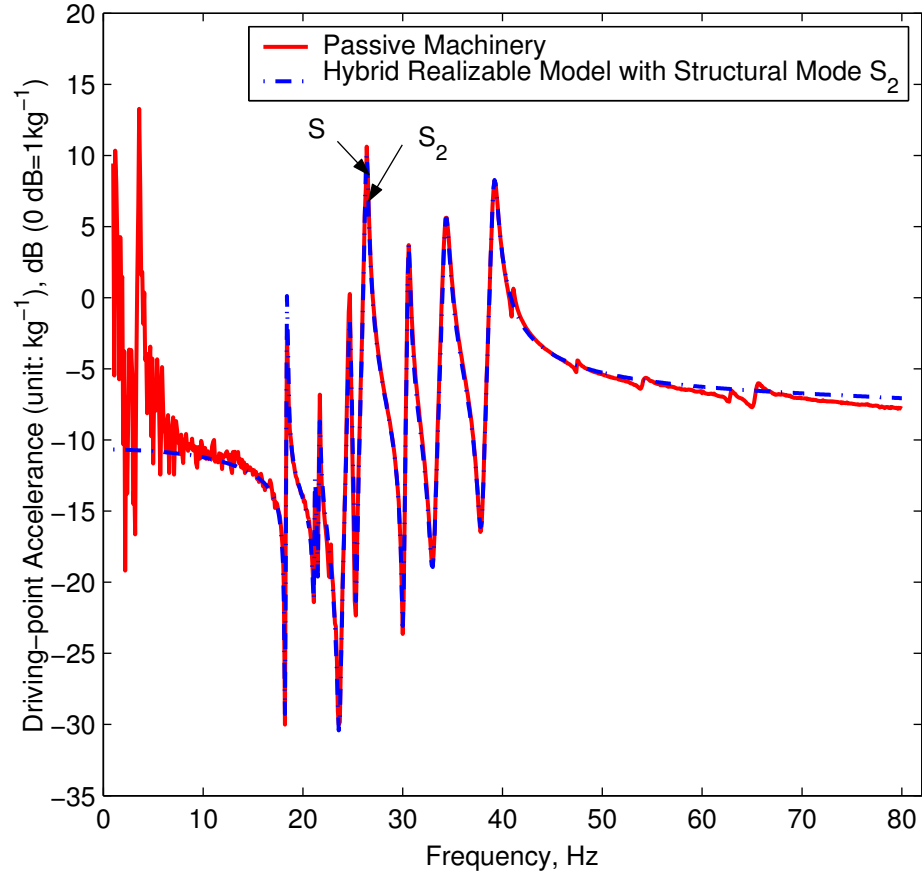


Figure 6.7: Comparison between the Passive Machinery and its Continuous and Lumped-parameter Hybrid Realizable Model: Realizable Model II.

large moments of inertia are carefully designed.

Due to the idealization during modeling of the emulator's structural mode in Subsection 5.1.3, the two identical vertical bars made of aluminum should not be milled to their desired width for the first run, but to a slightly greater value. Subsequently, one needs to carefully remove thin layers of material until the structural mode  $S_2$  of the passive emulator matches with the structural mode of the passive machinery  $S$ . A number of polymeric free damping layers or constrained damping layers should be applied, determined according to the desired loss factor and relations in (5.30) and (5.31) on the side surfaces of the vertical bars.

For the first emulator, the average actual width of the two identical vertical bars

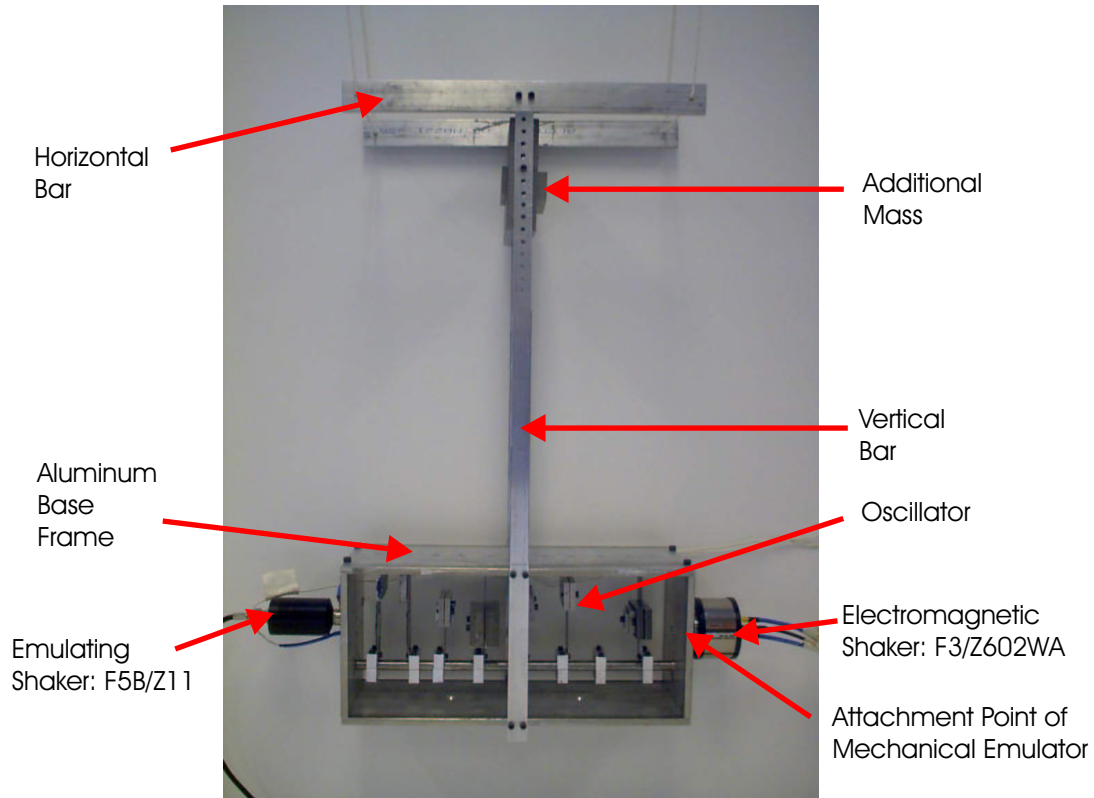


Figure 6.8: Example Passive Mechanical Emulator

is 0.604 inches. Thus, compared to the desired width  $t = 0.590$  inches as obtained in Subsection 6.3.1, the error between the actual width and the desired one is only 2.37%.

For the second passive mechanical emulator, the average actual width of the two identical vertical bars is 0.449 inches. Thus, compared to the desired width  $t = 0.451$  inches as obtained in Subsection 6.3.1, the error between the actual width and the desired one is only  $-0.42\%$ , where the negative sign means that the actual width is less than the desired one.

### 6.3.3 Performance Evaluation of the Passive Mechanical Emulators

The driving-point accelerance of the first passive emulator is compared to that of the passive machinery, as shown in Figure 6.9. The machinery and emulator do not match well, especially at modes  $B_5$  and  $B_6$ . This discrepancy mainly arises from the matching

between the structural mode of the passive mechanical emulator and the highest frequency major mode of the passive machinery despite their relatively large difference in mass.

The second emulator whose structural mode is matched with that of the passive machinery reproduces the driving-point accelerance well in the frequency range 0 Hz to 80 Hz, with some discrepancy in the small region around the modes  $B_3$  and  $S$ , as depicted in Figure 6.10. The amplitudes around these two modes are lower than desired, which may be attributed to two factors. The first factor is that damping in the emulator may exceed the desired value. The extra damping may arise due to the many screw joints between components. To reduce damping, connections between elements may be carried out by welding. Another factor may be an asymmetrical effect due to fabrication error in the two vertical bars connecting the additional mass and the aluminum base frame.

A passive mechanical emulator having a good agreement with its corresponding passive machinery provides the basis for active emulation. An active mechanical emulator was designed and implemented for the second passive emulator model with attachment point driving-point accelerance shown in Figure 6.10.

## 6.4 Design of an Active Mechanical Emulator

In active emulator design, a passive emulator is modified by adding an emulating shaker to reproduce the acceleration at the machinery attachment points due to machinery operation. This design step involves several important issues, including selection of the emulating shaker, selection of its mounting location, identification of the transfer function of the voltage applied to the shaker and the force that it generates, and finally design and implementation of the feedforward/feedback controller for the emulating shaker.

### 6.4.1 Selection of the Emulating Shaker and its Mounting Location

The emulating shaker and its mounting location is selected according to the principles discussed in Subsection 5.2.1. The mounting location of the shaker is selected on the

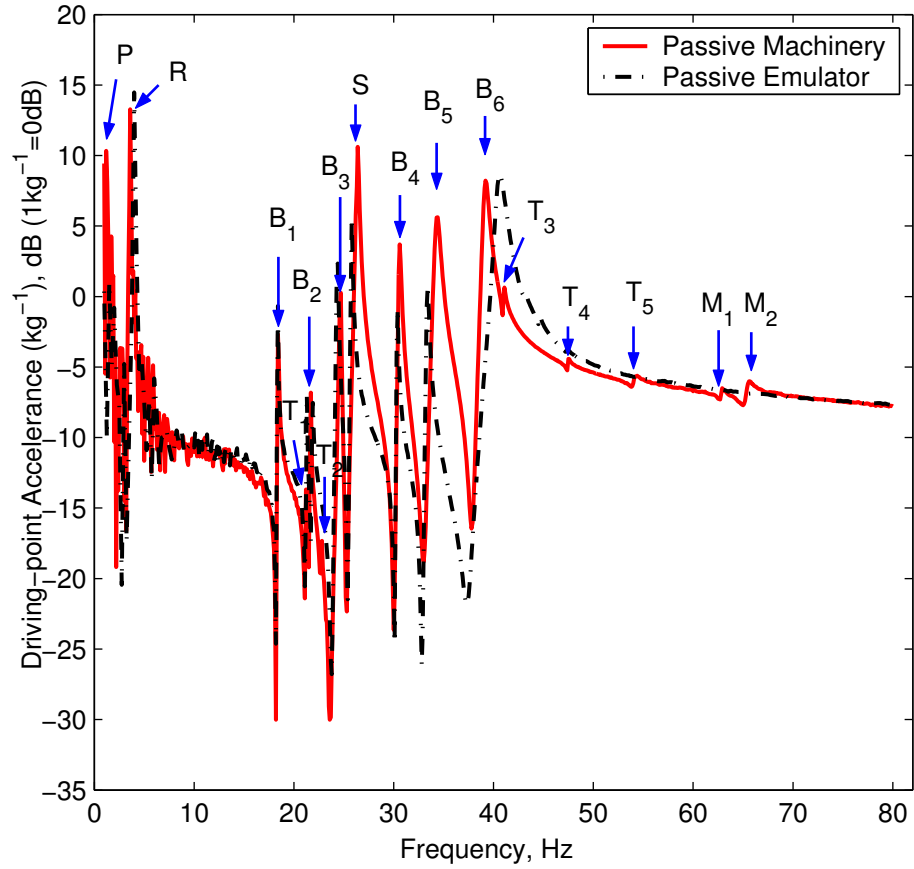


Figure 6.9: Driving-point Accelerance Comparison between Passive Machinery and its Passive Mechanical Emulator: Passive Mechanical Emulator I

aluminum base frame, as shown in Figure 6.8. A *Wilcoxon<sup>TM</sup>* Model *F5B/Z11* shaker, a reaction-type permanent magnet electromagnetic shaker, is used to reproduce the operating effect of the machinery. Its operating frequency ranges from 10 Hz to 10,000 Hz. The impedance head *Z11* includes an accelerometer with charge sensitivity of  $0.36 \text{ pC}/(m/s^2)$  and a force gage with charge sensitivity of  $56 \text{ pC}/N$ . The total weight of this shaker with the impedance head is  $0.170 \text{ kg}$ . The relation of the output force versus frequency and other detailed specifications can be found in [94].

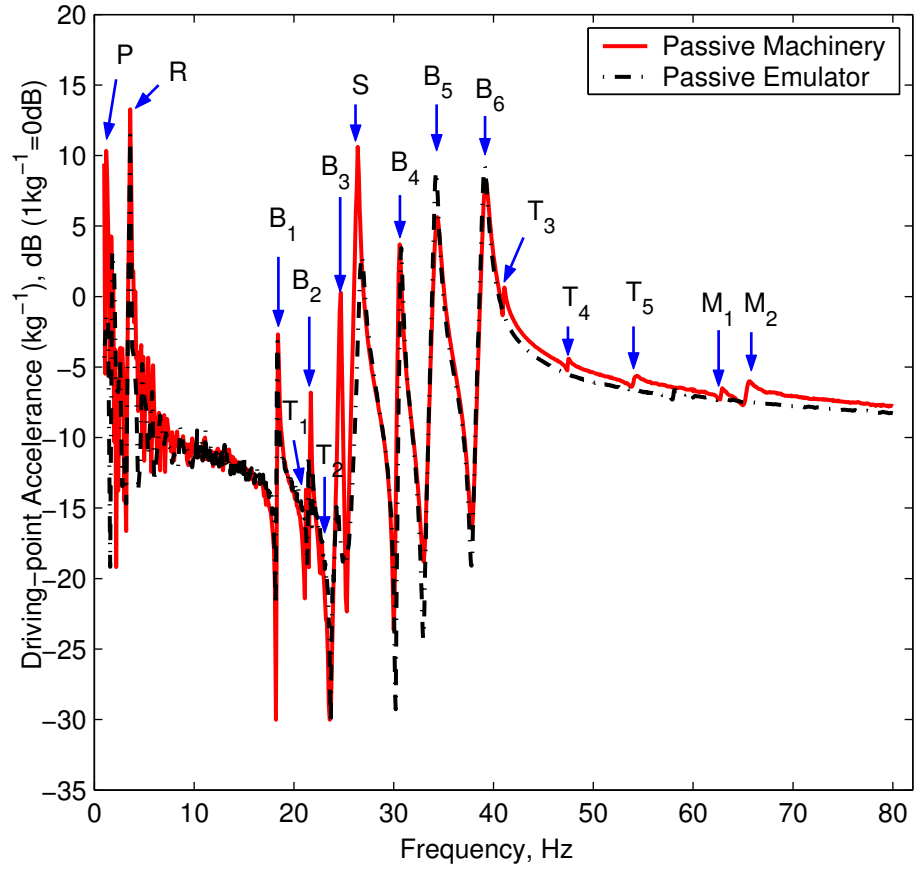


Figure 6.10: Driving-point Accelerance Comparison between Passive Machinery and its Passive Emulator: Passive Mechanical Emulator II

#### 6.4.2 Transfer Accelerance from the Emulating Shaker to the Attachment Point

The transfer accelerance  $A_{tf}(s)$  from the emulating shaker location to the attachment point was measured over a frequency range 1 Hz to 80 Hz, as shown in Figure 6.11, containing the two frequencies generated during machinery operation.

When reproducing the acceleration at the attachment point of active machinery, the values of the transfer accelerance  $A_{tf}$  should be read out at the two machinery frequencies. These values are used to calculate the desired forces by (5.33).

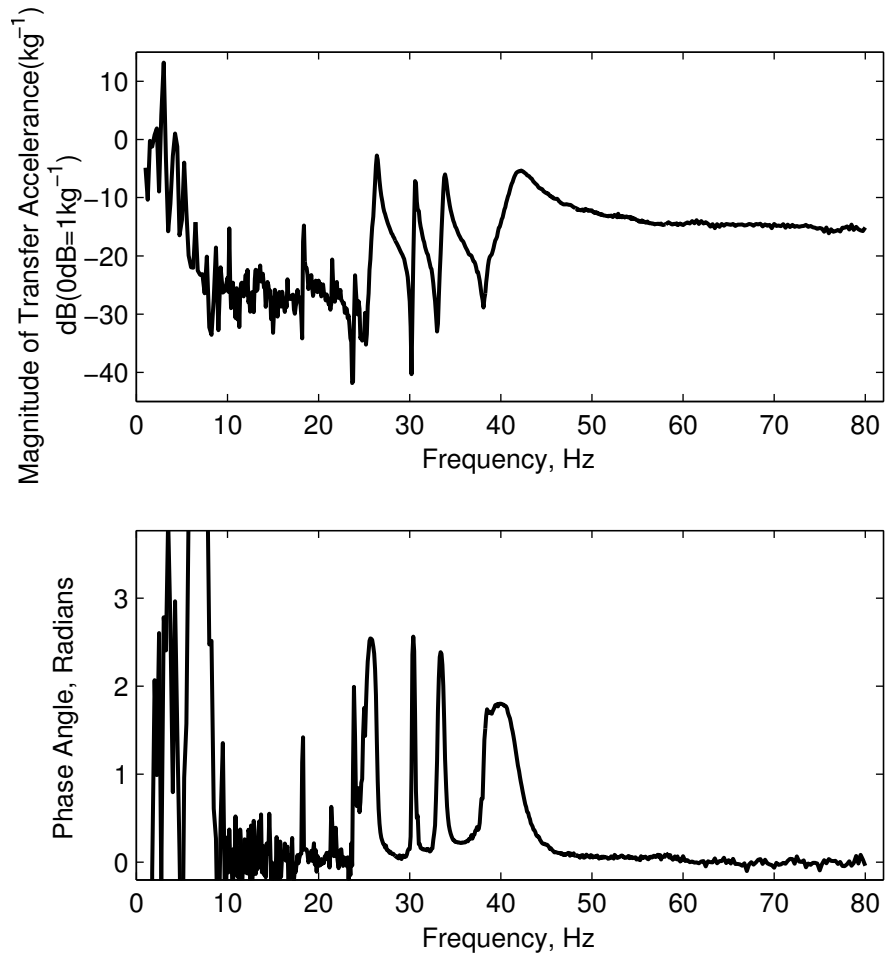


Figure 6.11: The Transfer Accelerance from the Acceleration Pickup Location to the Mounting Location of the Emulating Shaker

### 6.4.3 Identification of the Transfer Function $V(s)/F(s)$

Recall that a feedforward/feedback controller is used to drive the emulating shaker, discussed in Subsection 5.2.2. After mounting the emulating shaker at the chosen location, transfer function  $V(s)/F(s)$  can be obtained by a slow sinusoidal sweep, as shown in Figure 6.12. Due to the limit of the usable frequency range of the impedance head *Wilcoxon<sup>TM</sup>* Z11 (10 Hz to 10 kHz), the data below 10 Hz are quite noisy and not reliable. Therefore, during model identification, the cost function is defined with data from 10 Hz to 80 Hz.

By looking at its slopes in the low and high frequency ranges, it is enough to use a

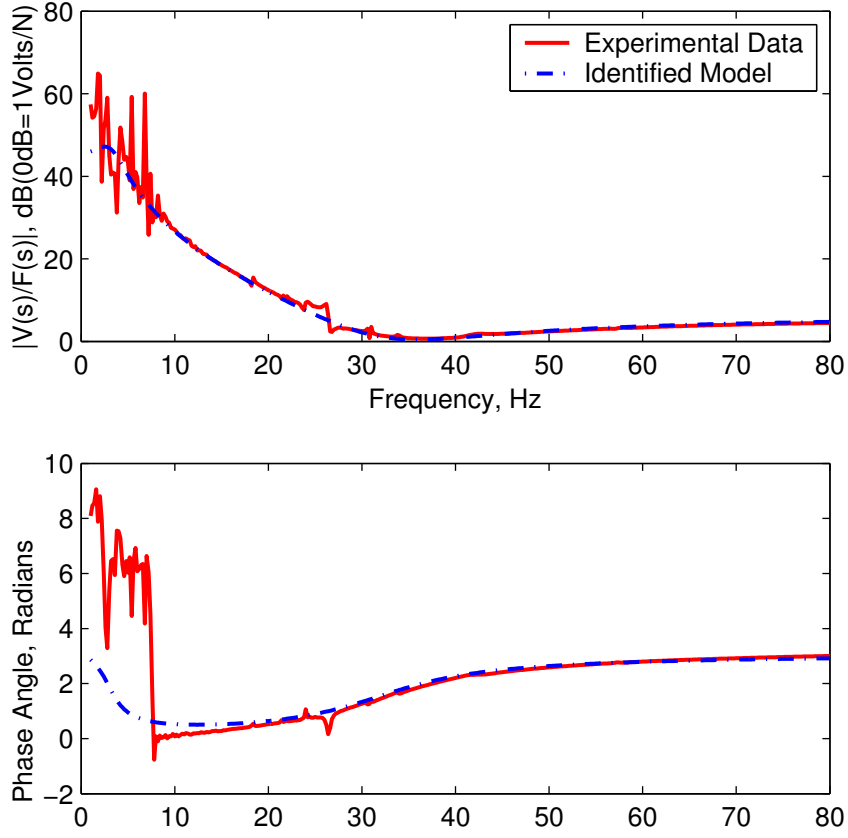


Figure 6.12: Comparison between the Identified Model and Experimental Data of the Transfer Function  $V(s)/F(s)$ , Voltage Applied to the Emulating Shaker to the Emulating Shaker Generated Force

second order transfer function to capture its major dynamics, which is defined as follows

$$\frac{V(s)}{F(s)} = -\frac{a_2s^2 + a_1s + a_0}{s^2 + 2a_4s + (a_4^2 + a_3^2)} \quad (6.1)$$

Here, the coefficients  $a_i$  ( $i = 0, 1, 2, 3, 4$ ) in the numerator and denominator are forced to be positive so that the transfer function to be obtained is a stable and minimum phase one. The pair of poles are  $-a_4 + a_3j$  and  $-a_4 - a_3j$ , where  $j = \sqrt{-1}$ .

In order to match the transfer function with the experimental data between 10 Hz and



80 Hz, the cost function is defined as the following weighted sum

$$J = \frac{\sum_{i=0}^{i=n} \left| \frac{1}{y_e(f_i)} \right|^2}{\sum_{i=0}^{i=n} |y_e(f_i)|^2} \sum_{i=0}^{i=n} |y_e(f_i) - y_m(f_i)|^2 + \sum_{i=0}^{i=n} \left| \frac{1}{y_e(f_i)} - \frac{1}{y_m(f_i)} \right|^2 \quad (6.2)$$

where  $y_e(f_i)$  and  $y_m(f_i)$  are the experimental data points and the frequency responses of the model (6.1) at the frequencies  $f_i$ 's, and  $n$  is the number of data points.

With the above cost function, the transfer function (6.1) is identified as

$$\frac{V(s)}{F(s)} = -\frac{2.007s^2 + 226.5s + 86670}{s^2 + 1.3153 \times 10^{-9}s + 355.00} \quad (6.3)$$

In the above model, the pair of conjugate complex poles of  $V(s)/F(s)$  are approximately  $18.8413j$  and  $-18.8413j$ , corresponding to a mode at 3 Hz. The frequency component corresponding to this pair of poles has a large amplitude and persists in the response of the transfer function due to a sinusoidal force input. Since it is undesirable to drive the emulating shaker with a large voltage, this frequency component should be attenuated quickly by introducing more damping. The cost function (6.2) however can not introduce more damping to the 3 Hz mode in that this mode locates outside of the frequency range of interest, In the identified model (6.3), damping thus is added by manually increasing the coefficient  $a_4$ . Since damping often has a localized effect around the modes in an oscillatory system, increasing damping does not cause much change in the frequency range between 10 Hz and 80 Hz even though the amplitude around this mode is significantly reduced. The frequency of the mode corresponding to the pair of poles does not shift. From the transfer function (6.3), the following transfer function is obtained by choosing the coefficient  $a_4 = 10$ .

$$\frac{V(s)}{F(s)} = -\frac{2.007s^2 + 226.5s + 86670}{s^2 + 20s + 455} \quad (6.4)$$

Compared to the experimental data, as depicted in Figure 6.12, very good agreement

is achieved in the frequency range between 10 Hz and 80 Hz except around 25 Hz. This transfer function (6.4) is used in the feedforward/feedback controller for the emulating shaker discussed below.

#### 6.4.4 Implementation of the Feedforward/feedback Controller

Implementation of the schematic for the feedforward/feedback controller in Figure 5.10 includes the software and hardware, shown in Figure 6.13. The former includes *MATLAB/SIMULINK*<sup>®</sup>, *Real Time Workshop*, *WINCON 3.1*, *Visual Studio C++ 6.0*, *Real Time Extension RTX*<sup>TM</sup> *5.0* and *Windows 2000*. The latter includes a *MultiQ-3*<sup>TM</sup> 16-bit AD/DA board (analog-to-digital converters and digital-to-analog converters), the impedance head *Z11* and the emulating shaker *F5B*.

The 16-bit AD/DA board *MultiQ-3*<sup>TM</sup> with 8 input channels and 8 output channels is used to acquire force and acceleration data, and control the emulating shaker [95]. Since real-time data acquisition and control is required, Real-time Extension *RTX*<sup>TM</sup> *5.0* is used to add real-time capabilities to Window 2000 [96]. The controller model of the feedforward/feedback controller is implemented in *MATLAB/SIMULINK*<sup>®</sup> [97]. This model is converted to real-time C code by *MATLAB/Real-Time Workshop*<sup>®</sup>, which is a software package for generating C code for models from *SIMULINK*<sup>®</sup>. This C code is compiled and linked by Visual C++ and downloaded to the *WINCON 3.1* client. *WINCON 3.1*, comprised of a client and a server, is a real time Windows 2000 based application software that runs code generated by *SIMULINK*<sup>®</sup> using *Real Time Workshop* [98]. Finally, the real-time controller code can be run on the *WINCON 3.1* client and real time control of the emulating shaker is achieved.

The force generated by the emulating shaker is measured by the first input AD channel and the acceleration at the attachment point of the active mechanical emulator by the second input AD channel. The desired force and the measured force are compared and their error is fed to the feedforward/feedback controller. The corrected voltage to the emulating shaker obtained by the controller is output to the emulating shaker through

one DA output channel.

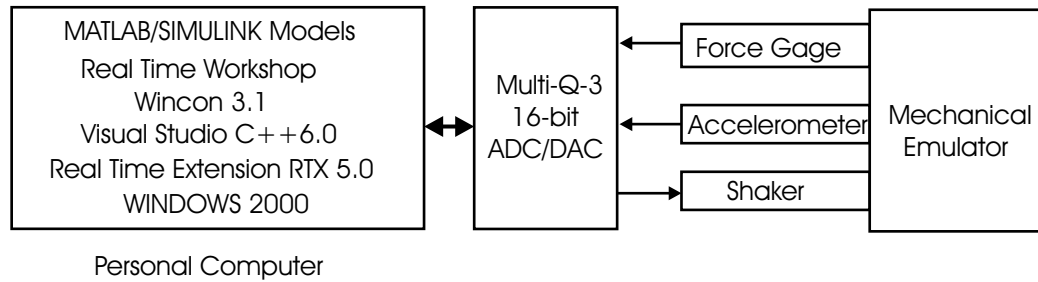


Figure 6.13: Implementation of the Feedforward/feedback Controller for Active Emulation

#### 6.4.5 Performance Evaluation of the Active Emulator

Three experiments were carried out to verify whether the active emulator can generate the same acceleration at the attachment point as does the active machinery. In the first experiment, the emulator and machinery were compared when they only act as vibration sources. The second experiment compares the emulator and machinery when an impulsive force is also applied at the machinery attachment point. The last one compares the emulator and machinery when a force input composed of 5 sinusoids is applied at the attachment point.

In most cases, machinery operates at a frequency higher than the first several lowest fundamental frequencies. When it is started, however, its operating frequency has to pass by these frequencies. Two unbalanced motors thus are chosen to operate at two different frequencies with one between the modes of the machinery and another higher than the modes of the machinery. As discussed in Subsection 6.1, the rotation speeds of the two DC motors have some drift around the desired values. In each experiment below, therefore, the actual rotation speeds must be obtained from the data.

#### Experiment 1: Active Machinery as a Vibration Source

This experiment is carried out to verify whether the active emulator can reproduce the attachment point acceleration of active machinery. In this experiment, no external

excitations are applied.

Two unbalanced motors on the machinery test bed are operated at frequencies of 37.70 Hz and 44.38 Hz, respectively, and the attachment point acceleration data is collected.

The magnitudes of forces which the emulating shaker needs to generate are calculated according to (5.33) in Table 6.2. Here the magnitudes of the transfer accelerance  $A_{tf}(s)$  are read out at the two motor frequencies from Figure 6.11. When machinery is running in steady state, the acceleration data at its attachment point can be measured. The magnitudes of the frequency components of active machinery then can be obtained by Fast Fourier Transformation (FFT) of the measured acceleration data.

The *SIMULINK*<sup>®</sup> model for the feedforward/feedback controller and the data acquisition of the attachment point acceleration is shown in Figure H.1 of Appendix H. The time domain profile comparison of the attachment point accelerations between the machinery and its emulator is shown in Figure 6.14. By FFT, the frequency domain comparison is shown in Figure 6.15. The actual magnitudes at 37.70 Hz and 44.38 Hz have  $0.0341 \text{ m/s}^2$  and  $0.0393 \text{ m/s}^2$ , respectively. Compared to their desired values, their relative errors are  $-4.75\%$  and  $-3.2\%$ , where the negative sign means the actual value is less than the desired. According to these comparisons, it can be concluded that the active emulator can generate approximately the same kind of acceleration at the attachment point as active machinery.

Table 6.2: Calculation of Desired Force for the Emulating Shaker, Experiment 1

Frequency $f$ (Hz)	37.70	44.38
Magnitude of Transfer Accelerance $A_{tf}(s)(kg^{-1})$	0.0572	0.378
Magnitude of Attachment Point Acceleration $a(s) (m/s^2)$	0.0358	0.0406
Force Magnitude $F(s)$ (N)	0.625	0.108

## Experiment 2: Active Machinery with an Impulsive Force Applied at the Attachment Point

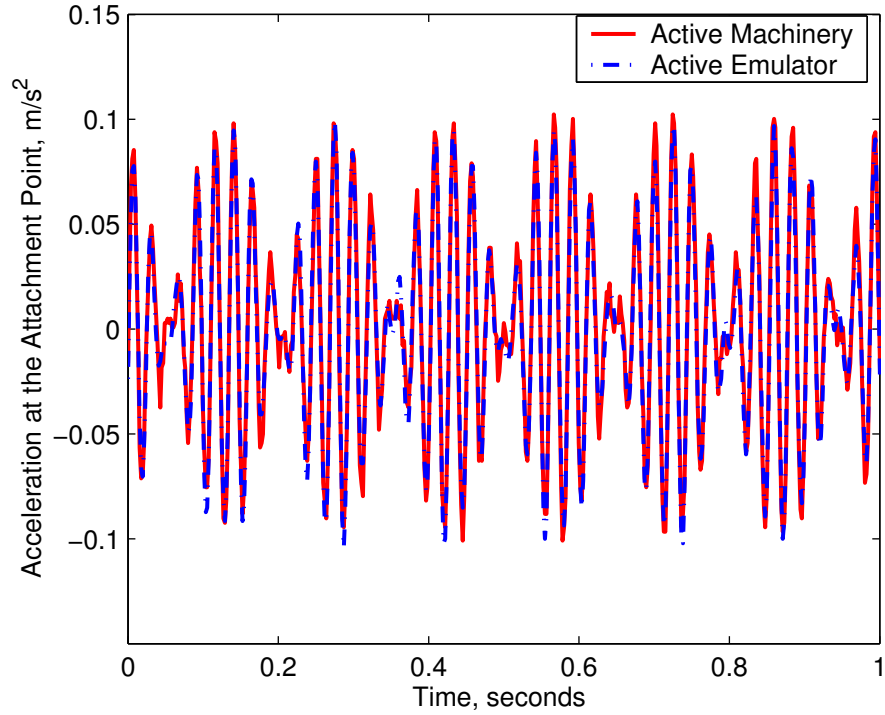


Figure 6.14: Comparison between the Active Machinery and Active Emulator

This test is adopted to see how well the active emulator performs when a transient input force is applied at the attachment point. The advantage of using an impulsive force is that it can simultaneously excite all modes within the frequency range of interest.

To produce this force, a *Wilcoxon<sup>TM</sup>* shaker *Model F3/Z602WA* is mounted at the attachment point of the active machinery. The attachment point acceleration of the active machinery is measured while the shaker is driven by a periodic impulse voltage with an amplitude of 0.1 Volts, a period of 10 seconds and an impulse width of 0.1 second.

Due to drift in the machinery motors, the forces that the emulating shaker should generate are recalculated in Table 6.3. Here, the magnitudes of the transfer acceleration  $A_{tf}(s)$  are read out at the two frequencies of the unbalanced motors in Figure 6.11. The magnitudes of the frequency components in the machinery attachment point acceleration are similarly obtained. The external excitation shaker *F3/Z602WA* is mounted at the attachment point of the active emulator and driven by the same impulse voltage.

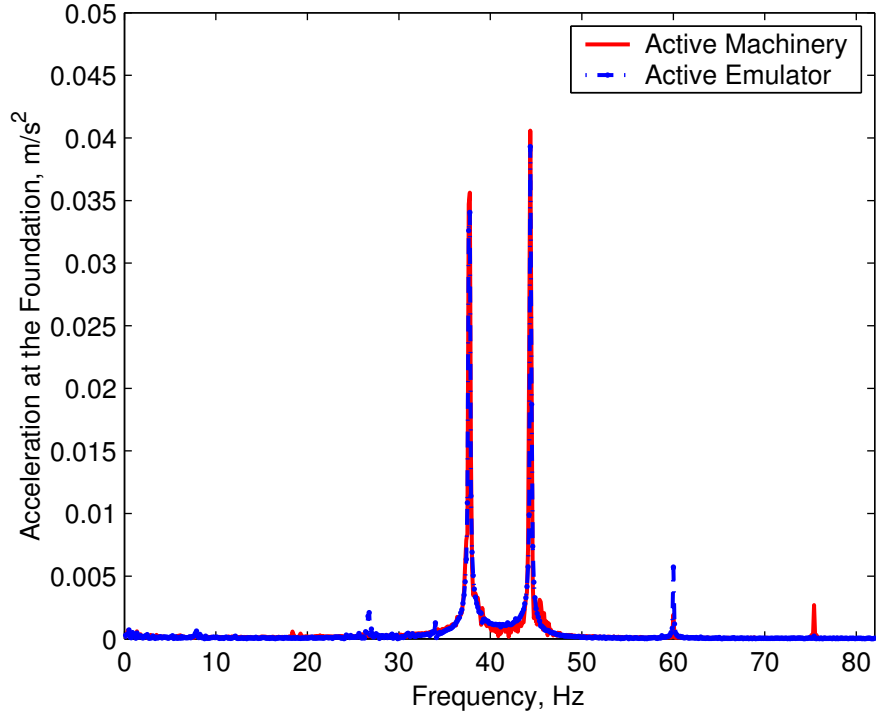


Figure 6.15: Comparison between Active Machinery and Active Emulator, Linear Scale

Table 6.3: Calculation of the Desired Force for the Emulating Shaker, Experiment 2

Frequency $f$ (Hz)	37.69	43.63
Magnitude of Transfer Accelerance $A_{tf}(s)$ ( $kg^{-1}$ )	0.0618	0.440
Magnitude of Attachment Point Acceleration $a(s)$ ( $m/s^2$ )	0.0217	0.042
Force Magnitude $F(s)$ (N)	0.352	0.0955

The *SIMULINK*<sup>®</sup> model for the feedforward/feedback controller and data acquisition of the attachment point acceleration is shown in Figure H.2 of Appendix H. Comparisons between the attachment point accelerations of the machinery and emulator are shown in Figure 6.16 and Figure 6.18. In order to see clearly how the active mechanical emulator performs, a comparison of the impulse response just before and after the impulse excitation is shown in Figure 6.17. The actual magnitudes at 37.69 Hz and 43.63 Hz are  $0.0210 m/s^2$  and  $0.0416 m/s^2$ , respectively, with their relative errors of  $-3.23\%$  and  $-0.95\%$ . Good agreement between the machinery and its emulator is achieved except for some magnitude

difference between 24 Hz and 26.5 Hz, and between 34.5 Hz and 36.5 Hz. This difference is attributed to the magnitude difference between the passive machinery and its passive mechanical emulator, as shown in Figure 6.10. If a passive mechanical emulator possessing better agreement with the machinery can be obtained, the magnitude difference in Figure 6.18 can be improved.

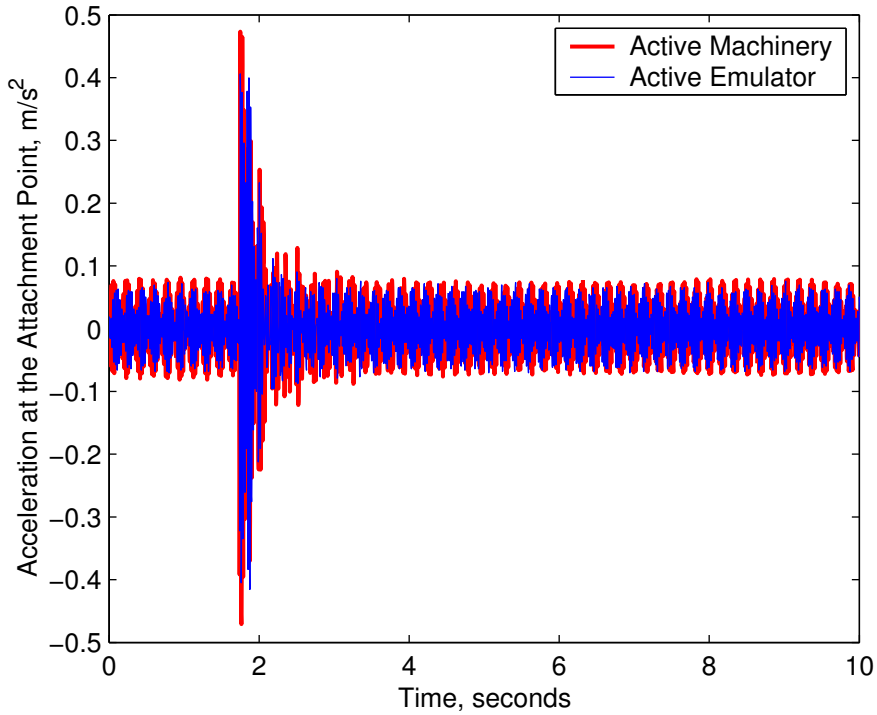


Figure 6.16: Time Domain Comparison between the Active Machinery and Active Emulator, Experiment 2

### Experiment 3: Active Machinery with Periodic External Forcing

As discussed in Chapter 1, machinery and its supporting structure exchange vibration energy at their interface. This test is adopted to verify how the active emulator performs when the active machinery also is experiencing an external input force composed of several harmonic frequencies. In this test, five harmonic frequencies were selected. The magnitudes and frequencies of these five sinusoids are listed in Table 6.4. The same *Wilcoxon<sup>TM</sup>*

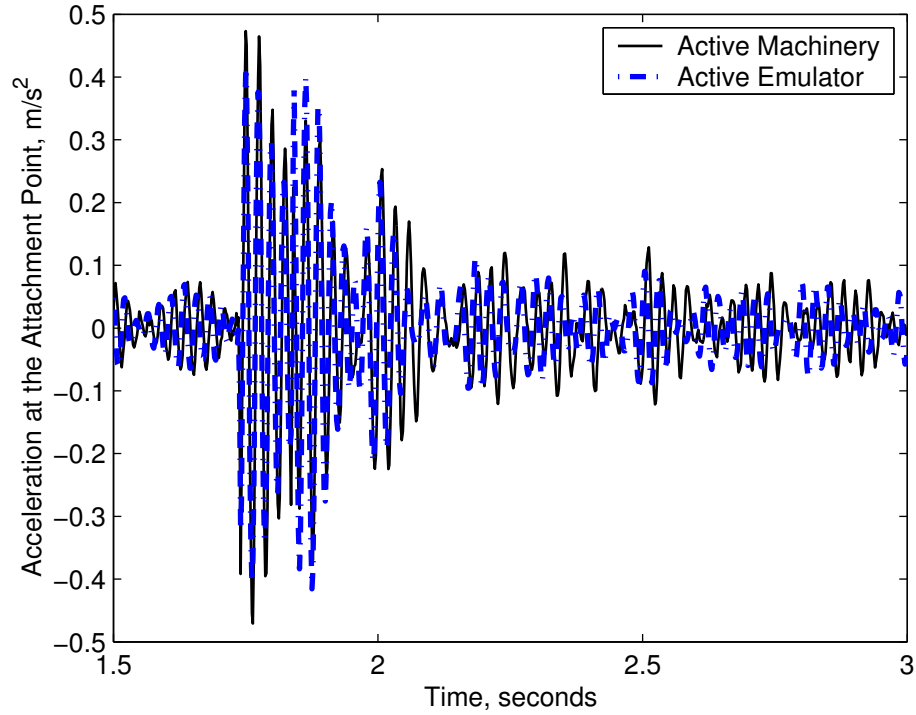


Figure 6.17: Time Domain Close-up Comparison between the Active Machinery and Active Emulator, Experiment 2

shaker *Model F3/Z602WA* as used in the second test was mounted at the attachment point of the active machinery and driven by the sum of these voltages. The attachment point acceleration data was then collected.

For active emulation, the magnitudes of forces that the emulating shaker needs to generate are determined in Table 6.5. Here the magnitudes of the transfer acceleration

Table 6.4: Magnitudes and Frequencies of Five Sinusoids, Experiment 3

Frequency (Hz)	20	28	32	40	50
Magnitude (Volts)	0.0037	0.0075	0.0025	0.005	0.0063

$A_{tf}(s)$  are read out at the machinery operating frequencies in Figure 6.11. The magnitudes of the two frequency components in the attachment point acceleration of active machinery are obtained by FFT.

The *SIMULINK*<sup>®</sup> model for the feedforward/feedback controller and the data ac-



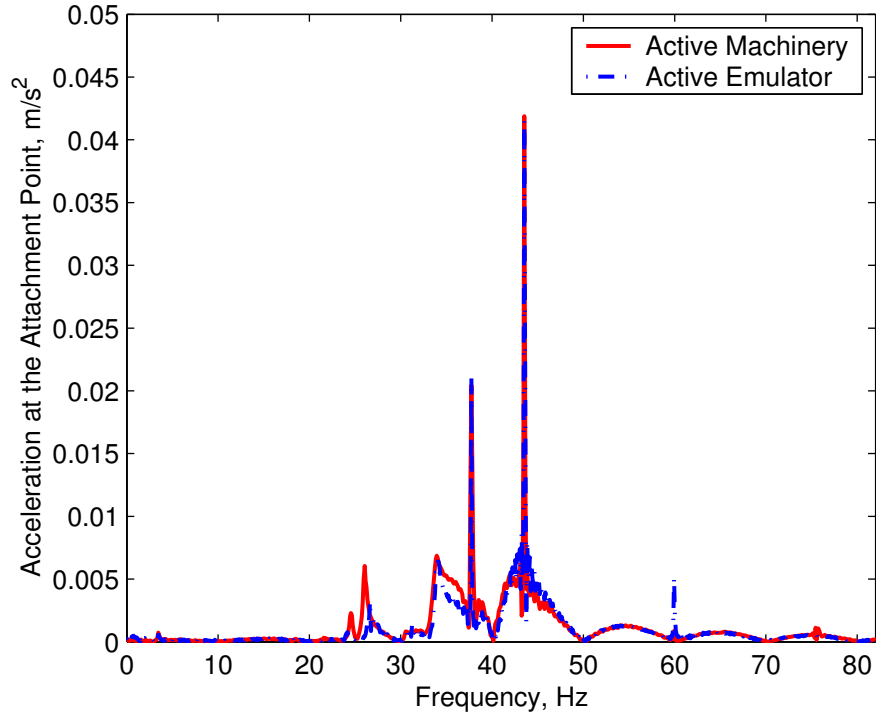


Figure 6.18: Frequency Domain Comparison between the Active Machinery and Active Emulator, Experiment 2

quisition for the attachment point acceleration is shown in Figure H.3 of Appendix H. The acceleration data at the attachment point of the active emulator is collected while the same *F3* shaker is mounted on the active emulator and excited by the same voltage as used in collecting machinery acceleration data. Comparisons between the attachment point accelerations of active machinery and its active mechanical emulator are shown in Figure 6.19 and Figure 6.20. The actual magnitudes at 37.88 Hz and 44.25 Hz are  $0.0352 \text{ m/s}^2$  and  $0.0179 \text{ m/s}^2$ , respectively, yielding relative errors of 6.67% and 1.13%. The magnitude comparison between the active machinery and its active emulator at the five excitation frequencies appears in Table 6.6, where the negative sign means that the former is greater than the latter. The magnitude errors associated with these frequencies can mainly be attributed to the driving-point accelerance error between the passive machinery and the passive mechanical emulator in Figure 6.10.

According to these comparisons, one can also conclude that the agreement between active machinery and its active emulator is very good in the frequency range of interest.

Table 6.5: Calculation of Desired Force for the Emulating Shaker, Experiment 3

Frequency $f$ (Hz)	37.88	44.25
Magnitude of Transfer Accelerance $A_{tf}(s)$ ( $kg^{-1}$ )	0.0485	0.382
Magnitude of Attachment Point Acceleration $a(s)$ ( $m/s^2$ )	0.0330	0.0177
Force magnitude $F(s)$ (N)	0.680	0.0465

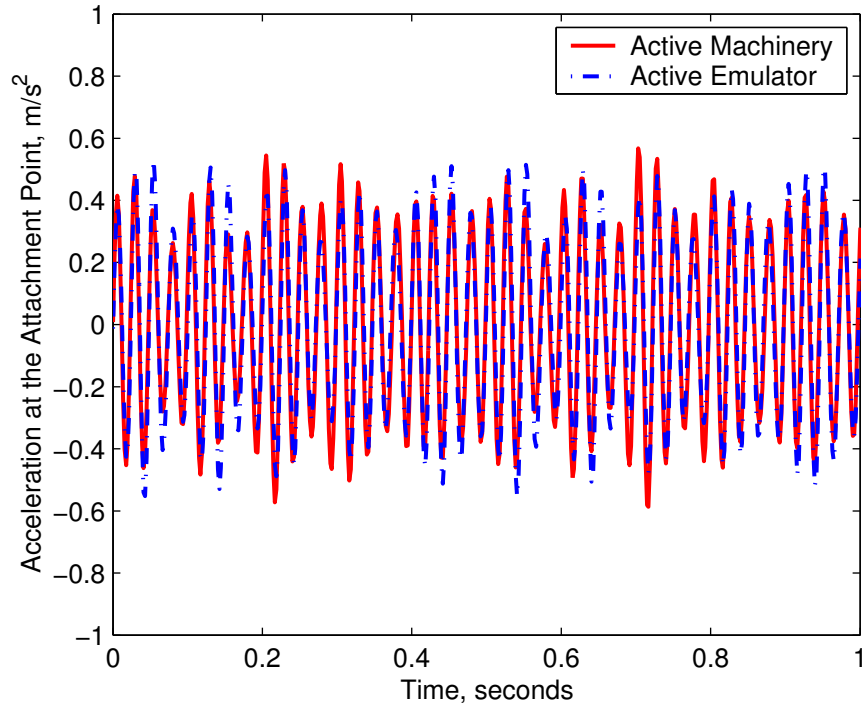


Figure 6.19: Time Domain Comparison of Active Machinery and Active Emulator, Experiment 3

Table 6.6: Acceleration Magnitude for the Active Machinery and its Active Emulator at the Five Excitation Frequencies, Experiment 3

Frequency (Hz)	20	28	32	40	50
Machinery Acceleration Magnitude ( $m/s^2$ )	$2.81 \times 10^{-3}$	0.0347	0.0164	0.385	0.0854
Emulator Acceleration Magnitude ( $m/s^2$ )	$2.66 \times 10^{-3}$	0.0316	0.0148	0.381	0.0926
Relative Acceleration Error	-5.34%	-8.93%	-9.76%	-1.04%	8.43%

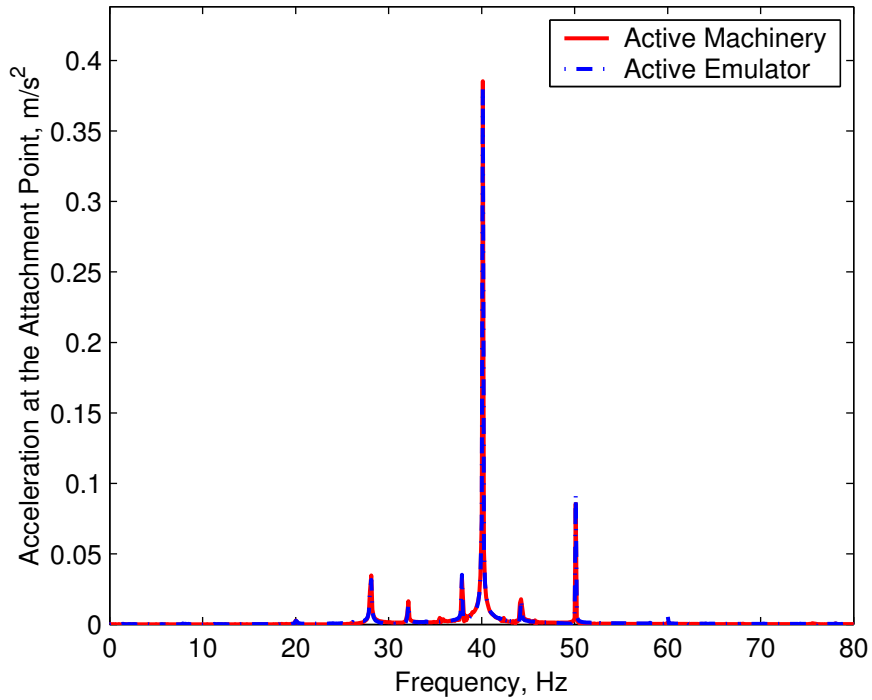


Figure 6.20: Frequency Domain Comparison of the Active Machinery and Active Emulator, Experiment 3

## Chapter 7

# Conclusions

The future cannot be predicted, but futures can be invented. It is our ability to invent the future which gives us hope and makes us who we are.

Dennis Gabor (1900-1979), Nobel Prize Winner in Physics, 1971

This dissertation has developed a mechanical realization theory for designing electromechanical dynamic systems possessing specified input-output properties. Although this research was initially motivated by machinery emulation, this theory can also be applied to the design of electromechanical filters and the design of vibration absorbers. A two-step realization process has been developed to obtain passive mechanical systems in the first step and to modify them into active ones in the subsequent step by incorporating active elements like shakers under closed loop control. With particular application to machinery emulation, the former are designed to emulate machinery when it is not operating, and the latter are used to reproduce the machinery motions at its foundation attachment points due to its operation. This dissertation distinguishes itself from prior work in the following aspects:

1. Multiple foundation attachment points are considered.
2. Many modes are considered for each coordinate direction.

3. Multiple coordinate directions can be accommodated.
4. Damping, both structural damping and general viscous damping, is incorporated in design and implementation.
5. Dynamics of interaction between the active elements and mechanical emulators are accounted for in active emulation.

The major contributions of this dissertation work are summarized as follows:

1. Two techniques have been developed to obtain realizable models for the design of passive mechanical systems with the specified input-output dynamic properties.
  - (a) The first technique involves searching for realizable models in the parameterized space of congruent coordinate transformations, each of which is related to a specific second order model. Each congruent coordinate transformation has been decomposed as a product of four components so that all components can be found in sequential order. The first component is used to mass normalize the given second order model. The second component, which is an orthogonal matrix, is applied to align the input and output influence vectors (or matrices) with the specified vector forms.  $QR$  factorization has been used to obtain this component. The third component, which is also an orthogonal matrix, has been parameterized by a finite set of free parameters, so that realizable models can be achieved by searching in this parameterized space. Under special circumstances, this component can be obtained by well known algorithms in matrix computation. Finally, the last component is obtained by solving the null space vector of the damping and stiffness matrices and scaling this null space vector properly.
  - (b) The second technique involves estimating realizable models, which can include both distributed and lumped mechanical elements, directly from experimental machinery data. This technique is based on an idea of optimization design.

To achieve good agreement at both resonance and antiresonance frequencies, a cost function was defined as a weighted sum of the error between the machinery accelerance experimental data and the corresponding accelerance of the specified model, and the error between the machinery dynamic mass experimental data and the corresponding dynamic mass of the specified model.

2. A design methodology for passive and active mechanical emulators has been developed.

(a) For the design of passive mechanical emulators, two design goals are satisfied, including matching of mass and moment of inertia between machinery and its passive mechanical emulator, and accelerance matching within a frequency range of interest. To meet these goals, a modular passive mechanical emulator configuration has been designed, based on a parallel stiffness realization. For emulating lightly damped machinery, this model has good performance without adding damping couplings between oscillators. For emulating highly damped machinery with strong damping coupling between modes, damping couplings between oscillators can be easily added.

(b) Active mechanical emulators have been designed to reproduce the desired level of vibration at the foundation attachment points associated with machinery operation by adding active elements to passive emulators.

A feedforward/feedback controller following the desired force has been designed and implemented with *MATLAB/SIMULINK*<sup>®</sup>. The dynamics between interaction of the emulating shaker and the passive mechanical emulator has been incorporated in the controller to overcome the shortcoming of a pure PD controller for mechanical systems with many modes.

3. Experimental evaluation of these techniques and design methodology has been successfully carried out through the design of a passive/active mechanical emulator for

a machinery test bed, which undergoes planar motion and has one attachment point. The implemented passive mechanical emulator has the following features:

- (a) In the vertical coordinate direction, it has the same total mass as the machinery.
- (b) In the rotational coordinate direction, it possesses the same moment of inertia with respect to its attachment point.
- (c) In the horizontal coordinate direction, it matches the apparent mass associated with the rigid body mode as well as the acceleration within the frequency range of interest.

The active mechanical emulator has been evaluated under a variety of testing conditions and good agreement has been achieved for all cases. Both numerical and experimental results have demonstrated that the techniques for both passive and active emulation are effective.

- 4. A comprehensive software design toolbox based on *MATLAB<sup>TM</sup>* for passive and active mechanical emulators has been developed.

There are several future directions for this dissertation work as stated briefly below:

- 1. Design and implementation of MIMO mechanical emulators for machinery with multiple attachment points and multiple coordinate directions.
- 2. Applications of this dissertation work in the design of electromechanical filters and vibration absorbers.
- 3. Applications of the idea of active mechanical emulators in active vibration control for structures.

# Appendix A

## State Space Realizations

This appendix presents three well known state space models with useful properties.

### 1. Modal Realization

$$\begin{aligned}\dot{x}_m &= A_m x_m + B_m u \\ y &= C_m x_m + D_m u\end{aligned}\tag{A.1}$$

where  $A_m = \text{diag}\left(\begin{bmatrix} \sigma_1 & \omega_1 \\ -\omega_1 & \sigma_1 \end{bmatrix}, \begin{bmatrix} \sigma_2 & \omega_2 \\ -\omega_2 & \sigma_2 \end{bmatrix}, \dots, \begin{bmatrix} \sigma_n & \omega_n \\ -\omega_n & \sigma_n \end{bmatrix}\right)$ ,  $\omega_i$ 's are damped frequencies and  $n$  is the number of modes.

### 2. McMillan Normal Form Realization [10]

$$\begin{aligned}\dot{x}_m &= A_m x_m + B_m u \\ y &= C_m x_m + D_m u\end{aligned}\tag{A.2}$$

where

$A_m = \text{diag}\left(\begin{bmatrix} 0 & 1 \\ -\omega_{n1}^2 & -2\zeta_1\omega_{n1} \end{bmatrix}, \begin{bmatrix} 0 & 1 \\ -\omega_{n2}^2 & -2\zeta_2\omega_{n2} \end{bmatrix}, \dots, \begin{bmatrix} 0 & 1 \\ -\omega_{nn}^2 & -2\zeta_n\omega_{nn} \end{bmatrix}\right)$  and  $\zeta_i$ 's are modal damping ratios.



### 3. Balanced Realization [11]

A state space model

$$\begin{aligned} \dot{x}_b &= Ax_b + Bu \\ y &= Cx_b + Du \end{aligned} \tag{A.3}$$

is a balanced realization if  $A$  is asymptotically stable and the following two Lyapunov equations hold

$$\begin{aligned} A\Sigma + \Sigma A^T + BB^T &= 0 \\ A^T\Sigma + \Sigma A + C^TC &= 0 \end{aligned} \tag{A.4}$$

where  $\Sigma = \begin{bmatrix} \sigma_1 & & & \\ & \sigma_2 & & \\ & & \ddots & \\ & & & \sigma_n \end{bmatrix}$  is both the controllability and the observability

gramian. Here, Hankel singular values of the transfer function,  $\sigma_i$ , are ordered in nondecreasing order, i.e.,  $\sigma_1 > \sigma_2 > \dots > \sigma_n$ , and  $\sigma_i$  is the index of controllability and observability of a state variable. If  $\sigma_i$  is greater than  $\sigma_j$ , this means the  $i$ 'th state variable is more controllable and observable than the  $j$ 'th state variable. The contribution of  $i$ 'th state variable to the output is larger than that of  $j$ 'th state variable. Balanced model reduction that is based on this balanced realization is carried out by removing states associated with small Hankel singular values [36].

## Appendix B

# Approximation of Nonproportionally Damped Mechanical Systems: An Example

In this appendix, an example is presented for which approximation by proportional damping introduces significant error. This result is typical for heavily damped systems. The example, shown in Figure B.1, is given by

$$\begin{aligned} M\ddot{x} + C\dot{x} + Kx &= Fu \\ y &= H\ddot{x} \end{aligned} \tag{B.1}$$

where the mass, damping and stiffness matrices are given by

$$M = \begin{bmatrix} 1.0000 & 0 & 0 & 0 \\ 0 & 0.2500 & 0 & 0 \\ 0 & 0 & 0.1800 & 0 \\ 0 & 0 & 0 & 0.3000 \end{bmatrix}$$

$$\begin{aligned}
C &= \begin{bmatrix} 1.6000 & -0.2400 & -0.8000 & -0.5600 \\ -0.2400 & 1.2400 & -1.0000 & 0 \\ -0.8000 & -1.0000 & 1.8000 & 0 \\ -0.5600 & 0 & 0 & 0.5600 \end{bmatrix} \\
K &= \begin{bmatrix} 16000 & -2400 & -8000 & -5600 \\ -2400 & 2400 & 0 & 0 \\ -8000 & 0 & 8000 & 0 \\ -5600 & 0 & 0 & 5600 \end{bmatrix} \\
F = H^T &= \begin{bmatrix} 1 & 0 & 0 & 0 \end{bmatrix}^T
\end{aligned} \tag{B.2}$$

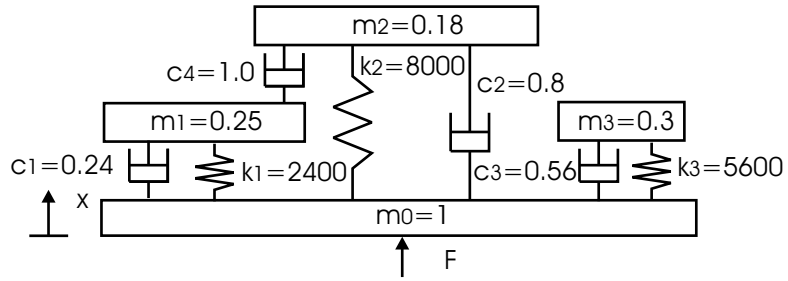


Figure B.1: Nonproportionally Damped Mechanical System

If the dashpot connecting masses  $m_1$  and  $m_2$  is removed, resulting in the approximate model in Figure B.2, the new damping matrix is proportional to the stiffness matrix, given by

$$C_a = 0.0001K \tag{B.3}$$

The frequency responses of the two models are compared in Figure B.3, showing that the approximate model has large errors around the modes of the oscillators associated with masses  $m_1$  and  $m_2$ , labeled  $O_1$  and  $O_2$ . It also introduces some error around the mode of the third oscillator from which no dashpot was removed. This example shows that approximation of vibratory mechanical systems by proportionally damped ones causes significant error, especially for highly damped mechanical systems if dashpots associated

with nonproportional damping are removed. In contrast, the error due to approximation may be modest for mechanical systems without strong damping coupling between modes, as shown in Figure B.4, when  $c_4$  is changed to  $0.1 N \cdot s/m$  in Figure B.1.

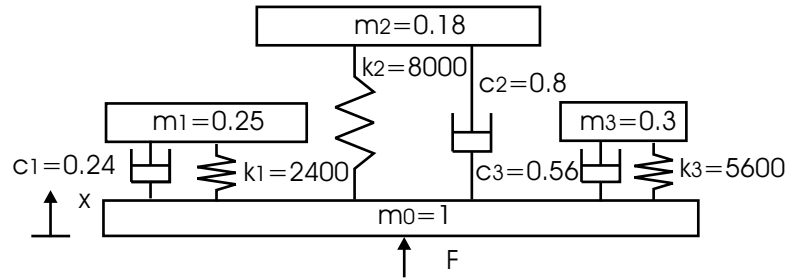


Figure B.2: Approximation of a Nonproportionally Damped Mechanical System by a Proportionally Damped One.

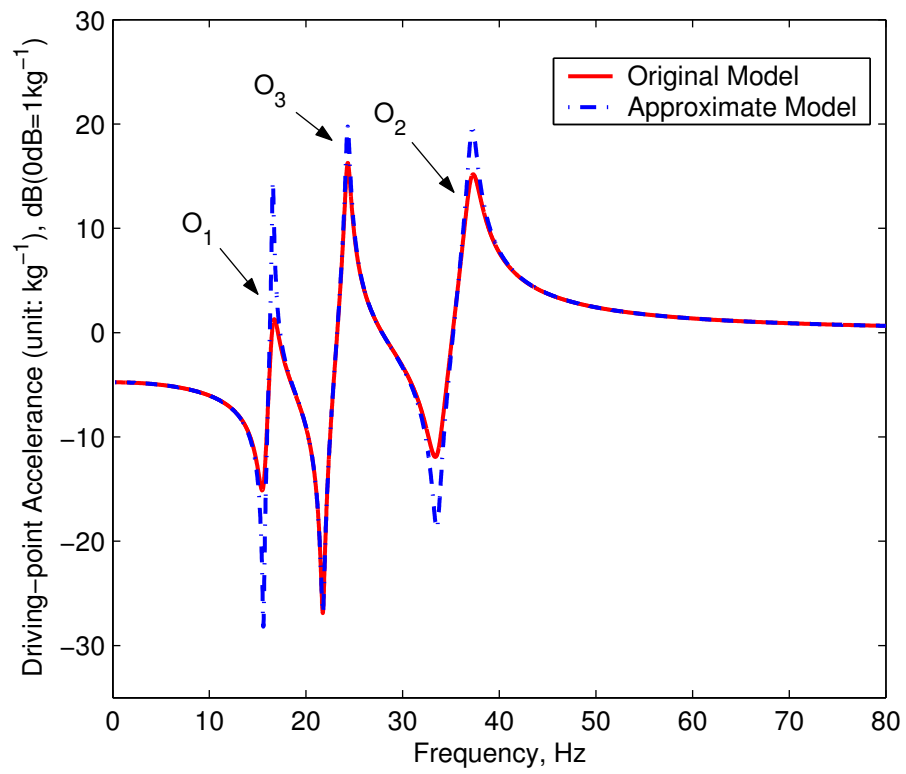


Figure B.3: Approximation of a Nonparallel Model by a Parallel Model: Strong Damping Coupling between Modes.

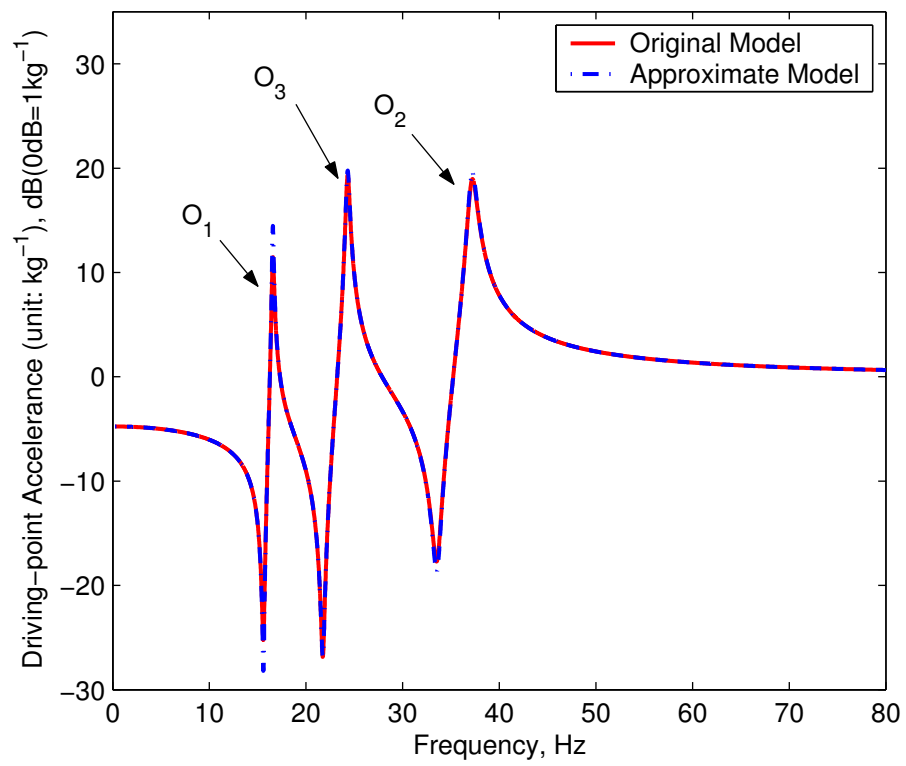


Figure B.4: Approximation of a Nonparallel Model by a Parallel Model: Weak Damping Coupling between Modes.

## Appendix C

# QR Factorization

This appendix defines  $QR$  factorization (or decomposition) and then applies it to a matrix with orthogonal columns.

**Theorem 1.** (*QR Factorization*)[67]

If  $A \in R^{n \times m}$  and  $n \geq m$ , there is an orthogonal matrix  $Q \in R^{n \times n}$  and an upper triangular matrix  $R \in R^{n \times m}$  such that  $A = QR$ .

A detailed description of  $QR$  factorization can be found in [67].

The following theorem applies  $QR$  factorization to a matrix with orthogonal columns, such as arises from the MIMO input and output influence matrices.

**Theorem 2.** If  $F_z = \begin{bmatrix} f_{z_1} & f_{z_2} & \cdots & f_{z_m} \end{bmatrix} \in R^{n \times m}$ , where  $f_{z_i}$  ( $i = 1, 2, \dots, m$ ) are the column vectors which are perpendicular to each other, that is,  $f_{z_i}^T f_{z_j} = 0$  for  $i \neq j$ , then its  $QR$  factorization has the following form

$$F_z = QR \tag{C.1}$$

where

$$R = \begin{bmatrix} \|f_{z_1}\|e_1 & \|f_{z_2}\|e_2 & \cdots & \|f_{z_m}\|e_m \end{bmatrix} \tag{C.2}$$

*Proof.* Suppose the  $QR$  factorization of the matrix  $F_z$  is given by

$$F_z = QR \quad (\text{C.3})$$

where  $Q$  is an orthogonal matrix and  $R$  is an upper triangular matrix.

Premultiplying  $Q$  on both sides of the above equation yields

$$R = Q^T F_z = Q^T \begin{bmatrix} f_{z_1} & f_{z_2} & \cdots & f_{z_m} \end{bmatrix} = \begin{bmatrix} Q^T f_{z_1} & Q^T f_{z_2} & \cdots & Q^T f_{z_m} \end{bmatrix} \quad (\text{C.4})$$

Since  $R$  is an upper triangular matrix,

$$Q^T f_{z_1} = \|f_{z_1}\| e_1 \quad (\text{C.5})$$

Because of the perpendicularity of the columns of  $R$ , the first element of the second column vector  $Q^T f_{z_2}$  has to be zero. Thus,  $Q^T f_{z_2}$  has to be equal to  $\|f_{z_2}\| e_2$ , that is,

$$Q^T f_{z_2} = \|f_{z_2}\| e_2 \quad (\text{C.6})$$

Following the same reasoning, it can be proved that

$$Q^T f_{z_i} = \|f_{z_i}\| e_i \quad \text{for } i = 3, 4, \dots, m \quad (\text{C.7})$$

Therefore, the upper triangular matrix has to be of the form

$$R = \begin{bmatrix} \|f_{z_1}\| e_1 & & & \\ & \|f_{z_2}\| e_2 & & \\ & & \cdots & \\ & & & \|f_{z_m}\| e_m \end{bmatrix} \quad (\text{C.8})$$

□



## Appendix D

# Properties of the Orthogonal Transformation $R_e$

As discussed in Chapter 3, the orthogonal component  $R_e$  in the orthogonal transformation  $R$  for a four-mass SISO driving-point mechanical system can be expressed as

$$R_e(\theta_1, \theta_2, \theta_3) = R_{\theta_1} R_{\theta_2} R_{\theta_3} \quad (\text{D.1})$$

Because of periodicity of the cosine and sine functions, the range for each angle is from 0 to  $2\pi$ . This orthogonal transformation has the following set of properties.

1. Property 1

$$R_e\left(\frac{\pi}{2} + \alpha, \frac{\pi}{2}, \alpha\right) = \begin{bmatrix} 1 & 0 & 0 & 0 \\ 0 & 0 & 0 & 1 \\ 0 & 1 & 0 & 0 \\ 0 & 0 & 1 & 0 \end{bmatrix} \text{ for any } \alpha.$$

This property means that all second order models along the line  $\left(\frac{\pi}{2} + \alpha, \frac{\pi}{2}, \alpha\right)$  in the angle space are the same. They are related to the original second order model by the permutation matrix  $R_e\left(\frac{\pi}{2} + \alpha, \frac{\pi}{2}, \alpha\right)$ .

2. Property 2

$$R_e\left(\frac{\pi}{2} + \alpha + \beta, \frac{\pi}{2}, \alpha\right) = \begin{bmatrix} 1 & 0 & 0 & 0 \\ 0 & -\sin\beta & 0 & \cos\beta \\ 0 & \cos\beta & 0 & \sin\beta \\ 0 & 0 & 1 & 0 \end{bmatrix}.$$

This is a generalization of Property 1. It implies that all second order models along the line  $\left(\frac{\pi}{2} + \alpha + \beta, \frac{\pi}{2}, \alpha\right)$  are identical to each other.

3. Property 3

$$R_e(\theta_1, \theta_2, \theta_3) = R_e(\theta_1 + \pi, \pi - \theta_2, \pi + \theta_3) \text{ or equivalently } R_e(\theta_1, \frac{\pi}{2} + \alpha, \theta_3) = R(\theta_1 + \pi, \frac{\pi}{2} - \alpha, \pi + \theta_3).$$

This property implies that all second order models repeat with a period of  $\pi$  along the  $\theta_1$  and  $\theta_3$  axes and have a mirror symmetry with respect to the  $\theta_2 = \frac{\pi}{2}$  plane. This also means that the second order model at  $\theta_1 = \pi$ ,  $\theta_2 = \pi$  and  $\theta_3 = \pi$  is the same as that at  $\theta_1 = 0$ ,  $\theta_2 = 0$  and  $\theta_3 = 0$ .

Let  $\begin{bmatrix} \theta_1 & \theta_2 & \theta_3 \end{bmatrix}^T = \begin{bmatrix} \frac{\pi}{2} + \alpha_1 & \frac{\pi}{2} + \alpha_2 & \alpha_3 \end{bmatrix}^T$ , then the following identity can be obtained

$$R_e\left(\frac{\pi}{2} + \alpha_1, \frac{\pi}{2} + \alpha_2, \alpha_3\right) = R_e\left(\frac{3\pi}{2} + \alpha_1, \frac{\pi}{2} - \alpha_2, \alpha_3 + \pi\right)$$

This implies that all the second order models around  $\left(\frac{\pi}{2}, \frac{\pi}{2}, 0\right)$  are equivalent to those around  $\left(\frac{3\pi}{2}, \frac{\pi}{2}, \pi\right)$ .

In addition, let  $\begin{bmatrix} \theta_1 & \theta_2 & \theta_3 \end{bmatrix}^T = \begin{bmatrix} \frac{3\pi}{2} + \alpha_1 & \alpha_2 & \frac{\pi}{2} + \alpha_3 \end{bmatrix}^T$ , then the following identity can be obtained

$$R_e\left(\frac{3\pi}{2} + \alpha_1, \alpha_2, \frac{\pi}{2} + \alpha_3\right) = R_e\left(\frac{\pi}{2} + \alpha_1, \pi - \alpha_2, \frac{3\pi}{2} + \alpha_3\right)$$

This implies that all the second order models around  $\left(\frac{3\pi}{2}, 0, \frac{\pi}{2}\right)$  are equivalent to those around  $\left(\frac{\pi}{2}, \pi, \frac{3\pi}{2}\right)$ .

4. Property 4

$$R_e \left( \frac{\pi}{2} + \alpha_1, \frac{\pi}{2} + \alpha_2, \alpha_3 \right) = R_e \left( \frac{\pi}{2}, \frac{\pi}{2}, 0 \right) R_e (\theta_1, \theta_2, \theta_3)$$

This property means that the second order models around  $\left( \frac{\pi}{2}, \frac{\pi}{2}, 0 \right)$  are related to those around the origin by congruent transformations with a permutation matrix  $R_e \left( \frac{\pi}{2}, \frac{\pi}{2}, 0 \right)$ .

5. Property 5

$$R_e \left( \frac{\pi}{2} + \alpha_1, \pi - \alpha_2, \frac{3\pi}{2} + \alpha_3 \right) = R_e \left( \frac{\pi}{2}, \pi, \frac{3\pi}{2} \right) R_e (\theta_1, \theta_2, \theta_3)$$

This property means that the second order models around  $\left( \frac{\pi}{2}, \pi, \frac{3\pi}{2} \right)$  are related to those around the origin by congruent transformations with a permutation matrix  $R_e \left( \frac{\pi}{2}, \pi, \frac{3\pi}{2} \right)$ .

Using these properties, the number of the realizable regions from exhaustive search in the solution space may be reduced to a single realizable region. Similar properties may be derived for systems with more masses.

## Appendix E

# Modeling the Base Structure of the Passive Mechanical Emulator

The base structure considered here is defined as the structure after removing all oscillators in Figure 5.1, which can be idealized as an elastic beam connecting two lumped masses at its two ends, as depicted in Figure E.1. The notation of all parameters in the figure is defined in Table E.1.

There are two methods for modeling this base structure. The first one is based on the Euler-Bernoulli continuous beam model while the second one uses a Finite Element Analysis (FEA) beam model. Both methods are presented below.

### E.1 Euler-Bernoulli Beam Model

Following a consistent set of sign conventions for the internal forces and moments, the base structure of the passive mechanical emulator can be modeled by the Euler-Bernoulli beam model as

$$E_b I_b \frac{\partial^4 y}{\partial x^4} + \rho A_b \ddot{y} = 0 \quad (\text{E.1})$$

with the following four boundary conditions

$$\begin{aligned}
(1) \quad & m_b(\ddot{y} - b_b \frac{\partial \ddot{y}}{\partial x}) + E_b I_b \frac{\partial^3 y}{\partial x^3} = F \quad \text{at } x = 0 \quad (\text{Force balance}) \\
(2) \quad & L_{C_b} \frac{\partial \ddot{y}}{\partial x} + E_b I_b b_b \frac{\partial^3 y}{\partial x^3} - E_b I_b \frac{\partial^2 y}{\partial x^2} = 0 \quad \text{at } x = 0 \quad (\text{Moment Balance}) \\
(3) \quad & m_a(\ddot{y} + b_a \frac{\partial \ddot{y}}{\partial x}) - E_b I_b \frac{\partial^3 y}{\partial x^3} = 0 \quad \text{at } x = L_b \quad (\text{Force balance}) \\
(4) \quad & L_{C_a} \frac{\partial \ddot{y}}{\partial x} + E_b I_b b_a \frac{\partial^3 y}{\partial x^3} + E_b I_b \frac{\partial^2 y}{\partial x^2} = 0 \quad \text{at } x = L_b \quad (\text{Moment balance})
\end{aligned} \tag{E.2}$$

Table E.1: Parameters of the Base Structure in the Passive Mechanical Emulator

Notation	Explanation
$E_b$	Young's modulus of the beam material
$E_{b_0}$	Elastic (or storage) modulus, a real number
$\rho_b$	Density of the beam material
$I_b$	Area moment of inertia
$L_b$	Length of the beam
$y$	Deflection of the beam
$A_b$	Area of the cross section of the beam
$m_b$	Mass of the base frame, round rod and mounting fixtures in Figure 5.1
$m_a$	Mass of the additional mass in Figure 5.1
$b_b$	Distance from the mass center of the mass $m_b$ to one end of the beam
$b_a$	Distance from the mass center of the mass $m_a$ to another end of the beam
$I_{C_b}$	Moment of inertia of the mass $m_b$ with respect to its mass center $C_b$
$I_{C_a}$	Moment of inertia of the mass $m_a$ with respect to its mass center $C_a$
$\eta_b$	Effective loss factor of the beam with damping treatments

To incorporate damping in the model, a complex Young's modulus of the beam should be used, which can be expressed as

$$E_b = E_{b_0}(1 + i\eta_b) \tag{E.3}$$

After the Laplace transformation of (E.1) and the four boundary conditions (E.2), the

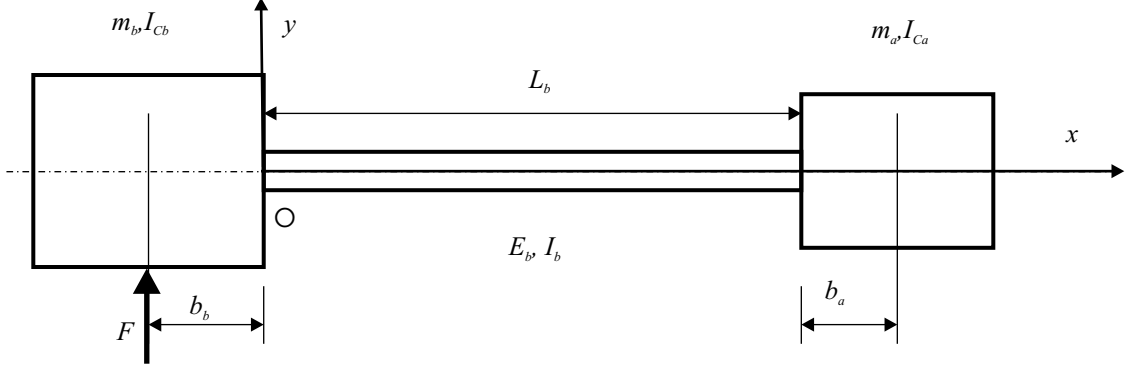


Figure E.1: Modeling the Base Structure of the Machinery Emulator

following set of equations in the frequency domain is obtained by substituting  $s = j\omega$

$$E_b I_b \frac{\partial^4 y}{\partial x^4} - \rho_b A_b \omega^2 y = 0 \quad (\text{E.4})$$

with the following four boundary conditions

$$\begin{aligned} (1) \quad & -m_b \omega^2 (y - b_b \frac{\partial y}{\partial x}) + E_b I_b \frac{\partial^3 y}{\partial x^3} = F \quad \text{at } x = 0 \quad (\text{Force balance}) \\ (2) \quad & -L_{Cb} \omega^2 \frac{\partial y}{\partial x} + E_b I_b b_b \frac{\partial^3 y}{\partial x^3} - E_b I_b \frac{\partial^2 y}{\partial x^2} = 0 \quad \text{at } x = 0 \quad (\text{Moment Balance}) \\ (3) \quad & -m_a \omega^2 (y + b_a \frac{\partial y}{\partial x}) - E_b I_b \frac{\partial^3 y}{\partial x^3} = 0 \quad \text{at } x = L_b \quad (\text{Force balance}) \\ (4) \quad & -L_{Ca} \omega^2 \frac{\partial y}{\partial x} + E_b I_b b_a \frac{\partial^3 y}{\partial x^3} + E_b I_b \frac{\partial^2 y}{\partial x^2} = 0 \quad \text{at } x = L_b \quad (\text{Moment balance}) \end{aligned} \quad (\text{E.5})$$

Denote  $\alpha_b = (\frac{\rho_b A_b \omega^2}{E_b I_b})^{\frac{1}{4}}$ . In general, the solution to the Euler-Bernoulli beam model can be expressed as [9].

$$y(x, \omega) = c_1 \sin \alpha_b x + c_2 \cos \alpha_b x + c_3 \sinh \alpha_b x + c_4 \cosh \alpha_b x \quad (\text{E.6})$$

where four unknown  $\omega$  dependent coefficients  $c_i$  ( $i = 1, 2, 3, 4$ ) can be solved with the above four boundary conditions.

Derivatives of (E.6) are given by the following equations

$$\begin{aligned}
\frac{\partial y(x, \omega)}{\partial x} &= \alpha_b (c_1 \cos \alpha_b x - c_2 \sin \alpha_b x + c_3 \cosh \alpha_b x + c_4 \sinh \alpha_b x) \\
\frac{\partial^2 y(x, \omega)}{\partial x^2} &= \alpha_b^2 (-c_1 \sin \alpha_b x - c_2 \cos \alpha_b x + c_3 \sinh \alpha_b x + c_4 \cosh \alpha_b x) \\
\frac{\partial^3 y(x, \omega)}{\partial x^3} &= \alpha_b^3 (-c_1 \cos \alpha_b x + c_2 \sin \alpha_b x + c_3 \cosh \alpha_b x + c_4 \sinh \alpha_b x)
\end{aligned} \tag{E.7}$$

Substituting  $y(x, \omega)$  in (E.6) and its derivatives into the four boundary conditions, yields

$$\begin{bmatrix} a_{11} & a_{12} & a_{13} & a_{14} \\ a_{21} & a_{22} & a_{23} & a_{24} \\ a_{31} & a_{32} & a_{33} & a_{34} \\ a_{41} & a_{42} & a_{43} & a_{44} \end{bmatrix} \begin{bmatrix} c_1 \\ c_2 \\ c_3 \\ c_4 \end{bmatrix} = \begin{bmatrix} F(\omega) \\ 0 \\ 0 \\ 0 \end{bmatrix} \tag{E.8}$$

where the elements in the matrix  $A(\omega)$  are given by

$$\begin{aligned}
a_{11} &= b_b m_b \omega^2 \alpha_b - E_b I_b \alpha_b^3 \\
a_{12} &= -m_b \omega^2 \\
a_{13} &= m_b b_b \omega^2 \alpha_b + E_b I_b \alpha_b^3 \\
a_{14} &= -m_b \omega^2 \\
a_{21} &= -L_{C_b} \omega^2 \alpha_b - E_b I_b b_b \alpha_b^3 \\
a_{22} &= E_b I_b \alpha_b^2 \\
a_{23} &= -L_{C_b} \omega^2 \alpha_b + E_b I_b b_b \alpha_b^3 \\
a_{24} &= -E_b I_b \alpha_b^2 \\
a_{31} &= -m_a \omega^2 \sin(\alpha_b L_b) - m_a \omega^2 b_a \alpha_b \cos(\alpha_b L_b) + E_b I_b \alpha_b^3 \cos(\alpha_b L_b) \\
a_{32} &= -m_a \omega^2 \cos(\alpha_b L_b) + m_a \omega^2 b_a \alpha_b \sin(\alpha_b L_b) - E_b I_b \alpha_b^3 \sin(\alpha_b L_b) \\
a_{33} &= -m_a \omega^2 \sinh(\alpha_b L_b) - m_a \omega^2 b_a \alpha_b \cosh(\alpha_b L_b) - E_b I_b \alpha_b^3 \cosh(\alpha_b L_b) \\
a_{34} &= -m_a \omega^2 \cosh(\alpha_b L_b) - m_a \omega^2 b_a \alpha_b \sinh(\alpha_b L_b) - E_b I_b \alpha_b^3 \sinh(\alpha_b L_b)
\end{aligned}$$

$$\begin{aligned}
a_{41} &= -L_{C_a}\omega^2\alpha_b\cos(\alpha_bL_b) - E_bI_b b_a\alpha_b^3\cos(\alpha_bL_b) - E_bI_b\alpha_b^2\sin(\alpha_bL_b) \\
a_{42} &= L_{C_a}\omega^2\alpha_b\sin(\alpha_bL_b) + E_bI_b b_a\alpha_b^3\sin(\alpha_bL_b) - E_bI_b\alpha_b^2\cos(\alpha_bL_b) \\
a_{43} &= -L_{C_a}\omega^2\alpha_b\cosh(\alpha_bL_b) + E_bI_b b_a\alpha_b^3\cosh(\alpha_bL_b) + E_bI_b\alpha_b^2\sinh(\alpha_bL_b) \\
a_{44} &= -L_{C_a}\omega^2\alpha_b\sinh(\alpha_bL_b) + E_bI_b b_a\alpha_b^3\sinh(\alpha_bL_b) + E_bI_b\alpha_b^2\cosh(\alpha_bL_b)
\end{aligned}$$

Equation (E.8) can be solved for the coefficients  $c_i$  at each frequency point. After obtaining these coefficients, the driving-point acceleration at the center of the mass  $m_b$  can be determined by

$$A_b(\omega) = -\frac{\omega^2 \left[ y - b_b \frac{\partial y}{\partial x} \right]_{x=0}}{F} \quad (\text{E.9})$$

which can be further simplified as follows

$$A_b(\omega) = -\omega^2 [c_2 + c_4 - b_b(c_1 + c_3)\alpha_b], \quad (\text{E.10})$$

which is the driving-point acceleration of the base structure of the passive mechanical emulator in Figure 5.1.

If the frequency of the structural mode is higher than the upper limit of the frequency range of interest, the base structure of the passive mechanical emulator in Figure 5.1 can be considered a rigid body. Otherwise, the structural mode of the base structure can be used to match one of the machinery modes in two ways, as discussed in Subsection 5.1.1.

The base structure can also be modeled according to the FEA beam model, which is discussed below.

## E.2 FEA Beam Model

Another modeling method for the base structure of the passive mechanical emulator in Figure 5.1 is based on an FEA beam model. When only the planar motion of a beam is



concerned as depicted in Figure E.2, the displacement vector can be chosen as follows

$$q_i = \begin{bmatrix} u_i & y_i & \alpha_i \end{bmatrix}^T \quad (i=1, 2) \quad (\text{E.11})$$

By choosing a proper set of shape functions, the mass matrix and stiffness matrix of this beam model can be obtained as follows [99]

$$M_b = \rho_b A_b L_b \begin{bmatrix} \frac{1}{3} & 0 & 0 & \frac{1}{6} & 0 & 0 \\ 0 & \frac{13}{35} & \frac{11}{210} L_b & 0 & \frac{9}{70} & -\frac{13}{420} L_b \\ 0 & \frac{11}{210} L_b & \frac{1}{105} L_b^2 & 0 & \frac{13}{420} L_b & -\frac{1}{140} L_b \\ \frac{1}{6} & 0 & 0 & \frac{1}{3} & 0 & 0 \\ 0 & \frac{9}{70} & \frac{13}{420} L_b & 0 & \frac{13}{35} & -\frac{11}{210} L_b \\ 0 & -\frac{13}{420} L_b & -\frac{1}{140} L_b^2 & 0 & -\frac{11}{210} L_b & \frac{1}{105} L_b^2 \end{bmatrix} \quad (\text{E.12})$$

$$K_b = \begin{bmatrix} \frac{E_b A_b}{L_b} & 0 & 0 & -\frac{E_b A_b}{L_b} & 0 & 0 \\ 0 & \frac{12E_b I_b}{L_b^3} & \frac{6E_b I_b}{L_b^2} & 0 & -\frac{12E_b I_b}{L_b^3} & \frac{6E_b I_b}{L_b^2} \\ 0 & \frac{6E_b I_b}{L_b^2} & \frac{4E_b I_b}{L_b} & 0 & -\frac{6E_b I_b}{L_b^2} & \frac{2E_b I_b}{L_b} \\ -\frac{E_b A_b}{L_b} & 0 & 0 & \frac{E_b A_b}{L_b} & 0 & 0 \\ 0 & -\frac{12E_b I_b}{L_b^3} & -\frac{6E_b I_b}{L_b^2} & 0 & \frac{12E_b I_b}{L_b^3} & -\frac{6E_b I_b}{L_b^2} \\ 0 & \frac{6E_b I_b}{L_b^2} & \frac{2E_b I_b}{L_b} & 0 & -\frac{6E_b I_b}{L_b^2} & \frac{4E_b I_b}{L_b} \end{bmatrix} \quad (\text{E.13})$$

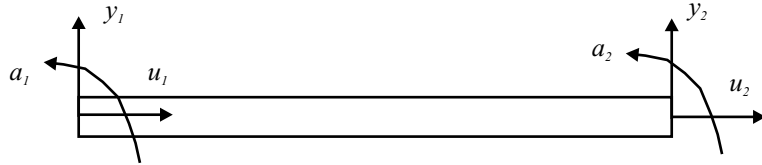


Figure E.2: FEA Beam Model

The mass matrix due to the lumped masses at both ends of the beam is given by

$$M_m = \text{diag}\left( \begin{bmatrix} m_b & m_b & I_{C_b} & m_a & m_a & I_{C_a} \end{bmatrix} \right) \quad (\text{E.14})$$

Therefore, the total mass matrix of the base structure is given by

$$M = M_m + M_b \quad (\text{E.15})$$

Thus, the driving-point accelerance can be obtained from the following second order model

$$\begin{aligned} M\ddot{x} + K_b x &= F u \\ y &= H \dot{x} \end{aligned} \quad (\text{E.16})$$

where  $x = \begin{bmatrix} q_1^T & q_2^T \end{bmatrix}$ ,  $F = \begin{bmatrix} 0 & 1 & 0 & 0 & 0 & 0 \end{bmatrix}^T$  and  $H = \begin{bmatrix} 0 & 1 & -b_b & 0 & 0 & 0 \end{bmatrix}$ .

## Appendix F

# Building Single-mode Oscillators from Distributed Mechanical Elements

While building oscillators in a passive mechanical emulator, lumped-parameter masses and springs are realized by rectangular steel blocks and thin spring steel plates with appropriate lengths between their mass centers and mounting fixtures, respectively. From the theoretical viewpoint, there are an infinite number of modes in each oscillator. In practice, however, it is enough to only consider the first oscillator mode of the bending of the spring steel plate with a mass at its tip. In this appendix, the conditions under which this experimental oscillator can well approximate a lumped-parameter oscillator are investigated.

### F.1 Modeling an Oscillator from Distributed Elements

Each oscillator built from distributed elements in Figure 5.1 can be idealized by the model shown in Figure F.1. The force from the round rod  $F$  is exerted at one end of the beam  $O$  and the oscillator mass  $m_o$  is attached at the other end of the beam. The notation is

defined in Table F.1. The block mass is attached at the end of a spring steel beam  $x = L_o$ . At  $x = 0$ , an input force  $F$  is applied. Since the oscillators are perpendicularly fixed to a far heavier base frame, the slope of the beam at  $x = 0$  can approximately be taken as zero. Consequently, this oscillator model can be imagined as one in which the oscillator vibrates with its left end sliding in a prismatic or translational joint. A mathematical model for this oscillator with consideration of the effect of the moment of inertia of the oscillator mass and geometric dimension of the oscillator mass will be obtained below since the dimension of the oscillator mass is comparable to the length of the beam.

Table F.1: Notation for Parameters in the Oscillator Model

Notation	Explanation
$E_o$	Complex Young's modulus of the beam material with damping treatments, $E_o = E_{o0}(1 + j\eta_o)$
$E_{o0}$	Elastic (or storage) modulus, a real number
$\rho_o$	Density of the beam material
$I_o$	Area moment of inertia of the cross section of the beam
$y$	Deflection of the beam
$A_o$	Area of the cross section of the beam
$m_o$	Oscillator mass
$b_o$	Distance from the mass center of the mass $m_o$ to one end of the beam
$L_o$	Length of the beam in the oscillator
$I_{C_o}$	Moment of inertia of the oscillator mass $m_o$ with respect to its mass center $C_o$
$\eta_o$	Effective loss factor of the beam with damping treatments

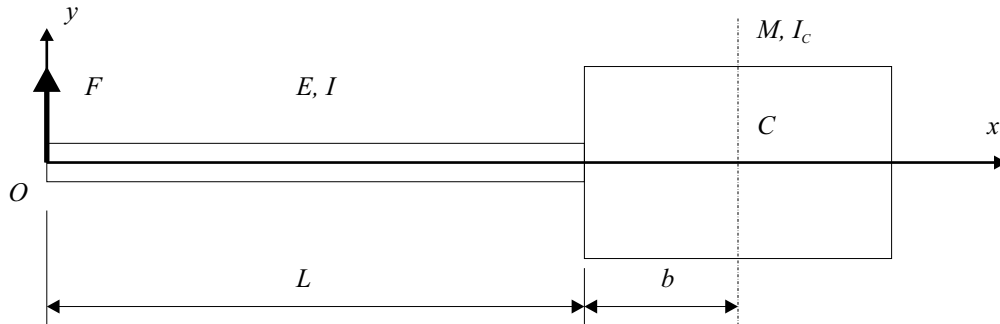


Figure F.1: Oscillator Model

The oscillator can be modeled by the Euler-Bernoulli beam model, given by

$$E_o I_o \frac{\partial^4 y}{\partial x^4} + \rho_o A_o \ddot{y} = 0 \quad (\text{F.1})$$

with the following four boundary conditions

$$\begin{aligned} (1) \quad & -E_o I_o \frac{\partial^3 y}{\partial x^3} + F = 0 & \text{at } x = 0 & \quad (\text{Force balance}) \\ (2) \quad & \frac{\partial y}{\partial x} = 0 & \text{at } x = 0 & \quad (\text{Zero slope}) \\ (3) \quad & m(\ddot{y} + b \frac{\partial \ddot{y}}{\partial x}) - E_o I_o \frac{\partial^3 y}{\partial x^3} = 0 & \text{at } x = L_o & \quad (\text{Force balance}) \\ (4) \quad & I_{C_o} \frac{\partial \ddot{y}}{\partial x} + E_o I_o b_o \frac{\partial^3 y}{\partial x^3} + E_o I_o \frac{\partial^2 y}{\partial x^2} = 0 & \text{at } x = L_o & \quad (\text{Moment balance}) \end{aligned} \quad (\text{F.2})$$

After the Laplace transformation of (F.1) and the four boundary conditions, the following equation in the frequency domain can be obtained by substituting  $s = j\omega$

$$E_o I_o \frac{\partial^4 y}{\partial x^4} - \rho_o A_o \omega^2 y = 0 \quad (\text{F.3})$$

with the following four boundary conditions

$$\begin{aligned} (1) \quad & -E_o I_o \frac{\partial^3 y}{\partial x^3} + F = 0 & \text{at } x = 0 & \quad (\text{Force balance}) \\ (2) \quad & \frac{\partial y}{\partial x} = 0 & \text{at } x = 0 & \quad (\text{Zero slope}) \\ (3) \quad & -m\omega^2(y + b \frac{\partial y}{\partial x}) - E_o I_o \frac{\partial^3 y}{\partial x^3} = 0 & \text{at } x = L_o & \quad (\text{Force balance}) \\ (4) \quad & -I_{C_o} \omega^2 \frac{\partial y}{\partial x} + E_o I_o b_o \frac{\partial^3 y}{\partial x^3} + E_o I_o \frac{\partial^2 y}{\partial x^2} = 0 & \text{at } x = L_o & \quad (\text{Moment balance}) \end{aligned} \quad (\text{F.4})$$

Denote  $\alpha = (\frac{\rho_o A_o \omega^2}{E_o I_o})^{\frac{1}{4}}$ . In general, the solution to (F.3) can be expressed

$$y(x, \omega) = A_1 \sin \alpha x + A_2 \cos \alpha x + A_3 \sinh \alpha x + A_4 \cosh \alpha x, \quad (\text{F.5})$$

where  $A_i$  ( $i = 1, 2, 3, 4$ ) are four unknown coefficients dependent on  $\omega$ .

It is desired to obtain the oscillator driving-point accelerance at  $x = 0$ , given by the

following equation

$$A_o(\omega) = \frac{\omega^2 y(0, \omega)}{F(\omega)} \quad (\text{F.6})$$

After substituting (F.5) and its derivatives (E.7) into the four boundary conditions, the following set of linear algebraic equations with four unknown coefficients  $A_i$  ( $i = 1, 2, 3, 4$ ) can be obtained

$$\begin{bmatrix} -a_1\alpha & 0 & -a_1\alpha & 0 \\ 0 & a_1 & 0 & -a_1 \\ a_2 & a_3 & a_4 & a_5 \\ a_6 & a_7 & a_8 & a_9 \end{bmatrix} \begin{bmatrix} A_1 \\ A_2 \\ A_3 \\ A_4 \end{bmatrix} = \begin{bmatrix} F(\omega) \\ 0 \\ 0 \\ 0 \end{bmatrix} \quad (\text{F.7})$$

where the elements in the  $4 \times 4$  matrix are given by

$$\begin{aligned} a_1 &= E_o I_o \alpha^2 \\ a_2 &= m\omega^2 [\sin(\alpha L_o) + b_o \alpha \cos(\alpha L_o)] - E_o I_o \alpha^3 \cos(\alpha L_o) \\ a_3 &= m\omega^2 (\cos(\alpha L_o) - b_o \alpha \sin(\alpha L_o)) + E_o I_o \alpha^3 \sin(\alpha L_o) \\ a_4 &= m\omega^2 [\sinh(\alpha L_o) + b_o \alpha \cosh(\alpha L_o)] + E_o I_o \alpha^3 \cosh(\alpha L_o) \\ a_5 &= m\omega^2 [\cosh(\alpha L_o) + b_o \alpha \sinh(\alpha L_o)] + E_o I_o \alpha^3 \sinh(\alpha L_o) \\ a_6 &= -I_{C_o} \alpha \omega^2 \cos(\alpha L_o) - E_o I_o \alpha^2 [\sin(\alpha L_o) + b_o \alpha \cos(\alpha L_o)] \\ a_7 &= I_{C_o} \alpha \omega^2 \sin(\alpha L_o) - E_o I_o \alpha^2 [\sinh(\alpha L_o) + b_o \alpha \cosh(\alpha L_o)] \\ a_8 &= -I_{C_o} \alpha \omega^2 \cosh(\alpha L_o) + E_o I_o \alpha^2 [\sinh(\alpha L_o) + b_o \alpha \cosh(\alpha L_o)] \\ a_9 &= -I_{C_o} \alpha \omega^2 \sinh(\alpha L_o) + E_o I_o \alpha^2 [\cosh(\alpha L_o) + b_o \alpha \sinh(\alpha L_o)] \end{aligned}$$

Subsequently, the coefficients  $A_i$  ( $i = 1, 2, 3, 4$ ) can be obtained by solving (F.7), given

by

$$\begin{aligned}
A_1 &= -\frac{1}{2a_1\alpha}F(\omega) \\
A_2 &= -\frac{a_9(a_2 - a_4) - a_5(a_6 - a_8)}{2a_1\alpha(a_5a_7 - a_3a_9)}F(\omega) \\
A_3 &= \frac{1}{2a_1\alpha}F(\omega) \\
A_4 &= \frac{a_7(a_2 - a_4) - a_3(a_6 - a_8)}{2a_1\alpha(a_5a_7 - a_3a_9)}F(\omega)
\end{aligned}$$

The driving-point accelerance of the oscillator at the mounting point  $O$  thus is given by

$$A_o(\omega) = -\frac{\omega^2 y(0, \omega)}{F(\omega)} = \frac{\omega^2 [(a_2 - a_4)(a_9 - a_7) + (a_6 - a_8)(a_3 - a_5)]}{2\alpha a_1 (a_5 a_7 - a_3 a_9)} \quad (\text{F.8})$$

The characteristic equation of the oscillator is obtained as follows

$$a_5 a_7 - a_3 a_9 = 0 \quad (\text{F.9})$$

which can be solved by any nonlinear zero finding technique.

## F.2 Distributed-parameter versus Lumped-parameter Oscillator

Given a lumped-parameter oscillator, this section addresses how to determine the length and loss factor of the beam, as shown in Figure F.2. If the cross section and Young's modulus of the beam are given, the length of the beam is the only parameter required to determine the stiffness. Since the fixed-base resonance frequency of an oscillator is not a simple function of the length of the beam, a nonlinear optimization technique [77] is used to determine the length of the beam  $L_o$  and loss factor of the beam  $\eta_0$ . In order to get

good matching at the resonance and anti-resonance, the objective function is defined as

$$J = \frac{\sum_{i=0}^{i=n} \frac{1}{|A_t(\omega_i)|^2}}{\sum_{i=0}^{i=n} \frac{1}{|\tilde{A}_t(\omega_i)|^2}} \sum_{i=0}^{i=n} |A_t(\omega_i) - \tilde{A}_t(\omega_i)|^2 + \sum_{i=0}^{i=n} \left| \frac{1}{A_t(\omega_i)} - \frac{1}{\tilde{A}_t(\omega_i)} \right|^2 \quad (\text{F.10})$$

where  $A_t(\omega_i)$  and  $\tilde{A}_t(\omega_i)$  are the attachment point driving-point accelerance of the base frame mounted with a continuous oscillator and the driving-point accelerance of the same base frame mounted with a lumped-parameter oscillator at the frequency point  $\omega_i$ . The accelerances  $A_t$  and  $\tilde{A}_t$  can be obtained according to (5.17).

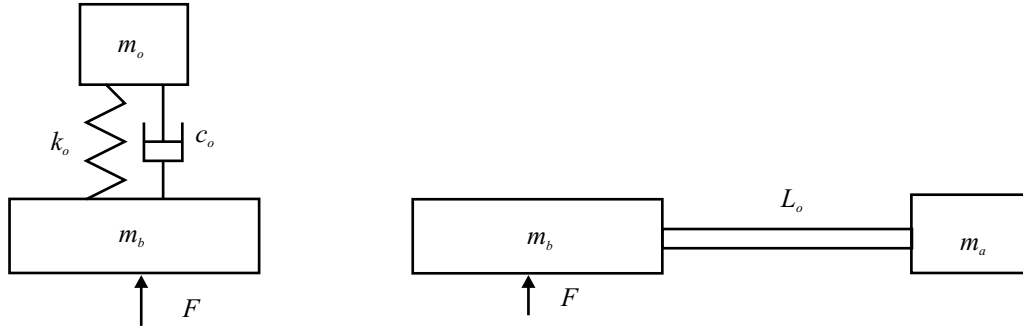


Figure F.2: Lumped-parameter and Distributed-parameter Oscillators



## Appendix G

# Analytical Model for Free-layer Damping Treatments

An analytical model for estimation of the modal loss factor associated with the free-layer damping treatments is discussed in this appendix. It is assumed that the structure under the free-layer damping treatments is a thin beam. The analytical expression for estimation of the modal loss factor is given by the following Oberst equation [100]

$$\eta = \frac{eh(3 + 6h + 4h^2 + 2eh^3 + e^2h^4)}{(1 + eh)(1 + 4eh + 6eh^2 + 4eh^3 + e^2h^4)}\eta_2 \quad (\text{G.1})$$

where  $\eta$  is the effective modal loss factor of the beam with free-layer damping layers,  $\eta_2$  is the loss factor of the damping material,  $e = E_2/E_1$  is the ratio of the Young's modulus  $E_2$  of the damping material to the Young's modulus  $E_1$  of the thin beam, and  $h = h_2/h_1$  is the ratio of the thickness of the damping layer  $h_2$  to the thickness of the thin beam  $h_1$ .

The Oberst equation does not include the damping of the beam material. Since vibration energy is dissipated by both the damping layers and the beam material, the Oberst equation may be modified as follows

$$\eta = \eta_0 + \frac{eh(3 + 6h + 4h^2 + 2eh^3 + e^2h^4)}{(1 + eh)(1 + 4eh + 6eh^2 + 4eh^3 + e^2h^4)}\eta_2 \quad (\text{G.2})$$

where  $\eta_0$  is the modal loss factor of the beam before the damping treatments.

Denote the thickness of each free damping layer as  $h_0$ . Substituting the thickness of  $n$  free damping layers  $nh_0$  into (G.2), the relation between the effective modal loss factor and the number of damping layers is given by

$$\eta = \eta_0 + \frac{eh [3 + 6nh_0 + 4(nh_0)^2 + 2e(nh_0)^3 + e^2(nh_0)^4]}{(1 + enh_0) [1 + 4enh_0 + 6e(nh_0)^2 + 4e(nh_0)^3 + e^2(nh_0)^4]} \eta_2 \quad (\text{G.3})$$

Since a ratio of two polynomials can be expressed as a MacLaurin series, it would be expected that a polynomial of the number of layers  $n$  can be used to model the relation between the effective loss factor and the number of free damping layers.

## Appendix H

# *MATLAB/SIMULINK*<sup>®</sup> Models for Active Emulation

This appendix includes three *SIMULINK*<sup>®</sup> models used in comparison experiments for active emulation. In these models, the gain  $K_a$  is determined by the sensitivity of the accelerometer in the impedance head *Z602WA* and the set gain of the signal conditioner. The gain  $K_f$  is dependent on the sensitivity of the force gage in the impedance head *Z11* and the gain set in the signal conditioner. The gains of the PD controller are carefully tuned such that the error between the actual force and desired force is small and the whole dynamic systems are stable. Saturation blocks are used to avoid overloading the emulating shaker *F5B*. Several virtual oscilloscopes are used to visually monitor accelerations and forces in real time.

The first *SIMULINK*<sup>®</sup> model consisting of two separate functional modules, as shown in Figure H.1, is used for the first comparison experiment discussed in Subsection 6.4.5. The top module is designed to measure the attachment point acceleration. The bottom module is the implementation of the feedforward/feedback controller in Figure 5.10. This model provides the basis for the other two experiments.

For the second comparison experiment in Subsection 6.4.5, a new *SIMULINK*<sup>®</sup> model

is obtained by adding a third module at the right top corner, as depicted in Figure H.2. The added module applies a periodic impulse voltage to the  $F_3$  shaker so that the  $F_3$  shaker can exert an impulse force excitation on the active mechanical emulator.

The last *SIMULINK*<sup>®</sup> model designed for the third comparison experiment in Subsection 6.4.5 is achieved by replacing the impulsive force module with one that can output a sum of five sinusoids to the  $F_3$  shaker. This model is depicted in Figure H.3.

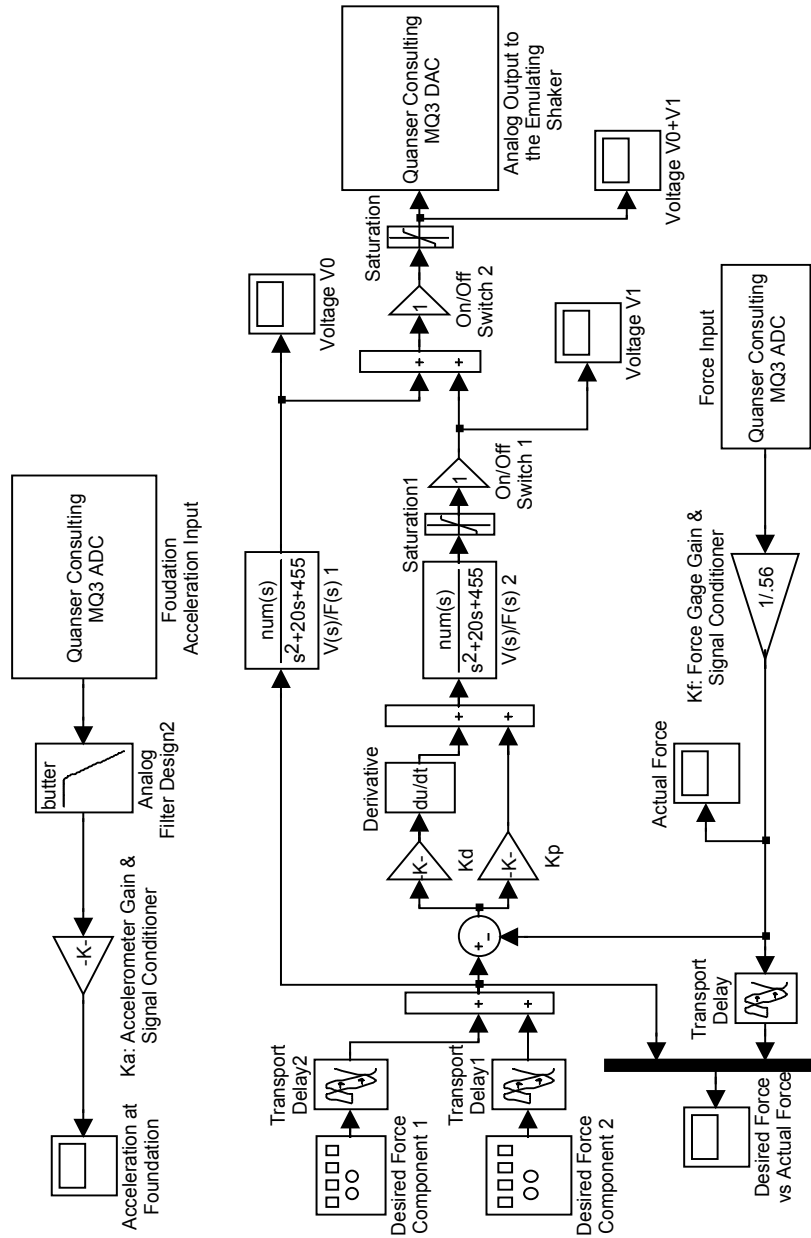


Figure H.1: *SIMULINK*<sup>®</sup> Model of Attachment Point Acceleration Measurement and Feedforward/feedback Controller, Experiment 1

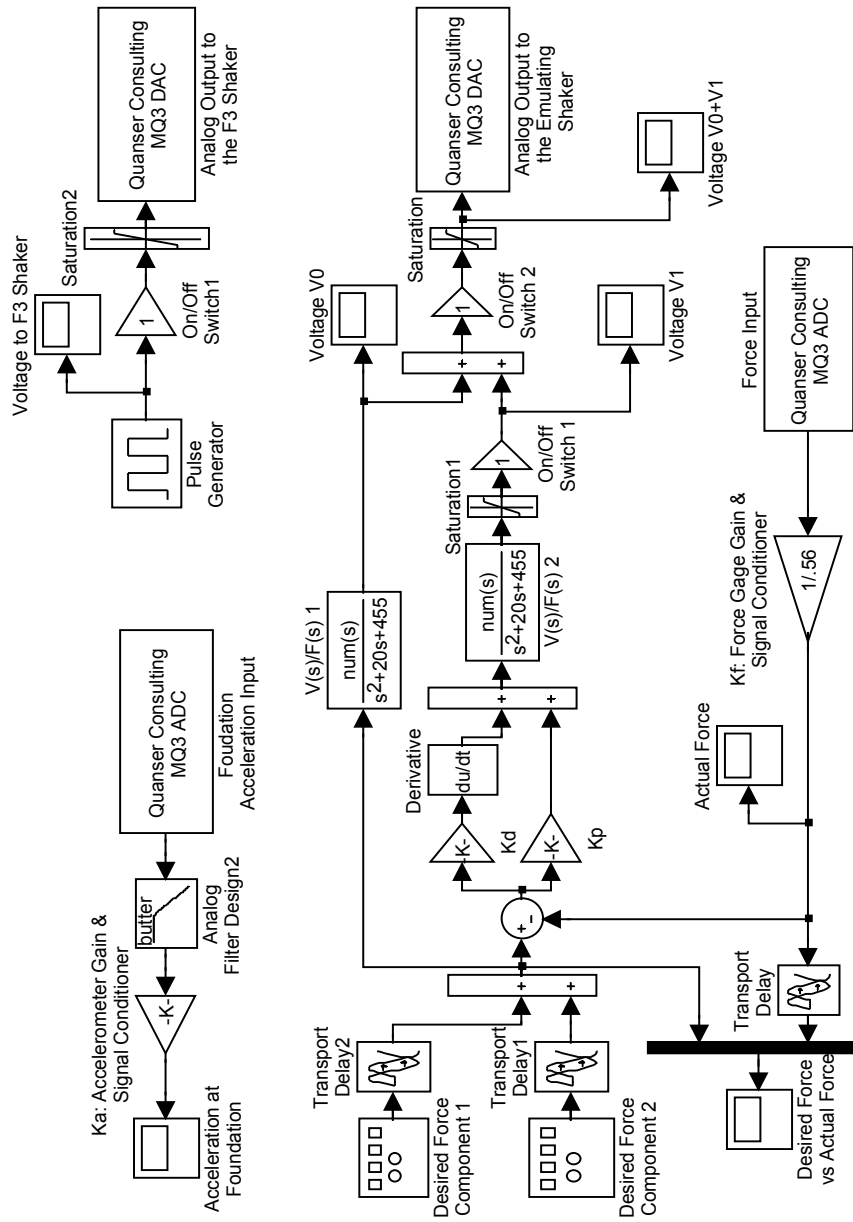


Figure H.2: *SIMULINK*<sup>®</sup> Model of Attachment Point Acceleration Measurement and Feedforward/feedback Controller, Experiment 2

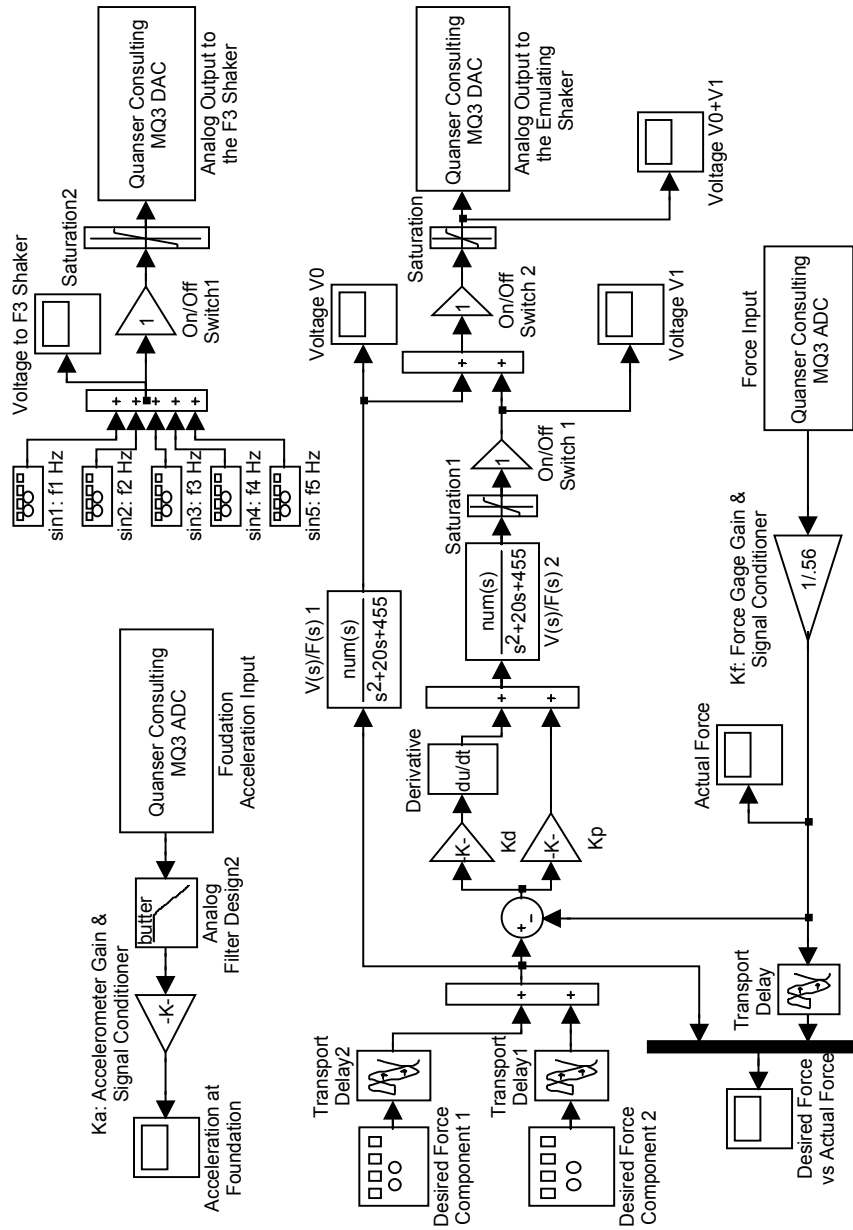


Figure H.3: *SIMULINK*<sup>®</sup> Model of Attachment Point Acceleration Measurement and Feedforward/feedback Controller, Experiment 3

# Bibliography

- [1] H. Baher. *Synthesis of Electrical Networks*. John Wiley & Sons, Inc., 1984.
- [2] Charles E. Crede and Jerome E. Ruzicka. Theory of vibration isolator. In Cyril M. Harris, editor, *Shock and Vibration Handbook*. McGraw-Hill, New York, fourth edition, 1996.
- [3] John D. Dickens. Review of methods to dynamically represent vibration isolators. *The Shock and Vibration Digest*, 34(6):447–453, 2002.
- [4] X. Huang, S. J. Elliott, and M. J. Brennan. Active isolation of a flexible structure from base vibration. *Journal of Sound and Vibration*, 263:357–176, 2003.
- [5] Leif Kari. On the dynamic stiffness of preloaded vibration isolators in the audible frequency range: Modeling and experiments. *Journal of the Acoustical Society of America*, 113(4):1909–1921, 2003.
- [6] Lennart Ljung. *System Identification: Theory for the User*. Prentice Hall, Englewood, NJ, 1987.
- [7] Sudhakar M. Pandit. *Modal and Spectrum Analysis: Data Dependent Systems in State Space*. John Wiley & Sons, Inc., New York, 1991.
- [8] A. A. Shabana. *Theory of Vibration*. Springer-Verlag, New York, 1991.
- [9] A. A. Shabana. *Vibration of Discrete and Continuous Systems*. Springer-Verlag, New York, 1997.
- [10] Dong-Huei Tseng, Richard W. Longman, and Jer-Nan Juang. Identification of a second-order mechanical system model from a state-space realization. In *Proceedings of AIAA Spaceflight Mechanics Meeting*, pages 347–360. Pasadena, CA, February 1993.
- [11] Michael Green and David J.N. Limebeer. *Linear Robust Control*. Prentice Hall, Englewood Cliffs, New Jersey, 1995.
- [12] Katsuhiko Ogata. *Modern Control Engineering*. Prentice-Hall, Inc., Upper Saddle River, NJ 07458, third edition, 1997.



- [13] K. F. Alvin. *Second-order Structural Identification via State Space-based System Realizations*. Ph.D. Dissertation, University of Colorado, Boulder, Colorado, 1993.
- [14] K. F. Alvin and K. C Park. second-order structural identification procedure via state space-based system identification. *AIAA Journal*, 32(2):397–406, 1994.
- [15] M. I. Friswell, S. D. Garvey, and J. E. T. Penny. Extracting second-order systems from state-space representations. *AIAA Journal*, 37(1):132–135, 1998.
- [16] David G. Meyer, Sriram Srinivasan, and Lloyd E. Barrett. 2nd-order balancing and 2nd-order model reduction. In *American Control Conference*, pages : 2116–2122. San Francisco, CA, June 1993.
- [17] David G. Meyer and Sriram Srinivasan. Balancing and model reduction for second-order form linear systems. *IEEE Transactions on Automatic Control*, 41(11):1632–1644, 1996.
- [18] K. F. Alvin, A. N. Robertson, G. W. Reich, and K. C. Park. Structural system identification: From reality to models. *Computers and Structures*, 81:1149–1176, 2003.
- [19] J. N. Juang, J. E. Cooper, and J. R. Wright. An eigensystem realization algorithm using data correlations(ERA/DC) for modal parameter identification. *Control Theory and Advanced Technology*, 4(1):5–14, 1988.
- [20] J. N. Juang and R. S. Pappa. An eigensystem realization algorithm for modal parameter identification and model reduction. *Journal of Guidance, Control and Dynamics*, 8(5):620–627, 1985.
- [21] Jer-Nan Juang. State-space system realization with input- and output -data correlation. Technical report, NASA Langley Research Center, Hampton, VA, April 1997.
- [22] Jer-Nan Juang. Unification of several system realization algorithms. *Journal of Guidance, Control, and Dynamics*, 20(1), 1997.
- [23] B. D. Anderson and R. E. Skelton. Generation of all Q-Markov covers. *IEEE Transactions for Circuits and Systems*, 35:375–384, 1988.
- [24] D. A. Wagie and R. E. Skelton. A projection approach to covariance equivalent realization of discrete systems. *IEEE Transactions for Automatic Control*, 31:1114–1120, 1986.
- [25] A. M. King, U. B. Desai, and R. E. Skelton. A generalized approach to Q-markov covariance equivalent realization of discrete systems. *Automatica*, 24:507–515, 1988.
- [26] M. Moonen, Vanderberghe DeMoor, and J. Vandewalle. On- and off-line identification of linear state-space models. *International Journal of Control*, 49:219–232, 1989.

- [27] Peter Van Overschee. N4SID: Subspace algorithms for the identification of combined deterministic– stochastic systems. *Automatica*, 30(1):75–93, 1994.
- [28] J. S. Lew, J. N. Juang, and R. W. Longman. Comparison of several system identification methods for flexible structures. *Journal of Sound and Vibration*, 167(3):461–480, 1993.
- [29] L. D. Peterson and K. F. Alvin. Time and frequency domain procedure for identification of structural dynamic models. *Journal of Sound and Vibration*, 201(1):137–144, 1997.
- [30] D. J. Ewins. *Modal Testing: Theory and Practice*. Research Studies Press LTD., Taunton, England, 1984.
- [31] D. J. Ewins and P. T. Gleeson. A method for modal identification of lightly damped structures. *Journal of Sound and Vibration*, 84(1):57–79, 1982.
- [32] M. H. Richardson and D. L. Formenti. Parameter estimation from frequency response measurements using rational fraction polynomials. In *Proceedings of the First International Modal Analysis Conference (IMAC I)*, pages :167–181. Orlando, Florida, 1982.
- [33] J. Schoukens and R. Pintelon. *Identification of Linear Systems*. Pergamon Press, 1991.
- [34] Robert J. Guyan. Reduction of stiffness and mass matrices. *AIAA Journal*, 3(2):380, 1965.
- [35] Harry G. Schaeffer. Part II: Finite element models. In Cyril M. Harris, editor, *Shock and Vibration Handbook*. McGraw-Hill, New York, fourth edition, 1996.
- [36] B. C. Moore. Principal component analysis in linear systems: Controllability, observability, and model reduction. *IEEE Transaction on Automatic Control*, 29:17–31, 1981.
- [37] Xin Chen and John T. Wen. Positive realness preserving model reduction with  $H_\infty$  norm error bounds. *IEEE Transaction on Circuits and Systems*, 42(1):23–29, 1995.
- [38] Pierre Dupont and Ann Stokes. Model reduction techniques for shock loaded equipment emulators. In *69'th Shock and Vibration Symposium*, St. Paul, MN, October 12-16, 1998.
- [39] Paul E. Barbone. Equipment representations for shock calculations: Time domain Dirichlet to Neumann maps. In *Proceedings of the ASME Symposium on Acoustics of Submerged Structures and Transduction Systems*, ASME Press, New York, September 17-21, 1995.
- [40] Daniel Goldman and Paul E. Barbone. Dirichlet to Neumann maps for the representation of equipment with weak nonlinearities. In *Proceedings of the ASME Noise Control and Acoustics Division*, volume NCA-Vol. 22, 1996.

- [41] Aravind Cherukuri and Paul E. Barbone. High modal density approximations for equipment in the time domain. *Journal of the Acoustical Society of America*, 104(4):2048–2053, 1998.
- [42] Paul E. Barbone, Aravind Cherukuri, and Daniel Goldman. Canonical representations of complex vibratory subsystems: Time domain Dirichlet to Neumann maps. *International Journal of Solids and Structures*, 37:2825–2857, 2000.
- [43] Daniel Boley and Gene H Golub. A survey of matrix inverse eigenvalue problems. *Inverse Problems*, 3(2):595–622, 1987.
- [44] Graham M. L. Gladwell. Inverse problems in vibration. *Applied Mechanics Review*, 39(7):1013–1018, 1986.
- [45] Graham M. L. Gladwell. Inverse problems in vibration. *Applied Mechanics Review*, 49(10):S25–S34, 1996.
- [46] G. M. L. Gladwell. On isospectral spring-mass systems. *Inverse Problems*, 11(2):591–602, 1995.
- [47] Moody T. Chu. Inverse eigenvalue problems. *SIAM Review*, 40(1):1–39, 1998.
- [48] Yitshak M. Ram and Sylvan Elhay. An inverse eigenvalue problem for the symmetric tridiagonal quadratic pencil with application to damped oscillatory systems. *SIAM Journal on Applied Mathematics*, 56(1):232–244, 1996.
- [49] L. Starek, D. J. Inman, and A. Kress. A symmetric inverse vibration problem. *Transactions of the ASME:Journal of Vibration and Acoustics*, 114:564–568, 1992.
- [50] L. Starek and D. J. Inman. A symmetric inverse vibration problem for nonproportional underdamped systems. *Journal of Applied Mechanics*, 64:601–605, 1997.
- [51] L. Starek and D. J. Inman. Symmetric inverse eigenvalue vibration problem and its application. *Mechanical Systems and Signal Processing*, 15(1):11–29, 2001.
- [52] G. M. L. Gladwell. Inverse vibration problems for finite-element models. *Inverse Problems*, 13(2):311–322, 1997.
- [53] Robert A. Johnson. *Mechanical Filters in Electronics*. John Wiley & Sons, Inc., 1983.
- [54] Sidney Darlington. A history of network synthesis and filter theory for circuits composed of resistors, inductors, and capacitors. *IEEE Transactions on Circuits and Systems, CAS*, 31(1):3–13, 1984.
- [55] C. T. C. Nguyen. Micromechanical resonators for oscillators and filters. In *Proceedings of 1995 IEEE International Ultrasonics Symposium*, pages 489–499, Seattle, WA, November 7-10, 1995.

- [56] K. Wang and C. T. C. Nguyen. High-order micromechanical electronic filters. In *Proceedings of 1997 IEEE International Micro Electro Mechanical Systems Workshop*, pages :25–30, Nagoya, Japan, January 26-30, 1997.
- [57] Liwei Lin, Roger T. Howe, and Albert P. Pisano. Microelectromechanical filters for signal processing. *Journal of Microelectromechanical Systems*, 7(3):286–294, 1998.
- [58] C. T. C. Nguyen. Micromechanical filters for miniaturized low-power communications. In *Proceedings of SPIE: Smart Structures and Materials (Smart Electronics and MEMS)*, Newport Beach, California, March 1-5, 1999.
- [59] Kun Wang and Clark T. C. Nguyen. High-order medium frequency micromechanical electronic filters. *Journal of Microelectromechanical Systems*, 8(4):534–557, 1999.
- [60] Ernst A. Guillemin. *Synthesis of Passive Networks— Theory and Methods Appropriate to the Realization and Approximation Problems*. John Wiley & Sons, Inc., 1957.
- [61] Van Valkenburg. *Introduction to Modern Network Synthesis*. John Wiley & Sons, Inc., 1960.
- [62] S. Falk. Die abbildung eines allgemeine schwingungssystems auf eine einfache schwingerkette. *Ingenieur-Archiv*, 23:314–328, 1955.
- [63] S. L. Chen and M. Géradin. An exact model reduction procedure for mechanical systems. *Computational Methods in Applied Mechanics and Engineering*, 143:69–78, 1997.
- [64] G. J. O’Hara and P. F. Cunniff. Elements of normal mode theory. Technical report, Naval Research Laboratory Report, 1963.
- [65] A. D. Pierce. Resonant-frequency-distribution of internal mass inferred from mechanical impedance matrices, with application to fuzzy structure theory. *Transactions of the ASME: Journal of Vibration and Acoustics*, 119:325–333, July 1997.
- [66] Leonard Meirovitch. *Principles and Techniques of Vibrations*. Prentice-Hall, Inc., Upper Saddle River, NJ, 1997.
- [67] Alan Jennings. *Matrix Computation*. John Wiley & Sons, 1992.
- [68] O. Rojo, R. Soto, and J. Egana. A note on the construction of a positive oscillatory matrix with a prescribed spectrum. *Computers and Mathematics with Applications*, 41:353–361, 2001.
- [69] R. Haberman. Frequency response characteristics of electrical cabinets and scale model simulators. Technical report, BBN Technical Memorandum No. NL-471, 1995.
- [70] R. Haberman. Equipment emulator design progress report. Technical report, Project M Progress Report Slides, May 1997.

- [71] Sudeep Deshpande. A systematic approach to active machinery emulation. M.S. Thesis, Department of Aerospace and Mechanical Engineering, Boston University, 2003.
- [72] Silva Maia and et al. *Theoretical and Experimental Modal Analysis*. Research Studies Press LTD., Taunton, England, 1997.
- [73] William H. Press and et al. *Numerical Recipes in C: the Art of Scientific Computing*. Cambridge University Press, New York, second edition, 1992.
- [74] Michael T. Heath. *Scientific Computing: An Introductory Survey*. McGraw-Hill, Boston, MA, 1997.
- [75] Randy L. Haupt and Sue Ellen Haupt. *Practical Genetic Algorithms*. John Wiley & Sons, New York, 1998.
- [76] G. H. Golub and C. F. Van Loan. *Matrix Computations*. John Hopkins University Press, Baltimore, MD, third edition, 1996.
- [77] R. Fletcher. *Practical Methods of Optimization*. John Wiley & Sons, Inc., New York, 1987.
- [78] J. C. Lagarias, J. A. Reeds, M. H. Wright, and P. E. Wright. Convergence properties of the Nelder-Mead simplex algorithm in low dimensions. *SIAM Journal of Optimization*, 9(1):112–147, 1999.
- [79] Jr., R. R. Graig. Substructure methods in vibration. *Transactions of the ASME: Special 50'th Anniversary Design Issue*, 117(1):207–213, 1995.
- [80] G. J. O'Hara and P. F. Cunniff. The shock spectrum dip effect. *Journal of Sound and Vibration*, 103(3):311–321, 1985.
- [81] P. F. Cunniff and G. J. O'Hara. A procedure for generating shock design values. *Journal of Sound and Vibration*, 134(1):155–164, 1989.
- [82] David I. G. Jones. Chapter 37: Applied damping treatments. In Cyril M. Harris, editor, *Shock and Vibration Handbook*. McGraw-Hill, New York, fourth edition, 1996.
- [83] Benjamin J. Lazan. *Damping of Materials and Members in Structural Mechanics*. Pergamon Press, Oxford, 1968.
- [84] Ahid D. Nashif, David I. G. Jones, and John P. Henderson. *Vibration Damping*. John Wiley & Sons, Inc., New York, 1985.
- [85] Donald Ross, Eric E. Ungar, and E. M., Jr Kerwin. Damping of plate flexural vibrations by means of viscoelastic laminae. In *Structural Damping*, pages 49–88. ASME, New York, 1959.
- [86] A. D. Nashif and T. Nicholas. Vibration control by a multiple-layered damping treatment. *The Shock and Vibration Bulletin*, 41(2):121–131, 1970.

- [87] S. H. Crandall. The role of damping in vibration theory. *Journal of Sound and Vibration*, 11(1):3–18, 1970.
- [88] D. I. G. Jones, A. D. Nashif, and M. L. Parin. Parametric study of multiple-layer damping treatments on beams. *Journal of Sound and Vibration*, 29(4):423–434, 1973.
- [89] Lynn C. Rogers and Ahid D. Nashif. Computerized processing and empirical representation of viscoelastic material property data and preliminary constrained layer damping treatment design. *The Shock and Vibration Bulletin*, 48(2):23–37, 1978.
- [90] Mohan D. Rao. Recent applications of viscoelastic damping for noise control in automobiles and commercial airplanes. In *2001 India-USA Symposium on Emerging Trends in Vibration and Noise Engineering*, 2001.
- [91] 3M<sup>TM</sup> Industrial Business Electronics Markets Materials Division. 3M<sup>TM</sup> viscoelastic damping polymer 110, 112 and 130, 2003.
- [92] Dynamic Control of North America, Inc. *Dynaplate<sup>TM</sup>* reference chart, 2001.
- [93] Wilcoxon Research. Model F3/Z602WA electromechanical shaker system.
- [94] Wilcoxon Research. Model F5B/Z11 electromechanical shaker system.
- [95] Quanser Consulting Inc., Ontario, Canada. *Quanser Manual*, 2000.
- [96] VenturCom, Inc., Cambridge, MA. *RTX 5.0 Release Notes*, 2001.
- [97] The Mathworks, Inc., Natick, MA. *SIMULINK<sup>®</sup>: Dynamic System Simulation for MATLAB<sup>®</sup>*, 2003.
- [98] Quanser Consulting Inc., Ontario, Canada. *Wincon 3.1*, 2000.
- [99] Jerry H. Ginsberg. *Mechanical and Structural Vibrations*. John Wiley & Sons, New York, 2001.
- [100] Von Hermann Oberst. Über die dämpfung der biegeschwingungen dünner fleche durch fest haftende belage. *Acustica*, 4:181–194, 1952.

# Vita

Wenyuan Chen was born in Taizhou City, Zhejiang Province, China in 1974, the third child of Guanyue Wu and Deqiu Chen. He attended Luqiao Middle School and graduated in 1992. The following fall he entered the Department of Mechanical Engineering of Zhejiang University (Website: <http://www.zju.edu.cn/english>) in Hangzhou. He was awarded the Bachelor of Engineering degree in Mechanical Manufacturing and Automation in the July of 1996. With privilege of exemption from Chinese National Entrance Exams for Graduate Schools, he entered the Graduate School of ZJU in 1996. He was awarded the Master of Engineering degree in Mechanical Manufacturing and Automation in the March of 1999. During pursuit for his master degree, he did research in development of an open architecture controller for a high precision machine tool under Dr. Zichen Chen in a joint research project of ZJU and Hangzhou Machine Tool Corporation.

On August 22, 1999, he came to the USA and entered the Ph.D. program in Mechanical Engineering of the Department of Aerospace and Mechanical Engineering at Boston University. Under the supervision of Dr. Pierre E. Dupont, he has been doing research in the areas of dynamics and control, acoustics and vibration and micro-electro-mechanical systems (MEMS).

Permanent Address: Xiayun Village, Hengjie Town, Luqiao District, Taizhou City, Zhejiang Province, People's Republic of China, 318056

# WENYUAN (WILLIAM) CHEN

21712 Septo Street, #209, Chatsworth, CA 91311

mewychen@yahoo.com

(617)416-8198(mobile)

## EDUCATION

Ph.D., Mechanical Engineering, Boston University, Boston, MA, May 2004

Ph.D. Dissertation: Mechanical Realization Theory and its Application to Machinery Emulation

M.E., Mechanical Manufacturing and Automation, Zhejiang University, China, 1999

Master Thesis: Study on CNC System Based on Industrial Personal Computer (IPCNC)

B.E., Mechanical Manufacturing and Automation, Zhejiang University, China, 1996

Bachelor Thesis: Study on Real-time Multi-task Partition, Scheduling, and Communications for Computer Numerically Controlled (CNC) Systems

Minor, Computer Science and Engineering (2.5 years program), Zhejiang University, China, 1996

## PROFESSIONAL EXPERIENCES

**Senior Design/Project Engineer**, Servo Dynamics Corporation, Chatsworth, CA

February 2004 to Present

Responsible for developing servo amplifiers based on the latest analog and digital technologies, with focus on DSP (Digital Signal Processor) firmware and FPGA (Field Programmable Gate Array) programming.

**Presidential Graduate Fellow/Research Assistant**, Boston University, Boston, MA



August 1999 to February 2004

Responsible for developing a realization theory for design of electromechanical systems with desired input-output dynamic properties in projects sponsored by US Office of Naval Research, with a wide variety of applications including scaled shock and vibration testing and design of vibration absorbers.

- Developed systematic design techniques for passive/active dynamic emulators of equipment and machinery, including searching the parameterized space of transformations and direct estimation of realizable models from experimental data.
- Designed, prototyped and tested passive/active mechanical emulators.
- Programmed a comprehensive software toolbox for mechanical emulator design.
- Developed a feedforward/feedback controller for a shaker to reproduce desired motions.
- Implemented several model reduction methods for complicated vibration systems, including Guyan's reduction, modal reduction and positive-realness preserving balanced reduction.
- Implemented a novel FEA method for solving a 2-D wave propagation problem.
- Studied dynamic properties of micro-electro-mechanical (MEMS) resonators.
- Modeled and tested damping properties of beams with polymeric damping treatments.

**Teaching Fellow for EK 303 Fluid Mechanics**, Boston University, Boston, MA

Summer 2003

Responsible for preparing lab equipment and instrumentation, and instructing students to do fluid mechanics labs and leading them to solve lab problems. These labs included Continuity Equation, Bernoulli's Principle, Flow Visualization Using Osborne Reynolds Apparatus and Friction Loss in Pipes.

**Mechanical Engineer**, Institute of Production Engineering, Zhejiang University, China

1999

Responsible for performance evaluations of an open architecture controller for a machine tool.

- Proved through tests that the developed miller controller has higher motion control precision.
- Evaluated its performance and reliability by machining sample parts.

**Development Engineer**, Hangzhou Machine Tool Corporation, Hangzhou, China

1996 to 1999

Responsible for development of a real-time open architecture controller for a high-precision machine tool in the province Key project jointly investigated by Hangzhou Machine Tool Corporation and Zhejiang University.

- Designed the hardware and software system of an open architecture controller.
- Developed and debugged real-time control software including GUI, input/output operation, machine tool condition monitoring and 3-axis motion control, using C/C++.

## HONORS AND ACTIVITIES

American Society of Mechanical Engineers (ASME), 2002- present

Presidential University Graduate Fellowship, Boston University, 1999

Graduate with Honors, Zhejiang University, 1999

Rockwell Automation MS Scholarship, Rockwell Automation and Zhejiang University, 1998

Siemens Prize, Siemens Corporation and Zhejiang University, 1997

Graduate with Honors (Medal), Zhejiang University, 1996

Graduate with Honors, Zhejiang Province, 1996

Distinguished Undergraduate Honors and Scholarships, Zhejiang University, 1992-1996

President, Vice President, Department Graduate Student Association, 1996-1998

Chinese Calligraphy Student Society of Zhejiang University, 1992-1998

## SELECTED PUBLICATIONS

- Dupont P., Chen, W., Mechanical Realization for Passive Scalar Transfer Functions, The First Pan-American/Iberian Meeting on Acoustics, Cancun, Mexico, 2-6 December, 2002, Abstract in Journal of Acoustical Society of America., Vol. 112, No. 5, pp. 2247, Pt. 2, November 2002.
- Chen, W. and Barbone P. E., Implementation of Nearly H1-Optimal Finite Element Method for Solving 2-D Helmholtz Equation, 73rd Shock and Vibration Symposium, Newport, RI, November 18-22, 2002 (full article).
- Dupont, P., Chen, W. and Deshpande, S., Design Techniques for Machinery Emulators, 73rd Shock and Vibration Symposium, Newport, RI, November 18-22, 2002 (abstract).
- Dupont, P. and Chen, W., Electromechanical Realization of Impedance Matrices, 141st Meeting of Acoustical Society of America, Palmer House Hilton Hotel, Chicago, IL, June 4-6, 2001, Abstract in Journal of Acoustical Society of America, Vol. 109, No. 5, pp. 2444, Pt. 2, May 2001.
- Chen, W., Wang, W. and Chen, Z., A Study on Real-time Multi-task Partition, Scheduling and Communications of CNC System Based on PC-Bus Industrial Computer, Journal of Zhejiang University (Science Edition), 1997.
- Chen, W., Wang, W. et al, The Software Design and Realization of a CNC System Based on A PC-Bus Industrial Personal Computer, Mechanical & Electrical Engineering Magazine, Vol. 16 (6), 1997.
- Zhang, Y., Ying, J., Chen, Z., Chen W., The Research on the Self Adaptive Fuzzy

Control System for Electric Discharge Machining, 1997 IEEE International Conference on Intelligent Processing System, Beijing, Vol 1: 364-367.

- Wang, W., Chen, W., Chen, Z., A Study on a New CNC System Based on Industrial Personal Computer, Mechanical & Electrical Engineering Magazine, Vol. 16 (6), 1997.